



VLT ERIS

Phase B

Sub-System Design & Performance Report - AO

Doc. No.: VLT-TRE-ERI-14403-3001

Issue: 1.0

Date: 05.12.15

| | | | |
|--------------|-----------------|-------|-------------------------|
| Prepared by: | A. Riccardi (*) | | <i>Armando Riccardi</i> |
| | Name | Date | Signature |
| Approved by: | | | |
| | Name | Date | Signature |
| Released by: | | | |
| | Name | Date | Signature |

(*) With contributions from: G. Agapito, J. Antichi, V. Biliotti, C. Blain, R. Briguglio, L. Busoni, L. Carbonaro, C. Del Vecchio, G. Di Rico, S. Egner, S. Esposito, C. Giordano, E. Pinna, A. Puglisi, P. Spanò, M. Xompero

| | | | |
|------------------------|-------------------------------------|------------------------------------|---|
| ERIS Consortium | ERIS Documentation Standards | Doc.-Ref. Issue Date Page | : VLT-TRE-ERI-14403-3001 : 1.0 : 05.12.15 : 2 of 136 |
|------------------------|-------------------------------------|------------------------------------|---|

CHANGE RECORD

| ISSUE | DATE | SECTION/PARAGRAPH AFFECTED | REASON/INITIATION DOCUMENTS/REMARKS |
|-------|----------|----------------------------|-------------------------------------|
| 1.0 | 05.12.15 | All | Initial release of the document |
| | | | |
| | | | |

| | | | |
|--------------------|---------------------------------|------------------------------------|---|
| ERIS Consortium | ERIS Documentation Standards | Doc.-Ref. Issue Date Page | : VLT-TRE-ERI-14403-3001 : 1.0 : 05.12.15 : 3 of 136 |
|--------------------|---------------------------------|------------------------------------|---|

TABLE OF CONTENTS

| | | |
|---------|--|----|
| 1 | Scope..... | 8 |
| 2 | References..... | 9 |
| 2.1 | Applicable documents | 9 |
| 2.2 | Reference documents | 10 |
| 2.3 | Acronyms | 12 |
| 3 | Introduction | 14 |
| 4 | Design report of Adaptive Optics and Warm Optics..... | 15 |
| 4.1 | The AO+WO general design guidelines..... | 15 |
| 4.2 | Constraints on choice on hardware devices for the AO | 18 |
| 4.2.1 | CCD220 Camera..... | 19 |
| 4.2.2 | SPARTA..... | 19 |
| 4.3 | HO/LO NGS WFS unit..... | 20 |
| 4.4 | LGS WFS unit | 22 |
| 4.5 | AO Control | 23 |
| 4.5.1 | AO Observing modes | 23 |
| 4.5.2 | Control loops in NGS mode | 24 |
| 4.5.2.1 | HO AO real-time loop:..... | 24 |
| 4.5.2.2 | Dark map update | 24 |
| 4.5.2.3 | NCPA offset..... | 25 |
| 4.5.2.4 | Pupil X-Y stabilization loop | 25 |
| 4.5.2.5 | Pupil rotator (K-mirror) loop | 25 |
| 4.5.2.6 | ADC loop | 25 |
| 4.5.2.7 | Differential pointing loop | 25 |
| 4.5.2.8 | Differential focus loop | 26 |
| 4.5.2.9 | Offloading | 26 |
| 4.5.3 | Control loops in LGS mode..... | 26 |
| 4.5.3.1 | HO AO real-time loop..... | 26 |
| 4.5.3.2 | LO AO real-time loop | 26 |
| 4.5.3.3 | LGS WFS focus loop | 27 |
| 4.5.3.4 | Dark map update | 27 |
| 4.5.3.5 | Laser focalization offset | 27 |
| 4.5.3.6 | Truth sensor loop and NCPA offset..... | 28 |
| 4.5.3.7 | Pupil X-Y stabilization loop | 28 |

| | | | |
|----------------------------|---|------------------------------------|---|
| ERIS Consortium | ERIS Documentation Standards | Doc.-Ref. Issue Date Page | : VLT-TRE-ERI-14403-3001 : 1.0 : 05.12.15 : 4 of 136 |
|----------------------------|---|------------------------------------|---|

| | | |
|----------|---|----|
| 4.5.3.8 | Pupil rotator (K-mirror) loop | 28 |
| 4.5.3.9 | ADC loop | 28 |
| 4.5.3.10 | Differential pointing loop | 28 |
| 4.5.3.11 | Differential focus loop | 28 |
| 4.5.3.12 | Offloading | 28 |
| 4.6 | HO NGS WFS trade-off..... | 29 |
| 4.7 | AO system simulation..... | 29 |
| 4.7.1 | Numerical simulation input parameters..... | 30 |
| 4.7.1.1 | Atmosphere | 31 |
| 4.7.1.2 | Emission and transmission | 32 |
| 4.7.1.3 | Total loop delay | 34 |
| 4.7.1.4 | EMCCD gain..... | 34 |
| 4.7.1.5 | Laser Guide Star specific parameters | 34 |
| 4.7.2 | AO system calibration simulation..... | 35 |
| 4.7.3 | LGS spot pattern modelling | 35 |
| 4.7.4 | EMCCD modelling | 36 |
| 4.7.5 | AO loop performance optimization..... | 36 |
| 4.7.6 | Selection of Centroid algorithm..... | 37 |
| 4.7.7 | Selection of sub-aperture FoV in NGS mode | 39 |
| 4.7.8 | Summary of AO performance | 41 |
| 4.7.9 | NGS-mode optimized parameters and performance | 44 |
| 4.7.10 | NGS-mode: contrast, speckle noise and ADI SNR | 45 |
| 4.7.11 | LGS-mode simulation results..... | 47 |
| 4.7.12 | Vibrations: NGS-mode..... | 48 |
| 4.7.13 | Variable seeing and robustness..... | 50 |
| 4.7.14 | Sensitivity Analysis | 52 |
| 4.7.15 | LGS spot elongation and truncation effect | 53 |
| 4.7.16 | Sodium layer profile variation..... | 54 |
| 4.8 | Optical Design..... | 57 |
| 4.8.1 | Overview | 57 |
| 4.8.2 | Warm Optics..... | 60 |
| 4.8.3 | WFS Optics | 64 |
| 4.8.4 | NGS Wavefront Sensor specific optics | 67 |
| 4.8.5 | LGS Wavefront Sensor..... | 68 |
| 4.8.6 | AO DM Simulator..... | 69 |

| | | | |
|----------------------------|---|------------------------------------|---|
| ERIS Consortium | ERIS Documentation Standards | Doc.-Ref. Issue Date Page | : VLT-TRE-ERI-14403-3001 : 1.0 : 05.12.15 : 5 of 136 |
|----------------------------|---|------------------------------------|---|

| | | |
|----------|---|----|
| 4.9 | Mechanical Design | 71 |
| 4.9.1 | Warm Optics..... | 71 |
| 4.9.2 | R-WFS - NGS HO/LO Wavefront Sensor..... | 74 |
| 4.9.2.1 | Dual-axis stage..... | 76 |
| 4.9.2.2 | Periscope..... | 77 |
| 4.9.2.3 | Pupil rotator | 78 |
| 4.9.2.4 | Technical camera | 79 |
| 4.9.2.5 | Pupil Stabilization Mirror | 80 |
| 4.9.2.6 | Filter Wheel | 81 |
| 4.9.2.7 | Collimator Lens..... | 81 |
| 4.9.2.8 | Fold mirror | 81 |
| 4.9.2.9 | ADC..... | 82 |
| 4.9.2.10 | HO/LO SH Lenslet switch | 82 |
| 4.9.2.11 | Camera Head Interface..... | 84 |
| 4.9.3 | LGS Wavefront Sensor..... | 85 |
| 4.9.3.1 | Focusing stage | 87 |
| 4.9.3.2 | Relay Lens..... | 87 |
| 4.9.3.3 | Shutter | 87 |
| 4.9.3.4 | K-mirror | 87 |
| 4.9.3.5 | Technical camera | 87 |
| 4.9.3.6 | Pupil Stabilization mirror | 87 |
| 4.9.3.7 | Collimator Lens..... | 87 |
| 4.9.3.8 | Lenslet mount..... | 87 |
| 4.9.3.9 | Camera Head Interface..... | 88 |
| 4.9.4 | Cables and Harnesses | 88 |
| 4.9.5 | Materials..... | 88 |
| 4.9.6 | Mass and Balance Budget..... | 89 |
| 4.10 | Control Electronic Design | 89 |
| 5 | Interaction Matrix (IM) calibration | 92 |
| 5.1 | Synthetic IM | 92 |
| 5.2 | On-sky IM calibration..... | 92 |
| 5.2.1 | Close loop operations..... | 92 |
| 5.2.2 | Modulation and demodulation..... | 93 |
| 5.2.3 | Iterative process | 93 |
| 5.2.4 | Multiplexing | 93 |

| | | | |
|------------------------|-------------------------------------|------------------------------------|---|
| ERIS Consortium | ERIS Documentation Standards | Doc.-Ref. Issue Date Page | : VLT-TRE-ERI-14403-3001 : 1.0 : 05.12.15 : 6 of 136 |
|------------------------|-------------------------------------|------------------------------------|---|

| | | |
|---------|--|-----|
| 5.2.5 | On-sky verification | 94 |
| 5.2.6 | Parameters optimization | 94 |
| 5.2.7 | Implementation on SPARTA..... | 94 |
| 6 | Pyramid WFS upgrade design for the NGS WFS | 95 |
| 6.1 | ERIS NGS Strehl ratio performances | 95 |
| 6.1.1 | Contrast, speckle noise and ADI SNR | 97 |
| 6.2 | Pyramid WFS Optical Design | 99 |
| 6.3 | Pyramid WFS Mechanical Design | 101 |
| 6.4 | Implementation in SPARTA..... | 102 |
| 7 | Analysis Report..... | 103 |
| 7.1 | Optical performances | 103 |
| 7.1.1 | Science Path Optical Performances | 103 |
| 7.1.2 | Sensitivity Analysis | 106 |
| 7.1.3 | Mechanical Performances | 111 |
| 7.1.4 | IR/VIS Dichroic FEA analysis and processing..... | 112 |
| 7.1.4.1 | Model..... | 112 |
| 7.1.4.2 | Geometry..... | 113 |
| 7.1.4.3 | Boundary conditions | 113 |
| 7.1.4.4 | Load cases | 113 |
| 7.1.4.5 | Results | 114 |
| 7.2 | NGS Opto-mechanical Performances..... | 115 |
| 7.2.1 | Optical Performances | 115 |
| 7.2.2 | Sensitivity Analysis | 116 |
| 7.3 | LGS Opto-mechanical Performances | 118 |
| 7.3.1 | Optical Performances | 118 |
| 8 | Alignment Concept..... | 118 |
| 8.1 | LGS WFS board internal alignment..... | 118 |
| 8.1.1 | Tools | 119 |
| 8.1.2 | Conventions | 119 |
| 8.1.3 | Alignment procedure | 119 |
| 8.2 | Internal Alignment of NGS WFS | 120 |
| 8.2.1 | Pre-requisites | 121 |
| 8.2.2 | Tools | 121 |
| 8.2.3 | Alignment procedure | 121 |
| 8.3 | Warm Optics and WFS boards alignments on ERIS Optical Plate..... | 124 |

| | | | |
|------------------------|-------------------------------------|------------------------------------|---|
| ERIS Consortium | ERIS Documentation Standards | Doc.-Ref. Issue Date Page | : VLT-TRE-ERI-14403-3001 : 1.0 : 05.12.15 : 7 of 136 |
|------------------------|-------------------------------------|------------------------------------|---|

| | | |
|-------|---|-----|
| 8.3.1 | Telescope's mechanical axis materialisation | 124 |
| 8.3.2 | Alignment of warm optics and WFS boards | 125 |
| 9 | Error Budget..... | 127 |
| 9.1 | WFE budget | 129 |
| 9.2 | Image Motion Budget | 131 |
| 10 | Compliance Status | 133 |
| 11 | Conclusions | 136 |

| | | | |
|---|--|--|---|
| <p style="text-align: center;">ERIS Consortium</p> | <p style="text-align: center;">ERIS Documentation Standards</p> | <p>Doc.-Ref. Issue Date Page</p> | <p>: VLT-TRE-ERI-14403-3001 : 1.0 : 05.12.15 : 8 of 136</p> |
|---|--|--|---|

1 Scope

The scope of this document is to provide the preliminary design of the Enhanced Resolution Imager and Spectrograph (ERIS) Adaptive Optics (AO) module developed in the framework of the ERIS Phase B study. This document provides also the preliminary design of Warm Optics (WO), i.e. the optics providing the relay of the telescope beam to the WFS units.

| | | |
|----------------------------|---|---|
| ERIS Consortium | ERIS Documentation Standards | Doc.-Ref. : VLT-TRE-ERI-14403-3001 Issue : 1.0 Date : 05.12.15 Page : 9 of 136 |
|----------------------------|---|---|

2 References

2.1 Applicable documents

The following applicable documents (AD) of the exact issue form part of the present document to the extent specified herein.

| AD Nr | Doc. Nr | Doc. Title | Issue | Date |
|-------|-------------------------|---|-------|----------|
| AD1 | VLT-SPE-ESO-14400-5252 | ERIS Top Level Requirements | 4 | 08.06.15 |
| AD2 | VLT-SPE-ESO-14400-5576 | ERIS System Technical Specifications | 2.4 | 31.07.15 |
| AD3 | VLT-TRE-ERI-14401-1010 | Back Focal Length Change Request for ERIS - Optical Concept | 1 | 15.12.15 |
| AD4 | ESO-262704 | ICD WFS-Cameras | 1 | 15.12.15 |
| AD5 | VLT-SPE-ESO-14400-5946 | ERIS WFS camera head technical specifications | 1 | 02.08.13 |
| AD6 | VLT-ICD-ESO-16800-4433 | Interface Control Document Between 4LGSF and Adaptive Optics | 2 | 30.10.10 |
| AD7 | VLT-PLA-ERI-14403-3901 | Sub-system MAIV plan – AO | 1 | 15.12.15 |
| AD8 | VLT-PRO-ESO-22000-5739 | AOF Control-calibration procedures | 2 | 15.05.13 |
| AD9 | VLT-TRE-ESO-22000- 5740 | AOF on-line optimization – Design Report | 2 | 15.05.13 |
| AD10 | VLT-SPE-ERI-14403-3501 | SPARTA user requirements for ERIS | 1 | 15.12.15 |
| AD11 | VLT-SPE-ERI-14401-1701 | ERIS – Instrumentation Software User Requirements Specification | 1 | 15.12.15 |
| AD12 | VLT-TRE-ERI-14400-1301 | Sub-System Design & Performance Report - Electronics | 1 | 15.12.15 |
| AD13 | VLT-TRE-ERI-14400-1004 | System Design and Analysis | 1 | 15.12.15 |

Table 1: Applicable documents

| | | |
|----------------------------|---|--|
| ERIS Consortium | ERIS Documentation Standards | Doc.-Ref. : VLT-TRE-ERI-14403-3001 Issue : 1.0 Date : 05.12.15 Page : 10 of 136 |
|----------------------------|---|--|

2.2 Reference documents

The following reference documents (RD) contain useful information relevant to the subject of the present document.

| RD Nr | Doc. Nr | Doc .Title | Issue | Date |
|-------|--|---|-------|----------|
| RD1 | VLT-TRE-ESO-14400-5563 | ERIS Phase A Adaptive Optics Design Report | 1 | 13.04.12 |
| RD2 | Esposito et al. SPIE 8447, 84470U (2012) | Natural guide star adaptive optics systems at LBT: FLAO commissioning and science operations status | | |
| RD3 | Morzinski et al. SPIE 9148, 914804 (2014) | MagAO: Status and on-sky performance of the Magellan adaptive optics system | | |
| RD4 | VLT-TRE-ESO-16100- 5513 | SPARTA – Vibration Rejection Algorithms for AO systems | 1 | 16.05.12 |
| RD5 | Pfrommer & Hickson A&A 565, A102 (2014) | High resolution mesospheric sodium properties for adaptive optics applications | | |
| RD6 | Thomas et al. MNRAS 371, 323 (2006) | Comparison of centroid computation algorithms in a Shack–Hartmann sensor | | |
| RD7 | VLT-TRE-OAA-14400-008 | Task B Report: Calibration strategy of PWM | 3 | 31.08.12 |
| RD8 | VLT-TRE-OAA-14400-0005 | Task D report: Simulations of PWM performance | 2 | 15.03.12 |
| RD9 | Pinna et al. SPIE 8447, 84472B (2012) | First on-sky calibration of an high order adaptive optics system | | |
| RD10 | VLT-TRE-OAA-11250-3642 | Fitting error analysis for the VLT deformable secondary mirror | 3 | 18.07.05 |
| RD11 | VLT-SPE-ESO-11250-4110 | Input parameters for the AO facility simulations: Design of the high order LGS WFS | 4 | 12.03.10 |
| RD12 | VLT-SPE-ESO-10000-3912 | Requirement for Visitor Instruments at VLT UT3 Visitor focus | 1 | 27.09.07 |
| RD13 | VLT-TRE-ESO-11250-4147 | AOF and SPHERE: WaveFront Sensor Camera System Design | 4 | 21.11.12 |
| RD14 | VLT-TRP-ESO-15600-6225 | MACAO Real Time Computer Software Upgrade to VLT2013 And feature enhancement Test Report | 1 | 25.11.14 |
| RD15 | VLT-ICD-ESO-14400-5565 | Interface Control Document between Adaptive Optics Facility and ERIS | 1 | 13.03.12 |
| RD16 | VLT-TRE-OAA-11250-4054 | DSM Optical Test report | 2 | 07/10/13 |

| | | | |
|----------------------------|---|-----------|--------------------------|
| ERIS Consortium | ERIS Documentation Standards | Doc.-Ref. | : VLT-TRE-ERI-14403-3001 |
| | | Issue | : 1.0 |
| | | Date | : 05.12.15 |
| | | Page | : 11 of 136 |

| RD Nr | Doc. Nr | Doc .Title | Issue | Date |
|--------------|--|--|--------------|-------------|
| RD17 | Carillet et al. Applied Optics, Vol. 49, No. 31 (2010) | Low-light-level charge-coupled de- vices for pyramid wavefront sensing on 8 m class telescopes: what actual gain? | | |
| RD18 | Guizard et al. SPIE 4003, 154 (2000) | Performance of active optics at the VLT | | |
| RD19 | VLT-TRE-ESO-14700-2768 | SINFONI image motion budget | 1 | 13.03.02 |
| RD20 | VLT-TRE-ERI-14402-2001 | Sub-System Design and Perfor- mance Report - NIX | 1 | 15.12.15 |

Table 2: Reference documents

| | | | |
|----------------------------|---|------------------------------------|--|
| ERIS Consortium | ERIS Documentation Standards | Doc.-Ref. Issue Date Page | : VLT-TRE-ERI-14403-3001 : 1.0 : 05.12.15 : 12 of 136 |
|----------------------------|---|------------------------------------|--|

2.3 Acronyms

| | |
|-------|--|
| ADC | Atmospheric Dispersion Correction |
| ADI | Angular Differential Imaging |
| AIT | Assembly, Integration and Test |
| AOF | Adaptive Optics Facility |
| CFRM | Cassegrain Flange Reference Mirror |
| CIF | Cassegrain Interface Flange |
| CoG | Center of Gravity |
| CRE | Change Request |
| CU | Calibration Unit |
| DM | Deformable Mirror |
| DSM | Deformable Secondary Mirror |
| ESO | European Southern Observatory |
| EMCCD | ElectroMagnified CCD |
| FEA | Finite Element Analysis |
| FoV | Field of View |
| FWHM | Full Width High Maximum |
| HW | Hardware |
| ICD | Interface Control Document |
| I/F | Interface |
| IM | Interaction Matrix |
| LUT | Look-Up Table |
| MPE | Max-Planck-Institut für extraterrestrische Physik (Garching) |
| NC | Non-conformance |
| NGS | Natural Guide Star |
| PDR | Preliminary Design Review |
| PSD | Power Spectra Density |
| PSM | Pupil Stabilization Mirror |
| PtV | Peak-to-valley |
| PWFS | Pyramid WFS |
| REQ | Requirement |
| RMS | Root Mean Square |
| RTF | Rejection Transfer Function |
| SH | Shack-Hartmann |

| | | | |
|----------------------------|---|------------------------------------|--|
| ERIS Consortium | ERIS Documentation Standards | Doc.-Ref. Issue Date Page | : VLT-TRE-ERI-14403-3001 : 1.0 : 05.12.15 : 13 of 136 |
|----------------------------|---|------------------------------------|--|

| | |
|------|----------------------------|
| SoW | Statement of Work |
| TBD | To Be Defined |
| TBC | To Be Confirmed |
| S/W | Software |
| WCoG | Weighted Center of Gravity |
| WO | Warm Optics |

| | | | |
|---|--|--|--|
| <p style="text-align: center;">ERIS Consortium</p> | <p style="text-align: center;">ERIS Documentation Standards</p> | <p>Doc.-Ref. Issue Date Page</p> | <p>: VLT-TRE-ERI-14403-3001 : 1.0 : 05.12.15 : 14 of 136</p> |
|---|--|--|--|

3 Introduction

ERIS, the Enhanced Resolution Imager and Spectrograph, is a 1-5 μm instrument for the Cassegrain focus of the UT4/VLT telescope equipped with the Adaptive Optics Facility (AOF).

The Top Level Requirements (TLRs) provided in AD1 explicitly require the following sub-systems:

- two **science instruments**, which receive their light via a dichroic beam-splitter located in the AO module.
 - **NIX** provides diffraction limited imaging, sparse aperture masking (SAM) and pupil plane coronagraphy capabilities from 1-5 μm (i.e. J-Mp), either in “standard” observing mode or with “pupil tracking” and “burst” (or “cube”) readout mode. NIX is a cryogenic instrument and it is equipped with a 2048 \times 2048 detector providing a field of view of, at least, 53 \times 53”
 - **SPIFFIER** is an upgraded version of SPIFFI, the 1-2.5 μm integral field unit used on-board SINFONI, that will be modified to be integrated into ERIS. Its observing modes are identical to those of SINFONI, possibly adding a high-resolution mode as a goal.
 - The two science instruments are not required to operate simultaneously.
- the **AO module** has wavefront sensing and real-time computing capabilities. It interfaces to the AOF infrastructure and provides the following observing modes:
 - LGS-mode: a WFS provides high-order AO correction using a LGS on-axis and a second WFS provides low-order correction using a NGS in the patrol field ($R \leq 1'$).
 - NGS-mode: a WFS provides high-order AO correction using a NGS in the patrol field;
- The **Calibration Unit** (CU), which provides facilities to calibrate the scientific instruments (remove instrument signature) and perform troubleshooting and periodic maintenance tests of the AO modules.

The ERIS AO concept maximizes the re-use of existing AOF sub-systems and components as explicitly requested by the TLRs. In particular the AO correction is provided by the AOF Deformable Secondary Mirror (DSM) and the artificial Laser Guide Star (LGS) is generated by the 4LGSF system. Moreover the ERIS AO sub-system uses components from the AOF GLAO systems (GALACSI and GRAAL), namely wavefront sensor camera detectors (CCD220) and a modified version of SPARTA as Real-Time Computer (RTC).

The design of the ERIS AO module is done according to the System Technical Specifications (defined in AD2, derived by the Top-Level Requirements defined in AD1).

In order to provide a global picture of the AO module design, this report describes the following main aspects: correction performance and error budget, opto-mechanical design, control strategy, system alignment and calibrations description. Compliance to the System Technical Specification is also provided.

| | | | |
|-----------------|------------------------------|-----------|--------------------------|
| ERIS Consortium | ERIS Documentation Standards | Doc.-Ref. | : VLT-TRE-ERI-14403-3001 |
| | | Issue | : 1.0 |
| | | Date | : 05.12.15 |
| | | Page | : 15 of 136 |

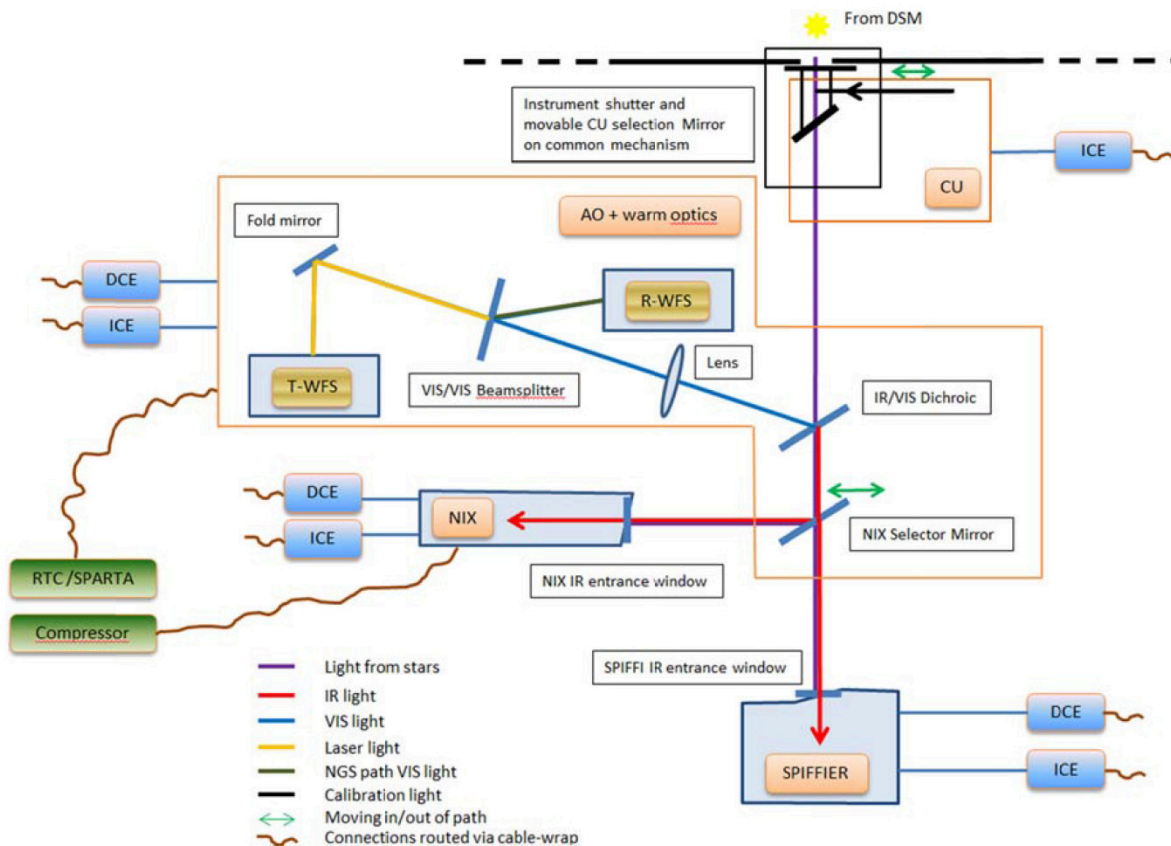


Figure 1 Conceptual scheme of the ERIS instrument

4 Design report of Adaptive Optics and Warm Optics

4.1 The AO+WO general design guidelines

Figure 1 shows the conceptual scheme of the ERIS instrument, including the Adaptive Optics (AO) sub-system (or module). The set of optical components, that relays the telescope optical beam out from the Cassegrain Flange to the science instruments and to the AO WFSs, is defined as Warm Optics (WO) and is considered part of the AO sub-system. The design of the AO module is developed according to the System Technical Specifications (TS) defined in AD2. Hereafter the TS requirements will be referenced using their identification number in the form TS-XXX-XXX-NNN as defined in AD2.

The ERIS instrument is installed at the UT4/VLT Cassegrain Focal Station (TS-ERIS-GEN-003). The beam from the telescope is split by an IR/VIS dichroic, transmitting the IR (1-5 μ m) light to the science instruments (TS-NIX-GEN-030) and the visible (<1 μ m) to the AO WFSs (TS-ERIS-GEN-010, TS-AO-GEN-029). The IR/VIS dichroic is the first component of the WO and has also the practical function of decoupling the alignment of the AO beam from the science beam. The size of the dichroic is constrained by the reflected AO patrol field of 2' diameter (TS-AO-OPS-031).

The two instruments (SPIFFIER and NIX) are simultaneously integrated in ERIS (TS-ERIS-GEN-002). SPIFFIER receives directly the beam from the IR/VIS dichroic (TS-SPIFFI-GEN-060), then feeding NIX requires an insertable mirror, the NIX Selector Mirror, still part of the WO.

| | | | |
|---|--|--|--|
| <p style="text-align: center;">ERIS Consortium</p> | <p style="text-align: center;">ERIS Documentation Standards</p> | <p>Doc.-Ref. Issue Date Page</p> | <p>: VLT-TRE-ERI-14403-3001 : 1.0 : 05.12.15 : 16 of 136</p> |
|---|--|--|--|

The AO module does not need to internally integrate any deformable mirror, interfacing for the WF correction to the external DSM facility (TS-ERIS-GEN-021), part of the AOF.

The requested operational modes for the AO module (TS-ERIS-OPS-005, TS-AO-GEN-028, TS-AO-OPS-031, TS-AO-OPS-032) are:

- **LGS-mode** (TS-AO-OPS-031): closing the High-Order (HO) AO loop with an on-axis LGS generated by any one of the Sodium beacons of the 4LGSF system (part of AOF, TS-ERIS-GEN-021) and simultaneously closing the Low-Order (LO) AO loop with an off-axis (max 1') NGS.
- **NGS-mode** (TS-AO-OPS-032): closing the HO AO loop with an on/off-axis NGS.
- **Seeing enhancer mode** (TS-AO-OPS-033): same as LGS-mode without the NGS loop.
- **Calibration mode**: in stand-alone mode or in combination with the CU. Night-time calibrations foresee the use of the telescope (TS-ERIS-OPS-005).

The LGS-mode requires the implementation of two WFSs, the HO LGS WFS and the LO NGS WFS, requiring the introduction in the WO of a VIS/VIS Beam-Splitter in the optical branch reflected by the IR/VIS Dichroic. It separates the narrow-band Sodium LGS light from the rest of the visible radiation. Hereafter, we will refer to the VIS/VIS beam-splitter also as WFS Dichroic. The baseline of the preliminary design joins the HO NGS functionality in the LO NGS WFS (see Sec. 4.6 resuming a trade-off analysis), separating the functionalities between the two WFSs in a purely on-axis LGS-dedicated WFS and an HO/LO NGS-dedicated WFS with off-axis capabilities. The LGS WFS is implemented in the beam transmitted through the WFS dichroic because the HO LGS loop is less sensitive with respect to the HO NGS loop to the aberrations introduced by the transmission through the WFS dichroic substrate.

In addition to the TSs, the AO WFSs opto-mechanical design has been constrained by the general design choice of using flat (or extremely slow) optics to relay the telescope beam to the AO WFSs to maximize the stability of Non Common Path Aberrations (NCPA). This is an opportunity, to be exploited, provided by telescopes with an adaptive secondary mirror, forcing no powered optics to integrate a DM in the AO module. As a direct consequence of this design choice, the selection of the Natural Guide Star (NGS) in the AO field is not performed by an optical field selector (tip-tilt mirror on a pupil image), but implementing each WFS units as a compact board supported by stages to scan the field (circular, about 32mm radius). The same approach is adopted for tracking the focus in both NGS and LGS WFS case. This design choice is the standard approach for the AO systems developed by INAF-OAA for telescopes with Adaptive Secondary Mirrors and successfully experienced on LBT-FLAO (RD2) and Magellan-AO (RD3).

The mechanical scanning of the WFS board to patrol the field requires inserting a telecentric lens between the IR/VIS and VIS/VIS dichroic to relay the telescope exit pupil (M2) to infinity and keep the chief ray of the beam parallel regardless the off-axis. This is an extremely slow optics having the focal length equal to the distance to M2 (14.9 m).

Figure 2 shows the implementation of the above described rational, where the CU Selector Mirror (CUSM) is also shown. The CUSM is located upstream the IR/VIS Dichroic to allow the CU providing all the calibration needs to all the sub-systems (TS-ERIS-GEN-001). The size of the CUSM is driven by the NIX FoV and contributes to constraint the available space for the WO components. The distance between the Cassegrain Flange and the top of SPIFFIER provides another major space constraint to fit the WO design. That requires to increase the Cassegrain Back Focal Length (BFL) by 250 mm with respect to the nominal VLT one, resulting in a formal Change Request to ESO (CRE ERIS-002) for a BFL=500. Details in AD3.

| | | | |
|-------------------------------|--|--|--|
| <p>ERIS Consortium</p> | <p>ERIS Documentation Standards</p> | <p>Doc.-Ref. : VLT-TRE-ERI-14403-3001 Issue : 1.0 Date : 05.12.15 Page : 17 of 136</p> | |
|-------------------------------|--|--|--|

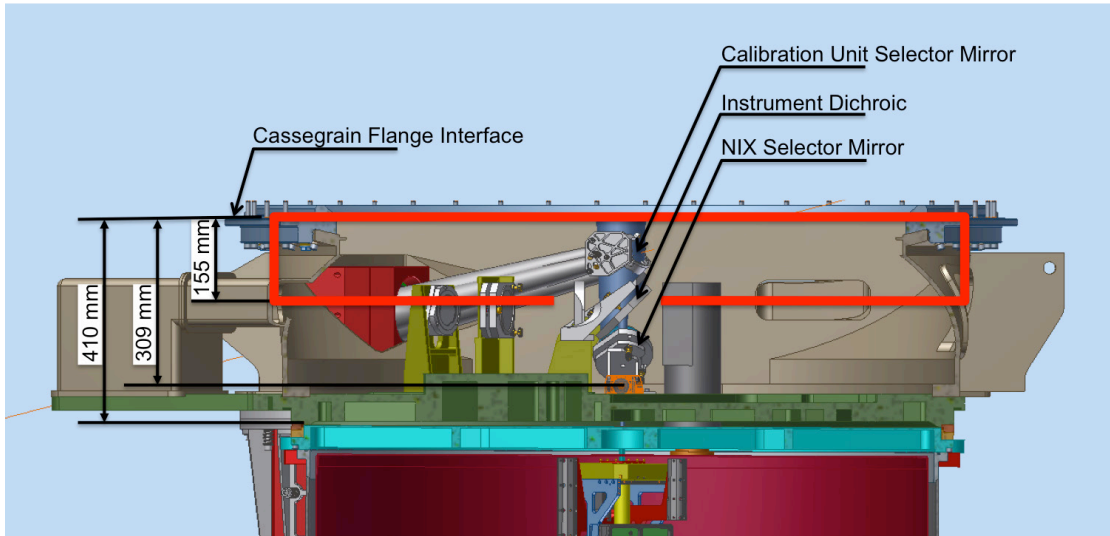


Figure 2 – Implementation WO with CU Selector Mirror. The red box highlights the volume available with the standard VLT BFL when SPIFFI is mounted.

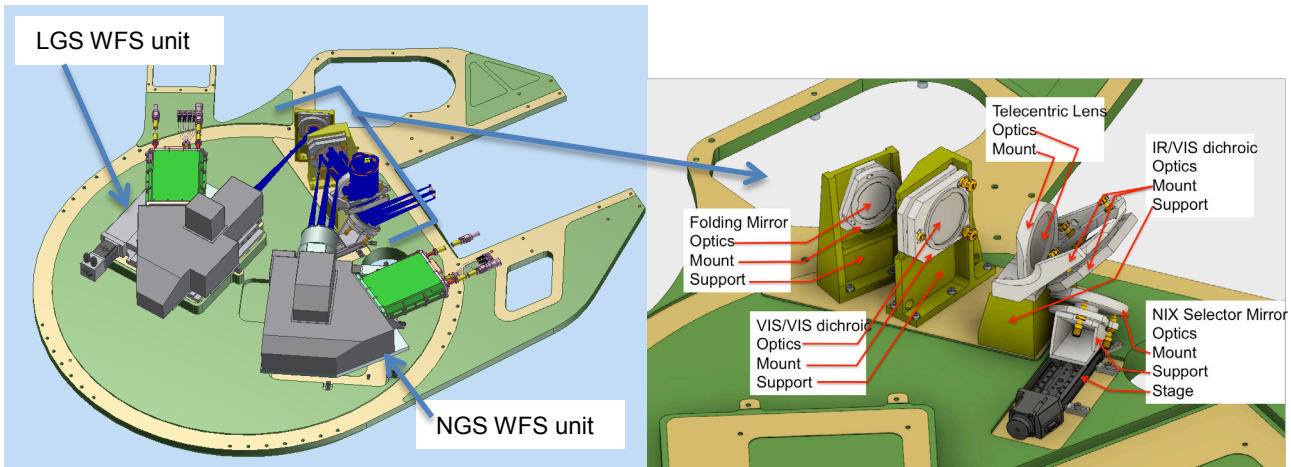


Figure 3 – WO and NGS WFS units mounted on the ERIS Optical Plate. All the other parts are hidden.

| | | |
|--------------------|---------------------------------|--|
| ERIS Consortium | ERIS Documentation Standards | Doc.-Ref. : VLT-TRE-ERI-14403-3001 Issue : 1.0 Date : 05.12.15 Page : 18 of 136 |
|--------------------|---------------------------------|--|

4.2 Constraints on choice on hardware devices for the AO

The following TSs provide constraints on the RTC, WFS camera and Control Electronics hardware to be used for the AO design:

| TS ID | TS description | Implication |
|-----------------|--|---|
| TS-ERIS-INT-024 | I/F to NGC | ERIS WFSs shall use the EMCCD WFS Cameras provided by ESO , including the related ESO's standard New General detector Controller (NGC) . Camera I/F description and specification are in AD4 and AD5, respectively. The ESO WFS Cameras are currently used for SPHERE and GALACSI/GRAAL in AOF. We will also refer to the ESO WFS Camera simply as CCD220. The format is 240x240 mm. The pixel size is 24 µm. For the LGS WFS the camera is provided with an internally integrated 40x40 Shack-Hartman lenslet array allocating 6x6 pixels per subaperture . The lenslets focal length provides 5"x5" FoV per subaperture . For the NGS WFS the camera is provided without lenslet array. |
| TS-ERIS-STD-011 | Detectors control electronics standard | |
| TS-ERIS-STD-014 | Wavefront Sensor Cameras standards | |
| TS-ERIS-INT-027 | I/F to the Real Time Computer | The ERIS real time computer system shall use the SPARTA Platform , provided by ESO |
| TS-ERIS-STD-013 | Real Time computer standards | The SPARTA implementation for ERIS is currently designed as a modified version of the SPARTA implementation for AOF (AD10). |
| TS-ERIS-GEN-021 | Use of the AOF | The baseline HO/LO NGS WFS is Shack-Hartmann , which is the defined standard of the AOF, as stated in an informative note of TS-AO-GEN-028. |
| TS-AO-GEN-028 | AO correction | An upgrade path for a more performing Pyramid Wavefront Sensor (PWFS) is reported in Sec. 6. |
| TS-ERIS-STD-010 | Control Electronics standards | Connection between control units and field devices shall be established with EtherCAT fieldbus (AD12), constraining the choice of available controllers for motion devices. |

In summary:

- WFS units shall use CCD220 cameras provided by ESO and related NGC controller.
- AO shall use the SPARTA Platform as RTC.
- The baseline for all the WFSs is Shack-Hartman type with 40x40 pupil sampling for the High-Order case (i.e. 6x6 CCD220 pixel per subaperture).
- EtherCAT fieldbus is the preferred standard for controlling field devices.

| | | | |
|---|--|--|--|
| <p style="text-align: center;">ERIS Consortium</p> | <p style="text-align: center;">ERIS Documentation Standards</p> | <p>Doc.-Ref. Issue Date Page</p> | <p>: VLT-TRE-ERI-14403-3001 : 1.0 : 05.12.15 : 19 of 136</p> |
|---|--|--|--|

The following two sections report more details on the constrained hardware.

4.2.1 CCD220 Camera

The WFS-Cameras for ERIS will be a copy of the cameras for AOF and SPHERE. They will use the CCD220 chip from e2v. To optimize the performance, the LGS WFS-Camera will use a stand-ard chip, while the NGS WFS-Camera will use a deep-depletion chip to achieve an overall better quantum efficiency and sensitivity. The amplifier, power-supply and temperature controller will be copies or similar units as used with the previous cameras. The two WFS-Cameras in ERIS will be operated in stand-alone mode with each having their dedicated LLCU. However, they share the power supply and the Peltier controller. For AIT purposes and for usage as spare parts, two power supplies and Peltier controllers are foreseen for ERIS.

The main difference with previous systems is that the lenslet array for the NGS WFS-Camera is not glued to the window of the camera allowing the possibility to switch between external LO and HO lenslet arrays.

More details on the design of the cameras, the power supply and Peltier controller can be found in the WFS camera design document (VLT-TRE-ESO-11250-4147). Additional information on the Peltier controller is given its manual (VLT-MAN-ESO-22000-6111). The mechanical drawings and description of the interfaces of the WFS-Camera can be found in the ICD (ESO-262704). The test plan for the WFS-Cameras is given in the MAIV Plan for the AO Module (VLT-PLA-ERI-14403-3901), and in the example test report (VLT-TRE-ESO-22000-5961).

4.2.2 SPARTA

The real-time computer for the AO system of ERIS will be a SPARTA system, as used already in other VLT instruments (in particular SPHERE and GRAAL, GALACSI as part of AOF). The real-time computation boards will be identical to these systems, only the workstation part will be adapted to the current standards at Paranal (e.g. blade-servers).

The FPGA firmware of the SPARTA system for ERIS will be modified to support the needs of ERIS (e.g. loop frequency, vibration reduction, truth sensing) as agreed in the SPARTA user requirement. Similarly, the non-real-time software, which is running on the workstation will be also up-graded to support the calibration and processing needs of ERIS.

The requirements for the SPARTA system for ERIS are given in the technical specifications (AD10: VLT-SPE-ERI-14403-3501). The interfaces with the instrument software are given in the SPARTA ICD (VLT-ICD-ERI-14404-3501, ESO-280345).

| | | | |
|-----------------|------------------------------|------------------------------------|--|
| ERIS Consortium | ERIS Documentation Standards | Doc.-Ref. Issue Date Page | : VLT-TRE-ERI-14403-3001 : 1.0 : 05.12.15 : 20 of 136 |
|-----------------|------------------------------|------------------------------------|--|

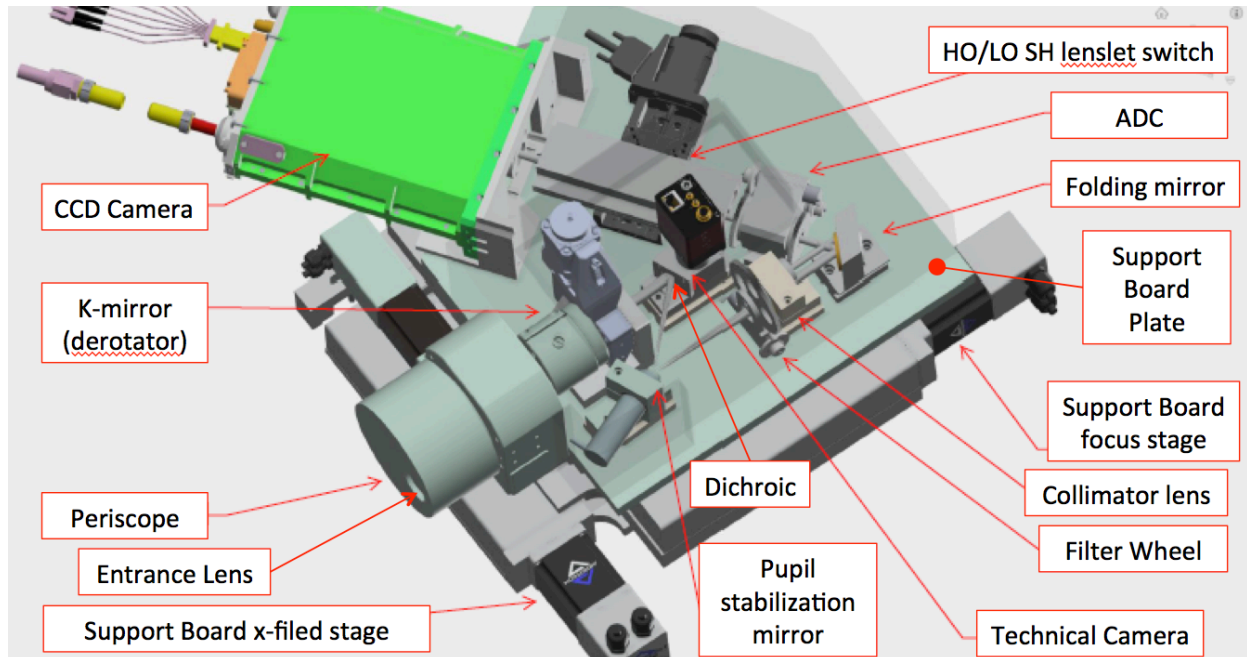


Figure 4 NGS WFS unit. The unit cover is hidden to show the content.

4.3 HO/LO NGS WFS unit

Figure 4 shows the preliminary design of the baseline NGS WFS implementation. It merges the HO and LO NGS WFS functionalities for the NGS and LGS mode, respectively. The HO configuration implements a 40x40 SH, i.e. the highest order WFS compliant to the SPARTA/AOF constraints. The LO configuration is pushed to the NGS faint end implementing a 2x2 SH array for measuring tip-tilt and focus.

The main components and functions are:

1. A dual axis stage supporting the WFS board. One (focus) stage moves in the direction of the input optical axis, the other (X stage) in the orthogonal direction, parallel to the plane of the WFS board. The focus stage is used to compensate for differential focus with respect to SPIFFIER and NIX, including drifts due to differential flexures and thermal expansion. The X stage, together with the periscope (see below), is used to patrol the NGS FoV ($R=1'$ or $R=32\text{mm}$) and to compensate for all the effects that introduce a differential image drift at the WFS focal plane with respect to the instrument one. Part of the travel budget of the stages is used for the initial optical alignment of WO and WFS units to the ERIS reference axis.
1. A board, supported by the dual axis stage, where all the WFS components are mounted. The board can be separated from the stage for maintenance; the alignment is reproduced by a set of mechanical references.
2. A rotary stage supporting the Entrance Lens and a periscope. The axis offset of the periscope is 32 mm, allowing to patrol the full NGS FoV combining the periscope rotation with the X stage motion. The periscope solution has been triggered by the vertical space constraints inside the ERIS central structure that does not allow implementing the vertical (Y) motion with a third stage.
3. The Entrance Lens produces a F/20 beam and relays the input telecentric focal plane to a tip-tilt mirror for pupil stabilization purposes (see below).

| | | | |
|-------------------------------|--|--|--|
| <p>ERIS Consortium</p> | <p>ERIS Documentation Standards</p> | <p>Doc.-Ref. Issue Date Page</p> | <p>: VLT-TRE-ERI-14403-3001 : 1.0 : 05.12.15 : 21 of 136</p> |
|-------------------------------|--|--|--|

4. A Pupil Rotator (named also K-mirror), implemented with an Abbe rotator prism, to de-rotate the actuator pattern of the DSM on the SH lenslet array when ERIS instrument rotator is operating in field tracking mode.
5. A beam splitter dichroic transmitting wavelengths shorter than 600nm to a technical camera that can be also used for NGS acquisition. The wavelengths in the range 600nm-1000nm are reflected toward the pupil stabilization mirror.
6. The pupil stabilization mirror on the F/20 focal plane used for stabilize the lateral decentering of the pupil on the SH lenslet array. The main contributors to the stroke requirement of the mirror are the pupil plane lateral drift due to alignment error between WFS and instrument rotator axis, PSF wobbling during K-mirror rotation due to residual alignment errors, flexures and thermal effects, and possible telescope exit pupil shift. The mirror implements a mask for a 2.5" field stop.
7. A 4-stop filter wheel hosting a beam stop for dark calibration, a pass-all filter for normal operations and two filters to reduce the light level and avoid CCD220 over-illumination with bright NGSs ($1 < mR < 2$ and $1 < mR < 7$ in the HO and LO configurations, TS-AO-PER-014)
8. A collimator lens relaying an image of the pupil on the SH lenslet array.
9. An ADC to compensate for atmospheric dispersion down to $z=70$ deg (TS-ERIS-ENV-010) and avoiding sensitivity reduction due to PSF elongation in the LO configuration.
10. A stage to switch between HO and LO SH lenslet arrays and related optics relaying the SH spots to the WFS Camera CCD. The HO and LO channel are implemented as two parallel barrels with a 40x40 and 2x2 SH arrays. The LO SH sampling (2x2) is the minimal to assure the measurement of both TT and focus with the aim of pushing the LGS-mode performance in the NGS faint-end. The HO SH sampling (40x40) is the maximum available with the constrained hardware (WFS Camera and RTC) to push the performances in the high-contrast NGS bright end.
11. The ESO's WFS Camera (CCD220) having 240x240 format. It is the same camera used for AOF, providing 6x6 pixel per subaperture in the HO configuration ($2.5''/6=0.42''/\text{pix}$). In the LO configuration the 2.5" FoV sampling is currently 8x8 ($0.31''/\text{pix}$), to be optimized in the next design phase.

| | | | |
|------------------------|-------------------------------------|------------------------------------|--|
| ERIS Consortium | ERIS Documentation Standards | Doc.-Ref. Issue Date Page | : VLT-TRE-ERI-14403-3001 : 1.0 : 05.12.15 : 22 of 136 |
|------------------------|-------------------------------------|------------------------------------|--|

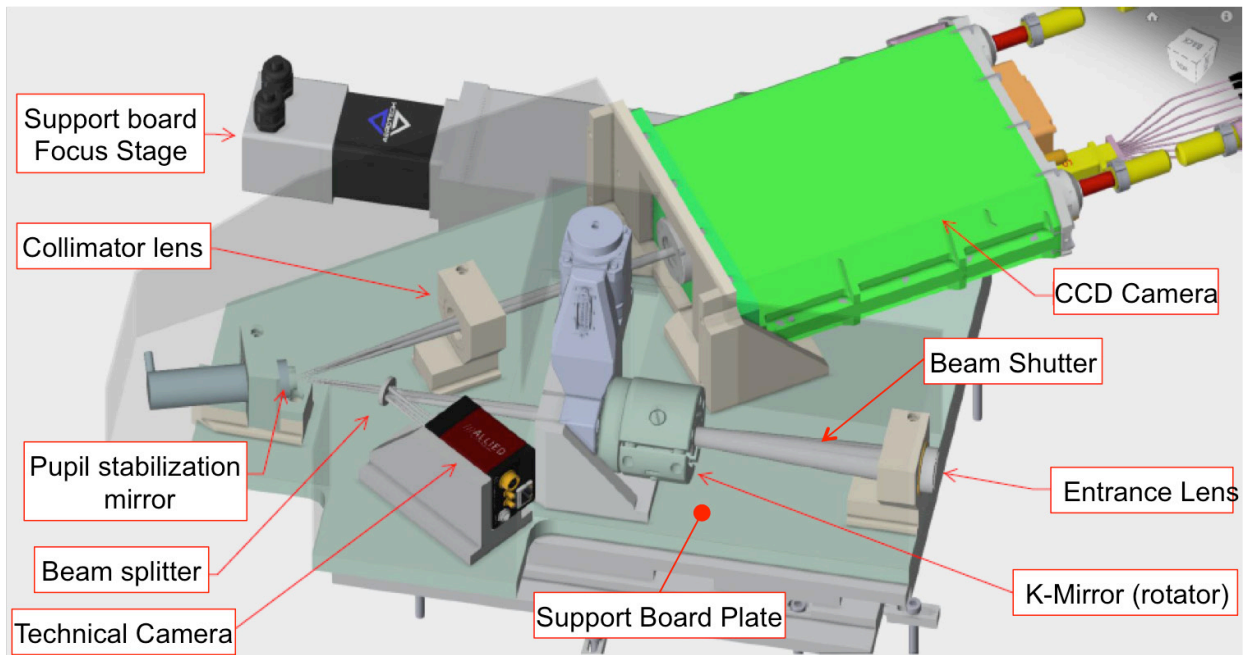


Figure 5 LGS WFS unit. The unit cover is hidden to show the content.

4.4 LGS WFS unit

Figure 5 shows the preliminary design of the baseline LGS WFS implementation. The main components and functions are:

1. A focus stage supporting the WFS board. The stage is used for tracking the best focus of laser beacon when changing its height with elevation and sodium profile evolution. The travel of the stage is also used for compensating differential focus positions with respect to SPIFFIER and NIX, including the focus drifts due to differential flexures and thermal expansion.
2. A board, supported by the focus stage, where all the WFS components are mounted. The board can be separated from the stage for maintenance; the alignment is reproduced by a set of mechanical references.
3. An Entrance Lens producing a F/20 beam and relaying the input telecentric focal plane to a tip-tilt mirror for pupil stabilization purposes.
4. A shutter to stop the incoming beam to protect CCD220 against over-illumination and calibrate dark frames.
5. A Pupil Rotator (the same as NGS WFS) to de-rotate the actuator pattern of the DSM on the SH lenslet array when ERIS instrument rotator is operating in field tracking mode.
6. A beam splitter reflecting 1% of the laser light to feed a technical camera that can be also used for LGS acquisition.
7. The pupil stabilization mirror on the F/20 focal plane used for stabilize the lateral decentering of the pupil on the SH lenslet array. The main contributors to the stroke requirement of the mirror are the pupil plane lateral drift due to alignment error between WFS and instrument rotator axis, K-mirror and flexures. The mirror implements a mask for a 5.0" field stop.
8. A collimator lens relaying an image of the pupil on the SH lenslet array.
9. The ESO's WFS Camera (CCD220) including a 40x40 lenslet array glued on the camera window with the same size of the CCD (5.76 mm). It is the same camera and SH array

| | | | |
|---|--|--|--|
| <p style="text-align: center;">ERIS Consortium</p> | <p style="text-align: center;">ERIS Documentation Standards</p> | <p>Doc.-Ref. Issue Date Page</p> | <p>: VLT-TRE-ERI-14403-3001 : 1.0 : 05.12.15 : 23 of 136</p> |
|---|--|--|--|

used for AOF, providing 6x6 pixel per subaperture with a FoV of 5" to accommodate the elongated spots of the LGS.

The LGS WFS operates only on-axis, therefore it does not require stages to patrol the field. LGS on-axis location and stabilization are devoted to the 4LGSF launcher, providing an internal large stroke field steering mirror for LGS acquisition and drift tracking, and a low stroke fast TT corrector. The interface to the 4LGSF system is described in AD6.

4.5 AO Control

This section describes the control strategy for ERIS AO for the different observing modes. The collection of control loops and LUTs that are required to drive the AO system are listed and analysed to derive the corresponding user requirements for SPARTA (AD10) and the Instrument Software (INS) (AD11). Most of the SPARTA requirements are constrained by the existing architecture and current implementation for AOF.

4.5.1 AO Observing modes

The AO module will support the following observing modes:

1. **SCAO LGS mode** with (any) one of the 4LGSF laser on-axis and one tilt star in the visible ($\lambda < 1\mu\text{m}$) that can be located anywhere in a patrol field with radius 1 arcmin around the LGS. The maximum zenith distance required for this mode is 60 deg.
2. **SCAO NGS mode** in the visible ($\lambda < 1\mu\text{m}$) with reference star that can be located on-axis or up to 1 arcmin off-axis. The maximum zenith distance required for this mode is 70 deg.
3. **Seeing Enhancer mode:** SCAO LGS with (any) one of the 4LGSF laser on-axis and no tilt star. Only the HO are corrected. It is a subset of the SCAO LGS mode, where the Active Optics Guider is used for tracking the Tip-Tilt.

There is another trivial mode, the **Seeing limited mode**, for which the AO is not operating. In this case the AO design has to guarantee that the no-operating state shall not prevent seeing limited observations.

The Active Optics "slow" servo-loop uses the Shack-Hartmann sensor located in the adapter at Cassegrain focus to correct for telescope aberration. This active optics loop, but also the guiding and field stabilization loops, cannot be operated when the "fast" AO servo-loop is running because conflicting with the DSM correction. However, we still keep the Active Optics SH operational, as a slow truth sensor, whose role is to probe the pseudo static biases propagated by the LGS high order loop to the DSM commands. Active Optics guider is instead used in Seeing Enhancer mode when the LO NGS WFS is not used because a suitable tilt star for AO is not available.

| | | | |
|-----------------|------------------------------|------------------------------------|--|
| ERIS Consortium | ERIS Documentation Standards | Doc.-Ref. Issue Date Page | : VLT-TRE-ERI-14403-3001 : 1.0 : 05.12.15 : 24 of 136 |
|-----------------|------------------------------|------------------------------------|--|

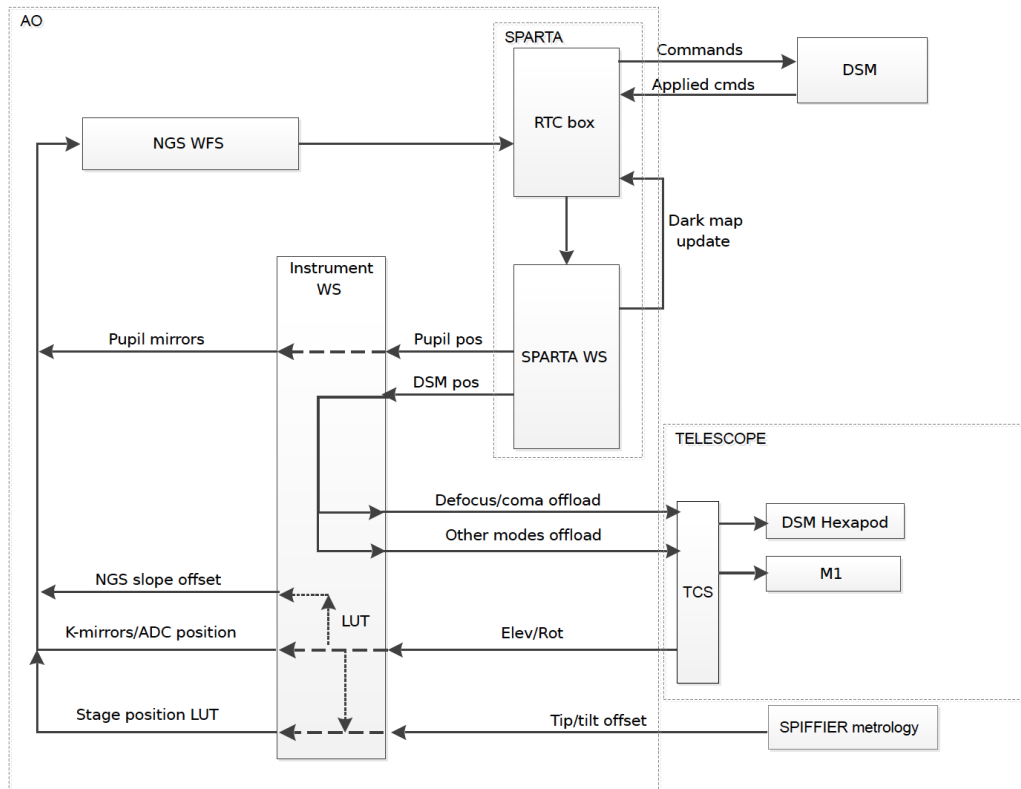


Figure 6 – AO NGS-mode: diagram of control loops and LUTs

4.5.2 Control loops in NGS mode

Figure 6 summarizes the system of control loops and LUTs in NGS mode. Only NGS WFS in HO configuration is operating in this mode.

4.5.2.1 HO AO real-time loop:

This is the real-time AO loop between the NGS WFS signals in HO configuration and the DSM. HO NGS WFS signals include also the tip-tilt. The baseline maximum loop frequency is 1 kHz.

The frames of the NGS WFS Camera are collected by SPARTA and processed to compute the DSM command vector. For a detailed description of the process see AD10 (Sec. 6 and 7).

SPARTA sends the command vector to the DSM and receives back the last successfully applied command to manage the DSM saturation check (AD10 Sec. 7.5). In case of saturation the DSM skips the saturating command and its shape is kept at last valid command.

The current implementation of SPARTA for AOF does not support Vibration Rejection algorithm (RD4), however a user requirement (AD10 [CC-30]) has been set for its implementation in ERIS because vibrations are a critical issue for performance (see Sec. 4.7.12 and 9.1).

4.5.2.2 Dark map update

SPARTA updates periodically the dark maps for the NGS WFS Camera CCD at least every 2 minutes. This update is based on a dark measurement done in a non-illuminated section of the detector. The measurement is done for every amplifier region of the chip. The aim is to avoid differen-

| | | | |
|----------------------------|---|-----------|--------------------------|
| ERIS Consortium | ERIS Documentation Standards | Doc.-Ref. | : VLT-TRE-ERI-14403-3001 |
| | | Issue | : 1.0 |
| | | Date | : 05.12.15 |
| | | Page | : 25 of 136 |

tial offset in slope computation between different amplifier regions in case of differential drift. See [AD10] Sec. 8.5 ([AL-9]).

4.5.2.3 NCPA offset

Non Common Path Aberrations (NCPA) for the NGS WFS are given as a pre-calibrated slope offset vector. The need of a LUT driven by elevation, instrument rotator angle, NGS off-axis and temperatures is still TBD and will be addressed in the next design phase. The INS uploads the slope offset vector to SPARTA (AD11 Sec. 4.9.2 [AOSL-05.2], AD10 7.3.2 [CC-6]), that adds it in the internal slope reference vector to be used as offset for the slope computation.

4.5.2.4 Pupil X-Y stabilization loop

SPARTA measures the X-Y offset of the relative position of the DSM with respect to the HO WFS SH lenslet array. The data are passed to the INS that transforms measured data in offset commands for the Pupil Stabilization mirror on-board the NGS WFS unit. The related SPARTA and INS user requirements are in AD10 Sec. 8.1.4 ([AL-5]) and AD11 Sec. 4.9 ([AOSL-04.1]). The algorithms are the same used for AOF and are described in AD9 Sec. 10.

The relative position of the DSM with respect to the HO WFS is a critical parameter of the AO system, defining the performance and in the worst case the stability of the loop (see Sec. 4.7.14). The loop has to keep the shift error below 0.1 subapertures.

4.5.2.5 Pupil rotator (K-mirror) loop

In order to stabilize the clocking of the DSM actuator pattern with the NGS SH lenslet array, the INS manages the open-loop tracking of the NGS WFS on-board k-mirror to counter-rotate the instrument rotator (See AD11 Sec. 4.1.2).

4.5.2.6 ADC loop

INS manages the tracking of the NGS WFS on-board ADC in open loop driven by current values of elevation (See AD11 Sec. 4.1.2). We remind that the ADC is located after the Pupil Rotator that stabilizes the elevation direction on the ADC.

4.5.2.7 Differential pointing loop

INS manages the open loop tracking of the NGS WFS position in the field using the X-stage and Periscope (See AD11 [AOSL-005.1]) to compensate the differential pointing error between the NGS WFS and the science instrument. It is done summing up the contribution of the following inputs:

- 1) **Differential flexures:** a pre-calibrated LUT applied in open loop compensating for shift of NGS WFS focal plane with respect to the instrument one due to gravity or thermal effects. The LUT inputs are the AltAz telescope coordinates, instrument rotator angle and temperature probes
- 2) **Pupil rotator (k-mirror) wobbling:** a pre-calibrated LUT applied in open loop compensating for the PSF shift during K-mirror rotation due to its residual alignment error and wobbling/eccentricity errors of the rotator stage. The LUT input is the pupil rotator angle.
- 3) **ADC wobbling:** Similar to Pupil rotator for the ADC. The LUT input is the ADC setting.
- 4) **Differential atmospheric refraction loop:** this is an open loop process by which the NGS WFS X-stage and Periscope are moved to compensate for the residual drift between the AO (visible) and the Science (infrared) image; it is driven by the elevation, instrument rotator angle and the atmospheric condition using a LUT.
- 5) **SPIFFIER internal metrology:** the internal metrology of SPIFFIER provides to the INS a measurement of internal flexures. This measurement is converted in field offset.

| | | | |
|---|--|--|--|
| <p style="text-align: center;">ERIS Consortium</p> | <p style="text-align: center;">ERIS Documentation Standards</p> | <p>Doc.-Ref. Issue Date Page</p> | <p>: VLT-TRE-ERI-14403-3001 : 1.0 : 05.12.15 : 26 of 136</p> |
|---|--|--|--|

4.5.2.8 Differential focus loop

INS manages the open loop tracking of the NGS WFS focal position using the focus stage (See AD11 [AOSL-005.1]) to compensate the differential focus error between the NGS WFS and the science instrument. It is done summing up the contribution of the following inputs:

- 1) **Differential flexures:** same as previous section for the focus
- 2) **SPIFFIER internal metrology:** same as previous section for the focus

4.5.2.9 Offloading

In order to prevent the saturation of the DSM actuators when integrating the correction of drifts, the following scheme of offloading is implemented:

- 1) SPARTA averages the position pattern of the DSM actuators (default 30s) and projects them to obtain Focus and Coma components (AD10 Sec. 8.1.2 [AL-2]). The same position pattern is also used for projecting M1 elastic modes (AD10 Sec. 8.1.2 [AL-3]). The data are used to:
 - a. **Focus and Coma Offload:** Tip-tilt, focus and coma are offloaded to M2 Hexapod (AD11 Sec. 4.9.3 [OFFL-001])
 - b. **M1 active optics offload:** M1 elastic modes are offloaded to the M1 active optics (AD11 Sec. 4.9.3 [OFFL-002])

The tip-tilt component of the average DSM position pattern is not considered here because it is managed directly by the M2 LCU with no interaction from the ERIS Instrument.

4.5.3 Control loops in LGS mode

Figure 7 summarizes the system of control loops and LUTs in LGS mode. Both the LGS and NGS WFSs are operating in this mode. The NGS WFS is set in the LO configuration.

4.5.3.1 HO AO real-time loop

This is the real-time AO loop between the LGS WFS signal, the DSM and the laser launcher jitter mirror (part of the 4LGSF system). The baseline maximum loop frequency is currently 1 kHz.

The frames of the NGS WFS Camera are collected by SPARTA and processed to compute the DSM command vector. The DMS command vector does not include the tip-tilt component that is used to produce the laser jitter mirror command to stabilize the LGS image in the WFS. For a detailed description of the process see AD10 (Sec. 6 and 7).

SPARTA sums the DSM command vector to the last available DSM tip-tilt vector from the LO loop and send it to the DSM. SPARTA receives back the last successfully applied command to manage the DSM saturation check (AD10 Sec. 7.5). In case of saturation the DSM skips the saturating command and its shape is kept at last valid command.

4.5.3.2 LO AO real-time loop

This is the real-time AO loop between the NGS WFS in LO configuration and the DSM. The baseline maximum loop frequency is currently 500 Hz for the current SPARTA configuration, requirement definition to push the frequency to 1 kHz are in progress.

The frames of the NGS WFS Camera are collected by SPARTA and processed to compute the DSM Tip-tilt vector implementing the Vibration Rejection Algorithm developed by ESO (AD10 [CC-30]). The focus term is also reconstructed and time averaged by SPARTA for the LGS focus loop (see below). For a detailed description of the process see AD10 (Sec. 6 and 7).

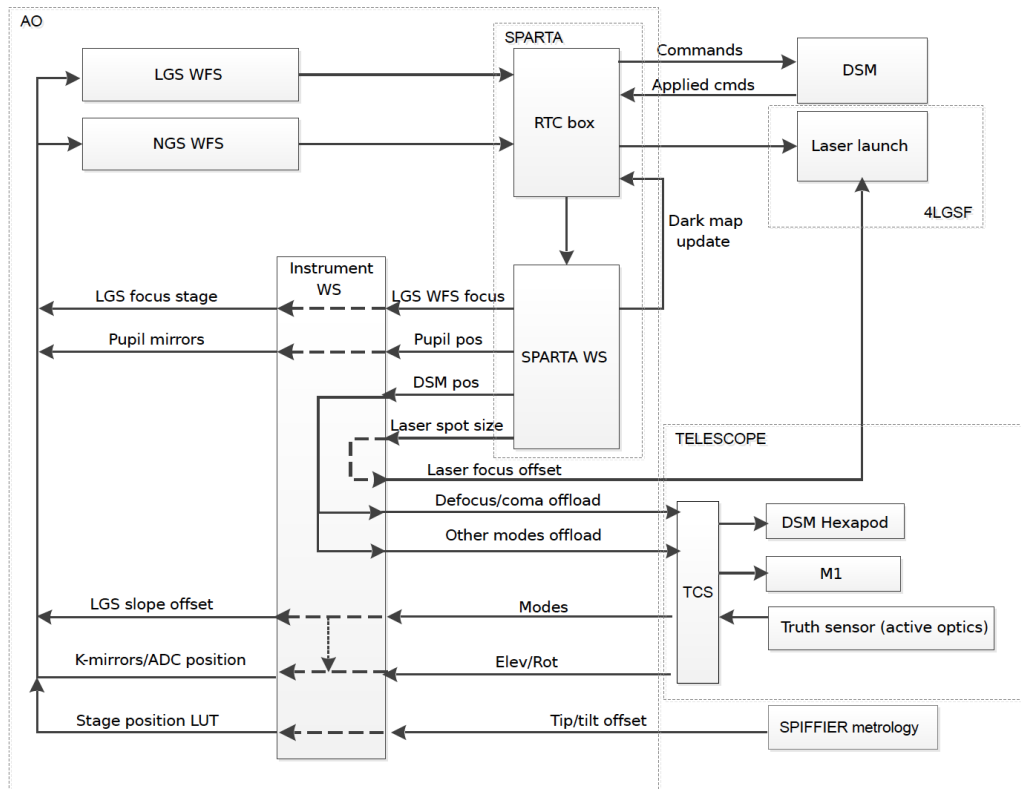


Figure 7 – AO LGS-mode: diagram of control loops and LUTs

In the presented baseline scheme the real-time focus term included in the DSM command vector is the one provided by the LGS WFS. That is not necessary the most performing solution due to the conical anisoplanatism affecting the LGS measurement. However, because the NGS focus is sensitive to source brightness and angular anisoplanatism, both scheme should be available to select the best performing depending on the NGS off-axis and brightness. The trade off-between the baseline “LGS-only real-time focus” and the “LGS/NGS-selectable real-time focus” schemes will be investigated at the beginning of the next design phase.

4.5.3.3 LGS WFS focus loop

The time averaged focus term from the LO NGS WFS is read by INS from SPARTA and, after device transformation, applied to the LGS focus stage to compensate for sodium altitude variation. See [AD10], section 8.2 and [AD11], section 4.9.2.

4.5.3.4 Dark map update

Same as for AO NGS mode, but here dark mask for both LGS and NGS CCDs are provided.

4.5.3.5 Laser focalization offset

In order to minimize the laser spot size, INS shall control the focalization of the laser in the sodium mesospheric layer. When observing with LGS, INS shall translate the average laser sport size into a focus correction to be sent to the LGS launch telescope (through 4LGSF). See AD11 section 4.9.2. [AOSL-002].

| | | | |
|----------------------------|---|-----------|--------------------------|
| ERIS Consortium | ERIS Documentation Standards | Doc.-Ref. | : VLT-TRE-ERI-14403-3001 |
| | | Issue | : 1.0 |
| | | Date | : 05.12.15 |
| | | Page | : 28 of 136 |

To compute the time averaged laser spot size, SPARTA shall acquire in closed loop (HO loop and jitter loop closed) one LGS WFS image averaged over a configurable duration (1 s during the bootstrap of the laser focus and 10 s during operation to update the weighting maps). The spot size is then estimated by the average value of the smaller axis of an elliptical Gaussian fitted to each sub-aperture's spot. See AD10 section 8.3 [AL-6] and [AL-7].

4.5.3.6 Truth sensor loop and NCPA offset

The Active Optics SH is kept operational in LGS mode to be used as a slow truth sensor. Its role is to probe the pseudo static biases propagated by the LGS high order loop to the DSM commands due to variation of the sodium profile (see Sec. 4.7.16). INS receives the input from the truth sensor (Active Optics SH sensor) and produces a truth sensor slope offset vector for the LGS WFS (AD11 4.9.2 [AOSL-003]) filtering out tip-tilt and focus. To be noted that a pre-calibrated NCPA LUT between Active Optics WFS and science instrument has to be also used for a proper computation of the truth sensor slope offset.

The truth sensor slope offset is added to the slope offset from NCPA LUT. The result is sent to SPARTA to add it in the internal slope reference vector used as offset for the slope computation.

4.5.3.7 Pupil X-Y stabilization loop

Same as for AO NGS mode, but here for the LGS WFS and LO NGS WFS.

Because of the large size of sub-apertures in the LO NGS WFS, it is possible that the pupil X-Y stabilization loop is not needed for this WFS, depending on the results of the detailed analysis on pupil stability that will be run in the next design phase.

4.5.3.8 Pupil rotator (K-mirror) loop

Same as for AO NGS mode, but here for both LGS and LO NGS WFS.

Because of the large sensitivity of the PSF wobbling introduced by the pupil rotator when observing close to the Zenith (see image motion budget in Sec. 9.2), the possibility to use a numerical dero-tator in the LO NGS WFS configuration will be considered in the next phase.

4.5.3.9 ADC loop

INS manages the tracking of the LO NGS WFS on-board ADC in open loop driven by current values of elevation (See AD11 Sec. 4.1.2). We remind that the ADC is located after the Pupil Rotator that stabilizes the elevation direction on the ADC.

4.5.3.10 Differential pointing loop

Same as for AO NGS mode, but here for the LO NGS WFS.

4.5.3.11 Differential focus loop

Same as for AO NGS mode for the LO NGS WFS.

4.5.3.12 Offloading

Same as for AO NGS mode, with the addition of the following offload to avoid laser jitter mirror saturation:

- 1) SPARTA averages in time the tip-tilt command of the laser jitter mirror (default 30s) and offloads it to the slow and large stroke steering mirror in the laser launcher.

| | | | |
|----------------------------|---|-----------|--------------------------|
| ERIS Consortium | ERIS Documentation Standards | Doc.-Ref. | : VLT-TRE-ERI-14403-3001 |
| | | Issue | : 1.0 |
| | | Date | : 05.12.15 |
| | | Page | : 29 of 136 |

4.6 HO NGS WFS trade-off

As already described in Sec. 4.1, the LGS-mode requires two separated WFS units: HO LGS WFS and a LO NGS WFS. To fulfil the requirements on the NGS-mode, the HO NGS WFS functionality have to be joined in the LGS or LO NGS WFS. We will refer to the first option as OptLGS and the latter as OptNGS.

The trade-off items between the two solutions are discussed in the following sections.

Performance

The laser spot elongation forces the LGS subaperture FoV to large values to avoid truncation effects (5as in our case). In OptNGS it is possible to optimize independently the FoV HO NGS WFS. Sec. 4.7.7 shows that reducing the FoV from 5as to 2.5as, the HO NGS WFS performance increases of $\Delta SR=5\%$ at short bands (J and H) around $\text{mag}R=13$.

Mechanics

In the OptNGS case the LGS WFS operates only on-axis requiring just a single stage for the LGS focus with a minimal travel of ~ 80 mm (see 4.8.1). No periscope is needed. The NGS WFS requires an increment of complexity due to the presence of the SH switching mechanism to swap between HO and LO configurations. However Sec. 4.9.2.10 shows that the solution found for the HO/LO switch is quite stable (e.g. only 15 on-sky mas from zenith to horizon due to torsional stiffness of the stage).

In the OptLGS case the LGS WFS requires to track both laser and natural star, requiring an increase of the focus stage travel from 80 mm to ~ 150 mm. Moreover a second stage and a periscope is required to patrol the NGS field. That produces an increment of WFS unit mass of at least 15 kg.

SPARTA interface

SPARTA is provided with a switch/transceiver box allowing to route data from multiple detectors. The use of two physical HO WFS is not a problem provided that only one HO WFS a time is served by the RTC.

The main drawback of the OptNGS is the presence of the HO/LO SH switch. However the repeatability of the positioning and the stability of the alignment with the gravity vector change seem to reduce the criticality of the device and the advantage in terms of performance becomes, at the end, the main point moving the trade-off choice on the OptNGS.

4.7 AO system simulation

In order to evaluate the ERIS AO module correction performance and sensitivity to main input parameters an extensive set of numerical simulations have been performed with the INAF AO simulations tool PASSATA, upgraded for the ERIS project to fully handle Shack-Hartmann WFSs both for NGS and LGS sources. The simulations constitute the end-to-end modelling of all the steps involving the AO system main functionality and the input disturbance generation and propagation. The following main steps are:

- Laser/Natural/Calibration Guide Source generation
- Wavefront generation
- Wavefront propagation
- WFS signals computation
- Delta correction vector computation via Control Matrix multiplication
- Correction vector computation via IIR filter

| | | | |
|-----------------|------------------------------|------------------------------------|--|
| ERIS Consortium | ERIS Documentation Standards | Doc.-Ref. Issue Date Page | : VLT-TRE-ERI-14403-3001 : 1.0 : 05.12.15 : 30 of 136 |
|-----------------|------------------------------|------------------------------------|--|

- Correction vector application via the Deformable Mirror
- PSF generation
- Performance estimation

Particular care has been dedicated to select and dimension the most complete set of input conditions allowing to have a representation of the AO module as close as possible to the real physical one.

The selected performance metric is the Strehl ratio at Ks band (2.145 μm) as requested in **TS-ERIS-PER-007** and **TS-ERIS-PER-008**.

4.7.1 Numerical simulation input parameters

The AO system parameters used to evaluate the baseline performance in the simulations are:

- **Telescope:**
 - Diameter of 8.118m with a central obstruction of 15.93% (see Sec. 4.8.1).
- **Observing conditions:**
 - Atmospheric turbulence (see **TS-ERIS-PER-005**): 0.87 arcsec seeing, $L_0=22\text{m}$, 10 turbulent layers and wind profile as reported in Table 3.
 - Sky background: 107 detected photons/arcsec²/m²/s (See Sec. 4.7.1.2).
- **Transmission** (Sec. 4.7.1.2):
 - NGS total transmission (atmosphere, optics and quantum efficiency): 0.344
 - LGS total transmission (optics and quantum efficiency): 0.480
 - Attenuation filters:
 - NGS-mode:
 - $1 \leq R \leq 2$: attenuation factor: 20.
 - $R > 2$: no attenuation filter.
 - LGS-mode (LO NGS WFS):
 - $6 < R \leq 10$: attenuation factor: 20
 - $R > 10$: no attenuation filter
- **Guide Star:**
 - NGS: G2V spectral type star (TS-ERIS-PER-007, TS-ERIS-PER-008)
 - 0-magnitude star brightness: 2.63×10^{10} ph/m²/s (1.05×10^9 ph/sa/s, HO case)
 - LGS Photon Flux at zenith: 7.7×10^6 ph/m²/s (3.08×10^5 ph/sa/s) at the telescope entrance pupil (see **TS-AO-PER-015**).
- **Deformable mirror:**
 - Simulated with the set of 1170 Influence Functions (IFs) obtained from the FEA model of the DSM (RD10).
- **WFS Camera detector:**
 - ESO's CCD220
 - RON values (EMCCD gain = 1): 80 e⁻/pixel/frame (ESO communication)
 - Excess noise simulated using proper statistics of electro-magnifying process (see Sec. 4.7.1.4)
 - Dark current:
 - 3.6 e⁻/pixel/s ($f_s \geq 900$)
 - 1.8 e⁻/pixel/s ($900 > f_s \geq 500$)
 - 1.4 e⁻/pixel/s ($500 > f_s \geq 360$)
 - 1.08 e⁻/pixel/s ($360 > f_s \geq 180$)
 - 0.84 e⁻/pixel/s ($f_s < 180$)
 - EMCCD gains in function of the magnitude is reported in 4.7.1.4.
- **LGS WFS:**

| | | | |
|-----------------|------------------------------|------------------------------------|--|
| ERIS Consortium | ERIS Documentation Standards | Doc.-Ref. Issue Date Page | : VLT-TRE-ERI-14403-3001 : 1.0 : 05.12.15 : 31 of 136 |
|-----------------|------------------------------|------------------------------------|--|

- 40x40 sub-aperture Shack Hartmann
- Sub-aperture FoV: 5.0x5.0 arcsec
- Central Wavelength: $\lambda_{wfs}=589\text{nm}$
- Pixel per sub-aperture: 6x6
- **HO NGS WFS:**
 - 40x40 sub-aperture Shack Hartmann
 - Sub-aperture FoV: 2.5x2.5 arcsec
 - Central Wavelength: $\lambda_{wfs}=768\text{nm}$
 - Bandwidth: 600 – 1000nm
 - Pixel per sub-aperture: 6x6
- **LO NGS WFS:**
 - 2x2 sub-aperture Shack Hartmann
 - Sub-aperture FoV: 2.5x2.5 arcsec
 - Central Wavelength: $\lambda_{wfs}=768\text{nm}$
 - Bandwidth: 600 – 1000nm
 - Pixel per sub-aperture: 8x8
- **AO RTC (SPARTA):**
 - Max frame frequency:
 - HO channel: 1 kHz
 - LO channel: 500 Hz
 - Slope computer algorithms (all available on SPARTA):
 - Center of Gravity (CoG) with pixel threshold = $3\sigma_R$ (where: σ_R read-out noise)
 - Quad Cell (QC) with threshold = $3\sigma_R$
 - Weighted Centre of Gravity (WCoG)
 - Nominal value of the average background is removed from the CCD frames before slope computation;
 - Modal control with static modal gains:
 - Modal base made of Zernike Tip, Tilt, Focus and higher order 1124 Karhunen–Loève modes fitted on the DSM influence functions.
 - Number of controlled modes is optimized in the simulation.
 - Temporal controller:
 - Simple integrator (gain optimized in the simulation)
 - Total time delay: As described in 4.7.1.3.
- **LGS specific information:**
 - LGS spot FWHM: 1.2 on-sky arcsec including up propagation (RD11).
 - Laser launcher position: see Figure 10 (AD6).
 - Sodium profile: “Single Peak” sodium profile from RD5 shown in Figure 11.

4.7.1.1 Atmosphere

- Reference: TS-ERIS-PER-005 in Technical requirement document and related AD VLT-SPE-ESO-11250-4110 (RD11) in it
 - $r_0=0.119\text{m}$ at 500 nm (seeing=0.87arcsec) along the line of sight at 30° off-zenith (airmass $am = 1.16$)
 - Outer scale $L_0=22\text{m}$
 - 10 turbulent layers and wind profile as reported in Table 3.
 - Note 1: "Height from ground" is the distance of the layer from the ground measured on Zenith direction
 - Note 2: "Distance from EnP" is the distance of the layer from the Entrance Pupil position in the line of sight. It is computed as: $am(h - 12) + 90$, with

| | | |
|----------------------------|---|--|
| ERIS Consortium | ERIS Documentation Standards | Doc.-Ref. : VLT-TRE-ERI-14403-3001 Issue : 1.0 Date : 05.12.15 Page : 32 of 136 |
|----------------------------|---|--|

$am=1.16$ ($z=30^\circ$). 12m is the height of M1 wrt ground and 90m is the distance of EnP below M1 (see Sec. 4.8.1).

Table 3. Turbulence profile. "Height from ground" is the distance of the layer from the ground measured on Zenith direction. "Distance from EnP" is the distance of the layer from the Entrance Pupil position in the line of sight.

| Layer number | 1 | 2 | 3 | 4 | 5 | 6 | 7 | 8 | 9 | 10 |
|--------------------------|------|------|------|------|------|------|------|------|-------|-------|
| Height from ground [m] | 30 | 140 | 281 | 562 | 1125 | 2250 | 4500 | 7750 | 11000 | 14000 |
| Distance from EnP [m] | 111 | 238 | 402 | 728 | 1381 | 2686 | 5296 | 9066 | 12836 | 16316 |
| Cn ² fraction | 0.59 | 0.02 | 0.04 | 0.06 | 0.01 | 0.05 | 0.09 | 0.04 | 0.05 | 0.05 |
| Speed [m/s] | 6.6 | 5.9 | 5.1 | 4.5 | 5.1 | 8.3 | 16.3 | 30.2 | 34.3 | 17.5 |

4.7.1.2 Emission and transmission

The emission and transmission parameters are computed for the NGS-mode between 600 nm and 1000 nm and are listed below:

- 0-magnitude emission:

$$e_0 = \int_{600}^{1000} e_s(w)dw$$

- Overall transmission:

$$T = \frac{\int_{600}^{1000} e_s(w)t_a(w)t_m(w)t_o(w)qe(w)dw}{\int_{600}^{1000} e_s(w)dw}$$

- WFS central wavelength:

$$\lambda_{wfs} = \frac{\int_{600}^{1000} t_a(w)t_m(w)t_o(w)qe(w)wdw}{\int_{600}^{1000} t_a(w)t_m(w)t_o(w)qe(w)dw}$$

- Detected sky background flux:

$$e_{b0} = \int_{600}^{1000} t_m(w)t_o(w)qe(w)e_b(w)dw$$

where:

- e_s is the NGS spectral emission (G2V star – see left part of Figure 8).
- t_a is the atmospheric transmission (see Figure 9). The value has been computed with **SKYCALC**¹. The settings used are: target at Zenithal distance $z=30\text{deg}$ (airmass, $am=1.16$), average profile on an entire night over an entire year cycle, Precipitable Water Vapor (PWV) average over a year, Monthly averaged solar flux 130 s.f.u.
- e_b is the atmospheric spectral emission (see right part of Figure 8). The value has been computed with **SKYCALC**. The settings used are: $z=30\text{deg}$, $z_{\text{moon}}=90\text{deg}$, distance target-moon $\gamma=60\text{deg}$, distance sun-moon= 90deg (~ 7 days after/before new moon); 1nm sampling bin from 300nm to 10um; all the other parameters as default.

¹ SkyCalc Sky Model Calculator issue 1:

<http://www.eso.org/observing/etc/bin/gen/form?INS.MODE=swspectr+INS.NAME=SKYCALC>

- t_m is the M1 + M2 transmission (see Figure 9 and RD12).
- t_o is the warm optics + WFS optics (see Table 38, Figure 9 and RD1).
- qe is the WFS detector CCD220 (see Figure 9 and RD13).

Table 4 shows the detected flux from the NGS for different magnitude computed taking into account t and e_o .

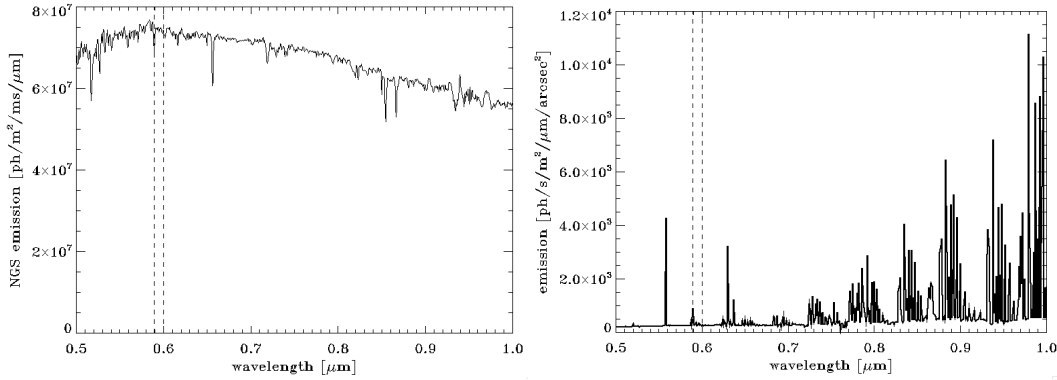


Figure 8. – left: G2V star spectrum, right: background. Dashed lines are LGS central wavelength @589nm and NGS lower limit wavelength @600nm.

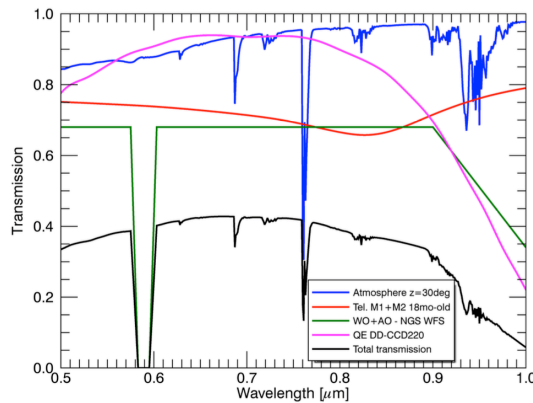


Figure 9. Atmospheric and NGS optics transmission, mirrors reflectance and detector quantum efficiency.

Table 4. Detected NGS flux per second on the whole telescope and on a 20x20cm sub-aperture for different magnitudes.

| R | 8 | 12 | 15 | 19 |
|-------------------------|-------------------|-------------------|-------------------|-------------------|
| Detected flux [ph/s] | $2.88 \cdot 10^8$ | $7.22 \cdot 10^6$ | $4.58 \cdot 10^5$ | $1.15 \cdot 10^4$ |
| Detected flux [ph/s/sa] | $2.28 \cdot 10^5$ | $5.74 \cdot 10^3$ | $3.61 \cdot 10^2$ | 9.08 |

4.7.1.3 Total loop delay

At the fastest rate for the HO WFSs (1 kHz), the time delay in SPARTA from starting the reading of the CCD220 and sending the last element of the command vector to the DSM is 1.2 ms (AD10). Considering the effective extra delay introduced by integration time + command hold (1 loop step) and half of the 0.8ms DSM settling time, the total time delay of the control loop is shown in Table 5. The delay is rounded to the upper integer for conservative performance results.

Table 5. Total number of frames delay taken into account in the simulations.

| Sampling freq. [Hz] | Total delay [frames] |
|---------------------|----------------------|
| $f_s < 334$ | 1 |
| $333 < f_s < 667$ | 2 |
| $667 < f_s < 1000$ | 3 |

4.7.1.4 EMCCD gain

The EMCCD gain is chosen to avoid that the upper limit of 10000ADU is reached, because over this value the EMCCD could be damaged. We use 5σ value to get a very high probability to stay below the upper limit. Note that system gain is $16e^-/ADU$. The gain with the average flux and the 5σ value is shown in Table 6 for LGS-mode and in Table 7 for NGS-mode.

Table 6. EM gain used in function of the R-magnitude on a SHS 2x2 at 500Hz.

| R-magnitude | 11 | 12 | 13 | 14 | 15 | ≥ 16 |
|-------------------------|-------|------|------|------|------|-------------|
| flux [ph/sa/ms] | 11900 | 4720 | 1880 | 748 | 298 | ≤ 120 |
| signal@ 5σ [ADU] | 7890 | 8130 | 6830 | 5880 | 7870 | ≤ 4890 |
| EM gain | 10 | 25 | 50 | 100 | 300 | 400 |

Table 7. EM gain used in function of the R-magnitude on a SHS 40x40 at 1kHz.

| R-magnitude | 3 | 4 | 5 | 6 | 7 | ≥ 8 |
|-------------------------|-------|------|------|------|------|-------------|
| flux [ph/sa/ms] | 23500 | 9350 | 3720 | 1480 | 590 | ≤ 235 |
| signal@ 5σ [ADU] | 7680 | 6270 | 6490 | 5480 | 9520 | ≤ 8580 |
| EM gain | 5 | 10 | 25 | 50 | 200 | 400 |

4.7.1.5 Laser Guide Star specific parameters

The geometry of the 4LGSF launchers with respect to the primary mirror is shown in Figure 10, in particular the launcher labelled as Laser1 is used in the simulations.

The sodium profile data are retrieved from RD5, reporting classes of typical sodium profiles. The profile used for the performance estimation is the one shown in Figure 11, corresponding to the "Single Peak" shape closest to standard Gaussian. The return flux is re-normalized to the value 7.7×10^6 ph/m²/s at the telescope entrance pupil as requested in TS-AO-PER-015.

| | | | |
|-------------------------------|--|--|--|
| <p>ERIS Consortium</p> | <p>ERIS Documentation Standards</p> | <p>Doc.-Ref. Issue Date Page</p> | <p>: VLT-TRE-ERI-14403-3001 : 1.0 : 05.12.15 : 35 of 136</p> |
|-------------------------------|--|--|--|

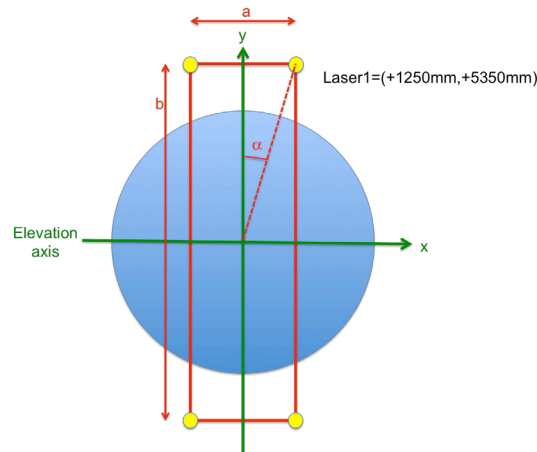


Figure 10. Primary mirror and launchers geometry. $a=2500\text{mm}$, $b=10700\text{mm}$ and $\alpha =13.15\text{degree}$. (RD15)

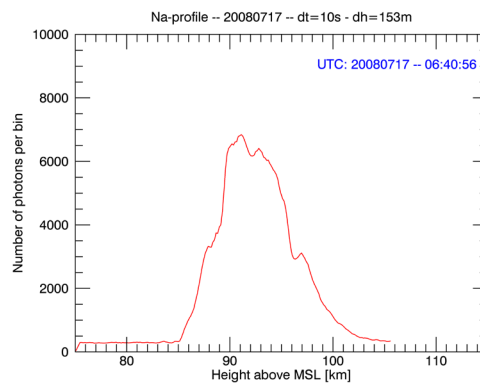


Figure 11. “Single Peak” sodium profile (UTC 20080717 – 06:40:56 from RD5).

4.7.2 AO system calibration simulation

The calibration is made without turbulence disturbance and without detector noise and it is used to estimate:

- Valid SHS sub-apertures.
- Reference slope vector.
- Interaction Matrix (IM).

The effect of the on-sky calibration of the interaction matrix will be evaluated with E2E simulations in the next design phase.

4.7.3 LGS spot pattern modelling

PASSATA computes the LGS spots for each sub-aperture as a convolution of the PSF of a point source affected by the residual turbulence in conic propagation and the extended LGS spots given by the laser geometry. The LGS spots are modelled taking into account a Gaussian shape broad-

| | | | |
|---|--|--|--|
| <p style="text-align: center;">ERIS Consortium</p> | <p style="text-align: center;">ERIS Documentation Standards</p> | <p>Doc.-Ref. Issue Date Page</p> | <p>: VLT-TRE-ERI-14403-3001 : 1.0 : 05.12.15 : 36 of 136</p> |
|---|--|--|--|

ened by upward propagation (FWHM=1.2", RD11), the geometry of the SH WFS, of the launcher and of the sodium profile. An example of LGS spot pattern is shown in Figure 12.

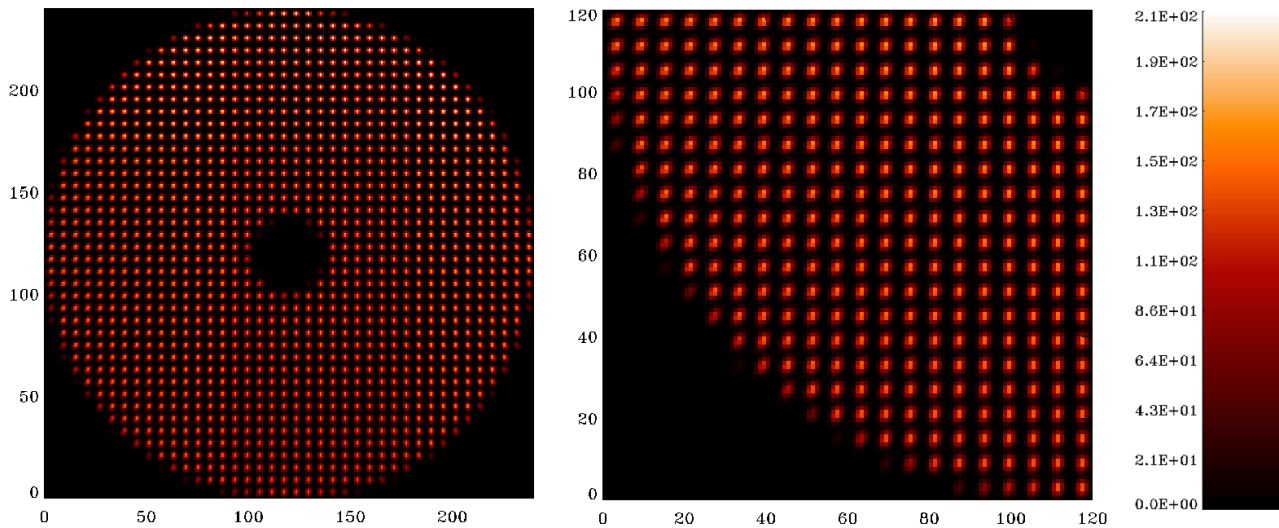


Figure 12 LGS WFS frame showing laser spots (no turbulence): left - full frame, right – zoom on the low left quadrant. Launcher is located in top-right, on bottom-left spot elongation is visible.

4.7.4 EMCCD modelling

The EMCCD is modelled in PASSATA by the following sequence of steps:

- Dark current is added to the input star flux.
- Poisson distribution is applied to the CCD frame.
- A gamma distribution is applied to the CCD frame to simulate the electron-multiplication effect.
- The read-out noise is applied as a Gaussian distribution.
- The CCD frame is converted to ADU.
- Finally, the black level is subtracted from the CCD frame.

The described sequence is represented in the sketch of Figure 13. It can be noted that the electron-multiplication noise effect is not simulated in PASSATA with the simplified $\sqrt{2}$ excess Poisson noise, but using the correct Gamma distribution noise, giving more accurate results at low level rate of photons (RD17).

4.7.5 AO loop performance optimization

The performance optimization is done exploring the free parameters for each NGS magnitude considered.

In the NGS-mode the optimized parameters are:

- CCD frame rate.
- Number of corrected modes.
- Integrator gain.
- Radius of the WCoG mask (when this slope algorithm is used).

In the LGS-mode the optimization of the HO LGS loop parameters is made once because the LGS flux does not change in the conditions evaluated in this work (TS-AO-PER-015). Instead, for each

| | | | |
|-----------------|------------------------------|------------------------------------|--|
| ERIS Consortium | ERIS Documentation Standards | Doc.-Ref. Issue Date Page | : VLT-TRE-ERI-14403-3001 : 1.0 : 05.12.15 : 37 of 136 |
|-----------------|------------------------------|------------------------------------|--|

NGS magnitude, we perform an optimization of the LO NGS loop parameters. The optimized parameters are:

- LGS WFS:
 - CCD frame rate.
 - Number of corrected modes.
 - Integrator gain.
- NGS WFS:
 - CCD frame rate.
 - Integrator gain.
 - Radius of the WCoG mask (when this slope algorithm is used).

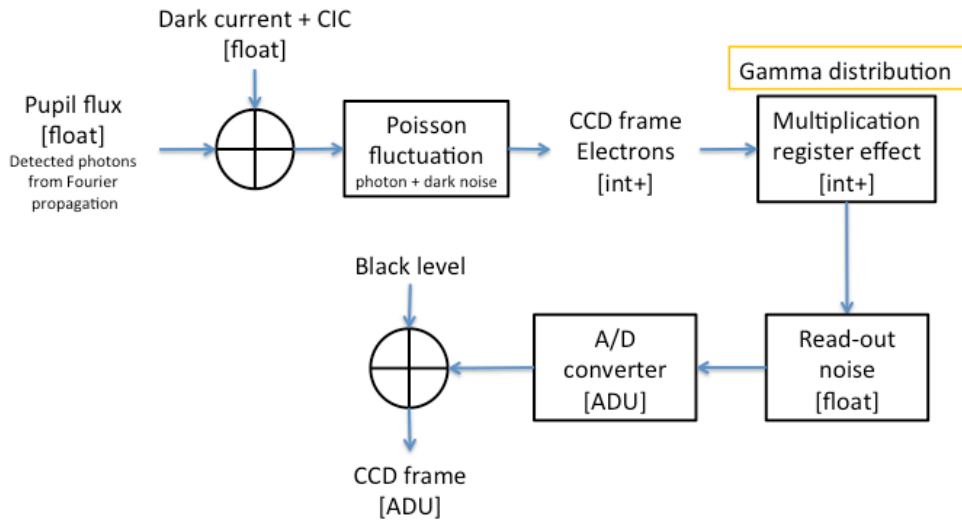


Figure 13. Schematic representation of the CCD model implemented in the E2E simulator.

4.7.6 Selection of Centroid algorithm

We have evaluated three centroid algorithms implemented in SPARTA (AD10):

- Centre of Gravity (CoG) with threshold, t .

$$i' = \begin{cases} I - t, & I - t > 0 \\ 0, & I - t \leq 0 \end{cases}, \quad s = \frac{\sum WI'}{I}$$

where s is the slope, I is the intensity measured by the detector and W is the distance from the centre of the sub-aperture in pixel.

- Quad Cell (QC).

$$s = \frac{\sum W_{QC} I}{I}$$

where W_{QC} is 1 if $W > 0$ and -1 if $W < 0$.

- Weighted Centre of Gravity (WCoG). Simplified weighting function: circular window, F_w , of radius r with value equal to 1 inside the window and 0 outside.

$$s = \frac{\sum WIF_w}{\sum IF_w}$$

- The threshold considered is $t = 3\sigma_R$, where σ_R is the RON of the detector. Before applying the threshold, the nominal average value of sky background flux per pixel is removed.

We chose the reference magnitudes reported in the Technical Specifications to compare the algorithms: 8 and 12 for NGS-mode and 12 and 19 for LGS-mode. WCoG shows the best performance as can be seen in Table 10, in agreement with the results in RD6. The optimized parameters are shown in Table 8 and Table 9 for NGS-mode and LGS-mode respectively. The last rows of the tables report the effective (i.e. cumulated on non-masked pixels of the subaperture) rms values of read-out (σ_R), dark (σ_D) and background (σ_B) noise.

The WCoG has been the last algorithm we implemented in PASSATA and, because time constraints, was not possible to produce performance results for a complete set of NGS magnitudes for the simulations in the NGS mode. For this mode only, the performance summary, reported in the Sec. 4.7.9, is related to the QC results as close, but conservative, approximation of the WCoG case, as shown in Table 10.

Table 8. Summary of the optimized parameters and of the fluxes for NGS-mode WFS with different centroid algorithms.

| R | | 8 | | | 12 | | |
|---------------------------|--|----------|------|------|-----------|------|------|
| Centroid algorithm | | CoG | QC | WCoG | CoG | QC | WCoG |
| NGS WFS | Fr. [Hz] | 1000 | 1000 | 1000 | 1000 | 1000 | 1000 |
| | int. gain | 0.35 | 0.35 | 0.35 | 0.15 | 0.20 | 0.55 |
| | No. modes | 945 | 945 | 945 | 860 | 702 | 860 |
| | Mask radius [pix] | - | - | 3 | - | - | 2 |
| | Flux [ph/sa/frame] | 235 | 235 | 235 | 5.9 | 5.9 | 5.9 |
| | σ_R [e-/sa/frame] | 1.2 | 1.2 | 1.1 | 1.2 | 1.2 | 0.7 |
| | σ_D [e-/sa/frame] | 0.36 | 0.36 | 0.32 | 0.36 | 0.36 | 0.21 |
| | σ_B [e-/sa/frame] | 0.17 | 0.17 | 0.15 | 0.17 | 0.17 | 0.10 |

Table 9. Summary of the optimized parameters and of the fluxes of the LGS-mode WFSs with different centroid algorithms.

| R | | 12 | | | 19 | | |
|--------------------|--------------------------|------|------|------|------|------|------|
| Centroid algorithm | | CoG | QC | WCoG | CoG | QC | WCoG |
| LGS WFS | Fr. [Hz] | 1000 | 1000 | 1000 | 1000 | 1000 | 1000 |
| | No. modes | 945 | 945 | 945 | 945 | 945 | 945 |
| | int. gain | 0.3 | 0.3 | 0.3 | 0.3 | 0.3 | 0.3 |
| NGS WFS | Fr. [Hz] | 500 | 500 | 500 | 200 | 333 | 500 |
| | int. gain | 0.45 | 0.55 | 0.45 | 0.30 | 0.35 | 0.55 |
| | Mask radius [pix] | - | - | 4 | - | - | 2 |
| | Flux [ph/sa/frame] | 3610 | 3610 | 3610 | 14.3 | 11.5 | 5.7 |
| | σ_R [e-/sa/frame] | 25.6 | 25.6 | 23.1 | 1.6 | 1.6 | 0.7 |
| | σ_D [e-/sa/frame] | 0.48 | 0.48 | 0.43 | 0.59 | 0.52 | 0.21 |
| | σ_B [e-/sa/frame] | 4.6 | 4.6 | 4.2 | 7.3 | 6.5 | 2.4 |

Table 10. Summary of the performance of the centroid algorithms

| R | | 8 | 12 | 12 | 19 |
|--------|------|----------|------|----------|------|
| Mode | | NGS mode | | LGS mode | |
| SR (K) | CoG | 91.0 | 78.5 | 72.6 | 26.2 |
| | QC | 91.9 | 80.2 | 72.6 | 52.3 |
| | WCoG | 91.8 | 81.2 | 72.6 | 53.6 |

4.7.7 Selection of sub-aperture FoV in NGS mode

We consider in the trade-off between two cases of sub-aperture FoV for the HO NGS WFS:

- **5.0"**: the same implemented in the LGS WFS, corresponding to a pixel scale of 0.83"/pix and a sub-aperture diffraction limited PSF sampled with 0.85pix/FWHM
- **2.5"**: corresponding to a pixel scale of 0.42"/pix and 1.70pix/FWHM

We remind that the 40x40 HO WFS configuration uses 6x6 pix per sub-aperture with the CCD220.

The performances are evaluated for the NGS Rmag=12, 13 and 14 using the WCoG algorithm, in proximity of the transition between NGS and LGS mode, where the difference is more sensitive. The SR results are reported in Table 11, showing a better SR in the 2.5" case of about $\Delta SR=4-5\%$ at the short-wavelengths (J and H). The optimized parameters are shown in Table 12.

Table 11. SR comparison of NGS mode with subaperture FoV 2.5" and 5.0" FoV and optimized WCoG.

| FoV ["] | Magnitude | J | H | Ks | K | L' | M' |
|---------|-----------|------|------|------|------|------|------|
| 2.5 | 12 | 53.4 | 69.3 | 80.3 | 81.2 | 93.3 | 95.7 |
| 5.0 | | 49.4 | 66.1 | 78.0 | 78.9 | 92.4 | 95.1 |
| 2.5 | 13 | 40.7 | 59.0 | 72.9 | 74.0 | 90.4 | 93.8 |
| 5.0 | | 35.6 | 54.4 | 69.3 | 70.5 | 88.9 | 92.8 |
| 2.5 | 14 | 24.6 | 43.7 | 60.7 | 62.2 | 85.2 | 90.4 |
| 5.0 | | 21.4 | 40.0 | 57.5 | 59.1 | 83.7 | 89.3 |

Table 12. Summary of the optimized parameters and of the fluxes for NGS-mode WFS with subaperture FoV 2.5" and 5.0" FoV and optimized WCoG.

| R | | 12 | | 13 | | 14 | |
|--------------|--|------|------|------|------|------|------|
| FoV [arcsec] | | 2.5 | 5.0 | 2.5 | 5.0 | 2.5 | 5.0 |
| NGS WFS | Fr. [Hz] | 1000 | 1000 | 1000 | 1000 | 600 | 600 |
| | int. gain | 0.20 | 0.25 | 0.25 | 0.30 | 0.40 | 0.50 |
| | No. modes | 860 | 702 | 702 | 560 | 495 | 377 |
| | Optimized radius [pix] of WCoG mask | 2 | 1 | 2 | 1 | 2 | 1 |
| | Flux [ph/sa/frame] | 3.5 | 3.5 | 1.4 | 1.4 | 0.9 | 0.9 |
| | σ_R [e-/sa/frame] | 0.8 | 0.4 | 0.8 | 0.4 | 0.8 | 0.4 |
| | σ_D [e-/sa/frame] | 0.21 | 0.12 | 0.21 | 0.12 | 0.19 | 0.11 |
| | σ_B [e-/sa/frame] | 0.10 | 0.11 | 0.10 | 0.11 | 0.12 | 0.14 |

In order to validate the simulation results we use a different code to estimate the WCoG measurement error versus FoV. The code implements a Montecarlo simulation of a single subaperture of the NGS HO SH WFS. Results are presented in Figure 14 (left) for magnitudes 12, 13 and 3 as "infinite" SNR reference case. The result confirms that the 2.5" FoV has lower noise propagation than the 5.0" FoV.

The presented results are also supported by the behaviour described in RD6 about the photon noise propagation in slope estimation. The right side of Figure 14 (from the paper) shows an evident change of photon noise propagation regime, rapidly increasing when the FWHM of the subaperture PSF is under sampled.

It has to be noted that the mask size optimization of the WCoG algorithm provided an effective 2x2 pixel mask in the 5.0" case and 4x4 pixel in the 2.5" case. The 2x2 case, working effectively as a QC, is also more critical in terms of linearity and corresponding handling of NCPA.

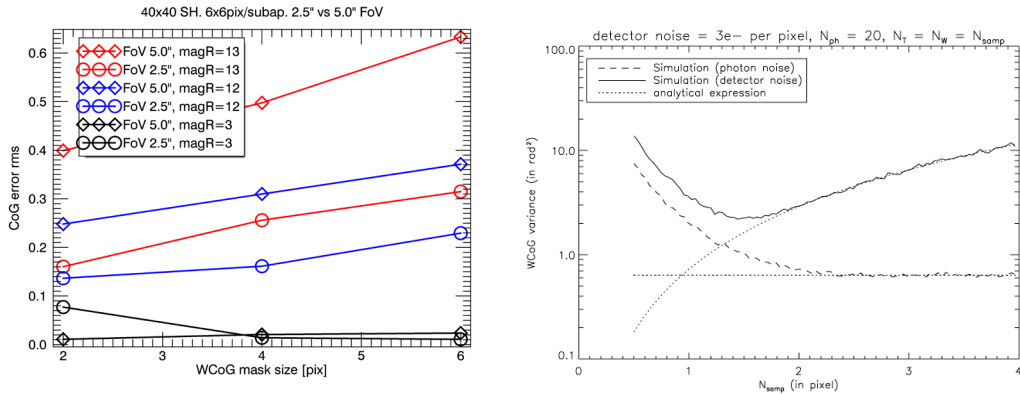


Figure 14. Left: WCoG error rms vs mask size for magnitudes 13, 12 and 3. Right: (figure from RD6) error variance of WCoG as a function of the subaperture PSF FWHM sampling N_{samp} for photon noise (dashed line). $N_{\text{ph}} = 20\text{ph/sa/frame}$ and WCoG window size $N_w = N_{\text{samp}}$.

4.7.8 Summary of AO performance

The overall NGS-AO system performance will be evaluated in terms of the Strehl Ratio (SR) in J, H, K, Ks, L', M' bands of the long-exposure AO-corrected PSF. The reference band for Technical Specification is Ks.

Figure 15 summarize the optimized performances achieved by the system working in the NGS- and LGS-modes. The plot shows the SR in Ks band as a function of the NGS star R-magnitude. The crossing point of better on-axis performance between LGS and NGS modes is at magnitude R=13.5. The error budget in Sec. 9.1 estimated the following contributions not provided by the end-2-end simulation:

NGS-mode: 110 nm rms WFE

LGS-mode: 150 nm rms WFE

The above contributions have been applied to the results in Figure 15 as SR attenuation factor computed with the Maréchal's approximation formula.

The system parameters (sampling frequency, number of controlled modes, and integrator's gains) have been optimized for each flux level. The parameters optimization for the NGS-mode case will be presented in Table 13 and for the LGS-mode in Table 15.

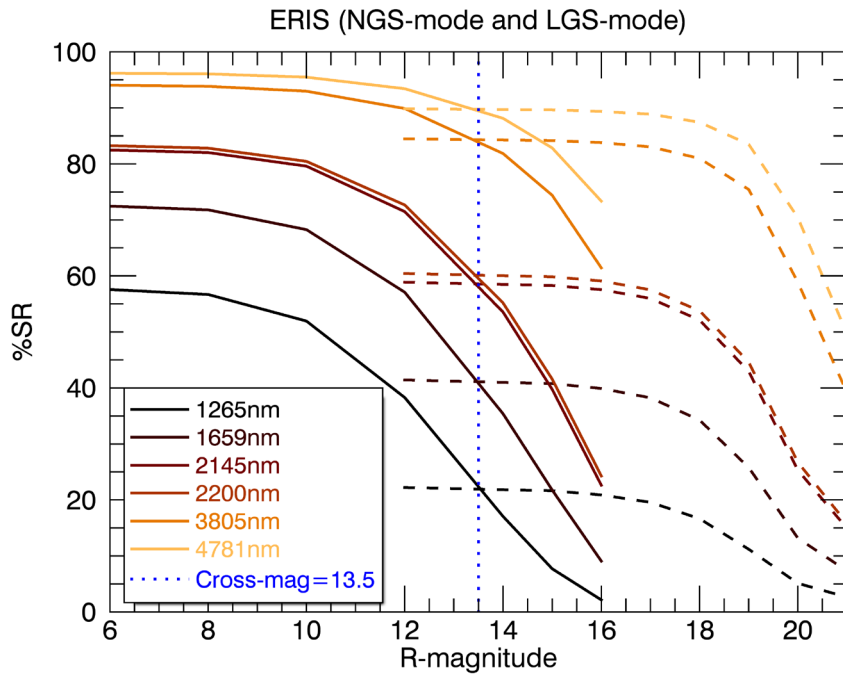
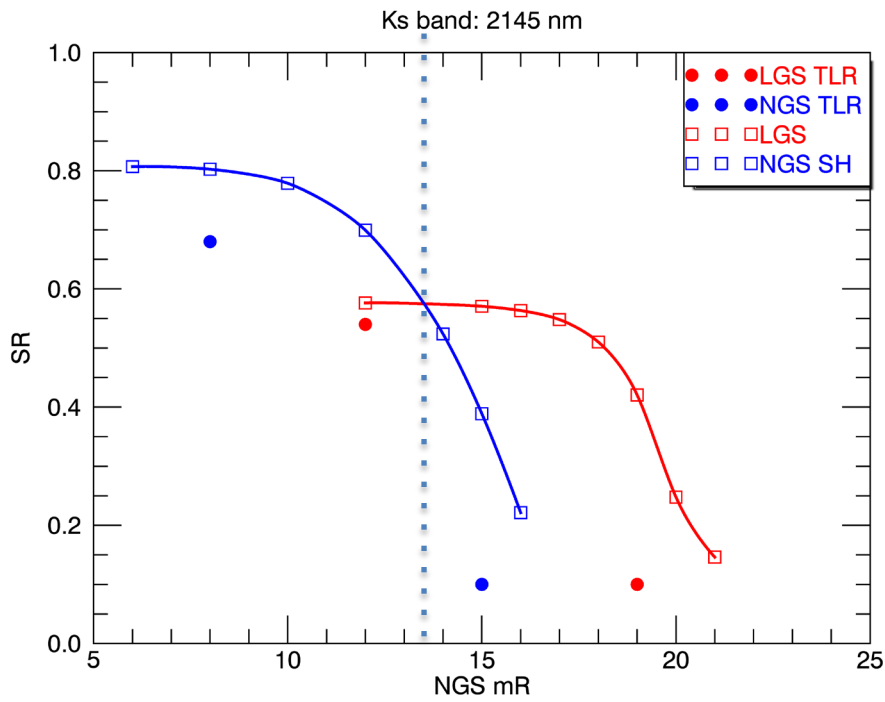


Figure 15 Top: overall ERIS performance in Ks band including the error budget contributions. The TLR values are also shown for comparison. Blue line is NGS-mode, red line is LGS-mode. The vertical dotted line at magR=13.5 represents the transition of better on-axis performance between NGS and LGS mode. Bottom: Resume of performance in J, H, Ks, K, L' and M' bands.

| | | | |
|------------------------|-------------------------------------|------------------------------------|--|
| ERIS Consortium | ERIS Documentation Standards | Doc.-Ref. Issue Date Page | : VLT-TRE-ERI-14403-3001 : 1.0 : 05.12.15 : 43 of 136 |
|------------------------|-------------------------------------|------------------------------------|--|

We compare off-axis results for LGS and NGS modes. These values are obtained using the following formula:

$$SR(\theta) = SR(0) SR_{off}(\theta)$$

where SR_{off} corresponds to the Strehl ratio coming directly from an anisoplanatic (NGS-mode) and anisokinetic (LGS-mode) study. These values are obtained by making open loop simulations with guide stars shifted from the line of sight and by subtracting the corresponding phase screens to the on-axis phase screen and by computing the RMS.

The two SR_{off} are shown in Figure 16.

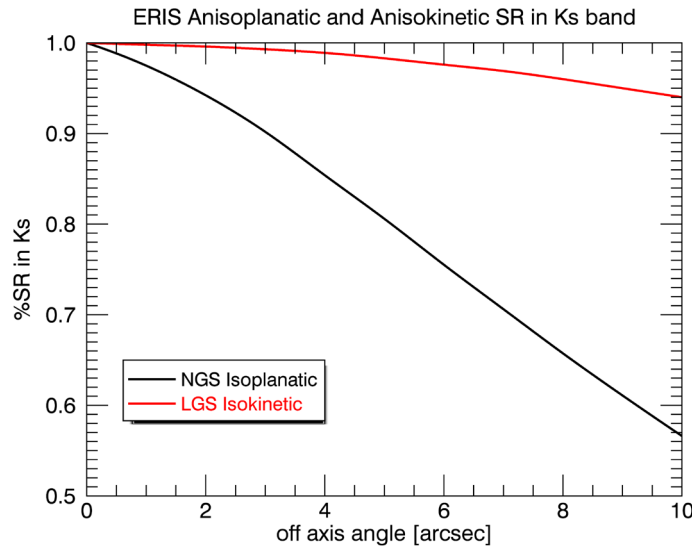


Figure 16. SR_{off} in Ks band from anisoplanatic (NGS-modes) and anisokinetic (LGS-modes) error.

From these values one can compute the isoplanatic angle for NGS-mode and isokinetic angle for LGS-mode using the following formula: $SR(\theta) = SR(0) e^{-(\theta/\theta_0)^{5/3}}$

- Isoplanatic angle (Ks band): $\theta_0 \approx 15$ arcsec
- Isokinetic angle (Ks band): $\theta_0 \approx 54$ arcsec

The Figure 15 shows the crossing magnitude between NGS- and LGS-modes in function of the off axis angle. Obviously the crossing magnitude decreases when the off-axis angle increases, being the LGS-mode more favourable in terms of Strehl Ratio. For NGS off-axis angle larger than 7.3 arcsec the LGS is always better performing than NGS (with standard atmosphere model). We remind that the plot of Figure 15 does not depend on the considered band in the Maréchal's approximation.

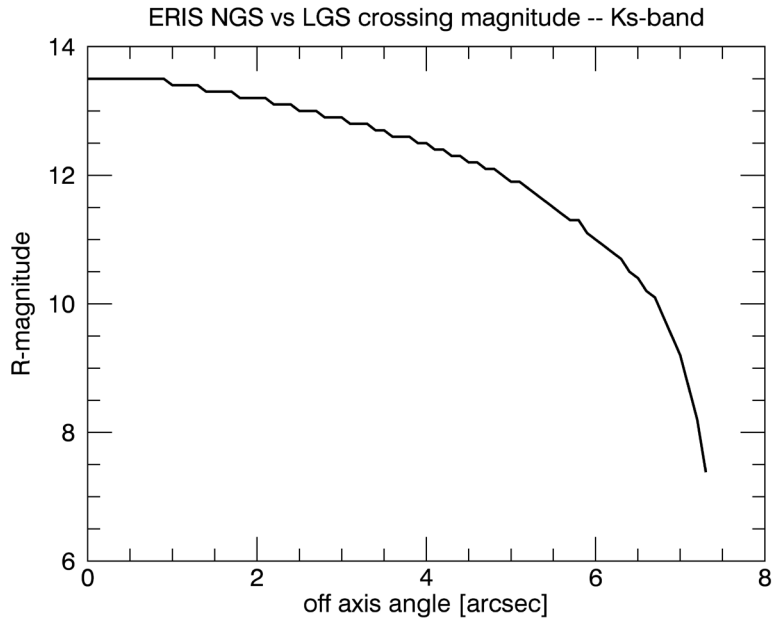


Figure 17. NGS vs LGS crossing magnitude as a function of the off axis angle (in arcsec).

In the following sections we report details of the simulations and results that are used to produce data for the plots in Figure 15. We remind that the contribution of the error budget is included only in the above figures.

4.7.9 NGS-mode optimized parameters and performance

We run simulations of 4 s if sampling frequency is 1kHz and of 8 s otherwise and we discard the first 250 steps to compute the performances. Figure 18 shows the summary of the best performance achieved with the parameters shown in Table 13 with the QC algorithm. In fact performance results for a complete set of NGS magnitude with WCoG algorithm has to be completed. The QC results presented here are a conservative approximation of WCoG (see in 4.7.6).

Table 13. Summary of the optimized parameters and of the fluxes of the NGS SH WFS.

| R | 6 | 8 | 10 | 12 | 14 | 15 | 16 |
|--------------------------|------|------|------|------|------|------|------|
| fr. [Hz] | 1000 | 1000 | 1000 | 1000 | 600 | 300 | 300 |
| no. modes | 945 | 945 | 860 | 702 | 377 | 189 | 119 |
| int. gain | 0.4 | 0.35 | 0.25 | 0.2 | 0.4 | 0.6 | 1.1 |
| Flux [ph/sa/frame] | 1480 | 235 | 37.2 | 5.9 | 1.6 | 1.2 | 0.5 |
| σ_R [e-/sa/frame] | 9.6 | 1.2 | 1.2 | 1.2 | 1.2 | 1.2 | 1.2 |
| σ_D [e-/sa/frame] | 0.36 | 0.36 | 0.36 | 0.36 | 0.33 | 0.36 | 0.36 |
| σ_B [e-/sa/frame] | 0.17 | 0.17 | 0.17 | 0.17 | 0.21 | 0.30 | 0.30 |

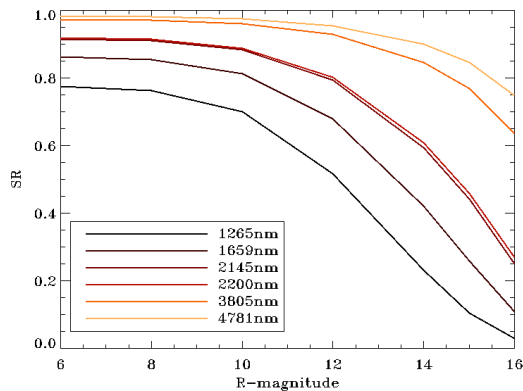


Figure 18. NGS-mode SH WFS, SR in function of R-magnitude.

4.7.10 NGS-mode: contrast, speckle noise and ADI SNR

We made 100 end-to-end simulations of the NGS-mode in the bright-end regime for the SH-WFS.

The simulations provided 100 PSFs in L' band with an integration time of 1 s each of a star magnitude L'=5 as requested by TS-NIX-PER-029. We computed the radial profile, the speckle noise and the ADI SNR. We use a binning equal to 0.1x0.1 arcsec.

The radial profile = average of the L' PSF profile in 0.1x0.1arcsec bins

$\sigma_{diff}(r)$ = rms of difference between two uncorrelated PSF in the bin (Here we have 50 couple of PSF)

$$ADI\ SNR = \frac{N_{planet}}{\sqrt{\sigma_{diff}^2 + 2 N_{planet} + 2 N_{star} + 2 N_{BG}}} \sqrt{n_{diff}}$$

where N_{planet} , N_{star} , N_{BG} are respectively the photon noise, from the planet and the star, and the sky background noise in the considered bin. They are computed from the following parameters:

- Star magnitude in L' = 5
- Background magnitude² in L = 3.9

The results are shown in the following figures.

Figure 19 shows a comparison between the different sources of noise and the total noise expressed in variance. As can be clearly seen the speckle noise is the dominant term up to $3\lambda/D$. Then, over this value the background noise gives the greatest contribution to the total noise.

Figure 20 shows the PSF contrast radial profile and the speckle noise profile both normalized to the unit total energy.

Figure 21 shows the SNR ADI (angular differential imaging) in the cases where the difference between the planet magnitude and the star magnitude is $\Delta mag = 10$ and 12 . These plots show that the SNR ADI is better than 5 before a radius of $3\lambda/D$ and remains stable after around $5\lambda/D$ because of the largest contribution of the sky background noise which is constant.

² <https://www.eso.org/gen-fac/pubs/astclim/paranal/skybackground/>

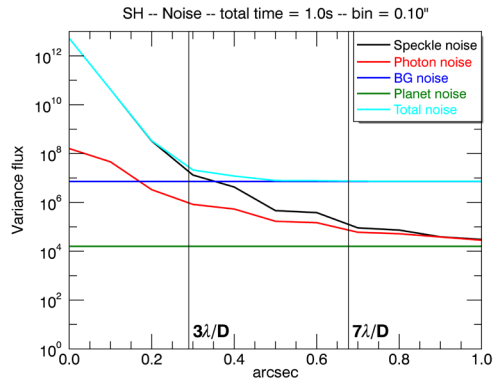


Figure 19. Comparison between different noise contributions (in variance).

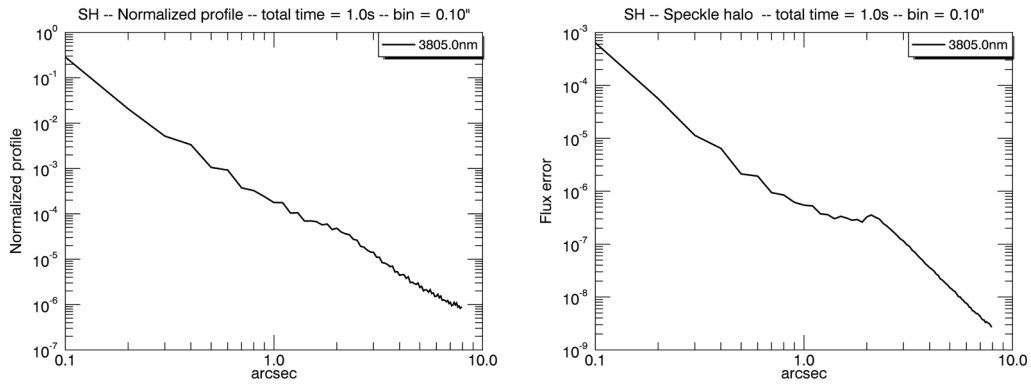


Figure 20. PSF contrast radial profile (Left). Speckle Noise (Right). In the plots the curves are normalized to unit total energy.

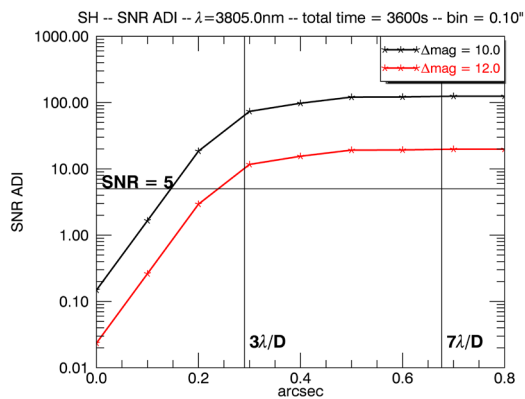


Figure 21. ADI SNR for planet L' magnitude 15 and 17. Star magnitude L'=5

Table 14. SNR ADI comparison for different radial distances.

| Radial distance | 2 λ /D | 3 λ /D | 7 λ /D |
|---------------------------|----------------|----------------|----------------|
| SNR ADI Δ mag = 10 | 19.5 | 59.6 | 123.7 |
| SNR ADI Δ mag = 12 | 3.1 | 9.5 | 19.6 |

4.7.11 LGS-mode simulation results

We run simulations of 4s at 500Hz and 6s at 333Hz and we discard the first 250 steps to compute the performance. Figure 22 shows the summary of the best performance achieved with the parameters shown in Table 15 and with the WCoG algorithm.

Table 15. Summary of the optimized parameters of the LGS and NGS WFSs.

| R | | 12 | 15 | 16 | 17 | 18 | 19 | 20 | 21 |
|---------|--------------------------|------|------|------|------|------|------|------|------|
| LGS WFS | Fr. [Hz] | 1000 | 1000 | 1000 | 1000 | 1000 | 1000 | 1000 | 1000 |
| | No. modes | 945 | 945 | 945 | 945 | 945 | 945 | 945 | 945 |
| | int. gain | 0.3 | 0.3 | 0.3 | 0.3 | 0.3 | 0.3 | 0.3 | 0.3 |
| NGS WFS | Fr. [Hz] | 500 | 500 | 500 | 500 | 500 | 500 | 333 | 333 |
| | int. gain | 0.45 | 0.40 | 0.40 | 0.30 | 0.35 | 0.55 | 0.60 | 0.10 |
| | Mask radius [pix] | 4 | 2 | 2 | 2 | 2 | 2 | 2 | 2 |
| | Flux [ph/sa/frame] | 3610 | 228 | 90.8 | 36.1 | 14.4 | 5.7 | 3.4 | 1.4 |
| | σ_R [e-/sa/frame] | 23.1 | 0.9 | 0.7 | 0.7 | 0.7 | 0.7 | 0.7 | 0.7 |
| | σ_D [e-/saframe] | 0.43 | 0.21 | 0.21 | 0.21 | 0.21 | 0.21 | 0.20 | 0.20 |
| | σ_B [e-/sa/frame] | 4.2 | 2.0 | 2.0 | 2.0 | 2.0 | 2.0 | 2.4 | 2.4 |

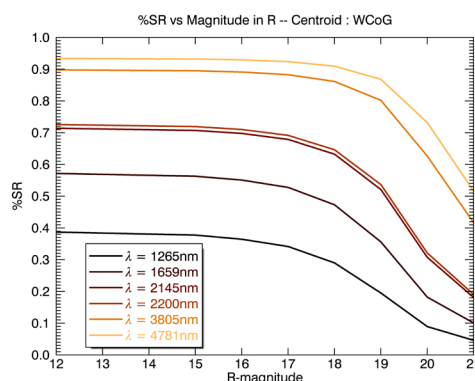


Figure 22. LGS-mode, SR in function of R-magnitude.

| | | | |
|---|--|--|--|
| <p style="text-align: center;">ERIS Consortium</p> | <p style="text-align: center;">ERIS Documentation Standards</p> | <p>Doc.-Ref. Issue Date Page</p> | <p>: VLT-TRE-ERI-14403-3001 : 1.0 : 05.12.15 : 48 of 136</p> |
|---|--|--|--|

4.7.12 Vibrations: NGS-mode

We get some data on telescope and instrument vibrations from RD14. The document reports results of on-sky closed-loop test for validation of Vibration Control Algorithm with the VLTI-MACAO system. The tip-tilt vibration frequencies are directly reported, while the strengths are deduced from the plots of the cumulated PSD. An example from RD14 is reported in Figure 14. From those data we define three different cases shown in Table 16 with frequencies ranging from 18 to 97Hz. We remind that MACAO is at the VLTI focal station, very different from the ERIS foreseen location except for the telescope (M1+M2) itself.

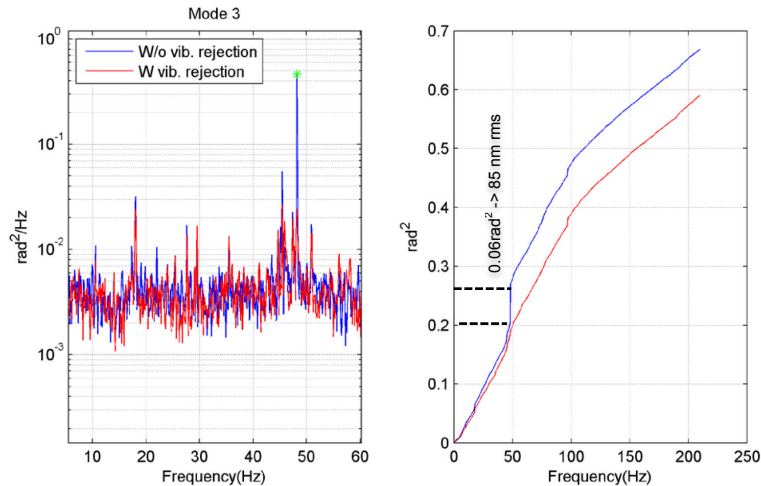


Figure 23 – example of VLTI-MACAO data from RD14. Tilt PSD and cumulative phase variance in K. The step in the cumulative curve is used to estimate vibration strength.

For each one of these cases we made two simulations of the NGS-mode with R-magnitude 8 with sampling frequency of 500 and 1000kHz. We optimized the integrator gain for two different sets: Tip-Tilt and other modes (see Table 17). The other parameters are shown in Table 13.

The results are summarized in Table 18. The greatest difference between the two sampling frequency is for the second case because the vibration at 48Hz is before the overshoot of Rejection Transfer Function (RTF) with a sampling frequency of 1000Hz and in the overshoot of the RTF with a sampling frequency of 500Hz (see Figure 24). The last case shows similar results because for both sampling frequency 97Hz is in the RTF overshoot.

Table 16. Summary of the three vibrations cases.

| Vibrations Case | 1 | | 2 | | | 3 | | | |
|------------------------|----------------|----|------------------|----|----|------------------|----|----|----|
| frequency [Hz] | 18 | 24 | 18 | 24 | 48 | 18 | 24 | 48 | 97 |
| Tip RMS [nm] | 40 | 60 | 40 | 60 | 45 | 40 | 60 | 45 | 60 |
| Tilt RMS [nm] | 40 | - | 40 | - | 80 | 40 | - | 80 | 50 |
| Total RMS | 82 nm 8 mas | | 123 nm 13 mas | | | 146 nm 15 mas | | | |

Table 17. Summary of the optimized parameters of the NGS WFS for the three vibrations cases.

| Vibrations Case | | 1 | | 2 | | 3 | |
|------------------------|--------------------|----------|------|----------|------|----------|------|
| fs [Hz] | | 500 | 1000 | 500 | 1000 | 500 | 1000 |
| gain | Tip/Tilt | 0.75 | 0.45 | 0.90 | 0.55 | 0.15 | 0.10 |
| | other modes | 0.60 | 0.35 | 0.60 | 0.35 | 0.60 | 0.35 |

Table 18. Summary of the performance for the NGS-mode for the three vibrations cases and, in the first column, for the case without vibrations

| Vibrations Case | NO | 1 | | 2 | | 3 | |
|---------------------------|-----------|----------|------|----------|------|----------|------|
| fs [Hz] | 1000 | 500 | 1000 | 500 | 1000 | 500 | 1000 |
| SR (K) | 90.5 | 88.5 | 89.7 | 81.0 | 85.8 | 71.6 | 73.0 |
| Tip/Tilt res. [nm] | 44.4 | 58.3 | 55.5 | 120.9 | 93.0 | 180 | 176 |
| [mas] | 4.5 | 5.9 | 5.6 | 12 | 9.5 | 18 | 18 |

| | | | |
|---|--|--|--|
| <p style="text-align: center;">ERIS Consortium</p> | <p style="text-align: center;">ERIS Documentation Standards</p> | <p>Doc.-Ref. Issue Date Page</p> | <p>: VLT-TRE-ERI-14403-3001 : 1.0 : 05.12.15 : 50 of 136</p> |
|---|--|--|--|

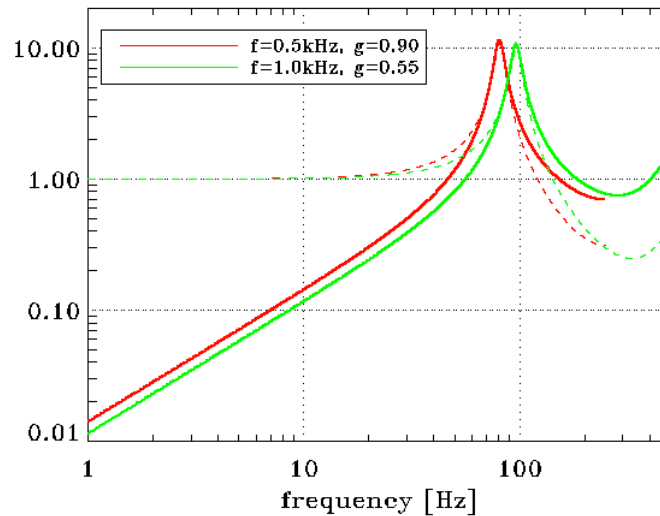


Figure 24. Solid lines: Rejection Transfer Function (solid curves) for Tip-Tilt in the vibrations Case 2.

From the estimated performance, we see that Case 2, and especially Case 3, are critical. Vibrations at 48 and 97 Hz are poorly rejected if not amplified by the system. **An assessment of Cas-segrain Focal station vibration scenario is mandatory for a performance estimation.** In case 48 and 97 Hz vibration are confirmed at the level experienced in RD14, advance Vibration Control Algorithm have to be implemented in the HO NGS loop control of SPARTA, currently only available in LO NGS loop of the LGS mode.

For error budget purposes we will use the intermediate case 2 as representative of average condition.

4.7.13 Variable seeing and robustness

In this section we report by numerical simulations the behaviour of closed loop NGS-mode and LGS-mode in case of seeing variation up to 1.5" (TS-AO-PER-017 and TS-AO-PER-018). The presented simulations consider two cases: system behaviour when seeing increase (left part of Figure 25) and decrease (right part of of Figure 25) with respect to the initial value where system parameters are optimized. The R-magnitude for NGS-mode is 13th and for LGS-mode is 17th. We optimized the NGS WFS parameters for the initial condition and then we let them unchanged. The SR time history is shown in Figure 26 for NGS-mode and Figure 27 for LGS-mode (left part increasing seeing, right part decreasing seeing). Note that we have taken into account LGS spots size changes due to seeing variations.

Table 19 Summary of NGS WFS optimized parameters for different seeing conditions

| Parameter | NGS-mode, R=13 | | LGS-mode, R=17 | |
|--------------------------|----------------|-------|----------------|-------|
| | 0.87" | 1.50" | 0.87" | 1.50" |
| Fr. [Hz] | 1000 | 1000 | 250 | 333 |
| No. modes | 629 | 560 | 2 | 2 |
| gain | 0.2 | 0.25 | 0.2 | 0.35 |
| Flux [ph/sa/frame] | 2.4 | 2.4 | 72.2 | 72.2 |
| σ_R [e-/sa/frame] | 1.2 | 1.2 | 1.6 | 1.6 |
| σ_D [e-/sa/frame] | 0.36 | 0.36 | 0.48 | 0.48 |
| σ_B [e-/sa/frame] | 0.17 | 0.17 | 4.6 | 4.6 |

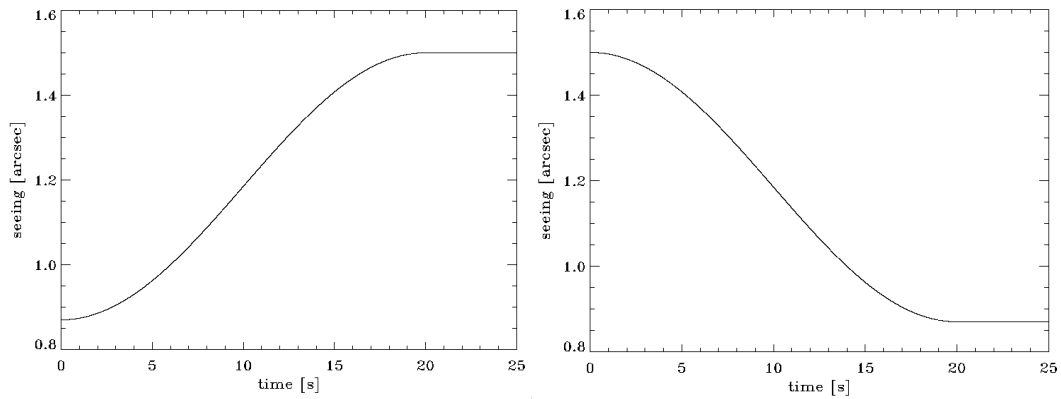


Figure 25. Seeing time history

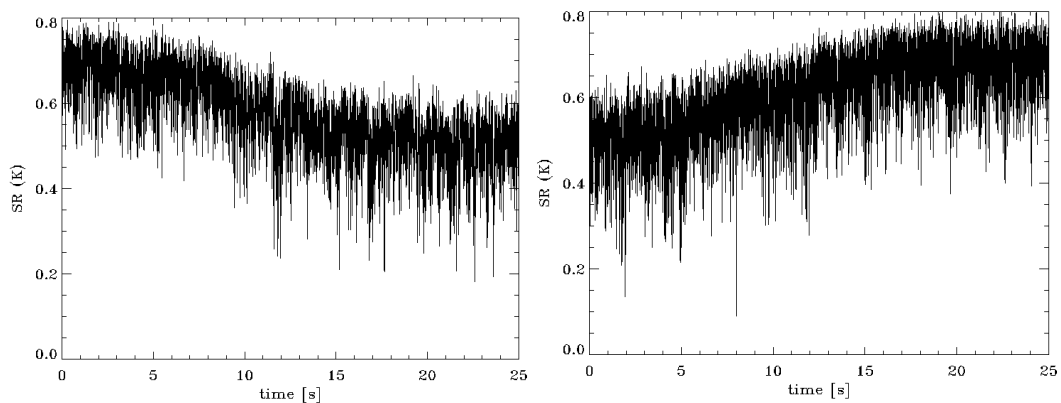


Figure 26. NGS-mode SR (K) time history

| | | | |
|---|--|--|--|
| <p style="text-align: center;">ERIS Consortium</p> | <p style="text-align: center;">ERIS Documentation Standards</p> | <p>Doc.-Ref. Issue Date Page</p> | <p>: VLT-TRE-ERI-14403-3001 : 1.0 : 05.12.15 : 52 of 136</p> |
|---|--|--|--|

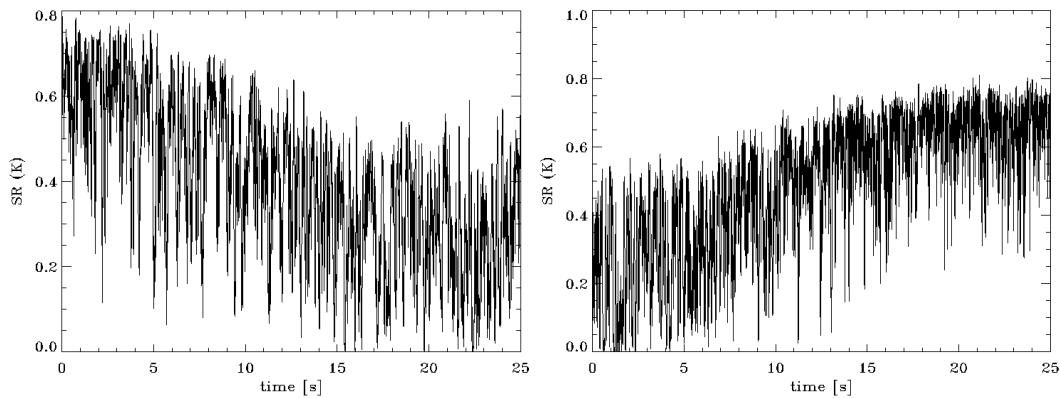


Figure 27. LGS-mode SR (K) time history

The first conclusion here is that the system is stable against seeing variation in both cases. In particular gain values optimized for 1.5 arcsec seeing still provide a stable loop at 0.87 arcsec seeing. No significant variation is found in the achieved SRs with optimal or not optimal gain values in both cases. We conclude this section saying that the system fulfils the specification to hold close loop when the seeing varies between 0.87 arcsec and 1.5 arcsec without operator intervention. A separate analysis should be dedicated to evaluate the impact on the close loop operations of the force limit of the DSM that may constrain the available seeing values range.

4.7.14 Sensitivity Analysis

In this section we evaluate the impact of a misalignment of the pupil w.r.t. the WFS in NGS-mode. The misalignments considered are:

- Shift
- Rotation

We made full end-to-end simulation at R-magnitude=8 and in the reference condition (See Sec. 4.7.1) with the misalignment and we measure SR and the differential residual RMS.

Pupil Shift

We simulated the closed loop performance with standard parameters for pupil mis-registration error shift on x and y-axis between 0 and 0.4 sub-apertures. In order to introduce a limited contribution in the wavefront error budget, we choose a maximum pupil shift error of 0.1 sub-apertures providing 15 nm RMS WFE per axis for a total contribution of 21 nm RMS WFE.

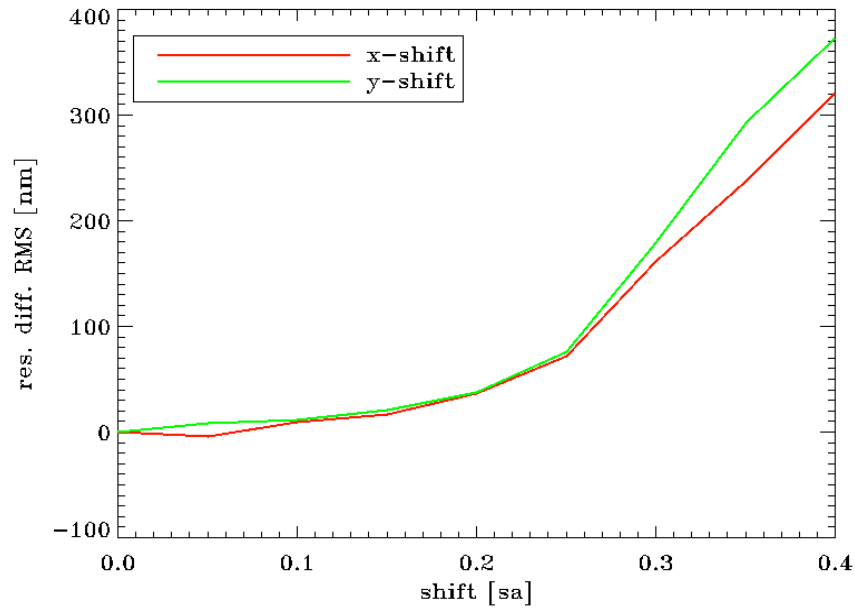


Figure 28. Residual difference RMS in function of pupil shift in fraction of sub-aperture.

Pupil Rotation

We considered rotations between 0 and 32arcmin, which corresponds to 0 and 0.4 sub-apertures at the edge of the pupil. The stabilization and reproducibility of the relative angular position between the instrument rotator and the WFS K-mirror is not limited by mechanics or electronics (encoder accuracy). Considering an extreme case of a 5s delay of the k-mirror angle update in a fast rotator condition (0.044 deg/s at z=5 deg), the angular mis-registration error is 0.22deg or 0.08 sub-apertures at the pupil edge with a contribution to the wavefront error budget of 8 nm RMS WFE.

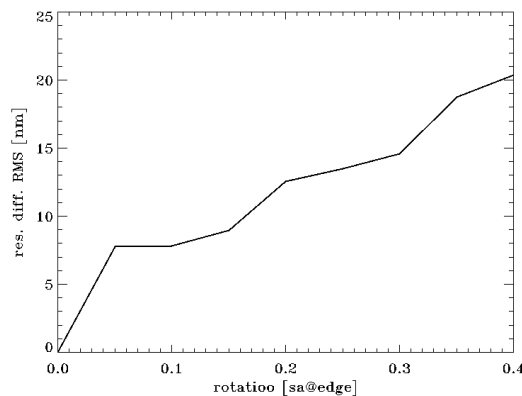


Figure 29. Residual difference RMS in function of pupil rotation in fraction of sub-aperture at the edge of the pupil.

4.7.15 LGS spot elongation and truncation effect

A critical aspect of the wavefront sensing is the spot elongation due to the finite size and distance from the telescope of the LGS reference source. The spot size being comparable to the sensor FoV may lead to spot truncation that results in an underestimate of the CoG position. The angular

| | | | |
|-------------------------------|--|--|--|
| <p>ERIS Consortium</p> | <p>ERIS Documentation Standards</p> | <p>Doc.-Ref. Issue Date Page</p> | <p>: VLT-TRE-ERI-14403-3001 : 1.0 : 05.12.15 : 54 of 136</p> |
|-------------------------------|--|--|--|

size of the spot elongation can be estimated using the well know geometrical formula $\theta \sim l \Delta h / h^2$ where l , Δh and h are the sodium layer thickness, subaperture distance to the laser launching unit and the sodium layer average altitude. Replacing the values for ERIS (8m, 20km, 90km) gives a spot size of about 4 arcseconds. Truncation of the SH spots is then a possible effect considering that the laser guide star has some residual tilt jitter and the ERIS AO LGS wavefront sensor FoV is designed to be 5 arcsecond. In the table below we report the LGS jitter effect in terms of cross-talk with Zernike modes as a function of the spots displacement from the centre. The figure shows that low order Zernike modes of the order of 20-50 nm can be generated with spot jitters in the range of 0.2-0.4 arcseconds.

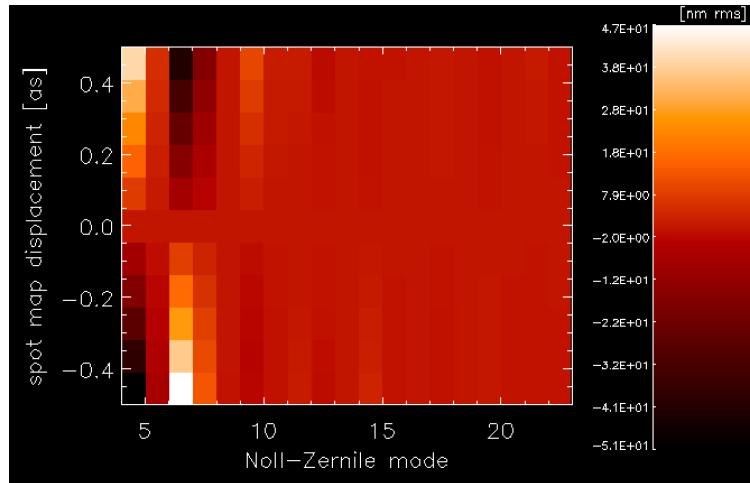


Figure 30 Double Peak profile case.

This analysis shows that it is important to take in account this effect in the end-to-end simulations, therefore we always added to the LGS spot positions a Gaussian distributed displacement due to an LGS residual jitter of 106 mas RMS per axis, as found in RD11.

4.7.16 Sodium layer profile variation

Because of the change of elevation, the LGS distance from the telescope entrance pupil changes with a speed ranging from zero at the meridian to ~20 m/s at 60deg elevation (minimum elevation requested for the LGS-mode), changing the best focus position of the LGS. Moving the LGS sensor stage following an elevation LUT controls this focus variation. In addition to this, the temporal changes in the sodium layer density will change the profile center of gravity altitude so adding another perturbation to the measured LGS best focus position. This focus variation is measured by the LO NGS WFS acting as truth sensor.

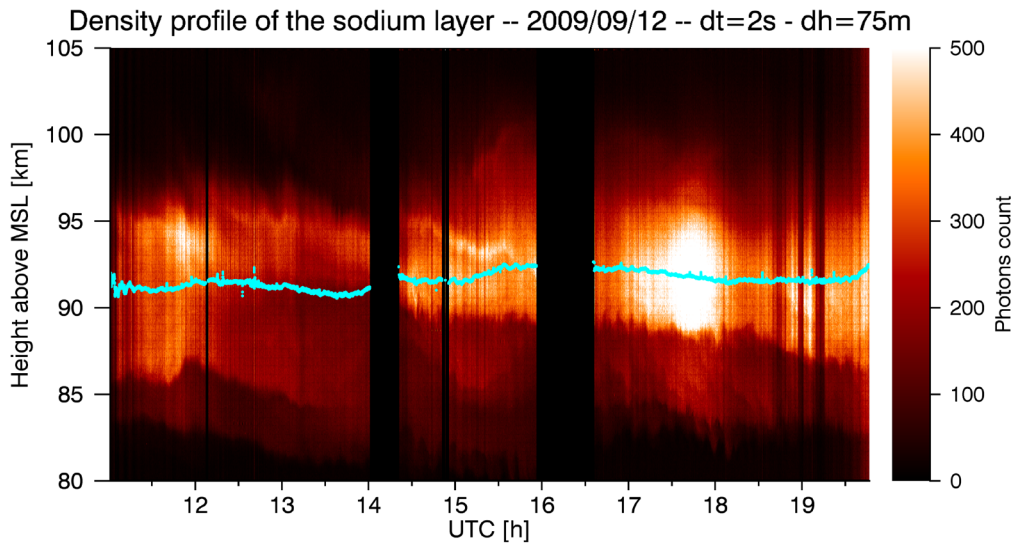


Figure 31. Example of sodium profile evolution with time and related barycentre variation (cyan line). Data from RD5.

SPARTA team reports that the truth sensor iteration rate can be set down to 5 seconds ([CC-1f] in AD10).

From RD5, the average PSD of the barycentre height fluctuations is:

$$PSD(\nu) = 34.4 \nu^{-1.87} [m^2/Hz]$$

where ν is the frequency in Hz. Filtering the PSD with the rejection function of a truth sensor integrator loop running at 0.2 Hz, the residual height fluctuation is 55 m RMS, equivalent to 16 nm WFE RMS focus residual³. In the same reference RD5 it is shown that the PSD coefficient (34.4 m²/Hz) easily spans 1 order of magnitude, therefore a factor $\sqrt{10}$ of margin is applied for the error budget (50 nm WFE rms).

The temporal variation of the sodium layer density changes the LGS beacon shape as seen from each SH subaperture introducing, due to change in the average spot shape, perturbations in the sensor measurements of spots CoG. Figure 33 summarizes the effect of a change in terms of reconstructed wavefront between the different profiles (a), (b) and (c) shown in Figure 32.

The figure shows that up to 50nm of astigmatism can be generated from such a profile change and even coma can reach values around 25nm. For such reason we require that the truth sensing loop has to control focus but even astigmatism and coma. The baseline option for the truth sensing is arranged so that the focus will be update from the NGS LO wavefront sensor (keeping the non common path aberration to a minimum) while astigmatism and coma will be measured by the VLT active optics system.

³ For this evaluation the gain of the integrator has been set to have 45° phase margin in the open loop transfer function.

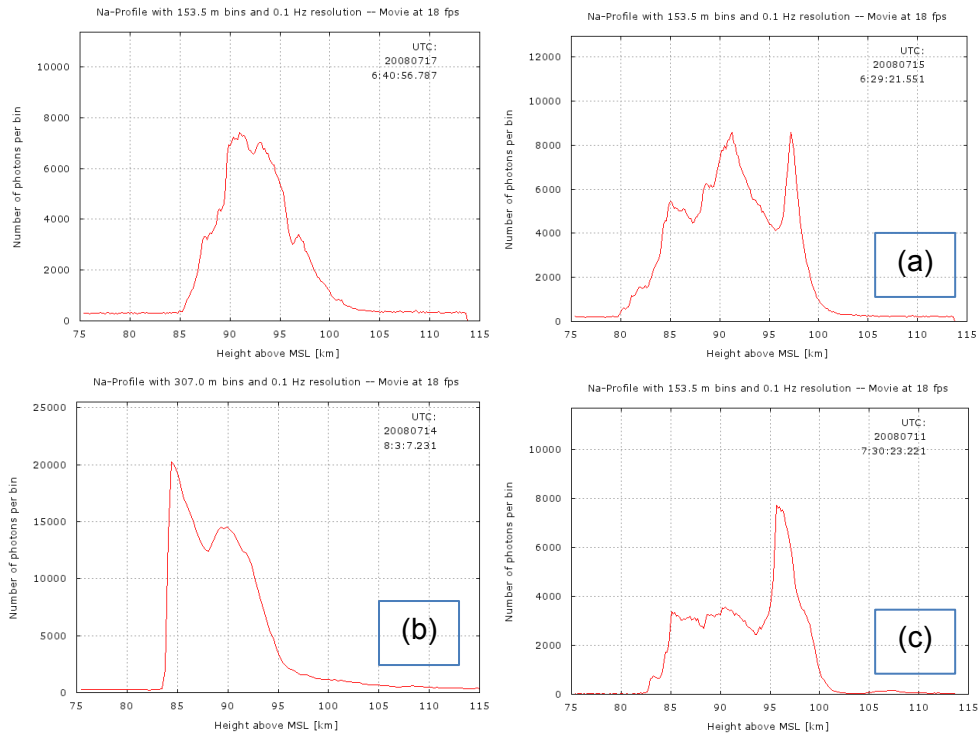


Figure 32. Different typical sodium profiles as reported in RD5. Top left is the profile used in the performance simulations, (a), (b) and (c) are the “Very-wide”, “Double Peak” and “Top Hat with Peak” profiles.

Referring to RD18, the intrinsic measurement accuracy of the active optics WFS is about 30 nm RMS for the astigmatism and about 20 nm RMS for the coma (fig. 3 in RD18), even if, in the standard active optics operation, the performances are reduced by the noise contribution of the atmospheric turbulence. However in the ERIS case, where the AO corrector (DSM) is upstream with respect to the active optics WFS, the atmospheric effect should be effectively reduced and we will consider the intrinsic measurement accuracy of the active optics as the sensitivity limit of the truth sensing.

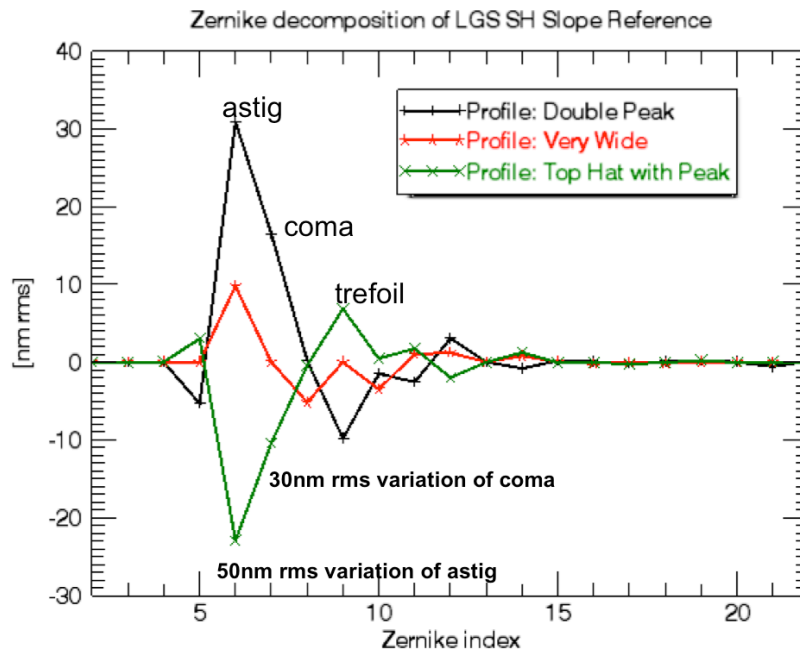


Figure 33 Modal reconstruction error using a reference reconstructor with different sodium profiles. No atmospheric turbulence is present in the simulation. The beacon is re-centered and the LGS WFS is re-focused to simulate the correction effect of the LGS jitter and focus loops.

4.8 Optical Design

4.8.1 Overview

Figure 34 shows the optical path from the telescope to the different subsystems. Light from the telescope is split by a first dichroic into two arms: the AO wavefront sensing unit and the science beam, alternatively feeding two instruments: NIX and SPIFFI, via a selector mirror. In the AO arm, a second dichroic split light into the LGS WFS and the NGS one. A calibration unit can illuminate the full system by inserting a mirror before the WFS dichroic.

Following sections give a description of the subsystems and related optical components, as identified in the scheme above.

It is assumed to have a “modified” VLT optical layout, with the BFL, as measured from the Cassegrain flange, to be 500 mm instead of the standard 250 mm. This change has been agreed with ESO and it is the subject of a formal Change Request (CRE number ERIS-002).

The telescope prescription used for the preliminary design of ERIS and implementing the BFL=500 mm is shown in Table 20 and the relative optical parameters are reported in Table 21. Details are available in AD3.

In the AO LGS-mode the telescope is used to relay the Sodium beacon. Assuming a conservative range of the Sodium layer barycenter from 85.0 km and 190 km (i.e., $95\text{km}/\cos(60)$), the LGS focal plane moves, respectively, 144 mm and 64 mm out from the NGS focal plane increasing the distance from M2 at the F/13.7 focal plane after the telecentric lens. That defines the **minimal requirement of 77 mm for the travel of the focus stage for the LGS WFS**. This is slightly smaller than 80 mm, because the LGS WFS is placed after a telecentric lens that will decrease the focal ratio from F/13.7 to F/13.4.

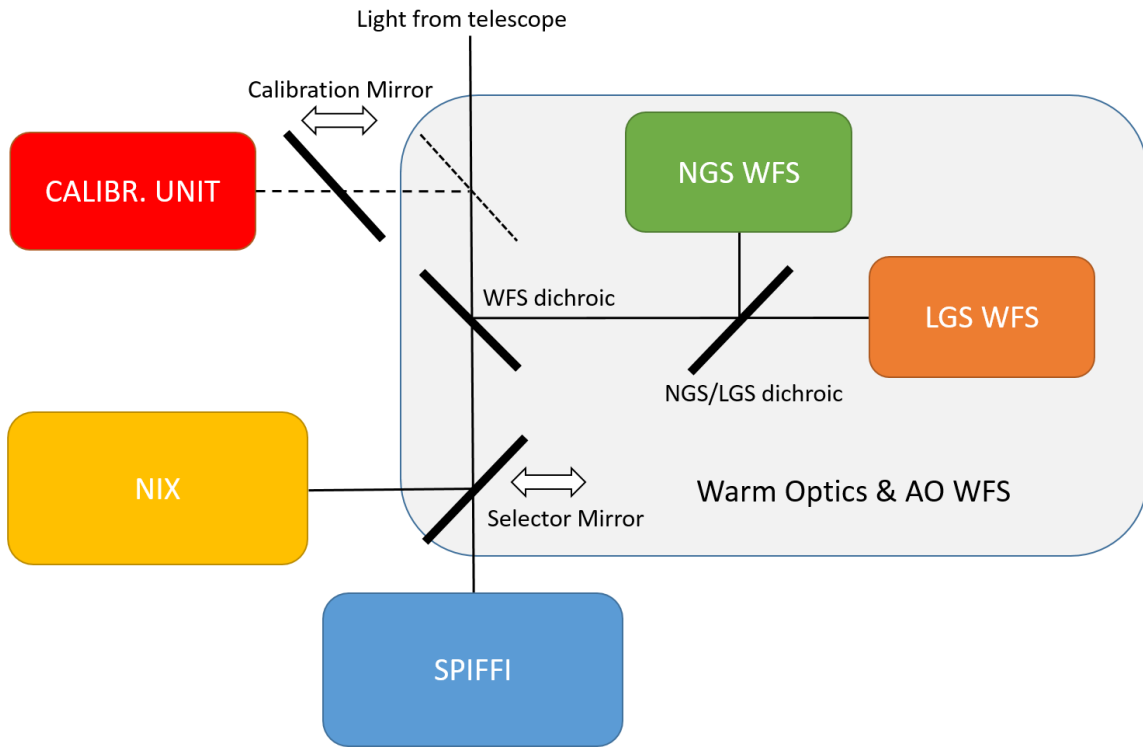


Figure 34 Schematic block diagram of the main optical subsystems.

Table 20 telescope optical prescription implementing BFL=500mm

| Surf | Type | Comment | Radius | Thickness | Glass | Semi-Diameter | Conic |
|------|----------|-------------------|-----------------|-----------------|----------|---------------|-------------|
| OBJ | Standard | | Infinity | Infinity | | Infinity | 0.00000000 |
| 1 | Standard | VLT-M1 | -28800.00000000 | -12420.32654000 | MIRROR | 4073.90924355 | -1.00469000 |
| STO* | Standard | VLT-M2 (DSM) | -4553.57100000 | 12420.32654000 | P MIRROR | 558.00000000 | -1.74235900 |
| 3 | Standard | VLT-M1 HOLE | Infinity | 2250.00000000 | | 127.20226010 | 0.00000000 |
| 4 | Standard | CASSEGRAIN FLANGE | Infinity | 500.00000000 | | 49.37488202 | 0.00000000 |
| IMA | Standard | FOCAL PLANE | -2028.68163000 | - | | 32.09155214 | 0.00000000 |

Table 21 Optical telescope parameters implementing BFL=500mm

| <i>Parameter</i> | <i>Value</i> | | |
|--|--------------|----------|-----------|
| Entrance Pupil dia. | EPD | 8117.7 | mm |
| Entrance position from M1 vertex (behind M1) | | 90344.6 | mm |
| Exit Pupil dia. | EXP | 1116.0 | mm |
| Exit Pupil position from focal plane (M2) | | 15170.33 | mm |
| Working F-Number | WFNO | 13.6332 | |
| On-axis plate scale | | 0.536 | mm/arcsec |
| Focal plane RoC (concavity towards M2) | | 2028.68 | mm |
| Effective Focal Length | EFL | 110348 | mm |
| Object Field of View diam. (unvignetted) | UFOV | 3.42 | arc-min |
| Image Field of View diam. (unvignetted) | UFOV | 109.8 | mm |

Table 22 Change of LGS with respect to NGS focal plane position. The WFE is dominated by Spherical Aberration

| Sodium layer distance [km] | Distance from NGS [mm] | on-axis WFE [nm rms] | F/number |
|----------------------------|------------------------|----------------------|----------|
| 85.0 | +144.4 | 4.3 | 13.8 |
| 190 | +64.3 | 2.4 | 13.7 |

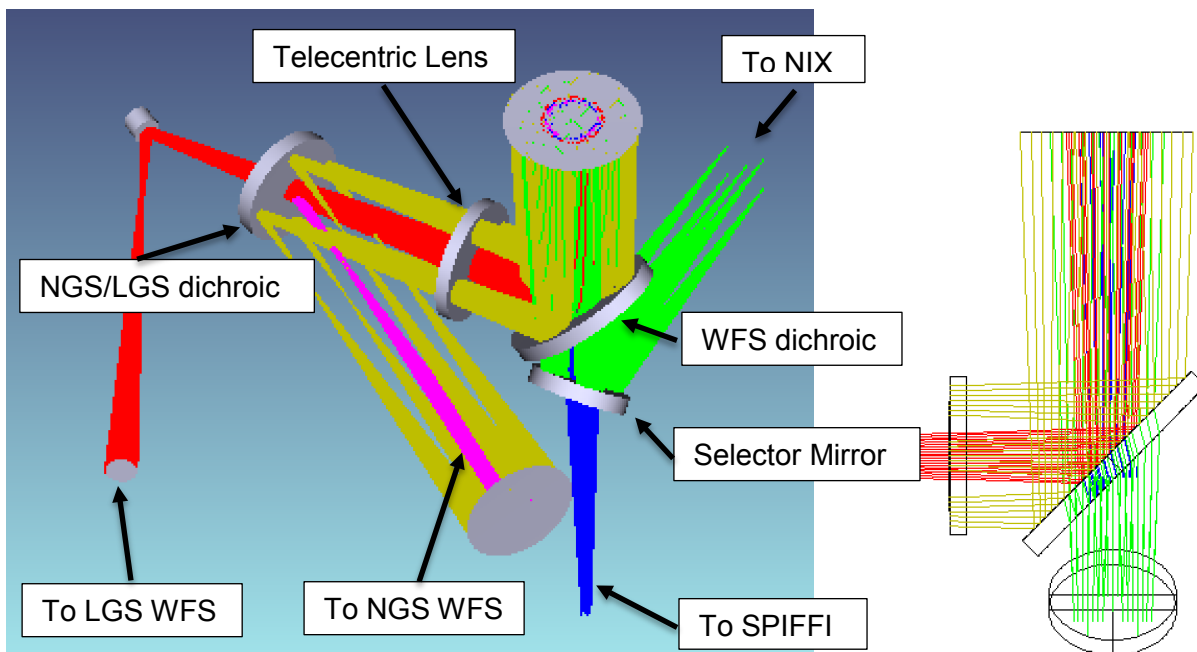


Figure 35 Layout of the Warm Optics.

| | | |
|------------------------|-------------------------------------|--|
| ERIS Consortium | ERIS Documentation Standards | Doc.-Ref. : VLT-TRE-ERI-14403-3001 Issue : 1.0 Date : 05.12.15 Page : 60 of 136 |
|------------------------|-------------------------------------|--|

4.8.2 Warm Optics

Figure 35 shows the optical layout of the Warm Optics. The first optical element in the light path is a tilted dichroic beam-splitter. It separates wavelengths between the science path (1.0-5.4 micron) and the WFS optics (500-1000 nm). The dichroic reflects shorter wavelengths to the WFS path. The transmitted beam feeds SPIFFI with a straight through path. A moving flat selector mirror is inserted to direct transmitted light to NIX. In the WFS path, a telecentric lens change the exit pupil position close to infinity, to avoid pupil wobbling while the NGS WFS is patrolling the field of view. The next optics in the line is the LGS dichroic to split light between the LGS WFS (in transmission) and the NGS WFS (in reflection). Angle of incidence is kept small to decrease NCPA. Finally a flat fold mirror is used to have a more compact layout of the AO optics.

Table 23, Table 24, Table 25, and Table 26 give WO prescriptions for the SPIFFI, NIX, LGS WFS, and NGS WFS arms respectively in tabular form from ZEMAX lens editor.

Table 23. SPIFFI warm optics prescriptions.

| Surf>Type | Comment | Radius | Thickness | Glass | Semi-Diameter | Conic | Par 0 (unused) | Par 1 (unused) | Par 2 (unused) | Par 3 (unused) |
|-----------|------------|----------------|------------|------------|---------------|----------|----------------|----------------|----------------|----------------|
| OBJ | Standard | Infinity | Infinity | | Infinity | 0.000 | | | | |
| 1 | Atmosphe.. | Atmosphere | Infinity | 0.000 | 4050.079 | 0.000 | | 0.000 | 2635.430 | 283.000 |
| 2 | Standard | Infinity | 1.300E+004 | | 4050.079 | 0.000 | | | | |
| 3 | Standard | VLT-M1 | -2.88E+004 | -1.24E+004 | MIRROR | 4049.730 | -1.005 | | | |
| * | Standard | VLT-M2 (DSM) | -4553.571 | 1.242E+004 | P MIRROR | 558.000 | U | -1.742 | | |
| 5 | Standard | VLT-M1 HOLE | Infinity | 2250.000 | | 103.404 | 0.000 | | | |
| 6 | Standard | CASSEGRAIN F.. | Infinity | 185.000 | | 21.277 | 0.000 | | | |
| 7 | Coordina.. | | 0.000 | - | 0.000 | | | 0.000 | 0.000 | -45.000 |
| 8* | Standard | INSTR. DICHR.. | Infinity | 12.000 | CAF2 | 18.260 | 0.000 | | | |
| 9 | Coordina.. | | 0.000 | - | 0.000 | | | 0.000 | 0.000 | -0.316 |
| 10* | Standard | INSTR. DICHR.. | 6.367E+004 | 0.000 | | 23.039 | 0.000 | | | |
| 11 | Coordina.. | | 0.000 | - | 0.000 | | | 0.000 | 0.000 | 0.316 |
| 12 | Standard | Infinity | -12.000 | T | 0.000 | U | 0.000 | | | |
| 13 | Coordina.. | | 12.000 | P | - | 0.000 | | 0.000 | 0.000 | 45.000 |
| 14 | Coordina.. | | 0.000 | - | 0.000 | | | 0.000 | 3.656 | 0.244 |
| 15 | Standard | Infinity | 307.418 | | 0.000 | U | 0.000 | | | |

Table 24. NIX warm optics prescriptions.

| Surf>Type | Comment | Radius | Thickness | Glass | Semi-Diameter | Conic | Par 0 (unused) | Par 1 (unused) | Par 2 (unused) | Par 3 (unused) | Par 4 (unused) |
|-----------|------------|----------------|------------|------------|---------------|----------|----------------|----------------|----------------|----------------|----------------|
| OBJ | Standard | Infinity | Infinity | | Infinity | 0.000 | | | | | |
| 1 | Atmosphe.. | Atmosphere | Infinity | 0.000 | 4066.560 | 0.000 | | 0.000 | 2635.430 | 283.000 | 750.000 |
| 2 | Standard | Infinity | 1.300E+004 | | 4066.560 | 0.000 | | | | | |
| 3 | Standard | VLT-M1 | -2.88E+004 | -1.24E+004 | MIRROR | 4064.207 | -1.005 | | | | |
| * | Standard | VLT-M2 (DSM) | -4553.571 | 1.242E+004 | P MIRROR | 558.000 | U | -1.742 | | | |
| 5 | Standard | VLT-M1 HOLE | Infinity | 2250.000 | | 117.656 | 0.000 | | | | |
| 6 | Standard | CASSEGRAIN F.. | Infinity | 185.000 | | 38.104 | 0.000 | | | | |
| 7 | Coordina.. | | 0.000 | - | 0.000 | | | 0.000 | 0.000 | -45.000 | 0.000 |
| 8* | Standard | INSTR. DICHR.. | Infinity | 12.000 | CAF2 | 39.648 | 0.000 | | | | |
| 9 | Coordina.. | | 0.000 | - | 0.000 | | | 0.000 | 0.000 | -0.316 | 0.000 |
| 10* | Standard | INSTR. DICHR.. | 6.367E+004 | 0.000 | | 43.450 | 0.000 | | | | |
| 11 | Coordina.. | | 0.000 | - | 0.000 | | | 0.000 | 0.000 | 0.316 | 0.000 |
| 12 | Standard | Infinity | -12.000 | T | 0.000 | U | 0.000 | | | | |
| 13 | Coordina.. | | 12.000 | P | - | 0.000 | | 0.000 | 0.000 | 45.000 | 0.000 |
| 14 | Coordina.. | | 0.000 | - | 0.000 | | | 0.000 | 3.637 | 0.242 | 0.000 |
| 15 | Standard | Infinity | 67.800 | | 0.000 | U | 0.000 | | | | |
| 16 | Coordina.. | | 0.000 | - | 0.000 | | | 0.000 | 0.000 | 7.574E-004 | V |
| 17* | Standard | NIX SELECTOR.. | Infinity | 0.000 | MIRROR | 40.000 | U | 0.000 | | | |
| 18 | Coordina.. | | -239.549 | - | 0.000 | | | 0.000 | 0.000 | 7.574E-004 | P |

Table 25. LGS WFS warm optics prescriptions.

| Surf>Type | Comment | Radius | Thickness | Glass | Semi-Diameter | Conic | Far 0 (unused) | Decenter X | Decenter Y | Tilt About X | Tilt About Y |
|-----------|------------|----------------|------------|-------|---------------|--------|----------------|------------|------------|--------------|--------------|
| OBJ | Standard | Infinity | 1.275E+008 | | 1546.596 | 0.000 | | | | | |
| 1 | Atmosphe.. | Atmosphere | Infinity | | 4045.165 | 0.000 | | 0.000 | 2635.430 | 283.000 | 750.000 |
| 2 | Standard | Infinity | 1.300E+004 | | 4045.165 | 0.000 | | | | | |
| 3 | Standard | VLT-M1 | -2.88E+004 | | 4045.415 | -1.005 | | | | | |
| * | Standard | VLT-M2 (DSM) | -4553.571 | | 558.000 | -1.742 | | | | | |
| 5 | Standard | VLT-M1 HOLE | Infinity | | 104.887 | 0.000 | | | | | |
| 6 | Standard | CASSEGRAIN F.. | Infinity | | 23.028 | 0.000 | | | | | |
| 7 | Coordina.. | | 0.000 | | 0.000 | | | 0.000 | 0.000 | -45.000 | 0.000 |
| 8* | Standard | INSTR. DICHR.. | Infinity | | 23.919 | 0.000 | | | | | |
| 19 | Coordina.. | | -80.000 | | 0.000 | | | 0.000 | 0.000 | -45.000 | 0.000 |
| 20* | Standard | TELECENTRIC .. | Infinity | | 45.000 | U | | | | | |
| 21* | Standard | TELECENTRIC .. | 7666.000 | | 45.000 | F | | | | | |
| 22 | Coordina.. | | 0.000 | | 0.000 | | | 0.000 | 0.000 | 0.000 | -17.000 |
| 23* | Standard | WFS DICHOIC.. | Infinity | | 42.000 | U | | | | | |
| 24* | Standard | WFS DICHOIC.. | Infinity | | 42.000 | U | | | | | |
| 25 | Coordina.. | | -12.000 | | 0.000 | | | 0.000 | 0.000 | 0.000 | 17.000 |
| 26 | Standard | | Infinity | | 8.907 | 0.000 | | | | | |
| 27 | Coordina.. | | 0.000 | | 0.000 | | | 1.254 | 0.000 | 0.000 | -32.000 |
| 28* | Standard | WFS-FM | Infinity | | 10.000 | U | | | | | |
| 29 | Coordina.. | | 62.599 | | 0.000 | | | 0.000 | 0.000 | 0.000 | -32.000 |
| 30 | Coordina.. | CR-SHIFT | 0.000 | | 0.000 | | | 0.000 | 0.000 | 0.000 | 0.000 |
| 31 | Standard | (FOCAL PLANE) | Infinity | | 1.332 | 0.000 | | | | | |
| 32 | Standard | WFS-T INTERF.. | Infinity | | 11.382 | 0.000 | | | | | |

Table 26. NGS WFS warm optics prescriptions.

| Surf>Type | Comment | Radius | Thickness | Glass | Semi-Diameter | Conic | Far 0 (unused) | Decenter X | Decenter Y | Tilt About X | Tilt About Y |
|-----------|------------|----------------|------------|-------|---------------|--------|----------------|------------|------------|--------------|--------------|
| OBJ | Standard | Infinity | 1.275E+008 | | 1546.596 | 0.000 | | | | | |
| 1 | Atmosphe.. | Atmosphere | Infinity | | 4045.165 | 0.000 | | 0.000 | 2635.430 | 283.000 | 750.000 |
| 2 | Standard | Infinity | 1.300E+004 | | 4045.165 | 0.000 | | | | | |
| 3 | Standard | VLT-M1 | -2.88E+004 | | 4045.415 | -1.005 | | | | | |
| * | Standard | VLT-M2 (DSM) | -4553.571 | | 558.000 | -1.742 | | | | | |
| 5 | Standard | VLT-M1 HOLE | Infinity | | 104.887 | 0.000 | | | | | |
| 6 | Standard | CASSEGRAIN F.. | Infinity | | 23.028 | 0.000 | | | | | |
| 7 | Coordina.. | | 0.000 | | 0.000 | | | 0.000 | 0.000 | -45.000 | 0.000 |
| 8* | Standard | INSTR. DICHR.. | Infinity | | 23.919 | 0.000 | | | | | |
| 19 | Coordina.. | | -80.000 | | 0.000 | | | 0.000 | 0.000 | -45.000 | 0.000 |
| 20* | Standard | TELECENTRIC .. | Infinity | | 45.000 | U | | | | | |
| 21* | Standard | TELECENTRIC .. | 7666.000 | | 45.000 | F | | | | | |
| 33 | Coordina.. | | 0.000 | | 0.000 | | | 0.000 | 0.000 | 0.000 | -17.000 |
| 34* | Standard | WFS DICHOIC.. | Infinity | | 42.000 | U | | | | | |
| 35 | Coordina.. | | 84.969 | | 0.000 | | | 0.000 | 0.000 | 0.000 | -17.000 |
| 36 | Standard | FOCAL PLANE | -1843.206 | | 31.612 | 0.000 | | | | | |
| 37 | Standard | WFS-R INTERF.. | Infinity | | 41.683 | 0.000 | | | | | |

The IR/VIS dichroic

The average angle of incidence is 45 degree. To correct for the astigmatism introduced on the transmitted beam, the rear surface of the dichroic has a small curvature and wedge. The required wavelengths in transmission ask for infrared materials. CaF2 seems a best compromise in term of refraction index, transmissivity, availability with proper homogeneity, and reasonable cost. Other materials have been investigated and dropped off, including ZnSe and Sapphire. ZnSe is sensitive to moist air, while Sapphire has high emissivity in M band.

A trade-off study between a cylinder vs. a sphere surface on the rear side of the dichroic compared manufacturability and performances of the two solutions. Table 37 (page 103) shows the characteristics and performances of the two different solutions. Performances are quite similar (Strehl ratio), and alignment sensitivities (Table 42, page 110) are low in both cases. The solution with the sphere surface has been selected as baseline for a relative advantage in manufacturing and test. Table 27 shows a preliminary list of specification for the baseline dichroic.

A preliminary feasibility and cost inquiry has been done with potential vendors, based on the preliminary specification given in Table 27. Very few of them are able to meet specifications and/or are willing to take the risk due to the very fragile behavior of the CaF2. For this reason, **early procurement of this component, or allow for some prototyping activity is strongly suggested.**

| | | |
|----------------------------|---|--|
| ERIS Consortium | ERIS Documentation Standards | Doc.-Ref. : VLT-TRE-ERI-14403-3001 Issue : 1.0 Date : 05.12.15 Page : 62 of 136 |
|----------------------------|---|--|

Table 27. WFS dichroic preliminary specifications.

| <i>Requirement</i> | Specification | Comment |
|--|-------------------------------------|--|
| <i>Substrate shape</i> | Plano circular | |
| <i>Diameter</i> | 110 mm | |
| <i>Clear Aperture</i> | >100 mm | |
| <i>Central thickness</i> | 12 mm | |
| <i>Substrate material</i> | CaF2 | |
| <i>Substrate wedge</i> | 19 arcmin | To correct for astigmatism |
| <i>Substrate rear side radius of curvature</i> | 64 meter Concave | To correct for astigmatism |
| <i>Coating type</i> | Dichroic on front + AR on rear side | |
| <i>Working angle of incidence</i> | 45 deg | |
| <i>F/number</i> | 13.6 | |
| <i>Transition wavelength</i> | 1000 nm | |
| <i>Average un-polarized reflectance</i> | >90% (goal 95%) 500-900 nm | 450-900 nm as a goal |
| <i>Average un-polarized transmittance</i> | >90% (goal 95%) 1.1-5.4 um | Feasible below 3.0 um, -5% above |
| <i>Absolute un-polarized transmittance</i> | >85% (goal 90%) 1.1-5.4 um | Feasible below 3.0 um, -5% above |
| <i>Storage temperature</i> | -30 +55 degC | |
| <i>Functional temperature</i> | -10 +30 degC | |
| <i>Humidity</i> | <95% RH (non condensing) | |
| <i>Durability</i> | As per MIL-C-48497 | |
| <i>Emissivity</i> | - | <5% at 3-4 um <10% at 4-5 um <50% above 5.5 um |

Telecentric lens

This is a plano-convex lens with EFL=14942 mm to place the telescope exit pupil at infinity. It is placed just after the WFS dichroic. Table 28 gives the preliminary set of specifications.

After the telecentric lens the F/number changes to 13.4 and the plate scale is 0.528 arcsec/mm for both NGS and LGS focal plane.

Table 28. Telecentric lens preliminary specifications.

| <i>Requirement</i> | Specification | Comment |
|------------------------|----------------------|----------------|
| <i>Substrate shape</i> | Circular | |

| | | | |
|------------------------|-------------------------------------|------------------------------------|--|
| ERIS Consortium | ERIS Documentation Standards | Doc.-Ref. Issue Date Page | : VLT-TRE-ERI-14403-3001 : 1.0 : 05.12.15 : 63 of 136 |
|------------------------|-------------------------------------|------------------------------------|--|

| | | |
|----------------------------------|---------------------------|----------------------|
| <i>Diameter</i> | 90 mm | |
| <i>Clear Aperture</i> | >80 mm | |
| <i>Central thickness</i> | 10 mm | |
| <i>Material</i> | N-Bk7 | |
| <i>Front Radius of curvature</i> | Infinity | |
| <i>Rear radius of curvature</i> | 7666 mm | |
| <i>Coatings</i> | A/R, R<0.5% at 500-900 nm | 450-950 nm as a goal |

NGS/LGS dichroic beam-splitter

After the telecentric lens, a second dichroic reflects the light to the NGS WFS optics and transmits it to the LGS WFS optics. After trade-off, the design has been simplified to a plano-plano beam-splitter, introducing a small astigmatism of 57 nm RMS, not dependent on LGS distance from focus. Table 29 gives the preliminary list of specifications. This beam-splitter acts as a dichroic notch filter, to transmit the sodium LGS light only. Wavelengths below the notch are still used by the NGS WFS for target acquisition (see also Section 4.8.4).

Table 29. NGS/LGS dichroic preliminary specifications.

| Requirement | Specification | Comment |
|---|--|------------------------|
| <i>Substrate shape</i> | Plano circular | |
| <i>Diameter</i> | 84 mm | |
| <i>Clear Aperture</i> | >76 mm | |
| <i>Central thickness</i> | 12 mm | |
| <i>Substrate material</i> | N-BK7 | |
| <i>Coating type</i> | Dichroic on front + AR on rear side | |
| <i>Working angle of incidence</i> | 17 deg | |
| <i>F/number</i> | 13.6 | |
| <i>Average un-polarized reflectance</i> | >90% (goal 95%) 610-900 nm >90% (goal 95%) 500-570 nm | (450-570 nm as a goal) |
| <i>Average un-polarized transmittance</i> | >90% (goal 95%) 585-595 nm | |

NIX Selector Mirror

The science beam can be switched between NIX and SPIFFI by a motorized flat folding mirror. Table 30 gives its characteristics.

Table 30. NIX Selector Mirror

| <i>Requirement</i> | <i>Specification</i> | <i>Comment</i> |
|-----------------------------------|------------------------------------|----------------|
| <i>Substrate shape</i> | Plano circular | |
| <i>Diameter</i> | 85 mm | |
| <i>Clear Aperture</i> | >74 mm | |
| <i>Substrate material</i> | Zerodur or equivalent | |
| <i>Coating type</i> | Protected Silver or Protected Gold | |
| <i>Working angle of incidence</i> | 45 deg | |

4.8.3 WFS Optics

This includes all the optical elements between the Warm Optics and the specialized WFS optics. The LGS and NGS WFS have the same optical design, to increase modularity, share spare parts and decrease cost.

Figure 36 shows the overall layout of the NGS WFS, used also as a reference for the description of the optical components.

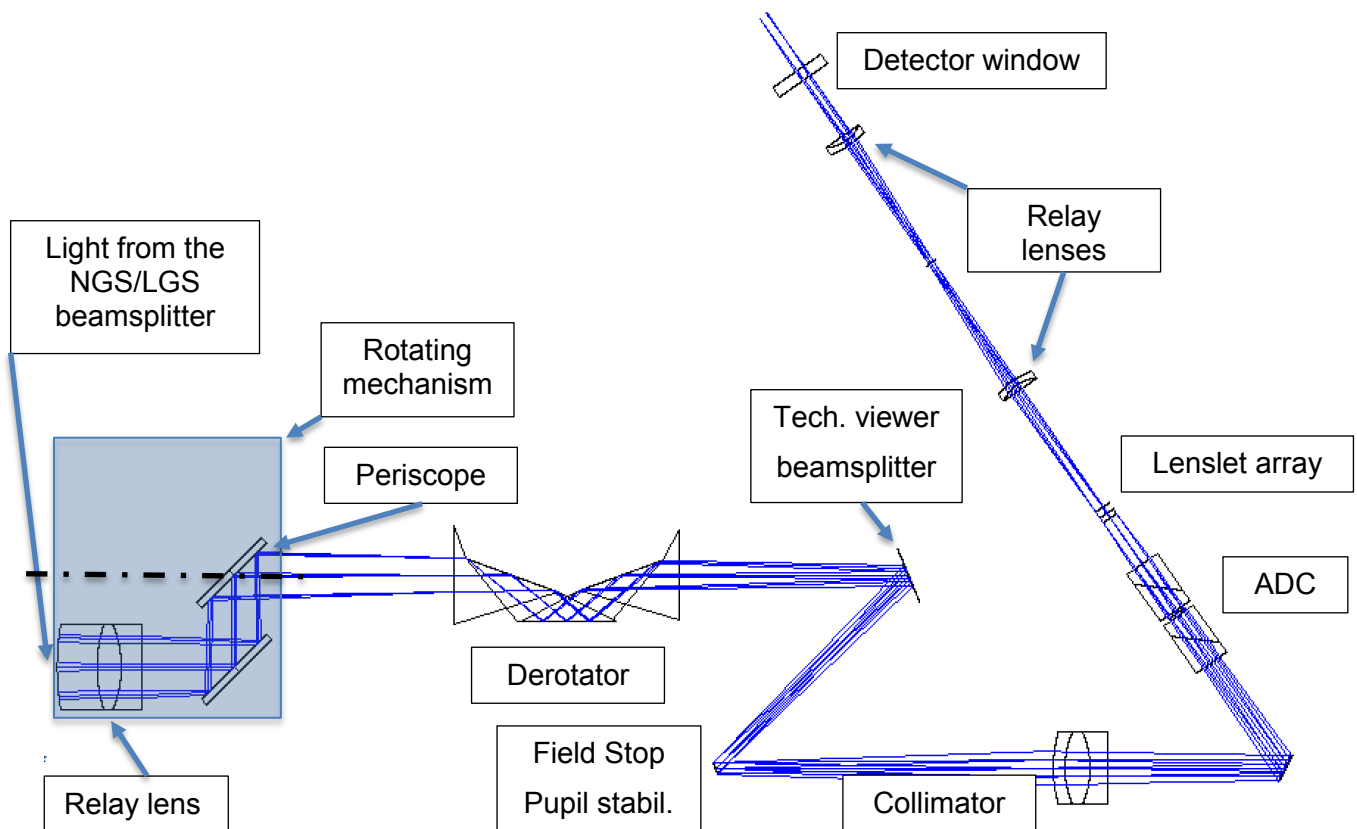


Figure 36 Layout of the NGS WFS optics.

| | | |
|----------------------------|---|--|
| ERIS Consortium | ERIS Documentation Standards | Doc.-Ref. : VLT-TRE-ERI-14403-3001 Issue : 1.0 Date : 05.12.15 Page : 65 of 136 |
|----------------------------|---|--|

Relay lens (LGS and NGS)

A triplet intercepts the incoming beam from the LGS/NGS beamsplitter and it refocuses it to F/20. It creates space for the periscope, an Abbe derotator and a field technical viewer. The lens focal length is 160 mm, and a 12 mm diameter pupil is generated 141 mm from the rear surface. The pupil longitudinal position produced by the Relay Lens does not change with the LGS or NGS WFS stage refocusing because of the input beam is telecentric.

This lens is attached to the periscope rotation mechanism, in order to patrol the field of view in coordination with the X stage. During the final design phase, we shall verify if it is better to have a lens cemented on the entrance surface of the periscope, in order to reduce the air-glass interfaces and reduce the size and complexity of the rotation mechanism itself.

Table 31. Relay lens prescription data.

| Surf:Type | Comment | Radius | Thickness | Glass | Semi-Diameter |
|-----------|----------|-----------|-----------|----------|---------------|
| 2 | Standard | F/13.4 fp | Infinity | | 4.000 |
| 3* | Standard | L1 S1 | 88.028 | N-LASF31 | 15.000 U |
| 4* | Standard | L1 S2 | 47.843 | S-FPM2 | 15.000 P |
| 5* | Standard | L1 S3 | -38.072 | P-SK57Q1 | 15.000 P |
| 6* | Standard | L1 S4 | -330.334 | | 15.000 P |
| 7 | Standard | | Infinity | M | 5.965 |
| IMA | Standard | | Infinity | | 5.884 |

Periscope (NGS only)

A periscope patrols the NGS WFS across the telescope field of view together with an XY-stage. The periscope rotates around the exit optical axis. The combined motion of the rotation angle of the periscope and one axis of the XY-stage is able to cover the full ERIS field of view.

The current design is based onto a two-mirror solution, with two precise aligned flat mirrors, 32 mm diameter, and a deviation distance of 32 mm, for a 64 mm total range across the field (2 arcmin diameter). During the Final Design phase the deviation distance could be slightly increased to account for a possible offset of the effective field centre produced by the optical alignment of the NGS WFS unit with the Warm Optics (see Sec. 8.3).

During final design phase, a full glass solution will be studied for the Entrance Lens + periscope because of its better stability and a more compact solution.

Derotator prism (NGS and LGS)

A reversion prism (Abbe Rotator) perform the pupil derotation. Image rotation angle is twice the rotation angle of the device with respect the incoming beam axis.

The current design is a Bk7 glass system, with 70 degrees internal incidence angle on the first and third reflection surfaces, 50 degrees incidence angle on the second reflection, working in total internal reflection for maximum throughput. Total optical path length (in the glass) is 90 mm. The clear aperture is 12 mm diameter. The entrance surface of the prism is at the pupil image created by the relay triplet. The derotator can be manufactured as two prisms cemented together (see Figure 37).

| | | |
|---|--|--|
| <p style="text-align: center;">ERIS Consortium</p> | <p style="text-align: center;">ERIS Documentation Standards</p> | <p>Doc.-Ref. : VLT-TRE-ERI-14403-3001 Issue : 1.0 Date : 05.12.15 Page : 66 of 136</p> |
|---|--|--|

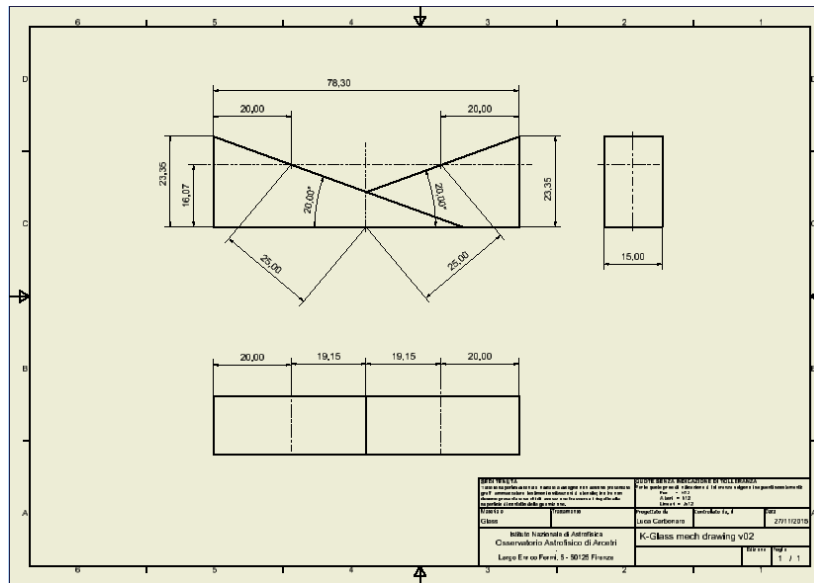


Figure 37 Abbe Rotator prism implementing the K-Mirror

Technical viewer beam-splitter (NGS and LGS)

After the derotator, a dichroic beam-splitter reflects light between 600 and 900 nm to the NGS WFS optics, and transmits shorter wavelengths to a small CCD camera used for field acquisition. With a typical pixel size of 7.4 μm , a typical CCD camera with 2kx2k pixels at the F/20 focal plane will see up to 19"x19" field with a plate scale of 9 mas/pixel. The maximum field of view is limited by the size of the other optical components, like the prism derotator. Currently a 15" diameter field is transmitted, during Final Design this parameter will be optimized.

Similar configuration is implemented in the LGS WFS using a regular beam splitter transmitting 10% of the laser light to the technical camera. The splitting ratio will be optimized in the next design phase.

Field stop – Pupil stabilizing mirror (NGS and LGS)

The field stop is placed at the F/20 focal plane, together with the pupil stabilizing mirror. The field stop can be performed by placing a mask just in front of the mirror, or by have the reflective coating on the required field of view only. The size of the field stop is 2.5" for the NGS WFS and 5.0" for the LGS WFS. The shape (circular or square) will be defined during the final design phase.

At the current F/20 focal ratio the plate scale is 773 $\mu\text{m}/\text{arcsec}$. The 2.5 arcsec FoV will project a 4.17x3.86 mm^2 aperture, rectangular in shape due to the 22.5 degree tilt angle of this mirror. The pupil is at 235 mm from the focal plane, so that the pupil motion sensitivity is 0.64 mrad/sub-aperture (40x40 sub-apertures case). A typical 1/10 sub-aperture resolution requirement will translate into a 64 μrad (13 arcsec) minimum resolution of this tip/tilt stage.

Collimator lens (NGS and LGS)

After the F/20 focal plane, a collimator lens will create a pupil image where lenslet arrays will be placed. This is a 115.2 mm focal length lens, in order to create a pupil of 5.76 mm diameter (or a 40 sub-apertures of 144 μm). Table 32 shows the lens prescription. The pupil is reimaged at 153 mm from the last lens surface, leaving enough space for the ADC in the NGS WFS case.

Table 32. Collimator lens prescription data.

| Comment | Radius | Thickness | Glass | Semi-Diameter |
|---------------|----------|-----------|---------|---------------|
| COLLIMATOR S1 | -45.180 | -4.066 | S-LAH75 | 12.700 U |
| COLLIMATOR S2 | -31.343 | -8.758 | PHM52 | 12.700 U |
| COLLIMATOR S3 | 31.629 | -6.029 | N-LAK8 | 12.700 U |
| COLLIMATOR S4 | Infinity | -62.000 | | 12.700 U |

4.8.4 NGS Wavefront Sensor specific optics

The optics following the Collimator lens are specific for each WFS. Here the NGS WFS specific ones are described.

ADC

The atmospheric dispersion corrector is based on two counter-rotating Amici dispersion prisms with apex angles of 42 degree, placed near the pupil provided by the collimator lens, to correct up to 70 degrees zenith angle. The selected glass pair is Schott N-LaK7 and BPH5 (now obsolete). This glass selection will be revised again during final design phase, to improve manufacturability.

High Order and Low Order WFS

The current NGS WFS is based onto a Shack-Hartmann design. The optics delivers a 5.76 mm circular pupil. In order to exchange between the high-order mode (40x40 sub-apertures across the pupil) and the low-order mode, two lenslet arrays will be interchanged at this pupil plane.

After the lenslet arrays, two lenses will relay the lenslet focal plane to the detector at the given plate scale. Detector pixel is 24 micron square. Two different relay optics have been designed, to optimize performances and make the exchange system relatively simple. See the mechanical section for a description of the exchange mechanism.

Relay optics and switching

In the high-order mode, the very short focal length of the microlens requires some extra lenses to relay the spot patterns onto the detector. A pair of identical doublets in a 1:1, 4-f, configuration will provide this relay system. Figure 38 shows the layout of the relay lenses. The total length between the lenslet array and the output vertex of the 2nd doublet is about 170 mm.

In low-order mode, the lenslet will be exchanged onto the same pupil plane and a separate set of relay lenses will deliver the lenslet focal plane onto the detector, without any displacement of the detector focus position. The current solution foresees a third identical doublet, near the lenslet, to replace the first doublet, while the second one in front of the detector will remain unchanged. This choice allows to have a simple exchange mechanism with a short barrel hosting the lenslet and the first doublet, while the second doublet is mounted near the detector. As a conservative approach during Preliminary Design, we opted for a full length barrel, hosting also the second doublet. During Final Design we shall make a proper trade-off between space envelope, alignment tolerances, repositioning tolerances. In the current design the full length barrel is 170mm length and the distance of the SH spots to the vertex of the 1st doublet is 50 mm. More details are given in Sec. 4.9.2.10. A preliminary sensitivity to barrel motion will affect the spot centroid positions is computed and results are given in Section 7.2.2.

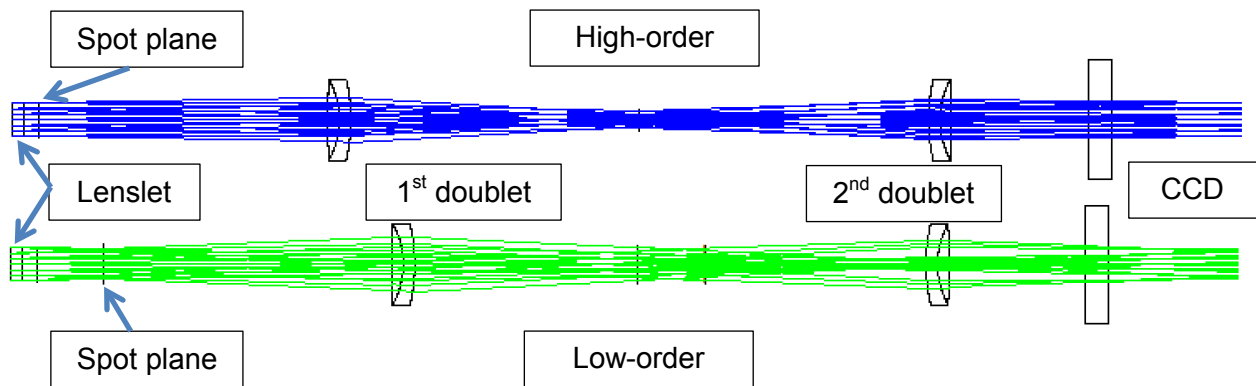


Figure 38. Lenslet relay lenses.

Microlens array

Two lenslet arrays will sample the pupil image of the telescope entrance aperture. All the major parameters are summarized in Table 33 for the HO and LO NGS SH. The pixel sampling of the FoV and lenslet design in the LO case is not yet optimized; however the modular design of the relay allows us to easily implement this change.

Table 33. Lenslet parameters.

| <i>Requirement</i> | NGS LO | NGS HO | LGS HO |
|-----------------------------------|---------------|---------------|---------------|
| | 2x2 | 40x40 | 40x40 |
| <i>Lenslet pitch (um)</i> | 2880 | 144 | 144 |
| <i>Focal length (mm)</i> | 11.2 | 8.4 | 4.2 |
| <i>F/ratio</i> | 3.9 | 59 | 29 |
| <i>Plate scale (arcsec/pixel)</i> | 0.31 | 0.42 | 0.83 |

4.8.5 LGS Wavefront Sensor

The LGS wavefront sensor optics shares most of the same optical components of the NGS WFS. Figure 39 shows the LGS optical components on board of the focusing motorized stage. No field patrolling is required. The first optical component is a relay triplet, identical to the one of the NGS WFS, that delivers a F/20 beam. A prism derotator is near the pupil image. Close to the focus, a tilted plate 10:90 beam-splitter sends 10% of the LGS light to a technical viewer for target acquisition and internal calibrations. A 5" field-stop and pupil stabilizer mirror is placed at the focus. A collimator lens will project a 5.76 mm diameter pupil image onto the lenslet array, with 40x40 sub-apertures (144 um lenslet pitch). The lenslet is placed within the detector head and pre-aligned by ESO with respect the CCD.

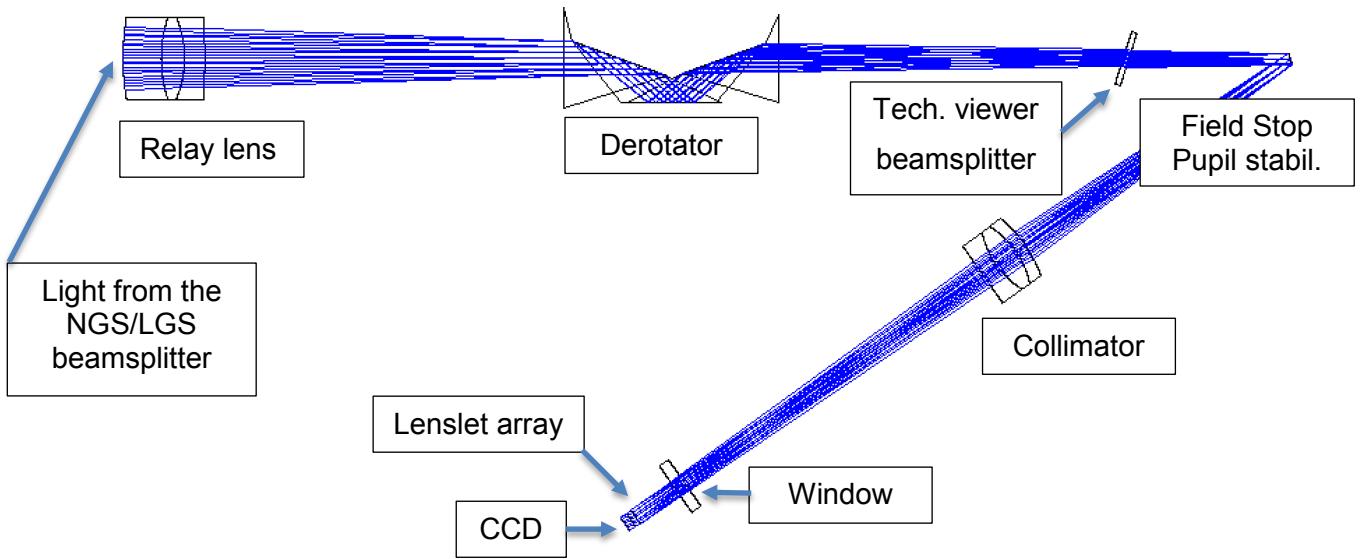


Figure 39. LGS wavefront sensor optics.

4.8.6 AO DM Simulator

This unit has been designed as a verification test tool during integration, alignment and verification phases, to produce known aberrations into the system that will be measured by the AO WFS units. It enables functional tests of many subsystems, including AO control loop. A commercial ALPAO deformable mirror (DM) will be used to simulate different aberration modes (low- to moderate order) with different amplitudes. A projection system will mimic the VLT optical interface.

Figure 40 shows the optical layout of the DM simulator. Two COTS (from Edmund Optics) off-axis parabola (OAP1, OAP2) works in a 1:1 relay system to create a collimated beam. The deformable mirror is on the 20 mm diameter pupil created by the first OAP. A pupil mask can reproduce the VLT pupil shape and size. A pinhole (or a monomode fiber) source will inject light into the system. The two parabola works at F/6.75. After the intermediate focal plane, a spherical mirror will create a F/13.7 beam to match the VLT focal ratio. A 45 degree folding mirror will direct light inside ERIS. A small hole in this folding mirror allows the light to pass through. The size of this hole is smaller than the secondary mirror projected shadow of the VLT, so no real vignetting of the simulated telescope exit pupil is created. Table 34 gives the optical prescriptions of the system.

The amount of spherical aberration introduced by the spherical relay mirror is only 16 nm RMS for a simulated NGS source. Mostly, this is a spherical aberration that can be removed by the DM. A small beam-splitter near the entrance focal plane allows to feed the system with both a NGS source and a LGS (589 nm) source at a given altitude. Figure 41 shows the two sources focal planes, for an LGS at 160 km. Fibers will inject light.

A preliminary assembly of the AO DM Simulator optical bench and its interface with the ERIS central structure is reported in the AO MAIV plan document (AD7).

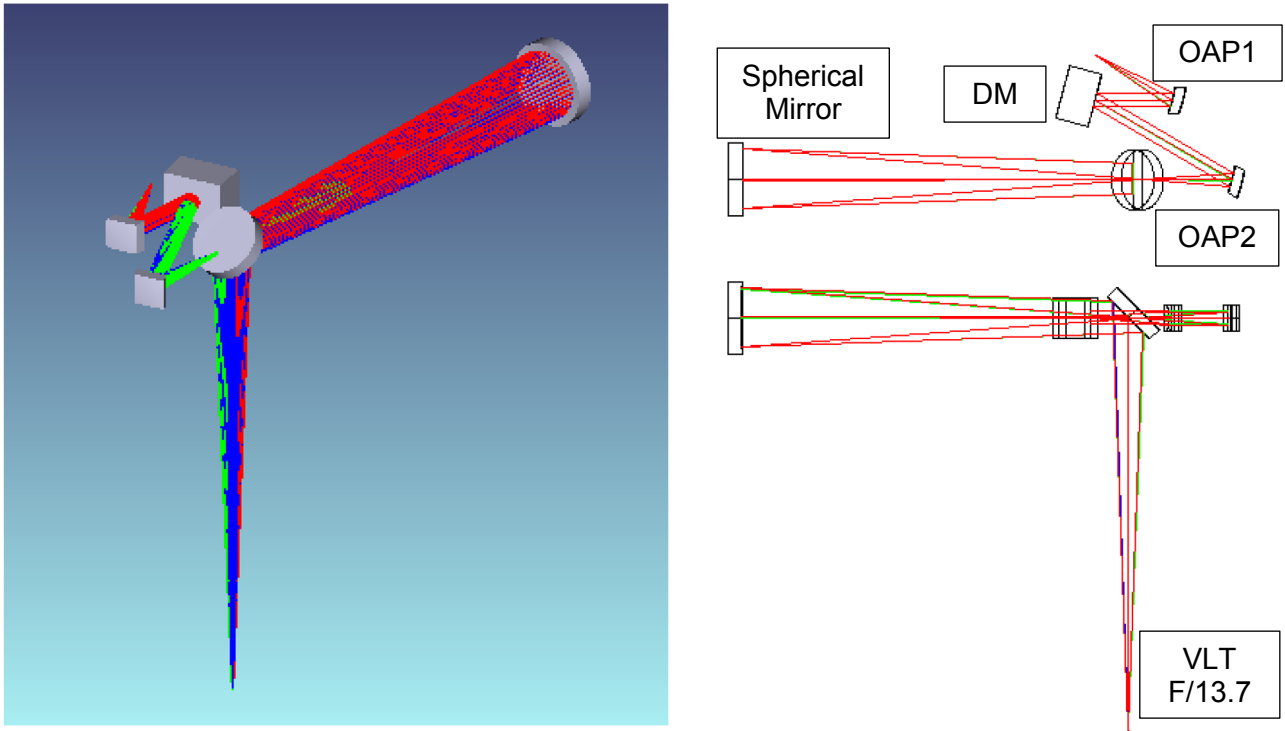


Figure 40. AO DM simulator optics.

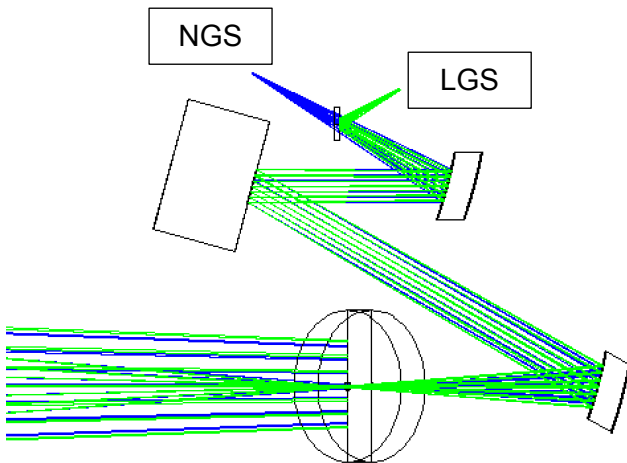


Figure 41. NGS and LGS sources injection.

Table 34. AO DM simulator optics prescriptions.

| Surf>Type | Comment | Radius | Thickness | Glass | Semi-Diameter | Conic | Par 0 (unused) | Decenter X | Decenter Y | Tilt About X | Tilt About Y |
|-----------|------------|--------------------|--------------|--------------|---------------|----------|----------------|------------|------------|--------------|--------------|
| OBJ | Standard | Infinity | -6.75E+005 | | 0.500 | 0.000 | | | | | |
| STO | Standard | Infinity | 6.754E+005 F | | 5.000E+004 U | 0.000 | | | | | |
| 2 | Standard | fiber | 0.000 | | 0.500 | 0.000 | | | | | |
| 3 | Standard | LGS fiber refocus | Infinity | | 0.500 | 0.000 | | | | | |
| 4 | Coordina.. | | -60.000 | - | 0.000 | | | 0.000 | 0.000 | 0.000 | 0.000 |
| 5 | Coordina.. | | 0.000 | - | 0.000 | | | 0.000 | 0.000 | 30.000 | 0.000 |
| 6* | Standard | beam-splitter | Infinity | MIRROR | 10.000 U | 0.000 | | | | | |
| 7 | Coordina.. | | -60.000 | - | 0.000 | | | 0.000 | 0.000 | 30.000 | 0.000 |
| 8 | Coordina.. | | 125.000 | - | 0.000 | | | 0.000 | 0.000 | -30.000 | 0.000 |
| 9* | Standard | OAP1 | -250.000 | MIRROR | 76.992 | -1.000 | | | | | |
| 10 | Coordina.. | | -125.000 | - | 0.000 | | | 0.000 | -66.987 C | 0.000 | 0.000 |
| 11 | Coordina.. | | 0.000 | - | 0.000 | | | 0.000 | 0.000 | 15.000 | 0.000 |
| 12 | Zernike .. | DM | Infinity | MIRROR | 10.357 | 0.000 | 1 | 0.000 | 0.000 | 0.000 | 0.000 |
| 13* | Standard | DM box | Infinity | 1.00,0.0 | 10.357 | 0.000 | | | | | |
| 14* | Standard | DM box | Infinity | F | 23.815 | 0.000 | | | | | |
| 15 | Standard | | Infinity | | 10.357 | 0.000 | | | | | |
| 16 | Coordina.. | | 246.300 | - | 0.000 | | | 0.000 | 0.000 | 15.000 F | 0.000 |
| 17 | Coordina.. | | 0.000 | - | 0.000 | | | 0.000 | -66.987 F | 0.000 | 0.000 |
| 18* | Standard | OAP2 | -250.000 | MIRROR | 76.798 | -1.000 | | | | | |
| 19 | Coordina.. | | 0.000 | - | 0.000 | | | 0.000 | 0.000 | -30.000 F | 0.000 |
| 20 | Standard | | Infinity | | 0.520 | 0.000 | | | | | |
| 21 | Standard | | Infinity | F | 1.736 | 0.000 | | | | | |
| 22 | Standard | | Infinity | | 0.520 | 0.000 | | | | | |
| 23 | Coordina.. | LGS sphere refocus | 0.000 | - | 0.000 | | | 0.000 | 0.000 | 0.000 | 0.000 |
| 24* | Standard | Spherical M | 801.985 | F | MIRROR | 55.000 U | 0.000 | | | | |
| 25 | Coordina.. | | 585.000 F | - | 0.000 | | | 0.000 | 0.000 | 0.000 | 0.000 |
| 26 | Coordina.. | | 0.000 | - | 0.000 | | | 0.000 | 0.000 | 0.000 | 45.000 |
| 27* | Standard | FOLD M | Infinity | MIRROR | 45.000 U | 0.000 | | | | | |
| 28* | Standard | hole obstrc | Infinity | | 34.992 | 0.000 | | | | | |
| 29 | Coordina.. | | -123.651 | - | 0.000 | | | 0.000 | 0.000 | 0.000 F | 45.000 F |
| 30 | Standard | Cassegrain flange | Infinity | | 100.000 U | 0.000 | | | | | |
| 31 | Standard | VLT F/13.7 | Infinity | | 1.052 | 0.000 | | | | | |
| 32 | Standard | LGS focus | Infinity | 1.512E+004 U | 1.052 | 0.000 | | | | | |
| 33 | Standard | exit pupil | Infinity | -1.51E+004 F | 567.253 | 0.000 | | | | | |
| IMA | Standard | | Infinity | - | 1.052 | 0.000 | | | | | |

4.9 Mechanical Design

In this section we report the mechanical design of the WO and WFS units.

4.9.1 Warm Optics

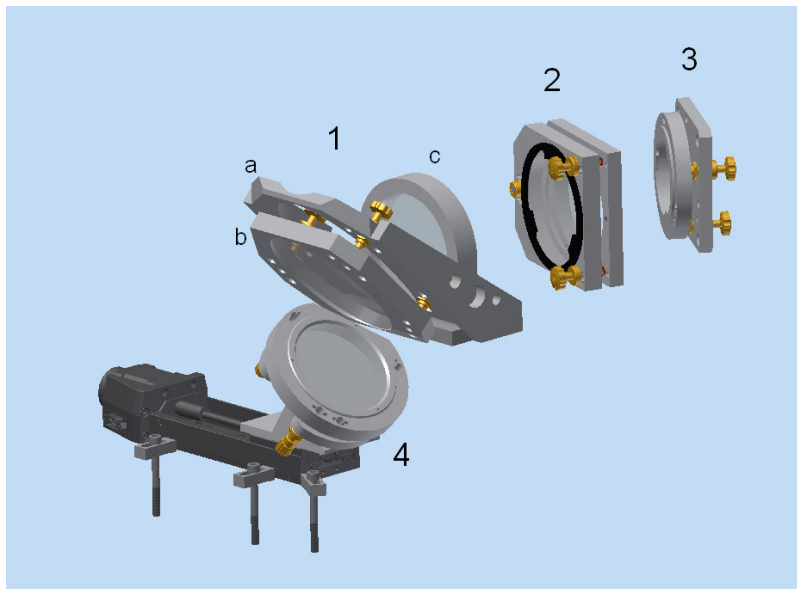


Figure 42 Warm optics components

The Warm Optics Assembly (see Figure 42) consists of 4 main components holding 5 optical elements. All of the components provide a Tip Tilt and Piston adjustment via three micrometric screws

| | | | |
|-----------------|------------------------------|-----------|--------------------------|
| ERIS Consortium | ERIS Documentation Standards | Doc.-Ref. | : VLT-TRE-ERI-14403-3001 |
| | | Issue | : 1.0 |
| | | Date | : 05.12.15 |
| | | Page | : 72 of 136 |

(Newport AJS100-0_5K) pushing on three kinematic references and secured by three pairs of retaining springs to ensure positional stability during operation and in the event of an earthquake.

The micrometric screws Newton AJS1004 coupled with cinematic inserts assure a minimum of 12.7 mm travel and, after adjustment, can be locked in position by a set screw lock (see Figure 44).

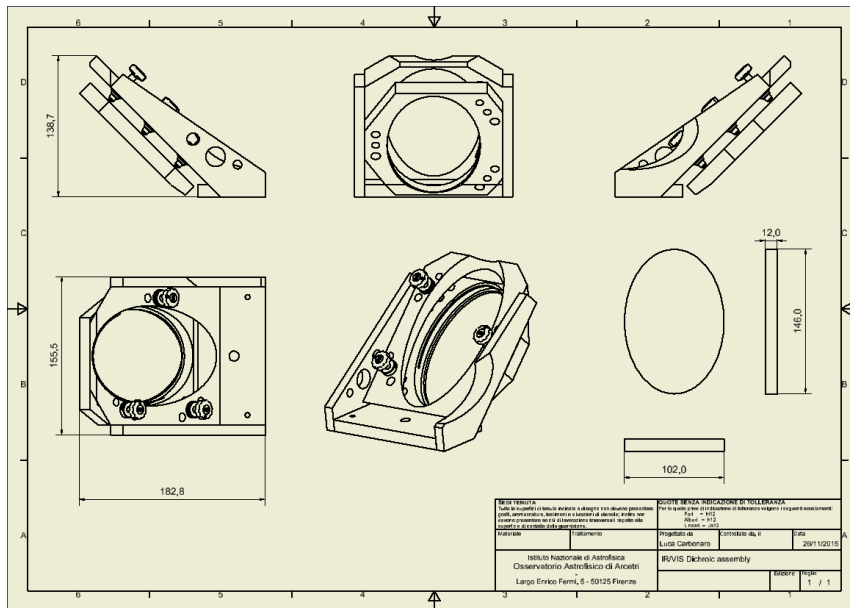


Figure 43: IR/VIS dichroic

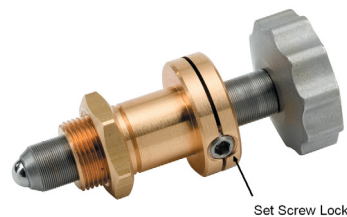


Figure 44. Newton AJS100-0.5K

- 1- **IR/VIS Dichroic assembly** – consisting in
 - a. A main mounting platform acting as a common interface for the Dichroic Holder and the Telecentric Lens Mount machined in Al6061-T6 black anodized and weighting 0.526 Kg

⁴ <http://search.newport.com/?x2=sku&q2=AJS100-0.5K>

| | | | |
|-------------------------------|--|--|--|
| <p>ERIS Consortium</p> | <p>ERIS Documentation Standards</p> | <p>Doc.-Ref. Issue Date Page</p> | <p>: VLT-TRE-ERI-14403-3001 : 1.0 : 05.12.15 : 73 of 136</p> |
|-------------------------------|--|--|--|

- b. The dichroic holder, weighting 0.252kg, adjustable in tip tilt and piston and realized in Al4032-T6 black anodized to match closely the CTE (see section 4.9.5) of the fragile 100x140 mm CaF2 optics component.
 - c. The Telecentric Lens Mount, in Al6061-T6 black anodized 0.329 in weight and adjustable only in clock due to the large positioning tolerances required.
- 2- VIS/VIS Dichroic mount – adjustable in Tip Tilt and Piston made of AL6061-T6 black anodized with a mass of about 0.60 Kg
- 3- Fold mirror mount - adjustable in Tip Tilt and Piston made of AL6061-T6 black anodized with a mass of about 0.45 Kg
- 4- NIX selector mirror consisting of:
 - a. NIX selector mirror mount adjustable in Tip Tilt and Piston made of AL6061-T6 black anodized with a mass of about 0.85 Kg
 - b. A PI-Micos PLS85⁵ precision linear stage with a travel range of 102 mm weighting 1.5kg with an unidirectional repeatability of 0.1um.

⁵ <http://www.pimicos.com/web2/en/1,4,150,pls85.html>

| | | | |
|------------------------|-------------------------------------|------------------------------------|--|
| ERIS Consortium | ERIS Documentation Standards | Doc.-Ref. Issue Date Page | : VLT-TRE-ERI-14403-3001 : 1.0 : 05.12.15 : 74 of 136 |
|------------------------|-------------------------------------|------------------------------------|--|

4.9.2 R-WFS - NGS HO/LO Wavefront Sensor

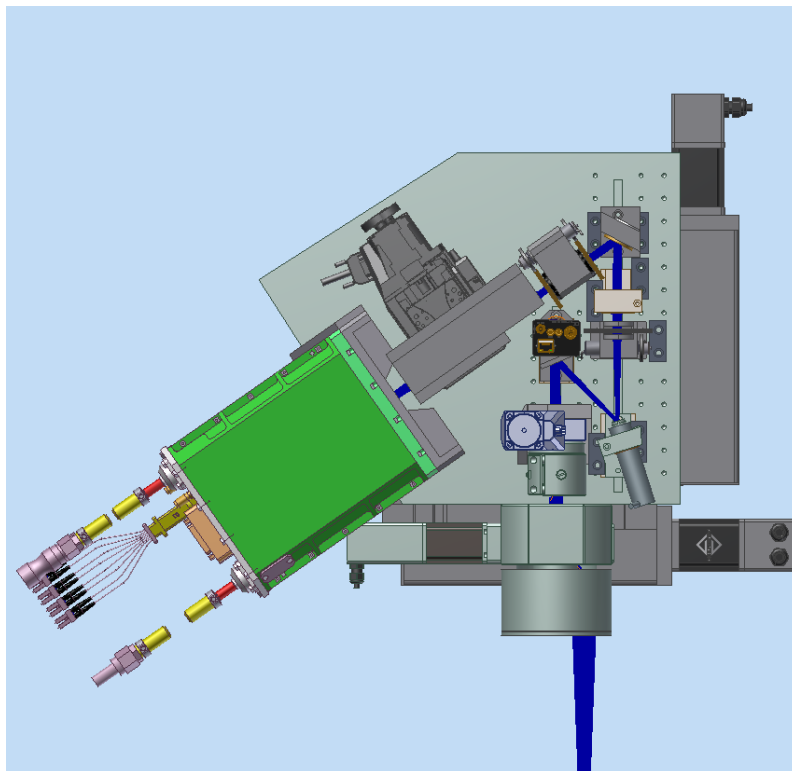
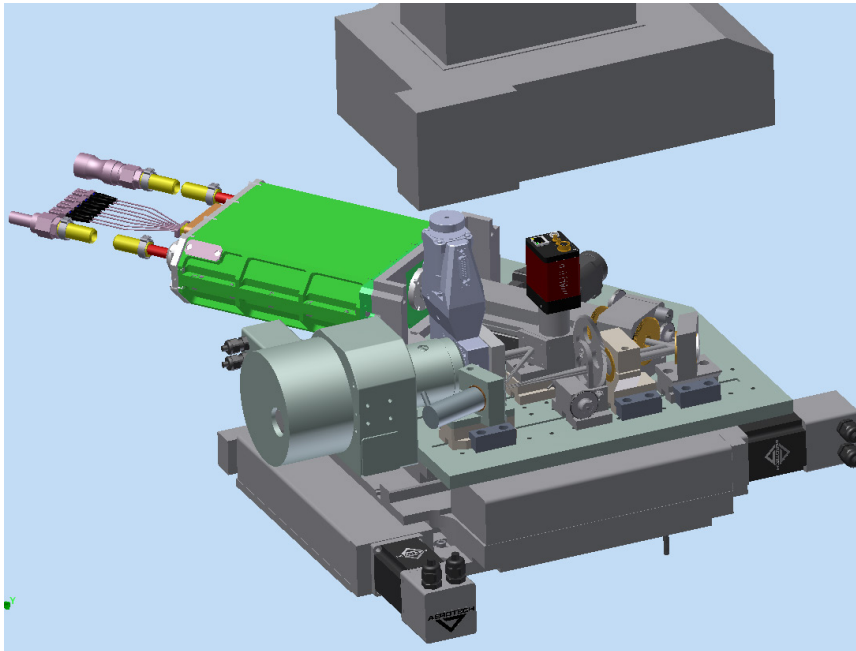


Figure 45 – Views of NGS WFS unit with cover removed

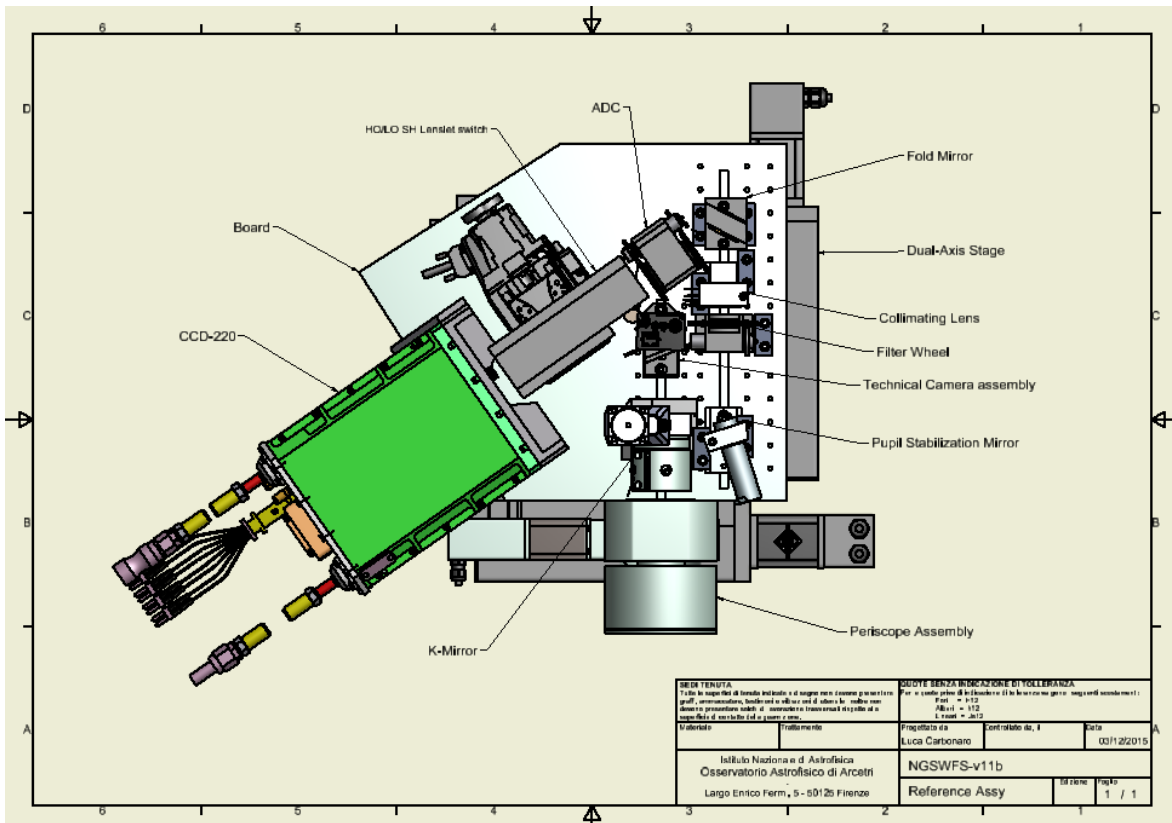
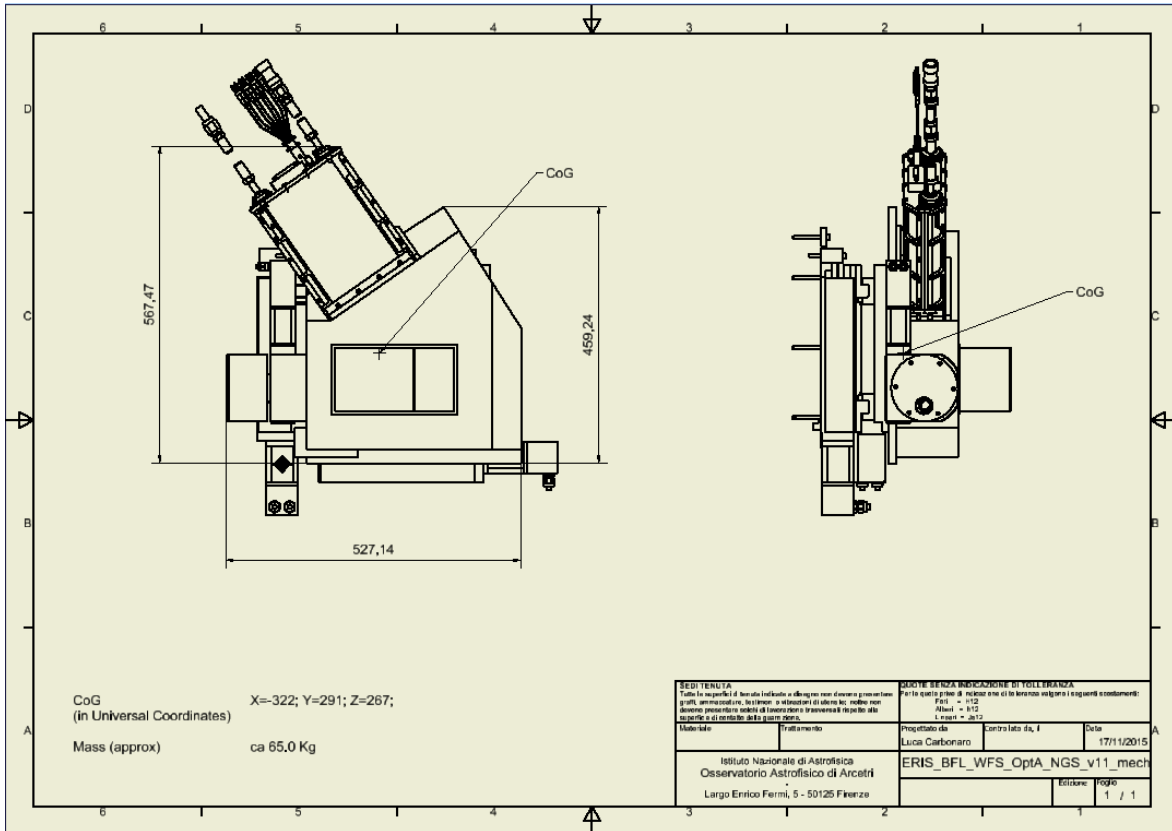


Figure 46 NGS WFS unit general dimensions and naming

The NGS WFS unit assembly consists of a base board (15mm thick aluminum plate) where all the components sits and a dual axis stage that will carry the board allowing field patrolling and focus. The optical axis of the system is located at 50mm above the board plane, provided of alignment rails and holes for the clampers securing the position stability of the components after the alignment. The rail and clamping mechanism has been experienced with success in the LBT-FLAO and Magellan AO WFS units.

The NGSWFS board sits atop a dual-axis stage to which is fixed by 6 M10 bolts. One reference pin and two adjustable reference points on the stage will be used during alignment to assure repeatability of positioning when the board is removed. All the optical components are enclosed in a 1.2mm aluminum plates shield structure bolted on top of the board.

Following sections describe the mechanics of the NGS WFS components in the order of the input beam.

4.9.2.1 Dual-axis stage

The WFS board sits on a dual-axis linear stage Aerotech ATS3610⁶ for focus compensation and field patrolling. The selection trade-off resulted in the choice of this stage due to the reduced vertical size with respect the other dual-axis stages on the market providing similar travel range and load capacitance.

The travel of this model is 100x100mm, covering the requirements (see Sec. 4.8.1). A complete customized analysis of our requirements in terms of stability and accuracy is currently in progress at Aerotech.

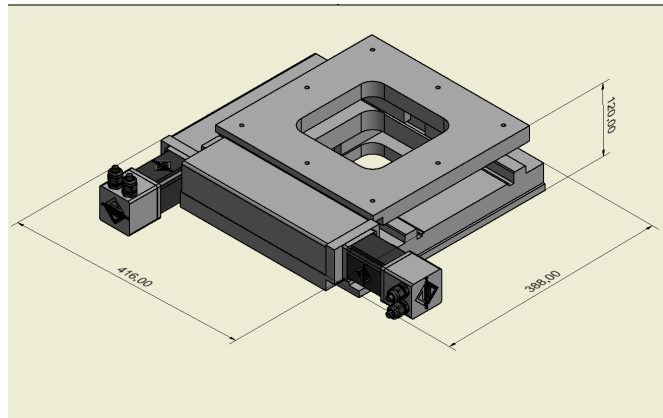


Figure 47 – Dual axis Aerotech stage

| Model | | ATS36210 |
|-------------------------------------|-------------------|--|
| Travel | | 100 mm |
| Drive System | | Brushless Servomotor (BMS60-A-D25-E1000ASH) |
| Bus Voltage | | Up to 160 VDC |
| Continuous Current | A_{pk} | Up to 2.3 A |
| | A_{rms} | Up to 1.6 A |
| Feedback | | Analog Sin/Cos 1Vpp Rotary Encoder (1000 line) |
| Resolution | LT Linear Encoder | 0.005 μ m - 1.0 μ m |
| Maximum Travel Speed ⁽¹⁾ | | 200 mm/s |
| Maximum Load ⁽²⁾ | | 90.0 kg |

⁶ <http://www.aerotech.com/product-catalog/stages/linear-x-y-stages/ats3600.aspx>

| | | | |
|------------------------|-------------------------------------|------------------------------------|--|
| ERIS Consortium | ERIS Documentation Standards | Doc.-Ref. Issue Date Page | : VLT-TRE-ERI-14403-3001 : 1.0 : 05.12.15 : 77 of 136 |
|------------------------|-------------------------------------|------------------------------------|--|

| Model | ATS36210 | | |
|-----------------------------|-------------------|----------------------|-------------------------------------|
| Accuracy | LT | HALAR ⁽³⁾ | ±2.0 µm (±80.0 µin) |
| | | Standard | ±4.0 µm |
| Bidirectional Repeatability | | | |
| | LT | | ±1.0 µm |
| Straightness and Flatness | Differential | | 1.0 µm/25mm |
| | Maximum Deviation | | ±2.0 µm |
| Pitch and Yaw | | | 10 arc sec |
| Nominal Stage Weight | Less Motor | | 22.8 kg |
| | With Motor | | 26.4 kg |
| Construction | | | Aluminum Body; Black Anodize Finish |

4.9.2.2 Periscope

The periscope is the opto-mechanical solution to vertically patrolling the field without using an additional vertical stage that would conflict with space restrictions and would reduce the overall assembly stiffness against gravity direction change. The periscope is composed by a mechanical mount hosting the WFS entrance lens and the two mirrors, implementing the optical periscope, and a rotary stage Aerotech AGR-50⁷. The Periscope assembly will be pre-aligned in laboratory and then integrated on the board.

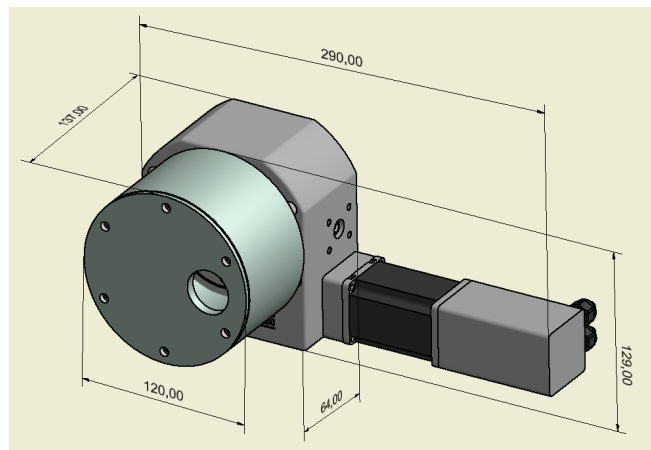


Figure 48 NGS-WFS Periscope Assembly

⁷ <http://www.aerotech.com/product-catalog/stages/rotary-stages/agr.aspx?p=%2fproduct-catalog%2fstages%2frotary-stage.aspx%3f>

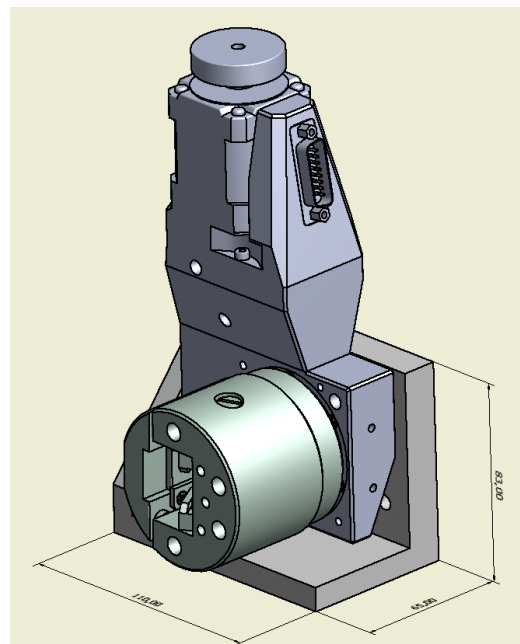
AGR Series SPECIFICATIONS

| Mechanical Specifications | | AGR50 | AGR75 | AGR100 | AGR150 | AGR200 |
|--|------------------------|--|--------------------------|--------------------------|-------------------------|-------------------------|
| Travel | | 360° (Limited Travel Versions Available) | | | | |
| Accuracy ⁽¹⁾ | Standard | 0.87 mrad (180 arc sec) | 0.58 mrad (120 arc sec) | | | |
| | Standard (HALAR) | 0.29 mrad (60 arc sec) | 0.24 mrad (50 arc sec) | | | |
| | Direct Encoder | 97 µrad (20 arc sec) | | | | |
| | Direct Encoder (HALAR) | 58 µrad (12 arc sec) | 49 µrad (10 arc sec) | | | |
| Repeatability (Uni-Directional) ⁽¹⁾ | Standard | 49 µrad (10 arc sec) | | | | |
| | Direct Encoder | 24 µrad (5 arc sec) | | | | |
| Repeatability (Bi-Directional) ⁽¹⁾ | Standard | 0.22 mrad (45 arc sec) | | | | |
| | Direct Encoder | 39 µrad (8 arc sec) | 29 µrad (6 arc sec) | | | |
| Tilt Error Motion | | 49 µrad (10 arc sec) | | | | |
| Axial Error Motion | | 5 µm | | | | |
| Radial Error Motion | | 10 µm | | | | |
| Gear Ratio | | 51:1 | 67:1 | 85:1 | 117:1 | 126:1 |
| Maximum Speed ⁽²⁾ | BWBMS | 180°/s | | | | 120°/s |
| | SM | 60°/s | | | 40°/s | |
| Maximum Acceleration ⁽²⁾ | | 720°/s ² | | | | 480°/s ² |
| Aperture | mm | 50 mm | 75 mm | 100 mm | 150 mm | 200 mm |
| Load Capacity | Axial | 40 kg | 100 kg | 200 kg | 300 kg | 425 kg |
| | Radial | 20 kg | 50 kg | 100 kg | 125 kg | 200 kg |
| | Moment | See Moment Load Curves | | | | |
| Maximum Torque Load to Stage Shaft | | 2.5 N-m | 3.5 N-m | 12 N-m | 20 N-m | 80 N-m |
| Rotor Inertia (Unloaded) | | 0.00052 kg-m ² | 0.0013 kg-m ² | 0.0035 kg-m ² | 0.011 kg-m ² | 0.076 kg-m ² |
| Stage Mass (No Motor) | Standard | 1.9 kg | 2.4 kg | 4.5 kg | 6.1 kg | 18.6 kg |
| | Direct Encoder | 2.5 kg | 3.1 kg | 5.6 kg | 7.6 kg | 21.7 kg |
| Material | | Aluminum | | | | |

Figura 1 - Aerotech AGR series specs

4.9.2.3 Pupil rotator

The Pupil rotator sub-unit (K-mirror) is an optical rotator to keep the relative geometry between the DSM actuator pattern and the SH lenslet array. It's composed by a rotary stage PI Micos DT-65N⁸ (equipped with the 2Phase-045 stepper motor and a rotary encoder) and a mechanical mount hosting the Abbe rotator. The optical component (see section 4.8.3) will be adjustable in tip and decentering. The optics will be pre-aligned in laboratory and then mounted on the rotary stage where centering will be mechanical assured by two pins. The so formed assembly will be bolted to the board via an interface that will allow for tip tilt and decentering to align the rotation axis with the optical axis of the board.



⁸ <http://www.pimicos.com/web2/en/1,5,100,dt65n.html>

The bidirectional repeatability is equivalent to 0.007 subaperture at the external edge producing negligible error for the error budget.

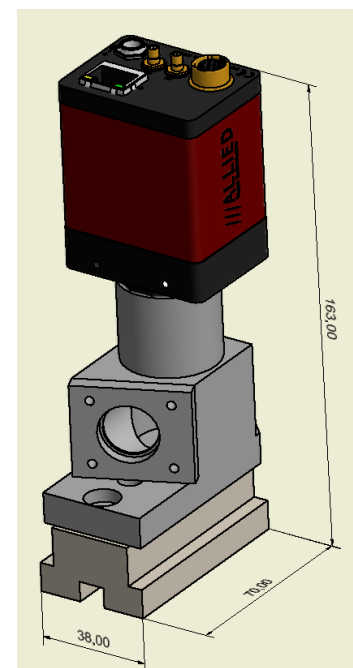
The effect of bearing decentering and wobbling on the PSF rotation will be estimated in Sec. 7.2.2 where the K-mirror sensitivity analysis is reported.

| Load Characteristics | <u>F_x</u> (N) | <u>F_z</u> (N) | <u>M_x</u> (Nm) | <u>M_z</u> (Nm) | <u>k_{ax}</u> (μ rad/Nm) |
|--|-----------------------------|-----------------------------|------------------------------|------------------------------|--|
| 2Phase-045 | 15 | 30 | 10 | 0.8 | 180 |
| Travel range (°) | 360, endless | | | | |
| Flatness (Bearings) (μ m) | ± 6 | | | | |
| Eccentricity (Bearings) (μ m) | ± 6 | | | | |
| <u>Wobble (Bearings) (μrad)</u> | ± 30 | | | | |
| <u>Weight (kg)</u> | 1.3 | | | | |
| Motor | 2Phase-045 | | | | |
| <u>Speed max. (°/sec.)</u> | 45 | | | | |
| <u>Resolution calculated (°)</u> | 0.01 (FS) | | | | |
| <u>Resolution typical (°)</u> | 0.002 | | | | |
| <u>Bi-directional Repeatability (°)</u> | ± 0.01 | | | | |
| <u>Uni-directional Repeatability (°)</u> | 0.002 | | | | |
| <u>Nominal Current (A)</u> | 1.2 | | | | |
| Worm gear reduction | 180:1 | | | | |
| <u>Velocity Range (°/sec.)</u> | 0.002 ... 60 | | | | |
| <u>Material</u> | Aluminum, black anodized | | | | |

Table 35 PI-Micos DT65 N specs

4.9.2.4 Technical camera

A mechanical mount will integrate the Technical Camera Dichroic (fixed), the Technical Viewer fold mirror and the Technical Camera CCD Prosilica GE-2040⁹. No internal alignment aid is foreseen at the moment. The mechanical interface will pivot (rotation $\pm 3.5^\circ$) under the first surface of the dichroic to help align the assembly.

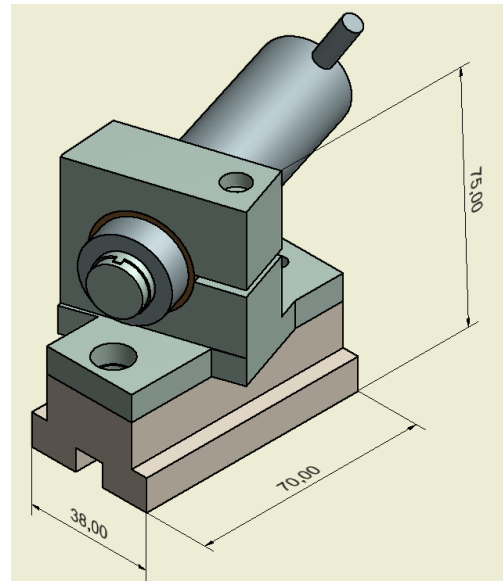


⁹ <https://www.alliedvision.com/en/products/cameras/detail/2040.html>

4.9.2.5 Pupil Stabilization Mirror

Holding a PI S-330.8SL¹⁰ two axis piezo stage, the mount will provide an eccentric ring for fine centering and $\pm 3.5^\circ$ pivoting under the mirror surface for alignment.

In the 40x40 subaperture case this unit provides a working range of ± 7.8 subap (0.64 mrad/subap) with a resolution of 1.6×10^{-3} subap.



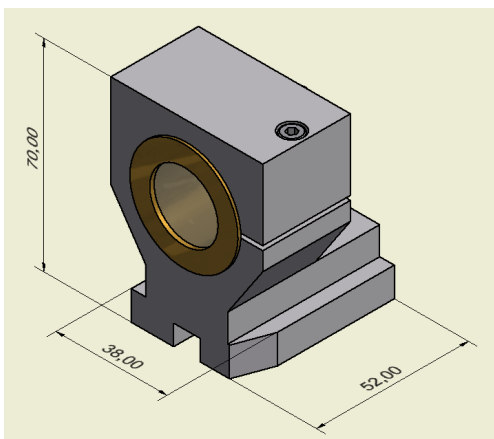
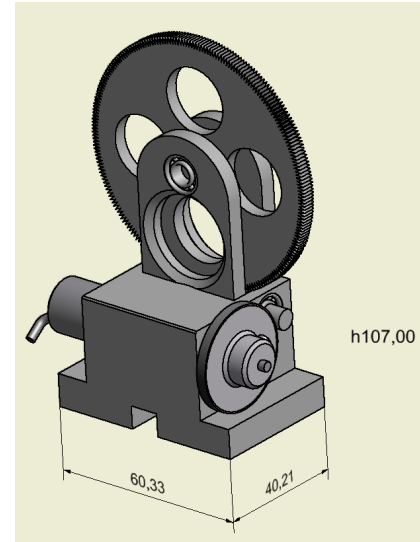
| | S-330.8SL | Unit | Tolerance |
|--|----------------------|------------------|------------|
| Active axes | θ_x, θ_y | | |
| Motion and positioning | | | |
| Integrated sensor | SGS | | |
| Closed-loop tilt angle in θ_x, θ_y | 10 | mrad | |
| Closed-loop resolution in θ_x, θ_y | 0.5 | μrad | typ. |
| Linearity error in θ_x, θ_y | 0.25 | % | typ. |
| Repeatability in θ_x, θ_y | 1 | μrad | typ. |
| Mechanical properties | | | |
| Resonant frequency, no load, in θ_x, θ_y | 3.1 | kHz | $\pm 20\%$ |
| Miscellaneous | | | |
| Operating temperature range | -20 to 80 | $^\circ\text{C}$ | |
| Material case | Steel | | |
| Material platform | Invar | | |
| Mass | 0.7 | kg | $\pm 5\%$ |
| Sensor / voltage connection | LEMO | | |

¹⁰ <http://www.physikinstrumente.com/product-detail-page/s-330-300700.html>

| | | | |
|-----------------|------------------------------|------------------------------------|--|
| ERIS Consortium | ERIS Documentation Standards | Doc.-Ref. Issue Date Page | : VLT-TRE-ERI-14403-3001 : 1.0 : 05.12.15 : 81 of 136 |
|-----------------|------------------------------|------------------------------------|--|

4.9.2.6 Filter Wheel

A four position filter wheel moved by a Faulhaber 1628T024 brushless motor equipped with an IE2-1024 incremental encoder¹¹

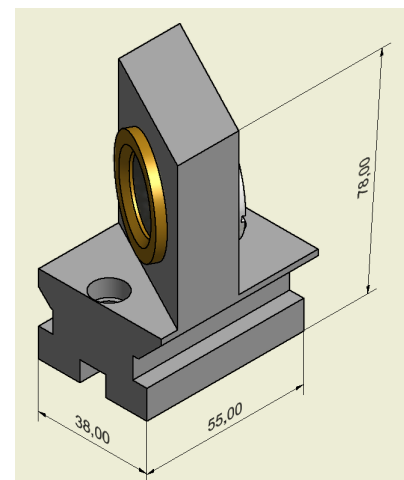


4.9.2.7 Collimator Lens

Collimating Lens holder: a very simple barrel with a tie clamping.

4.9.2.8 Fold mirror

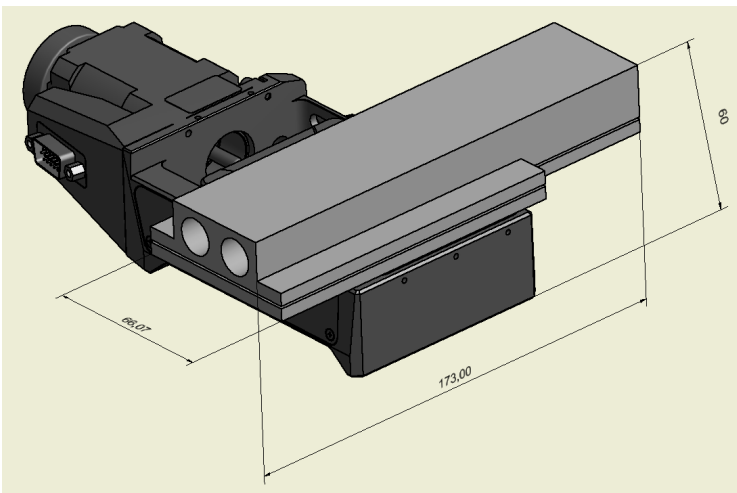
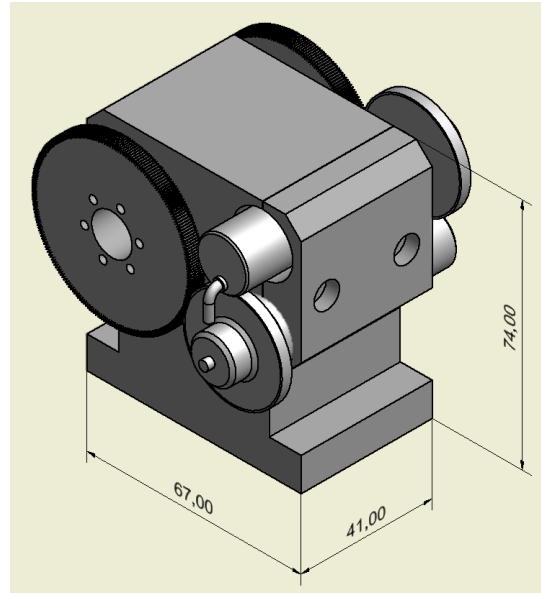
A barrel with a pre-tensioned spring pushing the mirror to a reference flange via a Teflon ring a $\pm 3.5^\circ$ rotation is available for alignment.



¹¹ https://fmcc.faulhaber.com/details/overview/PGR_4408_13822/PGR_13822_13814/en/GLOBAL/

4.9.2.9 ADC

Two counter rotating assemblies using bronze brushes to ensure smooth motion, hold the optical prisms each of them moved by a Faulhaber 1628T024 brushless motor equipped with an IE2-1024 incremental encoder.



4.9.2.10 HO/LO SH Lenslet switch

Composed by a PI-Micos PLS85-26 linear stage integrating the stepper motor 2Phase-45 and the optical mount of the SH lenslet relay. The stage is provided with linear encoder LS-012 to improve the positioning repeatability to 50 nm (unidirectional). The stage supports a single block mount, holding the relay optics and the SH arrays in two parallel mounting tubes, to switch between the low order and High order Shack Hartman configuration. A two-plate interface system will help in the alignment allow-

ing tip tilt and rotation for the mount. The block mount has an estimated mass of 0.4 kg and a height of its CoG from the stage interface plate of 11 mm. Given the torsional stiffness of the stage of 70 μ rad/Nm (see datasheet below), the maximum tilt of the block mount, when the telescope point to horizon, is:

$$70\mu\text{m/Nm} \times (0.4\text{kg} \times 0.011\text{m} \times 9.81\text{m/s}^2) = 3.0 \text{ urad}$$

that corresponds to just 15 mas of equivalent on-sky displacement from zenith to horizon.

Detailed design of the mount and related alignment mechanisms will be executed in the next design phase.

| Load Characteristics | F _x (N) | F _y (N) | F _z (N) | M _x (Nm) | M _y (Nm) | M _z (Nm) | k _{ax} (μ rad/Nm) | k _{ay} (μ rad/Nm) |
|----------------------|--------------------|--------------------|--------------------|---------------------|---------------------|---------------------|---------------------------------|---------------------------------|
| 2Phase-045 | 60 | 50 | 100 | 25 | 30 | 20 | 70 | 40 |

| | | | |
|----------------------------|---|------------------------------------|--|
| ERIS Consortium | ERIS Documentation Standards | Doc.-Ref. Issue Date Page | : VLT-TRE-ERI-14403-3001 : 1.0 : 05.12.15 : 83 of 136 |
|----------------------------|---|------------------------------------|--|

| | |
|--|------|
| Travel range (mm) | 26 |
| Straightness / Flatness (µm) | ± 1 |
| Pitch (µrad) | ± 60 |
| Yaw (µrad) | ± 60 |
| Weight (kg) | 0.9 |

| | |
|--|---------------------------|
| Motor (Pitch 1 mm) | 2Phase-045 |
| Linear scale | LS-012 |
| Speed max. (mm/sec) | 20 |
| Resolution calculated (µm) | 0.05 |
| Resolution typical (µm) | 0.05 |
| Bi-directional Repeatability (µm) | ± 0.1 |
| Uni-directional Repeatability (µm) | 0.05 |
| Nominal Current (A) | 1.2 |
| Velocity Range (mm/sec) | 0.001 ... 50 |
| Material | Aluminium, black anodized |

| | | | |
|-------------------------------|--|--|--|
| <p>ERIS Consortium</p> | <p>ERIS Documentation Standards</p> | <p>Doc.-Ref. Issue Date Page</p> | <p>: VLT-TRE-ERI-14403-3001 : 1.0 : 05.12.15 : 84 of 136</p> |
|-------------------------------|--|--|--|

4.9.2.11 Camera Head Interface

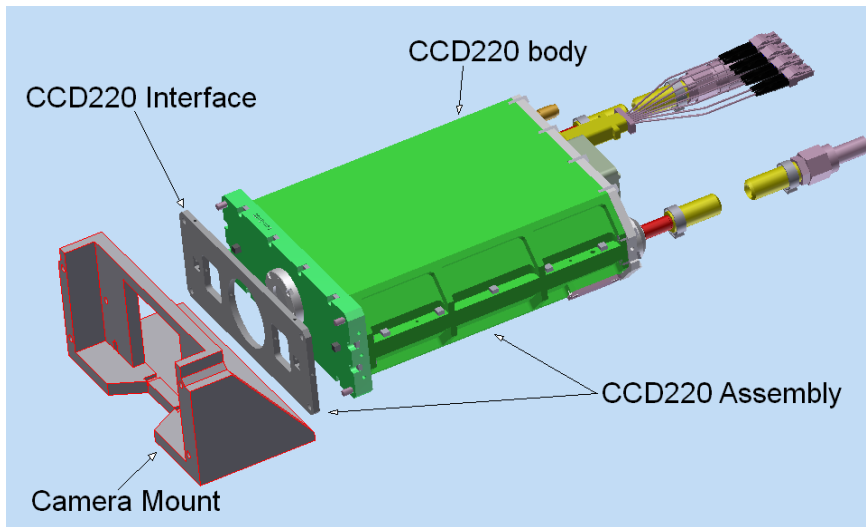


Figure 49 – Camera Head Interface components

It will consist of two units, one, named Camera Mount, acting as an interface between the camera and the WFS sensor board and allowing focusing and lateral positioning for alignment, and the other, the CCD220 Interface, acting as an interface between the CCD220 body and the Camera Mount and intended to compensate for any difference in CCD position between different units and allowing a fast switch between the various spares.

The camera alignment strategy foresees to firstly align all the CCD220 (including the spares) to their respective interfaces using a common alignment reference for all the cameras, so forming a series of commonly aligned assemblies that we'll name CCD220 Assembly (composed, as said, by the CCD220 and the CCD220 Interface).

The CCD220 Assembly will then be mounted on the Camera Mount, where two pins will assure assembly precision. The Camera Mount will finally be aligned to the NGSWFS optical path and then fixed to the board.

In case a replacement of the camera will be necessary we'll simply separate the CCD220 Interface from the Camera mount and replace it with another CCD220 Interface maintaining the original alignment of the Camera Mount and making unnecessary any further aligning procedure.

| | | | |
|-------------------------------|--|--|--|
| <p>ERIS Consortium</p> | <p>ERIS Documentation Standards</p> | <p>Doc.-Ref. Issue Date Page</p> | <p>: VLT-TRE-ERI-14403-3001 : 1.0 : 05.12.15 : 85 of 136</p> |
|-------------------------------|--|--|--|

4.9.3 LGS Wavefront Sensor

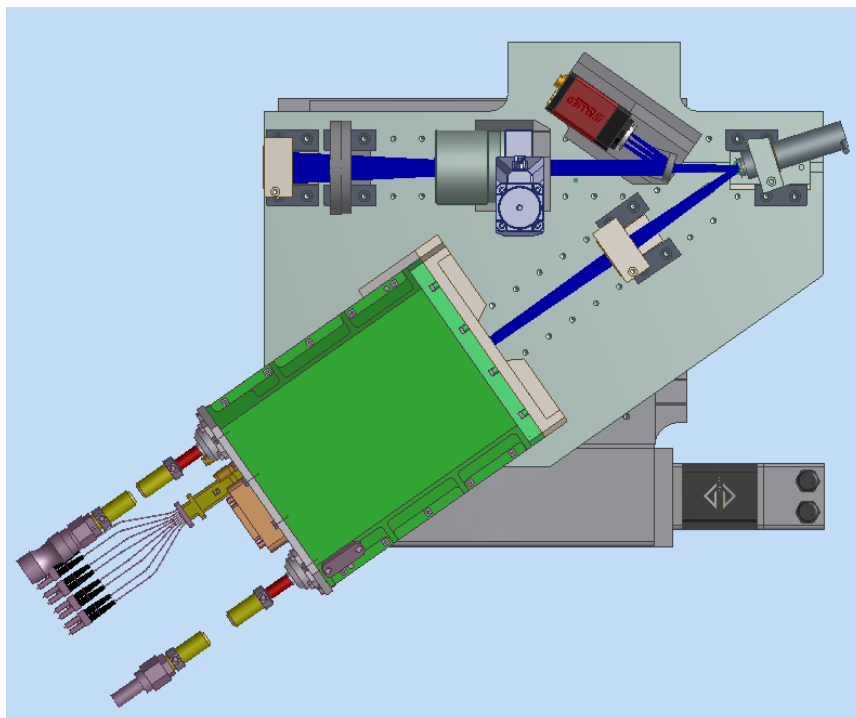
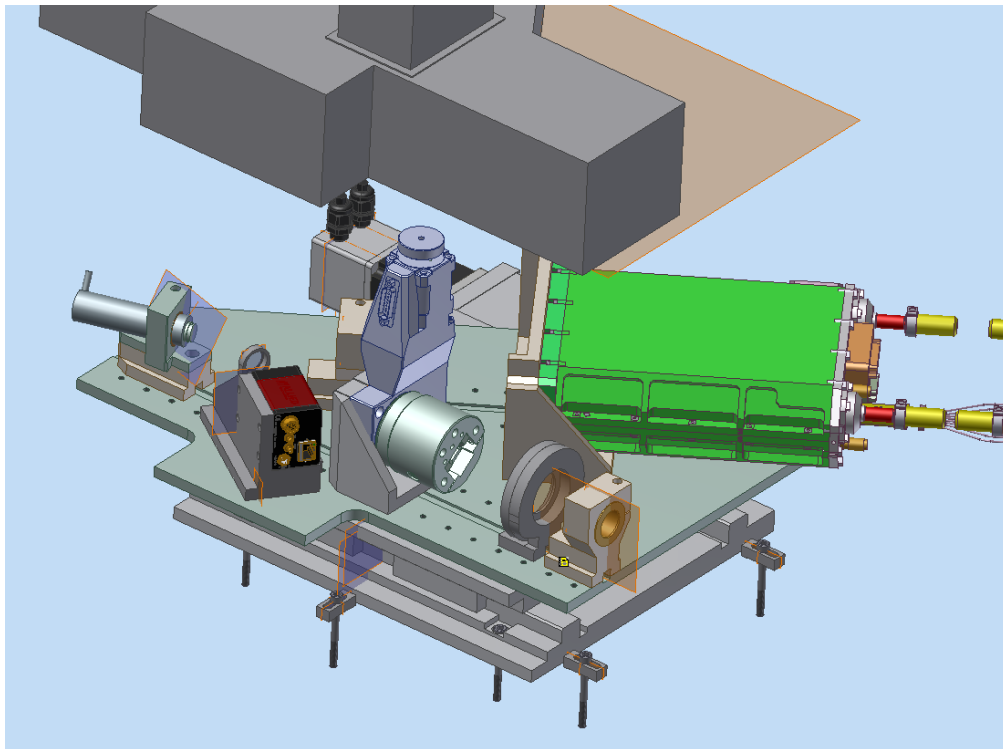


Figure 50 – views of LGS WFS with cover lifted

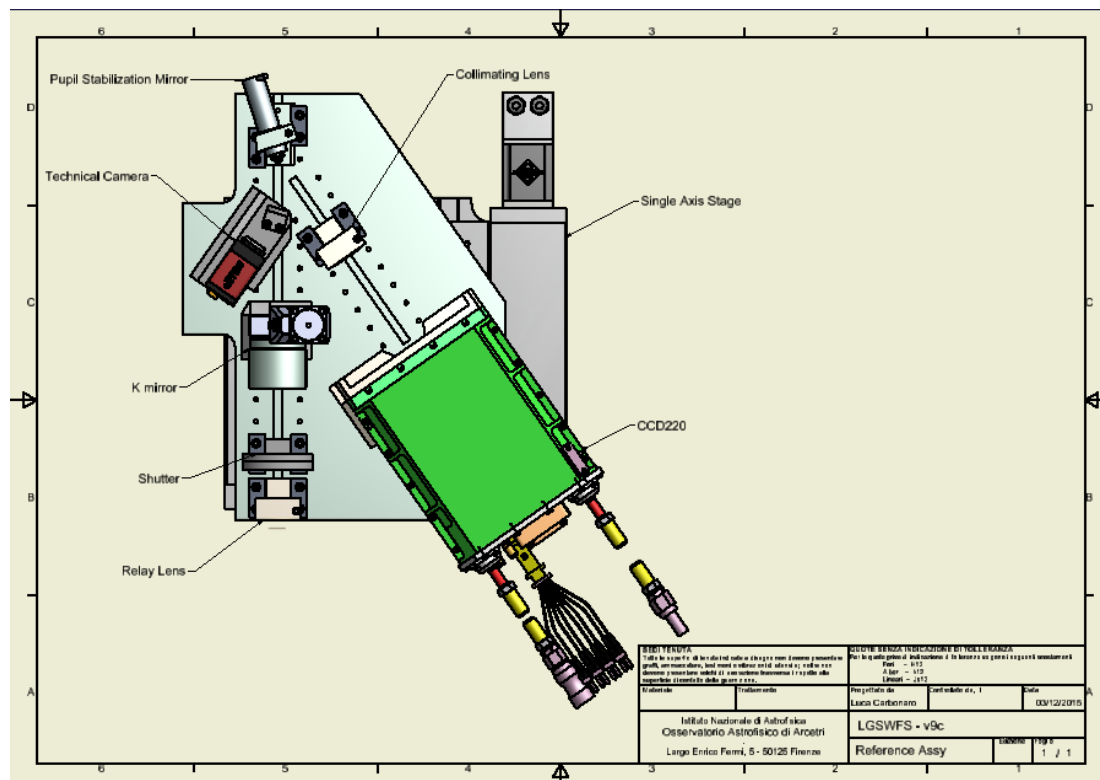
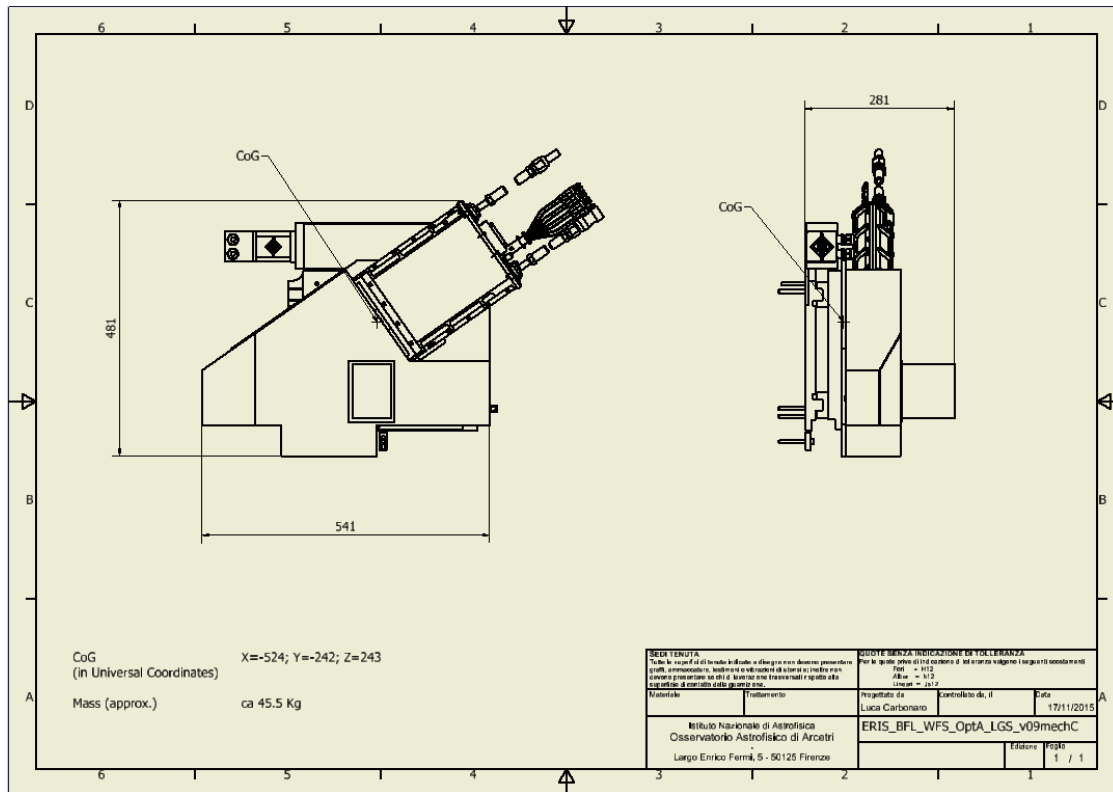
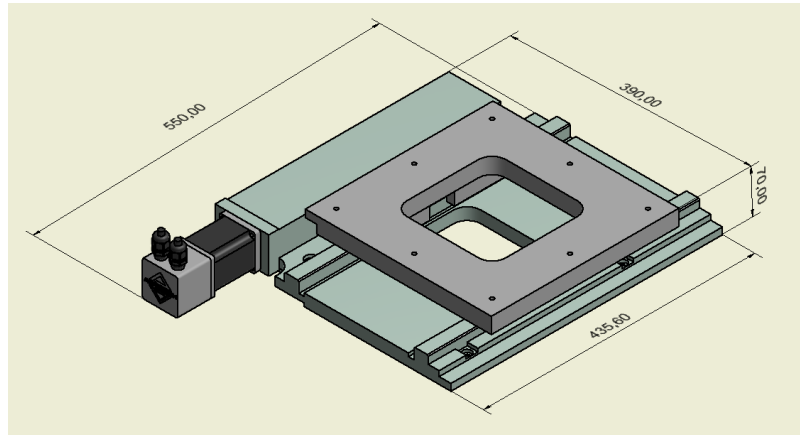


Figure 51 – LGS WFS general dimensions and parts naming

| | | | |
|-------------------------------|--|--|--|
| <p>ERIS Consortium</p> | <p>ERIS Documentation Standards</p> | <p>Doc.-Ref. Issue Date Page</p> | <p>: VLT-TRE-ERI-14403-3001 : 1.0 : 05.12.15 : 87 of 136</p> |
|-------------------------------|--|--|--|

4.9.3.1 Focusing stage

Same as the NGS stage, Aerotech ATS3600 series¹² but customized to have only one axis allowing focus adjustment and to increase the travel to 150mm maintaining the same width of a 100mm travel stage. General characteristics should be inherited from the two axis system but exact dimensioning and calculation of performances are currently under performing at Aerotech.



4.9.3.2 Relay Lens

Very similar to the NGSWFS Collimating Lens holder: a simple brass barrel with a tie clamping, an aluminum ring with elastic pushers acts on a Teflon ring to hold the lens in position.



4.9.3.3 Shutter

Commercial unit from Vincent associates model Uniblitz DSS35B0T1¹³ an interface will allow clamping to the LGS-WFS board

4.9.3.4 K-mirror

Same as NGS-WFS K-mirror

4.9.3.5 Technical camera

A single mount will host the camera, a Prosilica GE2040 from Allied Vision¹⁴ and a small dichroic. The mount will be clamped to the board and small adjustments in clock could be thence provided by moving the dichroic holder

4.9.3.6 Pupil Stabilization mirror

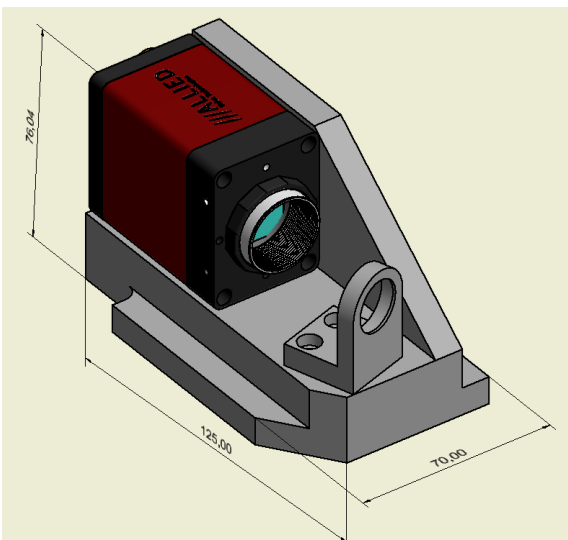
Same as NGS-WFS Pupil Stabilization mirror

4.9.3.7 Collimator Lens

Same as NGS-WFS Collimator Lens

4.9.3.8 Lenslet mount

The Shack Hartman Lenslet array is part of the



¹² <http://www.aerotech.com/product-catalog/stages/linear-x-y-stages/ats3600.aspx>

¹³ <https://www.uniblitz.com/product/dss35-shutter-system/>

¹⁴ <https://www.alliedvision.com/en/products/cameras/detail/2040.html>

| | | | |
|---|--|--|--|
| <p style="text-align: center;">ERIS Consortium</p> | <p style="text-align: center;">ERIS Documentation Standards</p> | <p>Doc.-Ref. Issue Date Page</p> | <p>: VLT-TRE-ERI-14403-3001 : 1.0 : 05.12.15 : 88 of 136</p> |
|---|--|--|--|

CCD220 camera and it is provide by ESO together with the SH lenslet array.

4.9.3.9 Camera Head Interface

Same as NGS-WFS Camera Head Interface

4.9.4 Cables and Harnesses

For a general view about the AO related cabling, refer to AD12..

Due to the stiffness of the CCD220 power cable a preliminary routing study has been performed. The minimum curvature radius of 200mm, the minimum free section of 1mm and the scarce flexibility¹⁵ forced the design of a stress relief mount and a possible cable chain to route the CCD220 cable down the cables ducts. Figure 52 shows 1m of cable to locate the clamping position, left for LGS and right for NGS WFS unit. In the first case the clamp can be easily implemented interfacing to the surrounding structure; in the NGS case an extension of the structure has to be provided.

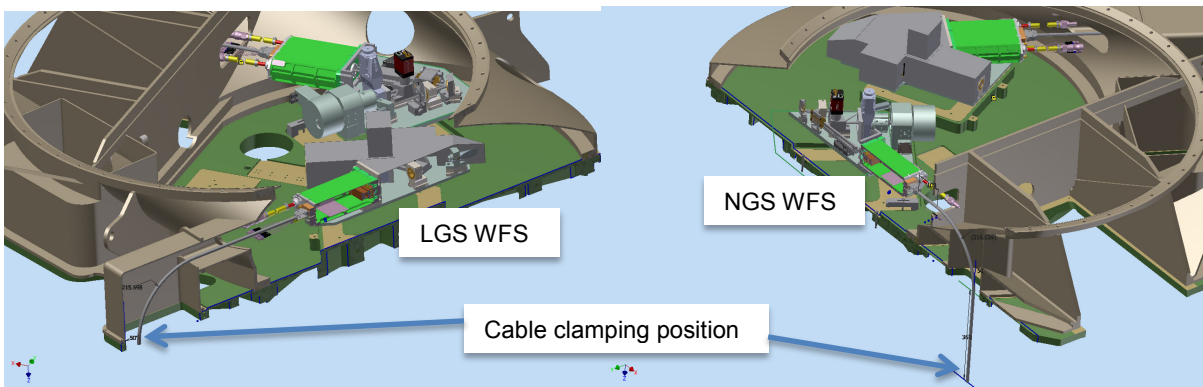


Figure 52 – Routing of the power cable of WFS Camera. Left: LGS WFS unit. Right: NGS WFS unit.

4.9.5 Materials

As far as it's possible all parts are designed to be realized in AL6061-T6 black anodized, only two exceptions are foreseen:

- some small components in direct contact with the optical parts will be made of TEFLON to ensure an intermediate CTE material between glass and aluminum
- the support of the Instrument Dichroic (CaF₂¹⁶) will be made of Al4032-T6 an aluminum-silicon alloy with a CTE¹⁷ almost perfectly matching (difference < 1ppm/°) that of the optical component, the part will be black anodized.

Here below a resuming table of the structural materials used with their main characteristics.

¹⁵ ESO delivered to INAF-Arcetri one cable to run stiffness measurement and characterize the amount of reaction force the cable applies to the WFS unit when moving for operation.

¹⁶ http://www.hellma-materials.com/html/seiten/output_adb_file.php?id=51

¹⁷ <http://www.matweb.com/search/datasheet.aspx?MatGUID=35707660584d4f7caef591324e592396>

| | | |
|------------------------|-------------------------------------|--|
| ERIS Consortium | ERIS Documentation Standards | Doc.-Ref. : VLT-TRE-ERI-14403-3001 Issue : 1.0 Date : 05.12.15 Page : 89 of 136 |
|------------------------|-------------------------------------|--|

| Material | Tensile Strength | Poisson Ratio | CTE ppm/°C | Modulus of elasticity |
|-----------|------------------|---------------|-----------------------------------|-----------------------|
| Al6061-T6 | 276 Mpa | 0.33 | 23.6 | 68.9 Gpa |
| Al4032-T6 | 379 MPa | 0.34 | 18 (-50°C/20°C) 19.4(20/100°C) | 78.3 Gpa |

4.9.6 Mass and Balance Budget

From an estimation based on the 3D model the actual masses and CoG location, wrt to the common reference system, of the mechanical components are listed in the table here below

| Item | Mass | CoG | | |
|--|------|--------|--------|--------|
| WO | [kg] | x [mm] | y [mm] | z [mm] |
| Intrument Dichroic + Telecentric lens | 2.9 | 0 | -29 | 194 |
| WFS Dichroic | 2.0 | -7 | -249 | 185 |
| WFS Folding mirror | 1.6 | -11 | 385 | 188 |
| NIX Selector Mirror + stage | 3.3 | -141 | -5 | 336 |
| LGS-WFS wo stages | 30 | -504 | -212 | 223 |
| NGS-WFS wo stages | 38.6 | -312 | 271 | 257 |
| LGS-WFS w stages | 45 | -524 | -242 | 243 |
| NGS-WFS w stages | 65 | -322 | 291 | 267 |

4.10 Control Electronic Design

The ERIS System Electronics has a modular architecture that allows to independently develop and operate its subsystems.

There is one Instrument Control Electronics (ICE) per science channel plus one for the AO+WO+CU subsystem (Figure 53). Each ICE is based on EtherCAT, a communication technology that has become an ESO standard for new instrumentation. This lead all instrument devices belonging to the same subsystem to be controlled by a single CPU-based PLC unit (Beckhoff CX2040). It communicates with a number of I/O, motion terminals and servo drives within each subsystem, to monitor and operate the devices connected to it. All the control electronics and power supplies of the AO subsystems are placed inside three cabinets mounted on the telescope, while motorized stages and other devices (sensors, technical cameras, WFS CCDs, etc.) are placed inside the two WFS units.

The AO subsystem is composed of the LGS and the NGS units. Since its limited number of controlled device, the WO has been considered as part of the LGS subsystem.

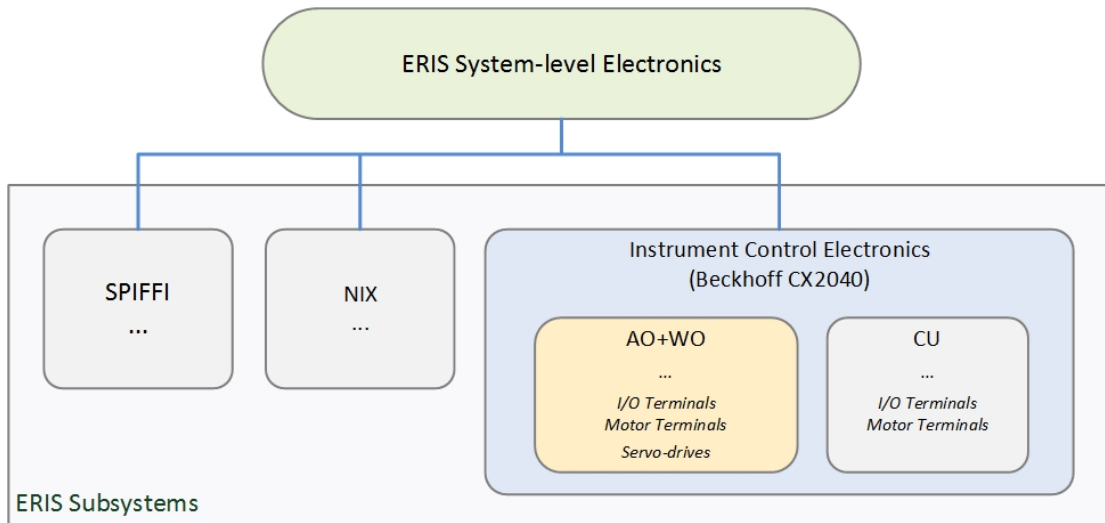


Figure 53 ERIS System Electronics layout

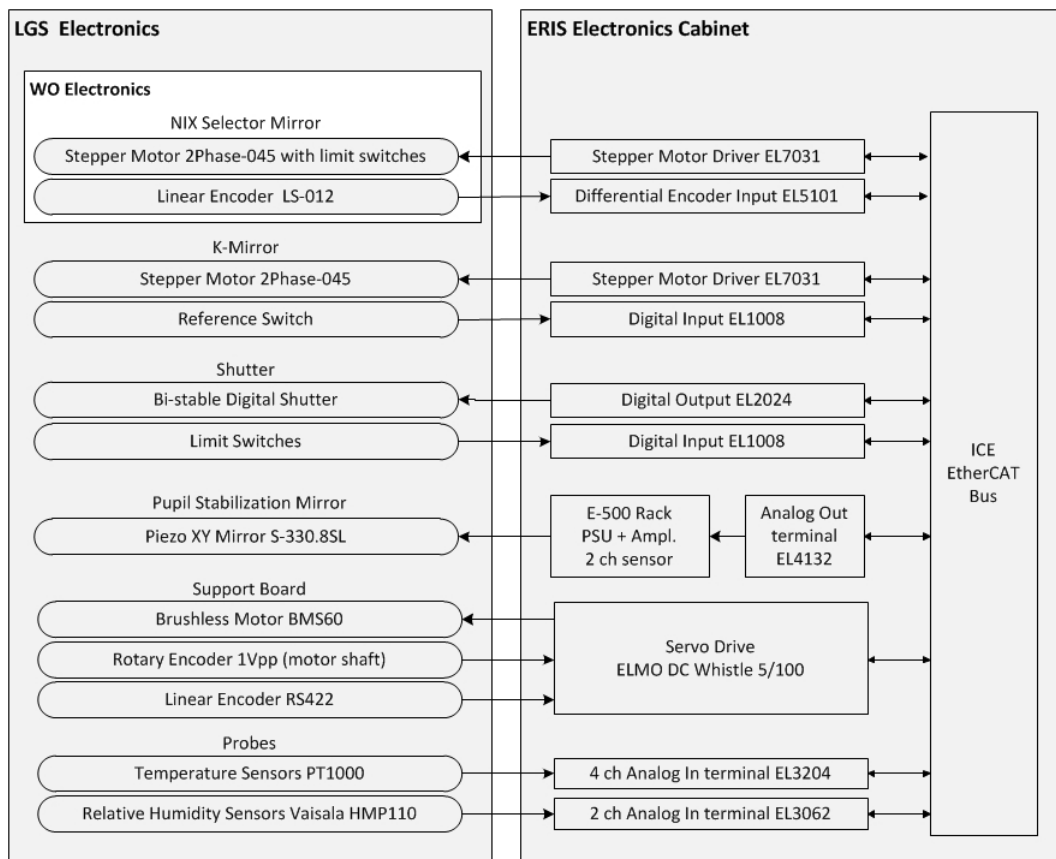


Figure 54 LGS+WO Electronics Architecture

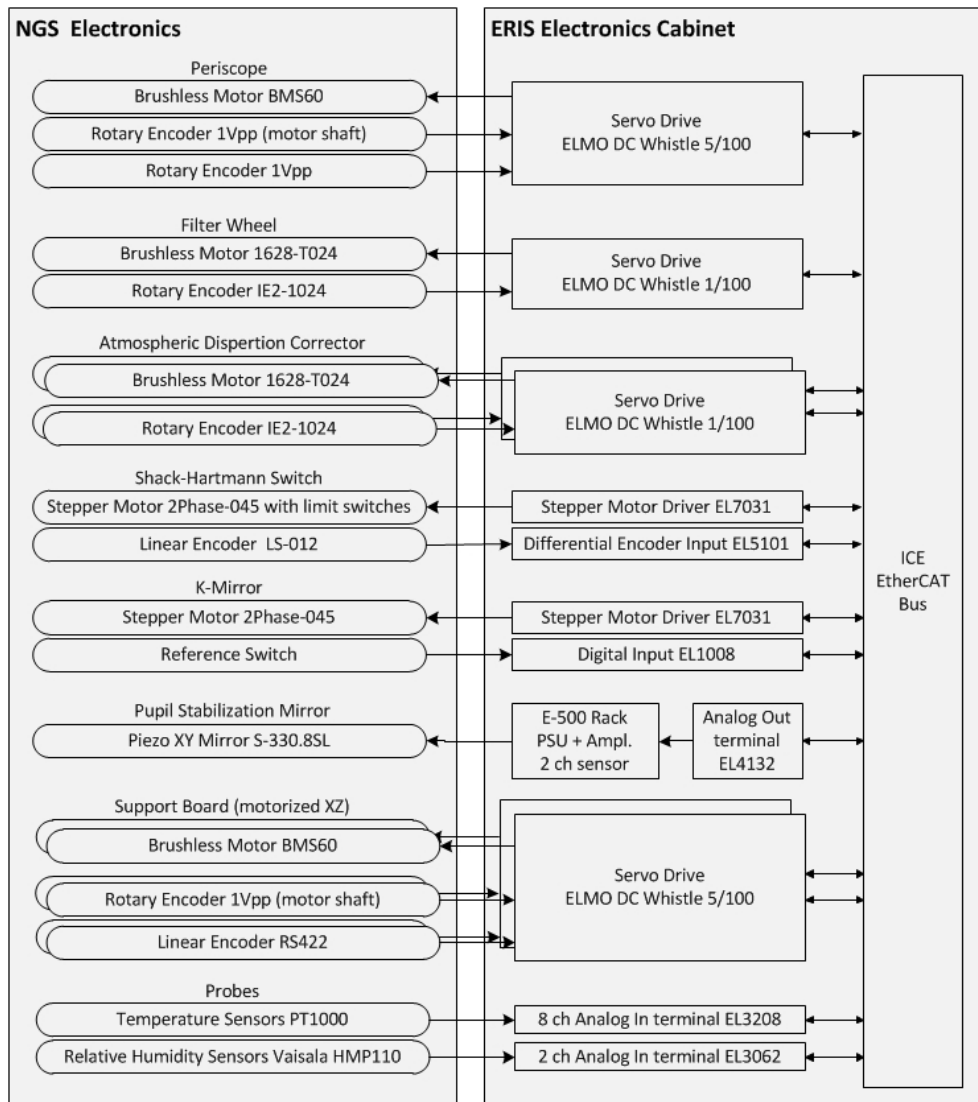


Figure 55 NGS Electronics Architecture

In Figure 54 the architecture of the LGS electronics is shown. The subsystem has 3 motorized stages (2 provided with stepper motor and 1 with brushless motor) a shutter and a piezo tit/tilt mirror. The last is controlled through an analog output terminal (EL4132) directly connected with the control electronics placed inside one of the three cabinets. The two stepper motors are interfaced with two Backhoff terminals (EL7031). One of them is also connected to an input terminal (EL5101) for the encoder feedback. The Support Board is provided with a brushless motor that is controlled by a ELMO DC Whistle 5/100 servo drive that (through the feedbacks from the rotary encoder on the motor shaft, and from the linear encoder on the stage) allows to perform a velocity-position control loop, to improve the performance of the device. Finally, 4 temperature sensors and 2 humidity sensors are used to monitor critical devices (motors heating, WFS CCD) and environmental conditions.

In Figure 55 the architecture of the NGS electronics is shown. The subsystem is composed a piezo tit/tilt mirror and 6 motorized stages. Among them, two have stepper motors (Shack-Hartmann Switch, K-Mirror derotator), the others are provided with brushless micromotors (Filter Wheel and

| | | | |
|----------------------------|---|-----------|--------------------------|
| ERIS Consortium | ERIS Documentation Standards | Doc.-Ref. | : VLT-TRE-ERI-14403-3001 |
| | | Issue | : 1.0 |
| | | Date | : 05.12.15 |
| | | Page | : 92 of 136 |

ADC) and more powerful brushless motors (Periscope and Support Board)¹⁸. Terminals and servo drives for this subsystem are of the same type as the ones used for the LGS subsystem.

Finally, 6 temperature sensors and 2 humidity sensors are used to monitor critical devices (motors heating, WFS CCD) and environmental conditions.

A detailed full description of the AO Electronics Design is reported in AD12.

5 Interaction Matrix (IM) calibration

The AO system calibration mainly consists in the measurement of the Interaction Matrix (IM) between the DM and the WFS. Such task is accomplished by recording the WFS signals associated with a set of DM offsets, which correspond to every single mode composing the modal basis chosen for the AO correction (typically KL modes). The ERIS AO system will not have the chance to measure its IM in diffraction limited conditions as could be using ASSIST. Therefore, the ERIS AO calibration will be performed with different techniques as the synthetic IM estimation and the on-sky measurement.

5.1 Synthetic IM

A synthetic IM is an estimation of the system IM based on numerical simulations. A synthetic IM (SIM) will be used to provide the first reconstructor allowing the closed loop, as required for the first iteration of the on-sky IM calibration (see sect. 5.2). The ERIS AO system will compute the synthetic IM using the same method developed for AOF and reported in in AD8. The computation is made by the SPARTA workstation (see AD10).

5.2 On-sky IM calibration

The on-sky calibration is the measurement of the system IM, using the light from a bright guide star (and the laser in the LGS mode) to illuminate the DM and provide the sensor with a WF signal. The on-sky calibration has to deal with the atmospheric noise; so, the calibration is run in (at least partial) close loop at a high frame rate. Moreover, in order to improve the signal SNR, the DM offsets are injected with a given frequency and then demodulated.

A more detailed discussion on the procedure concept may be found in RD7. The On-sky IM calibration for the AOF case is discussed in AD8. Experimental results in measuring a high-order IM on-sky at the LBT may be found in RD9.

5.2.1 Close loop operations

The seeing imposes that the on-sky measurement of the IM has to be done in closed loop. At least for the first calibration, the loop will be closed using a reconstructor obtained from a synthetic IM (see Sec. 5.1). It can happen that this reconstructor is not able to provide correction at all spatial frequencies, but a partial correction is enough during the initial step. The aim of this first closed loop is the control of vibrations and low order modes. As long as the procedure is carried out, the newly measured IM may be used to close the loop with a larger number of controlled modes and higher turbulence rejection.

¹⁸ It is important to note that to patrol the NGS WFS field to select the reference star, it is necessary to combine the circular motion of the periscope in the XY plane with the X-axis of the Support Board. Coordinated motion of the two devices is needed when science and NGS WFS target have differential non-sidereal motion.

| | | | |
|---|--|--|--|
| <p style="text-align: center;">ERIS Consortium</p> | <p style="text-align: center;">ERIS Documentation Standards</p> | <p>Doc.-Ref. Issue Date Page</p> | <p>: VLT-TRE-ERI-14403-3001 : 1.0 : 05.12.15 : 93 of 136</p> |
|---|--|--|--|

A bright reference star will allow running the loop at high frequency: then, the poor accuracy of the preliminary IM may be mitigated by adopting a low loop gain (and keeping the loop stable) and iterating the correction over multiple cycles.

5.2.2 Modulation and demodulation

The core of the on-sky calibration is the modulation-demodulation process. The modal offset is injected on the DM at a given high frequency. Such modulation method is valuable to spectrally decouple the signal to be measured from the atmospheric noise. A demodulation algorithm will be run on the collected data to retrieve the wanted modal signal at the modulation frequency.

Two approaches are viable for the modulation technique:

1. **The push-pull technique.**

It consists in injecting the modal command as a square wave, i.e. constant commands with alternate positive and negative amplitude. The modulation frequency should take into account the DM settling time and the measurements will be taken at a lower cadence to allow the DM reaching the command steady state. For push-pull the demodulation technique is pretty easy, consisting in averaging the entire dataset after correcting each frame for the command sign.

2. **The sinusoidal modulation technique.**

It consists in applying the modal command with amplitude varying as a sine in time. The demodulation algorithm filters the signal with a narrow temporal bandwidth. Such approach is greatly improving the atmospheric noise rejection allowing at the same time the simultaneous measurement of multiple modes at different modulation frequencies (multiplexing). For details on the demodulation algorithm refer to RD9.

The push-pull technique is currently used for the IM calibration on the AOF (refer to AD8). Here we will take the sinusoidal technique as our baseline, considering it has been successfully demonstrated on sky at the LBT (RD9). The push-pull will be considered as a backup solution.

5.2.3 Iterative process

At the beginning of the process, the loop is closed on low order modes using a reconstructor generated from a synthetic IM. The correction of a small number of modes is a conservative approach to avoid problems coming from sub-apertures mis-registration and poor accuracy of the IM in general and to guarantee a stable loop. Given such partial correction, the measurement of the IM will be limited to low orders only, as high orders will be affected by atmospheric noise; it is not convenient to sample a number of modes much larger than (twice) the number of the corrected ones.

The set of sampled modes are then collected together to produce a new, larger size, IM. With respect to the synthetic IM, the new one is expected to be more accurate as measured on the real system at the real working point. It can therefore be used to close the AO loop and collect a second IM increasing the number of measured modes. The calibration procedure is therefore iterative because of the need of close loop operations. As soon as a new IM is measured, it is used to close the loop and extend the number of sampled modes. At each step of the procedure, the modes previously measured will be sampled again, taking advantage of the improved atmospheric correction by the close loop.

5.2.4 Multiplexing

Through multiplexing a number of modes are superimposed and are measured together during the same sampling session in close loop. Such approach allows to significantly speed up the on-measurement process, reducing so the required time on-sky.

| | | | |
|---|--|--|--|
| <p style="text-align: center;">ERIS Consortium</p> | <p style="text-align: center;">ERIS Documentation Standards</p> | <p>Doc.-Ref. Issue Date Page</p> | <p>: VLT-TRE-ERI-14403-3001 : 1.0 : 05.12.15 : 94 of 136</p> |
|---|--|--|--|

The multiplexing consists in adding many DM modal offsets with a sinusoidal modulation at different frequencies; the demodulation algorithm will take care of separating, by means of spectral analysis, the signal associated with the single modes applied. The number of modes (or the number of frequencies) measured together depends on the DM and WFS bandwidth, in order to allow a proper frequencies spacing without going toward low frequency.

5.2.5 On-sky verification

At the beginning of each step of the iterative calibration procedure, performance verification in closed loop will be run to check the quality of the measured IM. In particular, an improvement in the correction degree shall be observed, in the range of modes that have been measured during the last calibration.

5.2.6 Parameters optimization

The optimization of the procedure parameters shall be tailored on the real sampling case; here we will report some generic guidelines, also outlined in Sec.5.2. and 5.3 in AD8.

The modulation frequency should be the highest compatible with DM settling time and WFS frame and diagnostic data rates. The optimal value can be found with a test measurement, in order to optimize the procedure versus mode spatial frequency, integration time, current seeing (e.g.). The test procedure is as follows:

1. The loop parameters, the integration time (i.e. the number of modulation cycles) and a set of modes and of frequencies are selected;
2. The modes are measured in close loop, obtaining a WFS signal for each frequency;
3. For each mode, the most performing modulation frequency is found by comparing the WFS realizations according to a given metric.

The command amplitude should be chosen considering three elements:

- a large amplitude is preferable to improve the SNR,
- avoid saturating the WFS nor the DM;
- the measurement is done in close loop, so that a large perturbation should be avoided as it will move the WFS far from its working point.

The first two points may be addressed with computation; for the latter, a good solution is to limit the modal amplitude to the (typical) atmospheric residuals. At the high order regime, where the DM saturation is encountered with very low modal amplitude, the SNR shall be improved with longer integration time.

5.2.7 Implementation on SPARTA

In the following the calibration procedure will be outlined, indicating the specific implementation and the associated user requirements on SPARTA as defined in AD10 (see also [CA-5] within the same document). The sinusoidal modulation technique will be considered as a baseline.

| | | |
|----------------------------|---|--|
| ERIS Consortium | ERIS Documentation Standards | Doc.-Ref. : VLT-TRE-ERI-14403-3001 Issue : 1.0 Date : 05.12.15 Page : 95 of 136 |
|----------------------------|---|--|

| Step # | Action | Associated REQ on SPARTA |
|--------|--|--------------------------|
| 1. | A sinusoidal command history with p modes, each individually modulated with frequency f_i and amplitude a_i and phase w_i is created and stored. | [CA-5] |
| 2. | The control matrix (produced as SIM or calibrated on sky) is loaded. | |
| 3. | The loop is closed with m modes at frequency f . | |
| 4. | The DM command history is started and is stopped after completion | [CC-18] |
| 5. | During time history execution, the DSM saturation is checked to record the event | [CC-28] |
| 6. | The slopes data s are recorded and downloaded at the completion of the time history. | [DR-1] Slopes |
| 7. | The slopes data s are processed according to the demodulation algorithm with the given parameters to extract the slope signal associated with each of the p modes. | [CA-5] |
| 8. | The slopes signal associated to each mode is normalized with the modal amplitude a_i and stored as column vector in the IM. | [CA-5] |

6 Pyramid WFS upgrade design for the NGS WFS

The Arcetri group worked in 2011-2013 to a Phase A study to assess the performance and feasibility of a Pyramid Wavefront sensor for ERIS to be used as NGS wavefront sensor. In this section we present the current ERIS NGS AO simulation performance when using a pyramid sensor and a sensor opto-mechanical design that matches the volume available in the current ERIS design. We consider that the simulations show a significant advantages of an NGS ERIS AO system using a PWFS with respect to the same system using a SH sensor.

6.1 ERIS NGS Strehl ratio performances

In this section we show the comparison of the NGS-mode performance when using a Pyramid and SH WFS. Figure 56 shows the SR in J, H and K band. The pyramid simulations shown here uses the same parameters of the AO loop identified in the phase A study (RD8). We note here that the gain apply only in a limited range of star magnitudes because for star fainter than 13.5th the ERIS AO system will use the LGS.

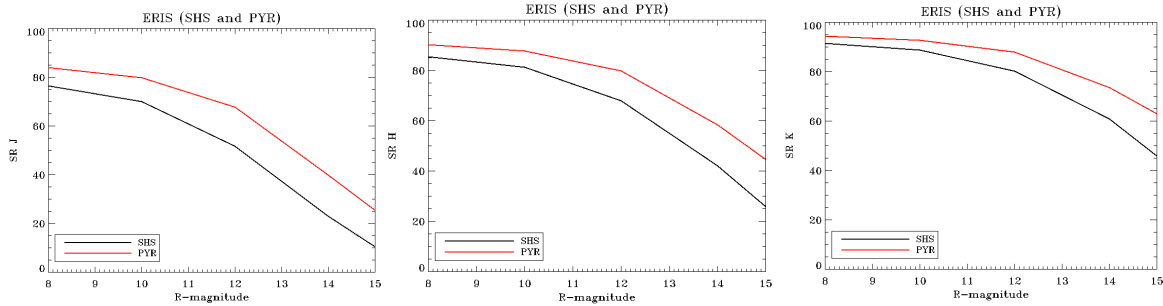


Figure 56. NGS-mode, Pyramid VS SH WFS, SR (J, H and K bands) as a function of R-magnitude

The increase in the SR values achieved with the PWFS with respect to the SH for the nominal conditions is reported in the figure below and translates in an improvement of the ERIS integration time and in the sustainable seeing to achieve the SR value required in TS-ERIS-PER-007. As we find below the maximum SR improvements in J, H and K band is respectively 1.57, 1.29 and 1.14 respectively.

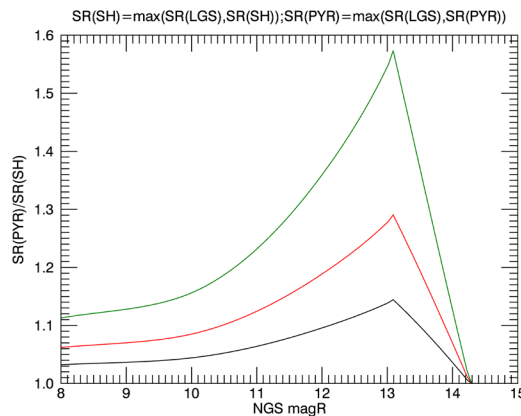
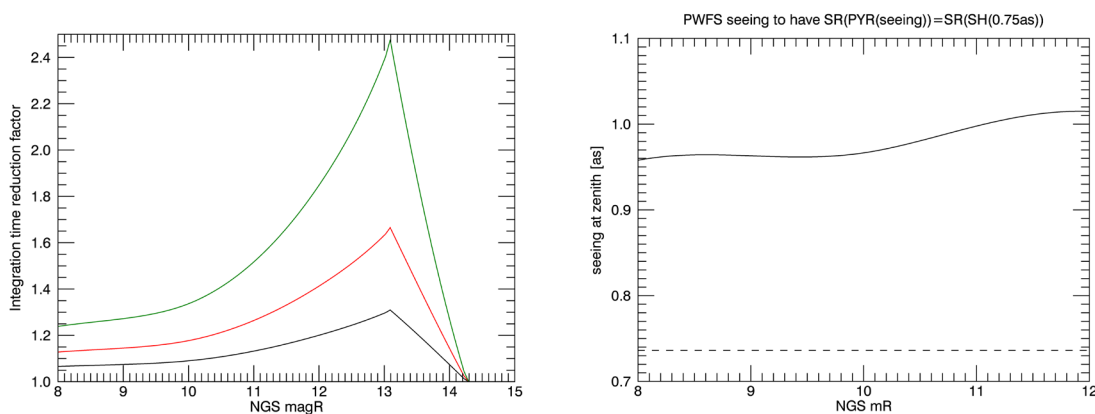


Figure 57 – The ratio of achieved SRs in J, H and K band (from top to bottom) for PWFS and SH sensor as a function of the reference star.

Using these data we can compute the improvement in exposure time for a given SNR and the increase in sustainable seeing conditions to match the SR requirements in TS-ERIS-PER-007. The results of the computations are shown in the figure below where we report exposure time gain and maximum seeing to achieve TS-ERIS-PER-007.



In summary we see that using a PWFS (a) the integration time to reach a given SNR is reduced by a factor up to 2.4 in the most favourable case and the average values for J, H and K are 1.15, 1.30 and 1.6, (b) the seeing value to match the SR technical specification (TS) is increased from 0.73 to an average of 0.98 that corresponds, considering the seeing value statistics of Paranal, an increase from 45% to 70% of observing nights matching the TS (see Figure 58).

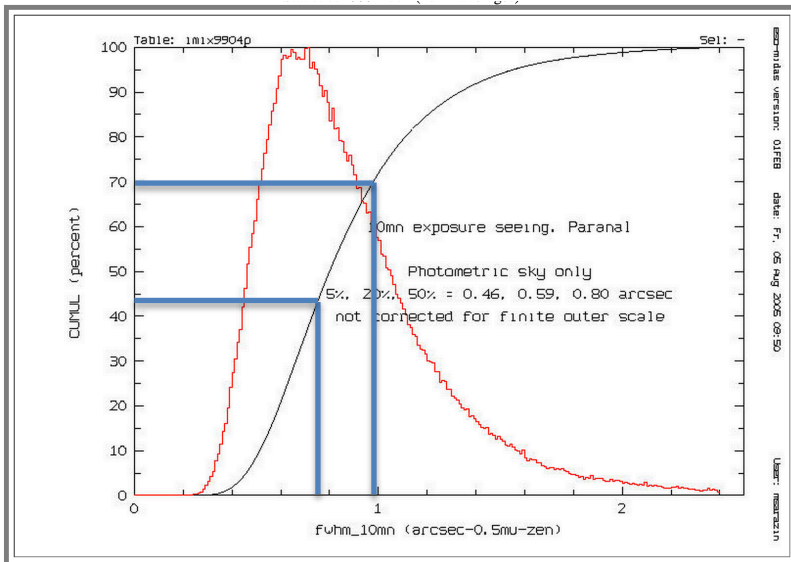


Figure 58 – Paranal seeing statistics.

6.1.1 Contrast, speckle noise and ADI SNR

We compare, in this part, the results on the noises and the SNR ADI for the SH-WFS and the Pyramid WFS.

The following figures show respectively the different noise contributions, the Normalized radial profiles, the normalized speckle noise profiles and the SNR ADI.

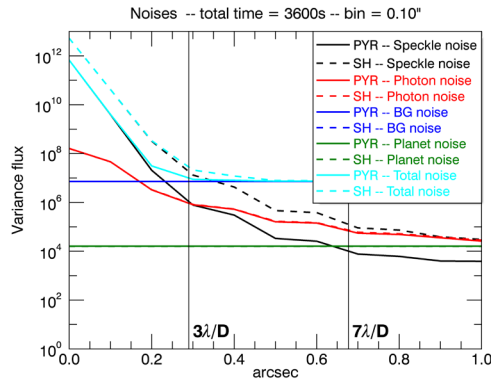


Figure 59. Comparison between different noise contributions (in variance). Solid lines: PYR-WFS. Dashed lines: SH-WFS.

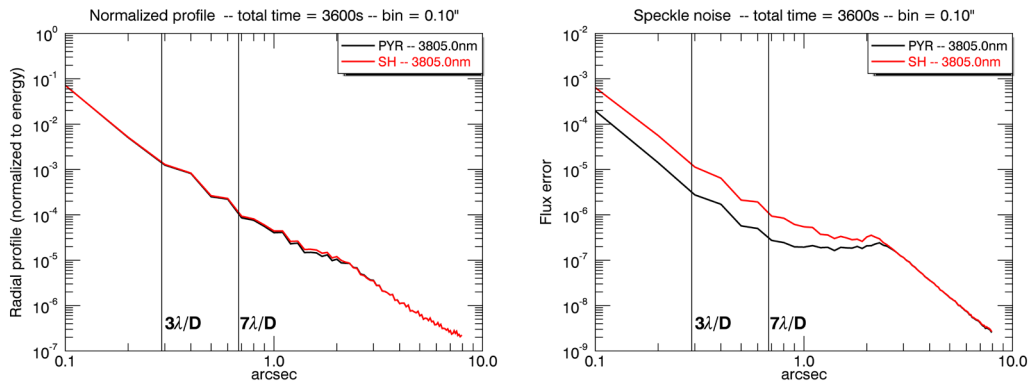


Figure 60. PSF radial profile (Left). Speckle Noise (Right). Black: PYR-WFS. Red: SH-WFS. In the plots the curves are normalized to unit total energy.

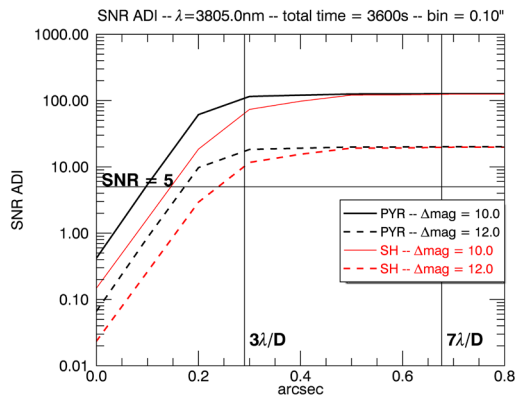


Figure 61. SNR ADI for different planet magnitudes. Black: PYR-WFS. Red: SH-WFS

Table 36. SNR ADI comparison for different radial distances.

| Radial distance | | 2 λ /D | 3 λ /D | 7 λ /D |
|---------------------------|-----|----------------|----------------|----------------|
| SNR ADI Δ mag = 10 | SH | 19.5 | 59.6 | 123.7 |
| | PYR | 50.0 | 105.5 | 126.4 |
| SNR ADI Δ mag = 12 | SH | 3.1 | 9.5 | 19.6 |
| | PYR | 7.9 | 16.7 | 20.1 |

In this case, assuming that the SNR scales with the square root of time we see that by using the PWFS, the integration time is reduced by a factor 6.6, 3.1 for 2 and 3 λ /D in the 10 magnitude difference case. Moreover the PWFS provides SNR above TS for a mag 12 while the SH sensor does not.

6.2 Pyramid WFS Optical Design

The high-order and low-order NGS WFS can be replaced by a pyramid WFS that is compatible with the current NGS WFS space envelope. The proposed design adopts most of the same optical components of the SH sensor presented above. Figure 62 shows the optical layout. As for the baseline SH sensor the patrolling of the FoV in transversal and longitudinal position is achieved by using a rotating periscope and an XY stage.

A different relay lens has been designed to accommodate a longer focal ratio at the pyramid (F/42.5 instead of F/20). The relay lens creates a pupil image of 16mm over a fast steering mirror that produces the fast angular modulation of the PSF. The angle of incidence on this mirror is 45 degree. Close to it, a double counter-rotating prism acts as ADC. This is based onto a similar design of the SH NGS WFS (see Section 4.8.3), but the larger pupil diameter requires smaller apex angles inside the prisms (19 deg). The derotator prism is placed between the ADC and the focal plane.

After the derotator, a dichroic beam splitter reflects shorter wavelengths for target acquisition to an acquisition camera. Due to the very long focal ratio, a focal reducer doublet is placed after the dichroic to shorten the focal ratio to F/20. The acquisition camera pixel scale and FoV are 9 mas/pix and 10arcsec, similar to the SH NGS Technical Viewer case.

On the other arm of the beam-splitter, the transmitted light is focused on a double-pyramid placed together with a field stop at the F/42.5 focal plane. Finally, a pupil relay lens (a triplet) reimages the four pupils onto the detector. Pupil images are shown in , they have the correct sampling of 40x40 pixels, with 8 pixels gap between adjacent pupils. Additionally the figure reports the ZEMAX drawing of the double pyramid unit.

The NGS LO configuration can be achieved by switching to a different camera lens set-up reducing the pupil images diameter to avoid summing up dark current and RON contributions. Optical design for such configuration will be studied in the next design phase.

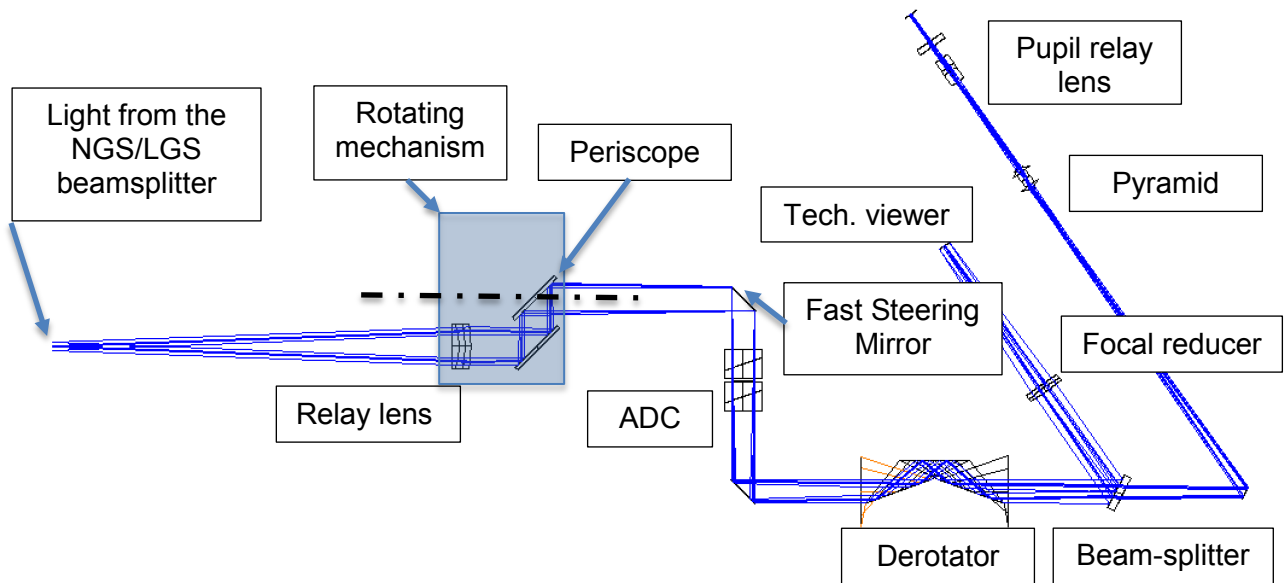
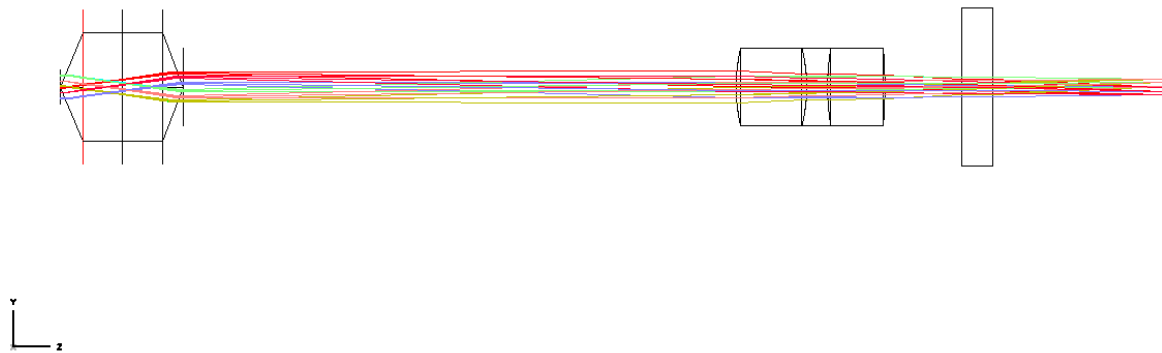


Figure 62. Pyramid WFS optical layout.



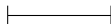
| | | |
|--|--|--|
| 3D LAYOUT | | |
| ERIS_NGS_WFS THU DEC 10 2015 SCALE: 1.5000 |  13.33 MILLIMETERS | ERIS_BFL500_WFS_OPTA_PWS_V07.ZMX CONFIGURATION 1 OF 2 |

Figure 63 – Optical layout from the Pyramid to the detector plane. The ray pattern corresponds to 2.5" FoV transmitted by the pyramid.

| | | | |
|-----------------|------------------------------|-----------|--------------------------|
| ERIS Consortium | ERIS Documentation Standards | Doc.-Ref. | : VLT-TRE-ERI-14403-3001 |
| | | Issue | : 1.0 |
| | | Date | : 05.12.15 |
| | | Page | : 101 of 136 |

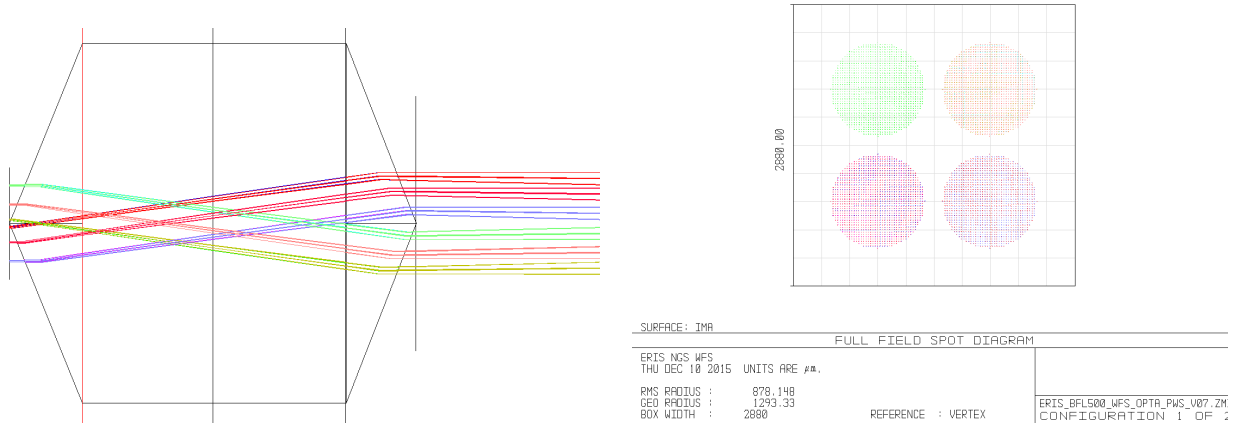


Figure 64 – Left: rays propagation in the pyramid. The FoV size defines the requirement of the pyramid thickness. Ray pattern of 2.5” FoV diameter are shown. Right: pupil images produced by the pyramid and pupil relay lens. Each pupil has 40 pixels diameter to match the sampling of the ERIS NGS WFS. The four images are fully included in a quarter (120x120 pix) of the CCD220.

6.3 Pyramid WFS Mechanical Design

In this section we show the mechanical arrangement of the NGS WFS when the pyramid is used as WFS. The general layout is very similar to the one of the NGS SH WFS of the baseline. The WFS board opto-mechanics is reported in Figure 65. Figure 66 provides a comparison between the NGS baseline option and the PWFS option in terms of placements and volumes.

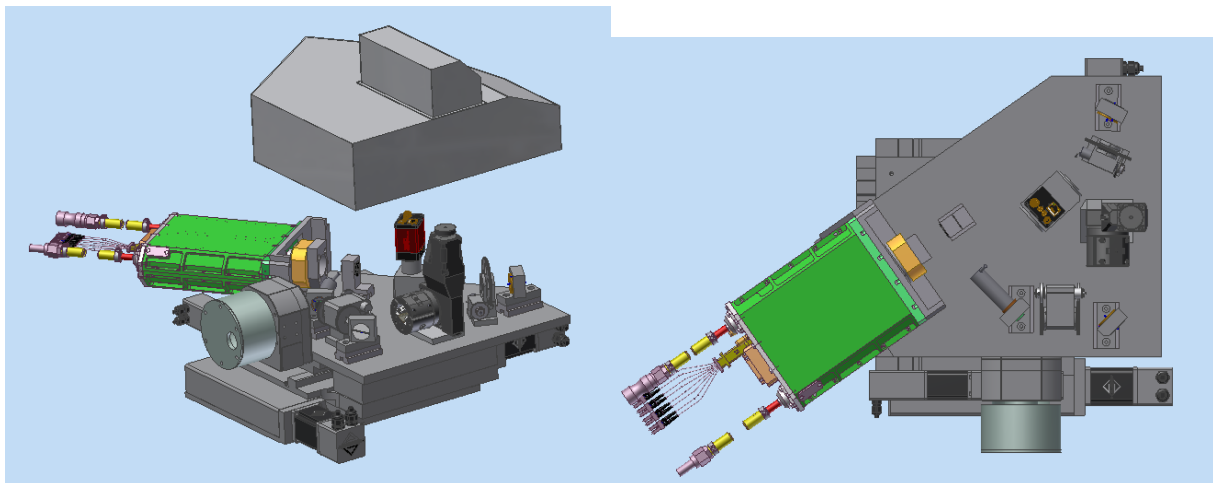


Figure 65 NGS WFS unit

| | | | |
|-------------------------------|--|--|---|
| <p>ERIS Consortium</p> | <p>ERIS Documentation Standards</p> | <p>Doc.-Ref. Issue Date Page</p> | <p>: VLT-TRE-ERI-14403-3001 : 1.0 : 05.12.15 : 102 of 136</p> |
|-------------------------------|--|--|---|

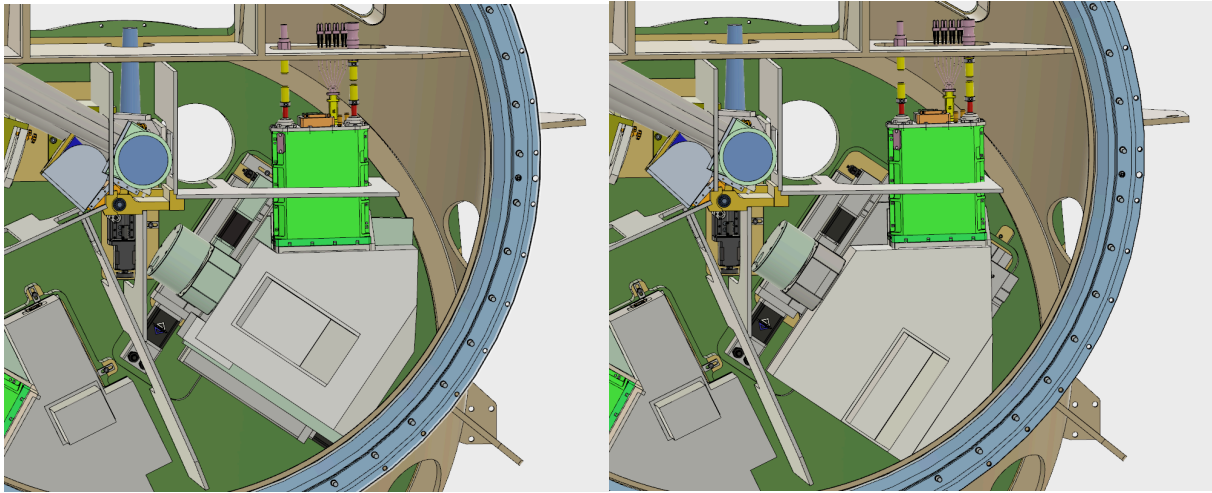


Figure 66 NGS WFS Unit view inside the ERIS Central Structure. Left: SH WFS. Right: Pyramid WFS.

Part re-used from the SH NGS WFS:

- Dual-axis stages (see Sec. 4.9.2.1)
- Periscope (mechanics, rotary stage and mirrors, see Sec.4.9.2.2)
- Technical camera (see Sec. 4.9.2.4)
- ADC (mechanics and motors, see 4.9.2.9)
- K-mirror (complete. See 4.9.2.3)
- Filter Wheel (mechanics and motors. See 4.9.2.6)
- Folding Mirror (complete. See Sec. 4.9.2.8)
- CCD Camera (including mount. See Sec. 4.9.2.11)

In conclusion we showed that the use of PWFS improves the ERIS NGS AO performance. An opto-mechanical design of the PWFS, using most of the parts already developed for the SH WFS, has been reported and is compatible with available volume in the ERIS central structure using the same I/F of SH WFS.

6.4 Implementation in SPARTA

In the Phase A study for the ERIS PWFS we identified several items to be considered when implementing the PWFS functionalities in SPARTA. In the view of minimizing the modification of SPARTA, only the following two have been selected as baseline requirements:

- 1) real time normalization of computed slopes to the average flux measured in previous frame. This one is unchanged from Phase A requiring an update of the SPARTA firmware.
- 2) fast change of modal gain for system optimization.

After various iteration with ESO in writing the SPARTA URD document, requirement 2) has been simplified and alternative implementations has been outlined:

- a) close the loop with a conservative set of gains, then run the already existing SPARTA functionality to compute optimize modal gains during closed loop and finally update the reconstruction matrix implementing the new gains.
- b) use the modal projection feature of the DSM to send commands in the modal space and use existing SPARTA IIR filters to adjust the gains more efficiently than changing the entire control matrix.

The best choice between these two options is still under consideration.

7 Analysis Report

7.1 Optical performances

7.1.1 Science Path Optical Performances

Strehl ratio

The nominal image quality across the field of view is reported as a Strehl ratio field map in Figure 67. SR is computed in K-band. Maximum WFE is 34nm RMS.

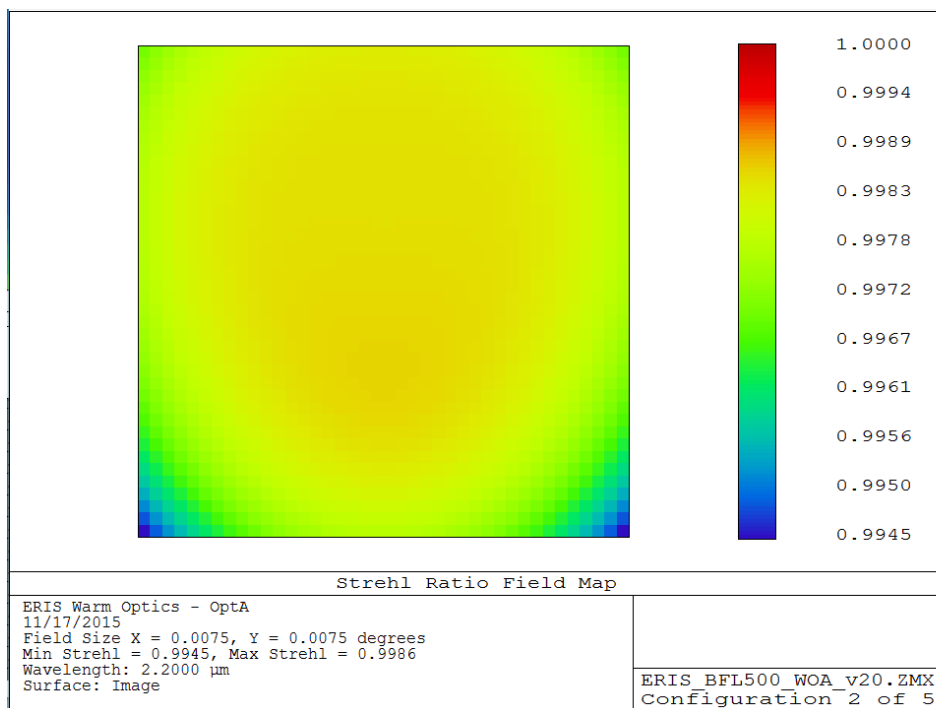


Figure 67. Map of the Strehl ratio across a 54x54 field of view.

Alignment sensitivities for image quality (i.e., Strehl ratio) are reported in Table 42. Pupil chromatism and anamorphism are generally quite low in both cases, the anamorphism being better for the spherical beamsplitter. Field distortion is low in both cases, being smaller than 0.05% (or 14 mas at the edge of the field).

Table 37. Comparison between cylindrical and spherical rear surface on the WFS dichroic.

| | Cylinder | Sphere |
|---------------------------------|-----------------|---------------|
| <i>Radius of curvature (km)</i> | 51 | 64 |
| <i>Wedge angle (arcmin)</i> | 24 | 19 |

| | | |
|---|---------------|--------|
| <i>Chief ray angle (arcmin)</i> | 19 | 14 |
| <i>Sag (um)</i> | 30 | 24 |
| <i>Strehl ratio (K band, full FOV)</i> | >99.0% | >98.4% |
| <i>Exit pupil position (m)</i> | -11(Y)/-15(X) | -12 |
| <i>Pupil chromatism (%/pupil diam., K band)</i> | 0.05 | 0.03 |
| <i>Pupil anamorphism (%/pupil diam.)</i> | 0.7 | 0.1 |
| <i>Field distortion over NIX FOV (%)</i> | -0.046 | -0.031 |

Geometric distortion

CAVEAT: current specification TS-NIX-PER-035 is based onto a geometric distortion definition where a partial linear transformation is allowed to calibrate observed distortion, not including anamorphism. However, if the full 4-term transformation is performed, much smaller distortions are obtained.

The maximum distortion induced by the only active element (WFS dichroic) over the 7×7 arcsec² (3.75×3.75 mm² at the F/13.6 focal plane) is 0.4% (14 mas) when anamorphism is not corrected, and 0.004% (0.14 mas) when linear component of anamorphism is removed.

TS-NIX-PER-035 requires distortion less than 1.5 mas in the 7×7 arcsec² field, therefore a corrective optics in NIX is needed to match the specification, unless the allowed transformation would include linear anamorphism.

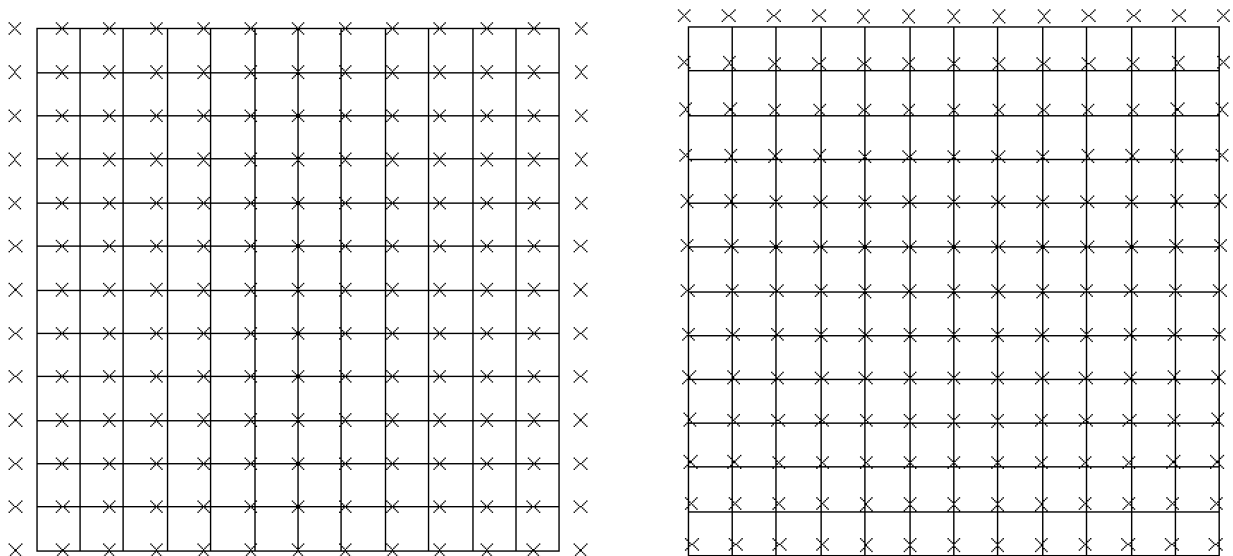


Figure 68. Distortion map over a 7×7 arcsec² field of view. Left: anamorphism is not corrected and distortion is exaggerated by a 20X factor. Right: anamorphism corrected, and distortion is exaggerated by 1000X.

Throughput

The overall system throughput has been estimated based on existing coating curves or measurements carried out in similar instruments. Table 38 gives the overall throughput of the AO subsystems, for both the science arms and the WFS optics. Data are for standard

Table 38. ERIS AO subsystems throughput budget (RD1).

| ERIS - Throughput Budget | | | | | | | | | |
|---------------------------------|---------------|---------------|---------------|-------------|-------------|-------------|-------------|-------------|-----------------------------|
| Channel | LGS HO | NGS HO | NGS LO | NIX J | NIX H | NIX K | NIX L | NIX M | |
| Wavelengths (um) | 0.589 | 0.6-0.9 | 0.6-0.9 | 1.1-1.4 | 1.45-1.85 | 1.95-2.45 | 3.0-3.8 | 4.6-5.4 | |
| Total throughput | 0.54 | 0.46 | 0.50 | 0.81 | 0.83 | 0.84 | 0.80 | 0.75 | Reference |
| Telescope | 0.76 | 0.72 | 0.72 | 0.88 | 0.90 | 0.92 | 0.92 | 0.92 | |
| M1 | 0.87 | 0.85 | 0.85 | 0.94 | 0.95 | 0.96 | 0.96 | 0.96 | VLT-SPE-ESO-10000-2723 |
| M2 | 0.87 | 0.85 | 0.85 | 0.94 | 0.95 | 0.96 | 0.96 | 0.96 | VLT-SPE-ESO-10000-2723 |
| Contamination losses | 0.0375 | 0.0675 | 0.0675 | 0.01 | 0.01 | 0.01 | 0.01 | 0.01 | ~0.25% per in-air surface |
| Warm Optics | 0.95 | 0.95 | 0.95 | 0.92 | 0.92 | 0.92 | 0.87 | 0.82 | |
| Dichroic #1 | 0.95 | 0.95 | 0.95 | 0.95 | 0.95 | 0.95 | 0.9 | 0.85 | Materion ROM quote |
| Folding Mirror (NIX) | | | | 0.97 | 0.97 | 0.97 | 0.97 | 0.97 | Protected Silver |
| WFS Optics | 0.95 | 0.95 | 0.95 | | | | | | |
| Telecentric Lens | 0.996 | 0.996 | 0.996 | | | | | | A/R coating (3 layers) |
| Dichroic #2 | 0.95 | 0.95 | 0.95 | | | | | | Estimate |
| WFS LGS Optics | 0.83 | | | | | | | | |
| Folding Mirror 1 | 0.99 | | | | | | | | Custom dielectric broadband |
| Triplet 1 | 0.98 | | | | | | | | A/R coating (2-3 layers) |
| K-prism | 0.98 | | | | | | | | A/R coating (2 layers) |
| Folding Mirror 2 | 0.99 | | | | | | | | Custom dielectric broadband |
| Triplet 2 | 0.985 | | | | | | | | A/R coating (2 layers) |
| Lenslet Array | 0.89 | | | | | | | | |
| WFS NGS Optics | | 0.76 | 0.82 | | | | | | |
| Triplet 1 | | 0.98 | 0.98 | | | | | | A/R coating (2-3 layers) |
| Periscope Mirror 1 | | 0.99 | 0.99 | | | | | | Custom dielectric broadband |
| Periscope Mirror 2 | | 0.99 | 0.99 | | | | | | Custom dielectric broadband |
| K-prism | | 0.98 | 0.98 | | | | | | A/R coating (2 layers) |
| Folding Mirror 1 | | 0.99 | 0.99 | | | | | | Custom dielectric broadband |
| Folding Mirror 2 | | 0.99 | 0.99 | | | | | | Custom dielectric broadband |
| Triplet 2 | | 0.985 | 0.985 | | | | | | A/R coating (2 layers) |
| Folding Mirror 3 | | 0.99 | 0.99 | | | | | | Custom dielectric broadband |
| ADC 1 | | 0.99 | 0.99 | | | | | | A/R coating (2 layers) |
| ADC 2 | | 0.99 | 0.99 | | | | | | A/R coating (2 layers) |
| Lenslet Array | | 0.89 | 0.96 | | | | | | |
| Relay Lens 1 | | 0.995 | 0.995 | | | | | | A/R coating (3 layers) |
| Relay Lens 2 | | 0.995 | 0.995 | | | | | | A/R coating (2 layers) |
| Detector Window | | 0.98 | 0.98 | | | | | | |
| All but telescope | 0.71 | 0.64 | 0.69 | 0.91 | 0.91 | 0.91 | 0.87 | 0.82 | |

Emissivity

TS-NIX-PER-40 requires a total thermal background emitted by the entire ERIS instrument warm optics elements to be smaller than 50% of the emission by the atmosphere and the telescope.

For the computation of the infrared emissivity due to the WO refer to Sec. 3.2.1 of AD13, showing that the specification is met producing the following ratios between the ERIS emissivity and telescope+atmosphere: K = 25%; L = 44%; M = 27%

| | | | |
|---|--|--|---|
| <p style="text-align: center;">ERIS Consortium</p> | <p style="text-align: center;">ERIS Documentation Standards</p> | <p>Doc.-Ref. Issue Date Page</p> | <p>: VLT-TRE-ERI-14403-3001 : 1.0 : 05.12.15 : 106 of 136</p> |
|---|--|--|---|

7.1.2 Sensitivity Analysis

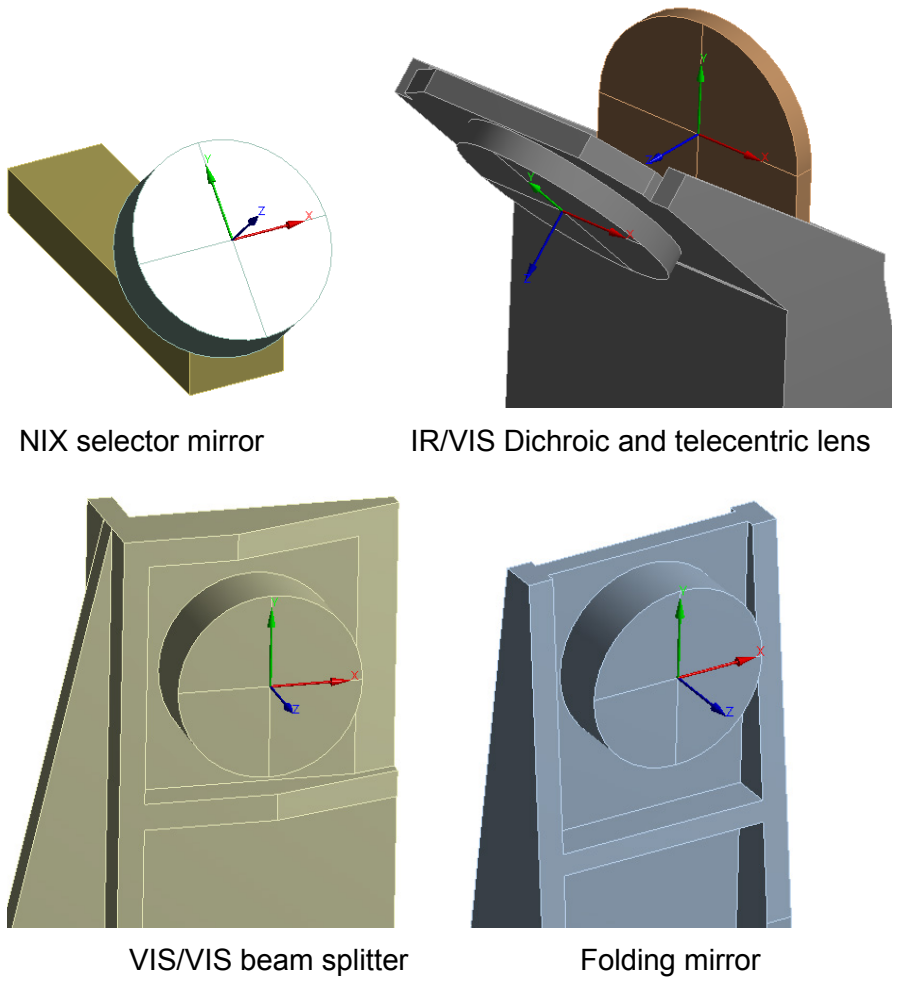
All the optical components at room temperature will need to be aligned, and the ERIS overall structure as well. Assuming typical mechanical tolerances for all those components, some residual differential WFE can be computed, that will affect both the science path and the WFS paths performances (WFE and NCPA budgets). However, very few, low-power optics are present along the beam, so that the computation shows that all those residuals are negligible, after adjustment of the pupil and image centroids, acting on its internal degrees of freedom, like tip/tilt of some optical components.

Method

A Zemax optical model of the ERIS warm optics was used. To simulate the alignment procedure, we defined as targets the pupil and image centroid for both WFS arms (8 targets), and as compensators we used the tip/tilts of 4 plano optics (two dichroics, two folding mirrors, 8 control degrees of freedom). Then, the alignment is performed, after inducing some misalignment of the system or some subsystems, by optimizing the variables/compensators in order to minimize the pupil and image decentering. The 8 DOFs are separated into two 4DOFs subsets, one controlled by the pupil and image positions of that WFS arm, so that the alignment can be done sequentially, without affecting the other. After this realignment, the variation of the WFE on-axis and off-axis is computed.

Results

All the sensitivities are reported in Table 39, Table 40, and Table 41 for the NIX, LGS WFS, and NGS WFS warm optics respectively. The X and Y definition for the WO components is shown in Figure 69.



NIX selector mirror

IR/VIS Dichroic and telecentric lens

VIS/VIS beam splitter

Folding mirror

Figure 69 – local coordinate definition of WO components

Table 39. NIX arm warm optics image and pupil motion sensitivity.

| | Image motion (arcsec) | | | Pupil motion (% pupil) | |
|-------------------|-----------------------|--------|---------------|------------------------|-------|
| | X | Y | Defocus (PTV) | X | Y |
| WFS Dichroic | | | | | |
| <i>DX = 1 mm</i> | -0.005 | | | | |
| <i>DY = 1 mm</i> | | -0.004 | | | |
| <i>DZ = 1 mm</i> | | 0.008 | | | |
| <i>RX = 1 deg</i> | | -0.16 | | | -0.2% |
| <i>RY = 1 deg</i> | 0.14 | | | 0.1% | |
| <i>RZ = 1 deg</i> | 0.03 | | | -0.1% | |
| Selector Mirror | | | | | |

| | | |
|------------------------|-------------------------------------|---|
| ERIS Consortium | ERIS Documentation Standards | Doc.-Ref. : VLT-TRE-ERI-14403-3001 Issue : 1.0 Date : 05.12.15 Page : 108 of 136 |
|------------------------|-------------------------------------|---|

| | | | | | |
|---------------------------------------|-------|-------|-------|-----|------|
| <i>DX = 1 mm</i> | | | | | |
| <i>DY = 1 mm</i> | | | | | |
| <i>DZ = 1 mm</i> | 2.64 | | 0.19 | | |
| <i>RX = 1 deg</i> | | 11.0 | | | -33% |
| <i>RY = 1 deg</i> | -15.6 | | | 47% | |
| <i>RZ = 1 deg</i> | | | | | |
| NIX (pivot at the image plane) | | | | | |
| <i>DX = 1 mm</i> | -1.87 | | | | |
| <i>DY = 1 mm</i> | | -1.87 | | | |
| <i>DZ = 1 mm</i> | | | -0.14 | | |
| <i>RX = 1 deg</i> | | | | | 24% |
| <i>RY = 1 deg</i> | | | | 24% | |
| <i>RZ = 1 deg</i> | | | | | |

Table 40. LGS WFS arm warm optics image and pupil motion sensitivity.

| | Image motion (arcsec) | | | Pupil motion (% pupil) | |
|-------------------------|------------------------------|-------|---------------|-------------------------------|------|
| | X | Y | Defocus (PTV) | X | Y |
| WFS Dichroic | | | | | |
| <i>DX = 1 mm</i> | | | | | |
| <i>DY = 1 mm</i> | | | | | |
| <i>DZ = 1 mm</i> | | -2.62 | -0.19 | | 0.1% |
| <i>RX = 1 deg</i> | | 26.6 | | | 47% |
| <i>RY = 1 deg</i> | -18.8 | | 0.009 | -33% | |
| <i>RZ = 1 deg</i> | | | | | |
| Telecentric lens | | | | | |
| <i>DX = 1 mm</i> | 0.04 | | | 0.1% | |
| <i>DY = 1 mm</i> | | 0.04 | | | 0.1% |
| <i>DZ = 1 mm</i> | | | -0.006 | | |
| <i>RX = 1 deg</i> | | 0.12 | | | |
| <i>RY = 1 deg</i> | -0.12 | | | | |
| <i>RZ = 1 deg</i> | | | | | |
| NGS Dichroic | | | | | |
| <i>DX = 1 mm</i> | | | | | |
| <i>DY = 1 mm</i> | | | | | |

| | | | |
|------------------------|-------------------------------------|-----------|--------------------------|
| ERIS Consortium | ERIS Documentation Standards | Doc.-Ref. | : VLT-TRE-ERI-14403-3001 |
| | | Issue | : 1.0 |
| | | Date | : 05.12.15 |
| | | Page | : 109 of 136 |

| | | | | | |
|---|-------|-------|--------|------|------|
| <i>DZ = 1 mm</i> | | | | | |
| <i>RX = 1 deg</i> | | 0.14 | | | |
| <i>RY = 1 deg</i> | -0.14 | | -0.004 | | |
| <i>RZ = 1 deg</i> | | | | | |
| Folding Mirror | | | | | |
| <i>DX = 1 mm</i> | | | | | |
| <i>DY = 1 mm</i> | | | | | |
| <i>DZ = 1 mm</i> | 2.01 | | 0.24 | | |
| <i>RX = 1 deg</i> | | -3.51 | | | -40% |
| <i>RY = 1 deg</i> | 4.14 | | | 47% | |
| <i>RZ = 1 deg</i> | | | | | |
| LGS WFS board (pivot at 270 mm from focal plane) | | | | | |
| <i>DX = 1 mm</i> | -1.89 | | | | |
| <i>DY = 1 mm</i> | | -1.89 | | | |
| <i>DZ = 1 mm</i> | | | -0.14 | | |
| <i>RX = 1 deg</i> | | -8.93 | | | 23% |
| <i>RY = 1 deg</i> | 8.93 | | | -23% | |
| <i>RZ = 1 deg</i> | | | | | |

Table 41. NGS WFS arm warm optics image and pupil motion sensitivity.

| | Image motion (arcsec) | | | Pupil motion (% pupil) | |
|-------------------------|------------------------------|-------|---------------|-------------------------------|------|
| | X | Y | Defocus (PTV) | X | Y |
| WFS Dichroic | | | | | |
| <i>DX = 1 mm</i> | | | | | |
| <i>DY = 1 mm</i> | | | | | |
| <i>DZ = 1 mm</i> | | -2.64 | -0.19 | | 0.1% |
| <i>RX = 1 deg</i> | | 20.5 | | | 47% |
| <i>RY = 1 deg</i> | -14.5 | | | -33% | |
| <i>RZ = 1 deg</i> | | | | | |
| Telecentric lens | | | | | |
| <i>DX = 1 mm</i> | 0.03 | | | 0.1% | |
| <i>DY = 1 mm</i> | | 0.03 | | | 0.1% |
| <i>DZ = 1 mm</i> | | | -0.004 | | |

| | | | |
|----------------------------|---|-----------|--------------------------|
| ERIS Consortium | ERIS Documentation Standards | Doc.-Ref. | : VLT-TRE-ERI-14403-3001 |
| | | Issue | : 1.0 |
| | | Date | : 05.12.15 |
| | | Page | : 110 of 136 |

| | | | | | |
|--|-------|-------|-------|------|------|
| <i>RX = 1 deg</i> | | 0.12 | | | |
| <i>RY = 1 deg</i> | -0.12 | | | | |
| <i>RZ = 1 deg</i> | | | | | |
| NGS Dichroic | | | | | |
| <i>DX = 1 mm</i> | | | | | |
| <i>DY = 1 mm</i> | | | | | |
| <i>DZ = 1 mm</i> | 1.11 | | 0.27 | | |
| <i>RX = 1 deg</i> | | -5.37 | | | -45% |
| <i>RY = 1 deg</i> | 5.62 | | | 47% | |
| <i>RZ = 1 deg</i> | | | | | |
| NGS WFS board (pivot at 270 mm from focal plane on the Entrance Lens vertex) | | | | | |
| <i>DX = 1 mm</i> | -1.89 | | | | |
| <i>DY = 1 mm</i> | | -1.89 | | | |
| <i>DZ = 1 mm</i> | | | -0.14 | | |
| <i>RX = 1 deg</i> | | -8.93 | | | 23% |
| <i>RY = 1 deg</i> | 8.93 | | | -23% | |
| <i>RZ = 1 deg</i> | | | | | |

Table 42 gives, as an example, the effect of dichroic misalignments on the science path, for both the current design based onto a spherical rear surface of the dichroic and a previous design based onto a cylindrical rear surface. Sensitivities are very small. All other optical components have no power and any decenter or tilt will have no effect on WFE or NCPA.

We assumed component decenters of the order of few millimeters, and tilts of a fraction of degree. For all the DOFs above, all difference in WFE and NCPA were always less (or much less) than 1 nm RMS, both on-axis and off-axis. We concluded that standard mechanical tolerances can be used to position optical components. Then, alignment of pupils and images will be done as per our alignment procedure.

Table 42. Alignment sensitivities of Strehl ratio, on- and off-axis, for cylindrical or spherical dichroic rear surface.

| | SR (on-axis) - Cylinder | SR (on-axis) - Sphere |
|--|--------------------------------|------------------------------|
| <i>Decenter X (ΔStrehl/mm)</i> | 0 | 0.001% |
| <i>Decenter Y (ΔStrehl/mm)</i> | 0.02% | 0.01% |
| <i>Decenter Z (ΔStrehl/mm)</i> | 0.007% | 0.01% |
| <i>Tilt X (ΔStrehl/arcmin)</i> | 0.005% | 0.006% |

| | | | |
|----------------------------|---|-----------|--------------------------|
| ERIS Consortium | ERIS Documentation Standards | Doc.-Ref. | : VLT-TRE-ERI-14403-3001 |
| | | Issue | : 1.0 |
| | | Date | : 05.12.15 |
| | | Page | : 111 of 136 |

| | | |
|--|---|---|
| <i>Tilt Y (ΔStrehl/arcmin)</i> | 0 | 0 |
| <i>Tilt Z (ΔStrehl/arcmin)</i> | 0 | 0 |

| | SR (off-axis) - Cylinder | SR (off-axis) - Sphere |
|--|---------------------------------|-------------------------------|
| <i>Decenter X (ΔStrehl/mm)</i> | 0 | 0.03% |
| <i>Decenter Y (ΔStrehl/mm)</i> | 0.06% | 0.05% |
| <i>Decenter Z (ΔStrehl/mm)</i> | 0.03% | 0.03% |
| <i>Tilt X (ΔStrehl/arcmin)</i> | 0.009% | 0.009% |
| <i>Tilt Y (ΔStrehl/arcmin)</i> | 0 | 0.003% |
| <i>Tilt Z (ΔStrehl/arcmin)</i> | 0 | 0.003% |

7.1.3 Mechanical Performances

AD8 reports the displacements and rotations under gravity of the WO optical components, the NIX entrance window and the WFS unit interfaces generated by a preliminary FEA in the following load cases:

- at zenith (z0)
- at z=45deg (z45)
- at horizon z=90deg (z90)

We assume ERIS is optically aligned at zenith, then the effective displacements and rotations producing optical misalignment are computed by subtracting the zenith load case (z0) data from the data of the load case of interest. The resulting displacements and rotations are transformed to local coordinates of the corresponding components in the ZEMAX optical prescription and inserted with a set of coordinate-break surfaces to simulate the gravity effect in ZEMAX. The longitudinal focus and lateral shifts of the on-axis chief ray of NGS WFS and NIX focal planes are recorded, are transformed in focus WFE RMS and on-sky tip and tilt taking into account the different F/number and focal plane scale and the difference is computed to provide the optical effect to the differential focus and flexures. We remind that only the NGS WFS is relevant in this analysis because it is the tip-tilt and focus reference both in NGS and LGS mode.

Table 43 summarizes the results, showing a limited optical effect of the gravity change: ≤ 130 mas and <18 nm WFE of focus rms from zenith to horizon. These results are preliminary because do not consider the change of instrument rotator angle and because the WO components, NIX and WFS units are modeled as infinitely internally rigid. Further FEA analysis will be performed in the next design phase.

| | | |
|----------------------------|---|---|
| ERIS Consortium | ERIS Documentation Standards | Doc.-Ref. : VLT-TRE-ERI-14403-3001 Issue : 1.0 Date : 05.12.15 Page : 112 of 136 |
|----------------------------|---|---|

Table 43 – differential focus and tip-tilt between NGS WFS and NIX. X and Y axis are NIX local focal plane coordinates as defined in AD8.

| Load case | Differential Focus WFE nm rms | Differential tilt-x on-sky mas | Differential tilt-y on-sky mas | Combined tilts on-sky mas |
|---------------|-------------------------------|--------------------------------|--------------------------------|---------------------------|
| z45-z0 | 5.1 | -21 | 61 | 65 |
| z90-z0 | 17.6 | -78 | 104 | 130 |

The focus and PSF motion due to flexures will be calibrated during the instrument AIV phase and verified during commissioning phase producing a LUT. For the error budget purposes we will consider a conservative factor of 1.5 with respect to the z90-z0 FEA results. Supposing 6 hours for tracking between zenith and horizon, the LUT rate of:

Focus drift: 4.5 nm RMS/hour TT drift: 32 mas/hour

For the error budget we will suppose the LUT will correct only 70% of the drift error to take into account calibration errors, hysteresis and other non linear effects.

7.1.4 IR/VIS Dichroic FEA analysis and processing

The dichroic analysis has been performed with COMSOL Multiphysics® and analyzed in order to characterize the WFE induced by the dichroic position variation against the gravity vector.

7.1.4.1 Model

The FEA model was performed accordingly the following parameters:

| Topic | Parameters |
|---------------------|--|
| Geometry | Cylinder with elliptical base of dimensions built from optical input data: 146 x 102 mm and 12 mm thickness |
| Boundary conditions | Edge clamping in 3 points and lateral support on the mean thickness. Three sets of points on the outer edge, 120deg apart (total 9 points): 1) on the the mid thickness: azimuthal and radial position constraints 2) on the top surface: axial position constraint 3) on the bottom surface: axial position constraint See |
| Material | Calcium Fluoride with: <ul style="list-style-type: none"> • Young's modulus 75.8e9 N/m² • Poisson's modulus 0.26 • density 3180 kg/m³ |
| Load case | The simulation has been performed simulating the gravity vector effect on three telescope elevation/rotator combinations (90-0 deg; 0-0 deg; 0-90 deg) |
| Results processing | The results have been verified in terms of nodal reaction forces in order to verify the static equilibrium. The deformations are given in terms of displacements at the mesh points. As post-processing, a Monte Carlo analysis has been performed on 10000 |

| | | | |
|-----------------|------------------------------|------------------------------------|---|
| ERIS Consortium | ERIS Documentation Standards | Doc.-Ref. Issue Date Page | : VLT-TRE-ERI-14403-3001 : 1.0 : 05.12.15 : 113 of 136 |
|-----------------|------------------------------|------------------------------------|---|

| | |
|-----------------------|--|
| | random patches for NGS case. Single patch on centre for LGS case. |
| Load topology | Uniform gravity field interesting the material. The load applied is the body load given by the material density multiplied by the gravity. $G=9.81 \text{ m/s}^2$ |
| Type of elements used | 71774 tetrahedral elements, 13986 nodes with average spatial resolution of 1.25 mm The static analysis is carried out using the physics defined by the software "Solid Mechanics Interface", whose elements are defined with 3 degrees of freedom (the 3 displacements) per node. |

7.1.4.2 Geometry

The geometry of the object is matching the optical and mechanical design. The dichroic is an elliptical lens with major axis 146 mm and minor axis 102 mm of Calcium Fluoride, 12 mm thick.

The holder clamps have been not simulated as physical object but in this phase we preferred to simply properly adding simulation restrains.

7.1.4.3 Boundary conditions

The restrains are applied on the dichroic edge with a 120-degrees symmetry.

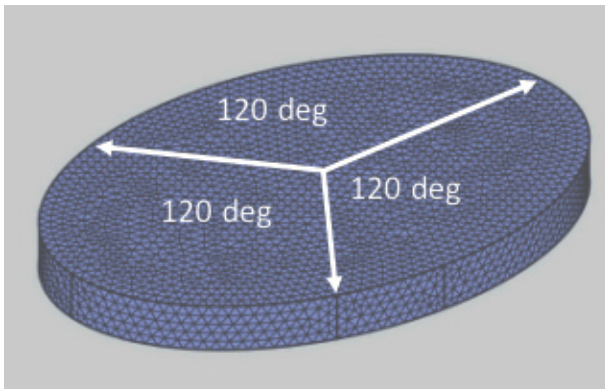


Figure 70: Bounds symmetry

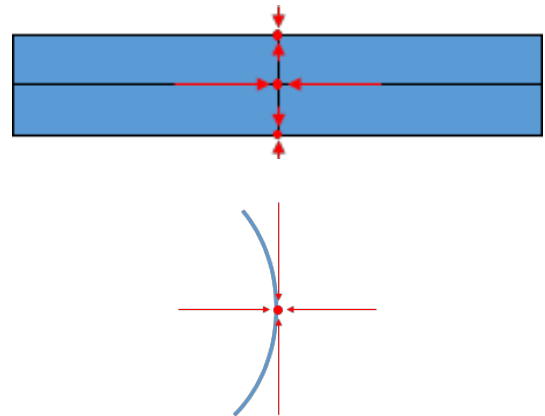


Figure 71: Restraints applied to the edges. Top and bottom normal to the surface. Middle normal and tangential to the edge.

On each angular displacement, the bounds are set on three point distributed on the front, on middle, and on the back surfaces of the dichroic. The point on the top and on the bottom surfaces are constrained normally to the surface to simulate a clamping, while the point on the middle is constrained radially to simulate a lateral support and tangentially to constraint rotations.

7.1.4.4 Load cases

The simulated load cases take into account the main worst cases for dichroic deflection. The considered positions are corresponding to a telescope elevation of 90 deg and 0 deg (named H90 and

| | | | |
|------------------------|-------------------------------------|------------------------------------|---|
| ERIS Consortium | ERIS Documentation Standards | Doc.-Ref. Issue Date Page | : VLT-TRE-ERI-14403-3001 : 1.0 : 05.12.15 : 114 of 136 |
|------------------------|-------------------------------------|------------------------------------|---|

H0). This last elevation was simulated for two instrument rotator positions of 0 deg and 90 deg (named R0 and R90). Clearly Load cases H90-R0 and H0-R0 provide the same deformation with reverse sign.

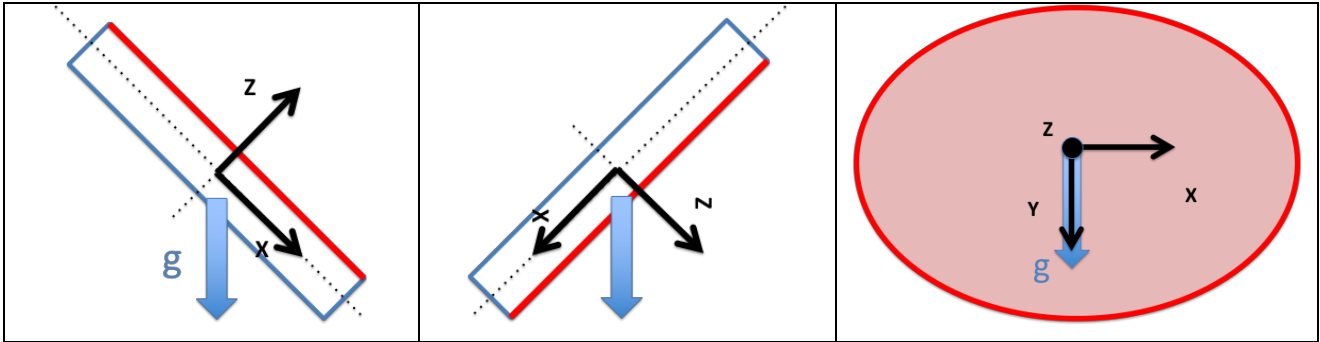


Figure 72: Load cases elevation/rotator: H90-R0; H0-R0; H0-R90

7.1.4.5 Results

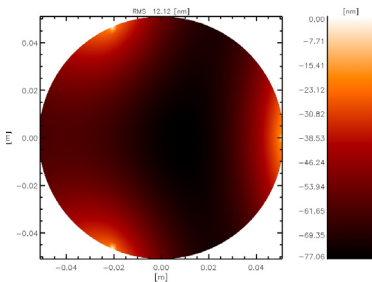


Figure 75: case H90-R0

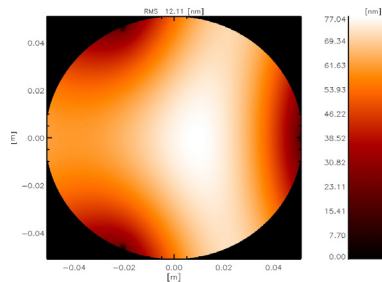


Figure 73: case H0-R0

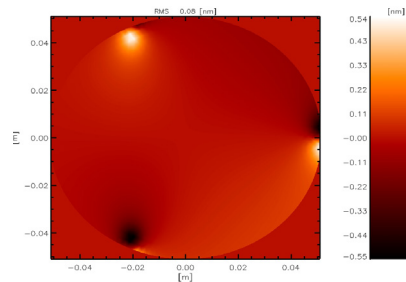


Figure 74: case H90-R0

The results of the FEA were reported in Figure 75, Figure 74, Figure 73. The deformations are shown as WFE perpendicular to the optical axis. The total amount of deformation is 12.1 nm RMS for the H90-R0 case, 12.1 nm RMS form the H0-R90 case and 0.08 nm RMS for the H0-R0 case.

The post-simulation analysis has been performed considering the optical footprint for NGS case (circle 25.4 mm) and LGS case (circle 35.4 mm).

The LGS case is a single evaluation on the optical footprint at the centre of the dichroic. The NGS case is performed on 10000

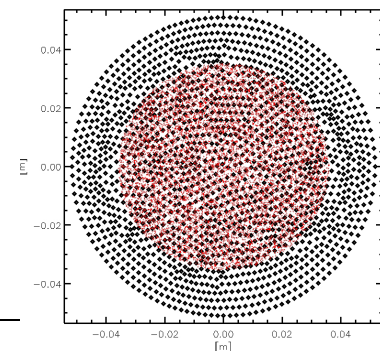


Figure 76: Monte Carlo population of random centres

patches randomly distributed on the clear aperture (optical radius reduced of 3 mm) and the worst case was selected.

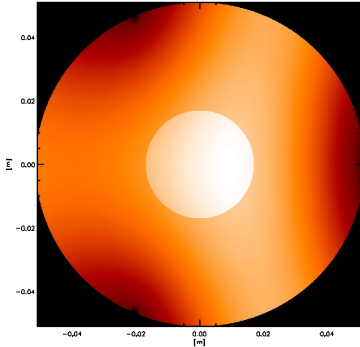


Figure 78: Optical footprint LGS case

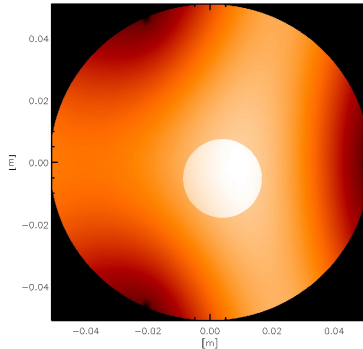


Figure 77: Sample optical footprint NGS case

The maximum values among the footprints are reported in the Table 44. For the Tip-Tilt, the differential value with respect to the zenith load case (ref) is shown, affecting the image motion during elevation change. The last column shows the maximum RMS WFE among the patches after removing the tip-tilt; this contributes to NCPA budget.

| | Cases | WFE nm | TT ref subtracted WFE nm | TT ref subtracted WFE mas (on-sky) | RMS (tilt removed) WFE nm |
|------------|--------|--------|--------------------------|------------------------------------|---------------------------|
| LGS | H90-R0 | 3.01 | 0.00 | 0.00 | 1.14 |
| | H0-R0 | 3.01 | 5.58 | 0.57 | 1.14 |
| | H0-R90 | 0.01 | 2.79 | 0.28 | 0.01 |
| NGS | H90-R0 | 11.21 | 0.00 | 0.00 | 1.67 |
| | H0-R0 | 11.12 | 22.09 | 2.25 | 1.61 |
| | H0-R90 | 0.11 | 11.08 | 1.13 | 0.07 |

Table 44: WFE FEA analysis result over optical footprints. The tilt is reported with respect to the H90-R0 case used as tilt reference.

7.2 NGS Opto-mechanical Performances

7.2.1 Optical Performances

Nominal wavefront errors of the NGS WFS have been minimized. Figure 79 shows the WFE map at the center and the edge of the 2 arcmin diameter WFS field of view. Residual aberrations are 5 nm RMS on-axis and up to 12 nm RMS off-axis, contributing to the NCPA. For the error budget (on-axis) calculation we consider a conservative 10 nm RMS waiting for the result of tolerance analysis that is foreseen for the next design phase.

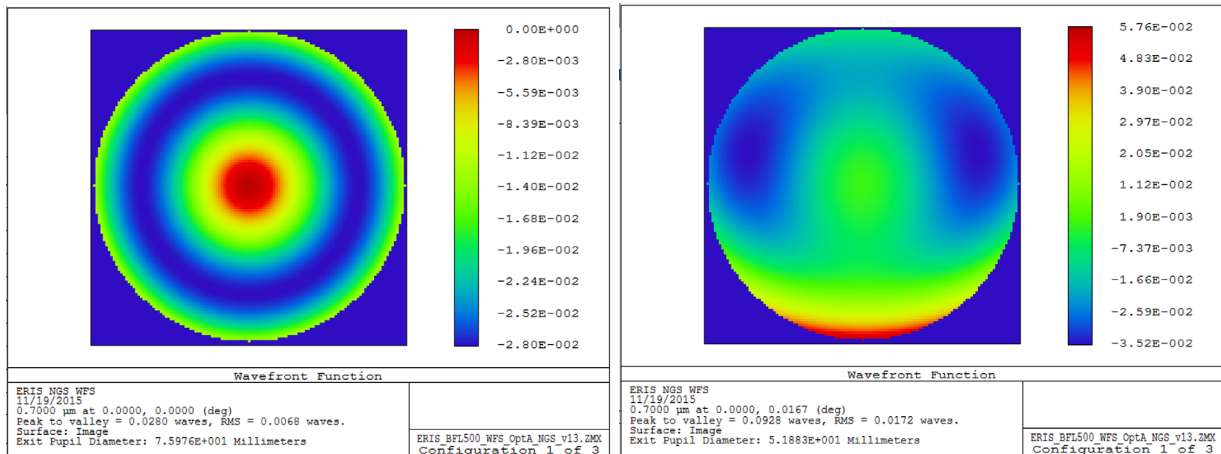


Figure 79. NGS WFS OPD at the lenslet pupil, both on-axis (left) and 1 arcmin off-axis.

ADC correction over the full 0-70 deg zenith angle range is always better than 10 mas, as shown in Figure 80. The ADC design has an undeviated wavelength of 720 nm, quite close to the barycenter of the WFS bandwidth.

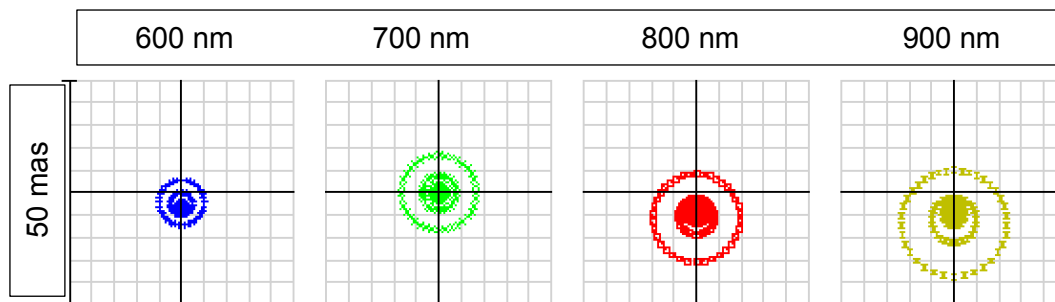


Figure 80. ADC residual chromatic dispersion at the image plane at the maximum zenith angle (70°).

7.2.2 Sensitivity Analysis

This is a place-holder for the full NGS WFS sensitivity analysis. During preliminary design, we checked the alignment sensitivity of the most critical item, i.e. the prism derotator and the NGS lenslet switching mechanism hosting the two relay lens barrels.

Switching mechanism

The most sensitive layout is the High Order barrel, with the largest 900 mas/pixel plate scale. A pivot located near the centre of the mechanical switching mechanism will induce:

- Decenter Sensitivity: 37.5 milliarcsec/micron
- Tilt Sensitivity: 5 milliarcsec/microrad

Prism derotator

The prism derotator is quite sensitive to small misalignments during operation. The image rotation angle is twice the mechanical angular rotation around the optical axis. However the optical axis

| | | | |
|----------------------------|---|-----------|--------------------------|
| ERIS Consortium | ERIS Documentation Standards | Doc.-Ref. | : VLT-TRE-ERI-14403-3001 |
| | | Issue | : 1.0 |
| | | Date | : 05.12.15 |
| | | Page | : 117 of 136 |

must be perfectly aligned with a given rotational mechanical axis, otherwise the image will also precess around a moving center of rotation, as shown in the examples of Figure 81.

Maximum image motion is:

- Decenter Sensitivity: 2.6 milliarcsec/micron
- Tilt Sensitivity: 0.4 milliarcsec/microrad

The image motion (in mm at the F/20 focal plane) is twice the prism decenter (in mm).

Combining the rotary stage specification data in 4.9.2.3 with the results of the k-mirror sensitivity, the radius R_w of focal plane circular drift due to rotator wobbling (30urad) is:

$$R_w = 30\text{urad} \times 0.4 \text{ mas/urad} = 12 \text{ mas}$$

Providing a PSF shift per degree of instrument rotator

$$2\pi R_w/360 = 0.21 \text{ mas/deg}$$

The PSF drift radius R_d due to the rotator eccentricity (6um) gives:

$$R_d = 6\text{um} \times 2.6 \text{ mas/um} = 15.6 \text{ mas}$$

giving a PSF shift per degree of instrument rotator:

$$2\pi R_d/360 = 0.27 \text{ mas/deg}$$

The PSF wobbling due to pupil rotator is the major contribution to image motion for observations close to the Zenith (see Sec. 9.2). Because the misalignment of the prism with respect to the rotary stage mechanical axis provides an additional contribution to the PSF wobbling, we constrain the accuracy of this alignment to have similar contributions to the ones estimated for the rotary stage specifications. Considering the alignment of the prism to the mechanical axis needs to be as good as 10 um in decentering and 20 arcsec in tilt, the image motion rate per degree of instrument rotator angle is:

$$10 \text{ um decentering: } 0.45 \text{ mas/deg}$$

$$20 \text{ arcsec: } 0.18 \text{ mas/deg}$$

The linear sum of the four terms will be used for the error budget analysis: 1.1 mas/deg.

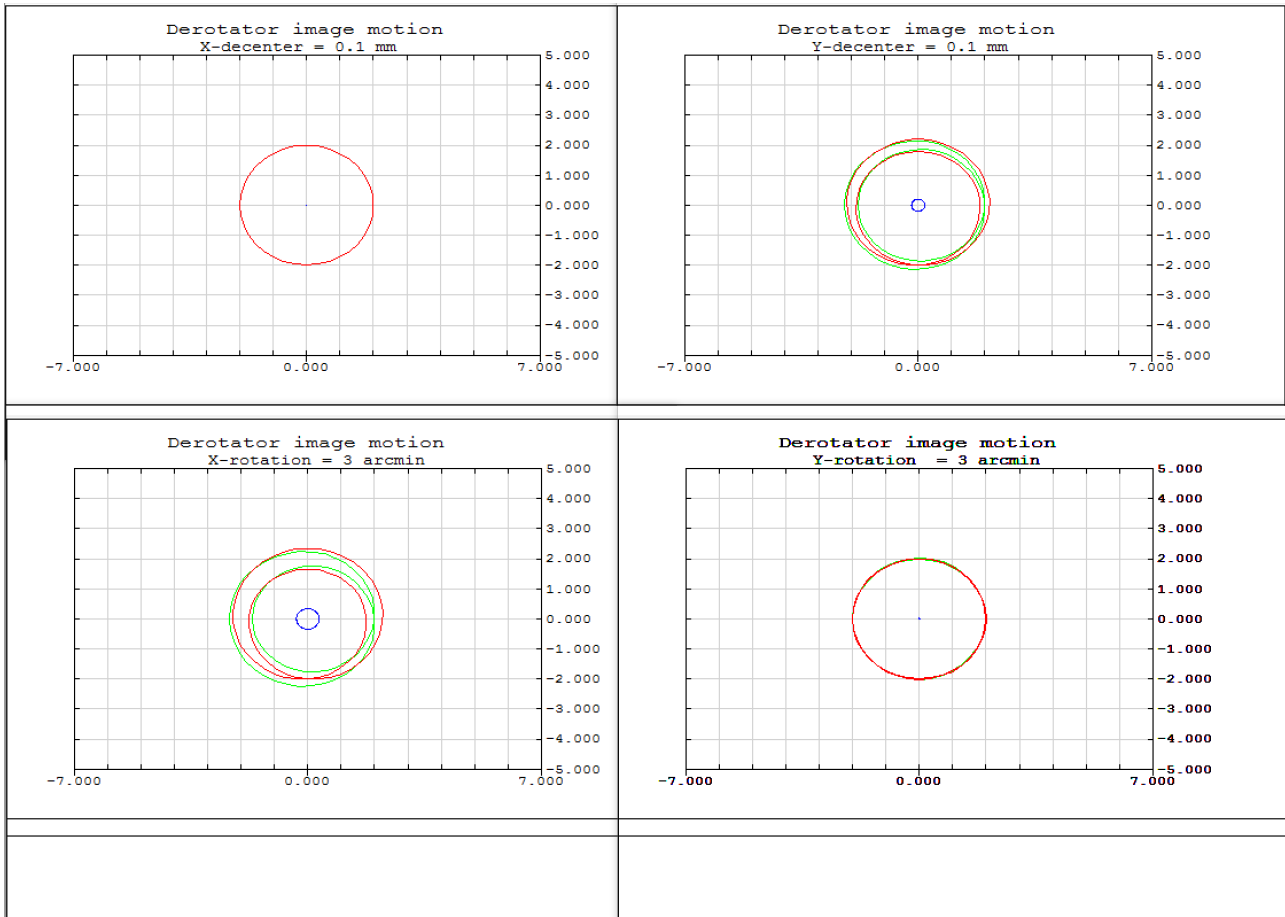


Figure 81. Image motion at the F/20 image plane after the derotator. Different mis-alignments are simulated.

7.3 LGS Opto-mechanical Performances

7.3.1 Optical Performances

The LGS WFS optics will have image performances quite similar to the NGS High-Order WFS optics, because its design is almost identical up to the lenslet array. The only difference is the LGS/NGS dichroic that transmits the light to the LGS optics, thus introducing a very small astigmatism (66 nm RMS), that will be measured and calibrated. This amount of aberration is a small fraction of the LGS WFS slope error budget.

8 Alignment Concept

8.1 LGS WFS board internal alignment

This section reports the sequence of operations required to perform the internal alignment of the LGS WFS units. The aim of the presented procedure is to identify tools and degrees of freedom that are needed to make the alignment. The details of the procedure and the accuracy required for each step will be studied in the next design phase.

| | | | |
|---|--|--|---|
| <p style="text-align: center;">ERIS Consortium</p> | <p style="text-align: center;">ERIS Documentation Standards</p> | <p>Doc.-Ref. Issue Date Page</p> | <p>: VLT-TRE-ERI-14403-3001 : 1.0 : 05.12.15 : 119 of 136</p> |
|---|--|--|---|

8.1.1 Tools

- ObjInf: An optical device that provides an extended object (like an F) at infinite distance
- Pointer: A device that produces a collimated laser beam of 1-2mm of diameter. This device is mounted on a replica of the Entrance Lens mount and aligned in such a way that materializes the Entrance Lens axis. This device can shine the beam in both direction (inside and outside the LGS WFS board) by reversing the device and it is used for the internal alignment and the alignment of the LGS WFS with the external optics
- F/13.4 source: A device that produces a laser F/13.4 beam with a pupil image at infinite mimicking the telescope LGS beam. This device is mounted outside of the LGS WFS board to reproduce the on-axis telescope beam. It is aligned to the LGS WFS axis using the Pointer shining outside the LGS WFS board.
- Shearing Interferometer: A commercial shearing interferometer to check beam collimation
- CameraFlange: A device that is mechanically identical to the flange of the CCD camera and materializes the nominal plane on which the SH lenslet array is located with the respect to the external mount of the CCD Camera. It is used to properly conjugate the lenslet array plane with the pupil image.
- AlignmentCamera: A laboratory small camera without optics used for alignment purpose.

8.1.2 Conventions

We refer in the following to the Z axis as the axis of optical propagation axis, the X axis is perpendicular to Z and parallel to the board plane, the Y axis is perpendicular to the board plane. Rx, Ry and Rz are the rotation around the corresponding axes.

8.1.3 Alignment procedure

Alignment will be done accordingly to the following steps:

1. K mirror alignment

The K-mirror sub-unit is supposed already internally aligned

 - a. Z alignment.

The K mirror must be positioned along the Z axis to have the pupil plane imaged on its first optical surface. The pupil plane Z position on the board is determined using the ObjInf device. A mechanical reference is positioned on the board.
 - b. X, Y, Rx, Ry alignment

The K mirror devices is mounted on the board in the Z position found in the previous step. The Entrance Lens is removed and replaced by the Pointer shining inside the LGS board. The X, Y, Rx and Ry degrees of freedom are adjusted minimizing the wobble of the Pointer beam on the AlignmentCamera when the K mirror is spinning.
2. Beam splitter
 - a. The beam splitter is inserted in the optical path centered on the Pointer beam and Rx, Ry angles are adjusted to center the Pointer beam in the center of the Technical Camera
3. Pupil Stabilization Mirror
 - a. Z alignment

The F/13.4 source is used. The Entrance Lens is mounted. The PSM is adjusted to have its surface in the focal plane produced by the F/13.4 source.
 - b. Rx, Ry alignment

| | | | |
|---|--|--|---|
| <p style="text-align: center;">ERIS Consortium</p> | <p style="text-align: center;">ERIS Documentation Standards</p> | <p>Doc.-Ref. Issue Date Page</p> | <p>: VLT-TRE-ERI-14403-3001 : 1.0 : 05.12.15 : 120 of 136</p> |
|---|--|--|---|

The Entrance Lens is removed and the Pointer is used toward the inside of the LGS board. The AlignmentCamera is installed on the PSM reflected beam. Rx is adjusted to keep the beam's height over the board constant. This is checked translating the AlignmentCamera on the board.

The CameraFlange is mounted in the nominal position of the CCD Camera and the PSM Ry angle is roughly adjusted to center the reflected beam on the Camera-Flange target.

4. Collimator Lens

a. Z alignment

The F/13.4 source is used. The Entrance Lens is mounted. The Collimator Lens (CL) is installed in its nominal position and Z is adjusted using the Shearing Interferometer checking that the output beam is collimated. A mechanical reference for the CL Z-position is installed on the board

b. X, Y alignment

The Entrance Lens is removed and the Pointer is used toward the inside of the LGS board. The Alignment Camera is mounted after the Collimator Lens. The Collimator Lens is removed and the Pointer beam position is stored. The Collimator Lens is mounted back and its X, Y are adjusted in order to restore the Pointer beam position.

5. CCD Camera

We remind that the LGS camera is delivered with the internal SH already aligned with certified Z position with respect to its interface flange.

a. Z alignment

The ObjInf device is used, the Pointer is removed and the Entrance Lens is installed, The CameraFlange is installed and adjusted in Z in order to have the pupil image conjugated to the target plane. A mechanical reference is installed on the board

The CameraFlange is removed and the CCD Camera is installed and it is Z-adjusted to the mechanical reference.

b. X, Y alignment

F/13.4 is installed and the CCD Camera X and Y position are adjusted to properly illuminate the nominal subapertures.

c. Rx, Ry alignment

The CCD Camera is rotated around Rx and Ry in order to have the spots centered on the nominal pixels of each subaperture

8.2 Internal Alignment of NGS WFS

This section reports the sequence of operations performing the internal alignment of the NGS WFS units. The aim of the presented procedure is to identify tools and degrees of freedom that are needed to make the alignment. The details of the procedure and the accuracy required for each step will be studied in the next design phase.

| | | | |
|---|--|--|---|
| <p style="text-align: center;">ERIS Consortium</p> | <p style="text-align: center;">ERIS Documentation Standards</p> | <p>Doc.-Ref. Issue Date Page</p> | <p>: VLT-TRE-ERI-14403-3001 : 1.0 : 05.12.15 : 121 of 136</p> |
|---|--|--|---|

8.2.1 Pre-requisites

- The barrel containing the periscope optics (Barrel) can be removed from the Periscope rotator and mounted back maintaining the optical alignment with a sufficient accuracy
- The 2 Lenslet barrels have been previously internally aligned. Moreover, the barrels, mounted on the stage have been aligned in Z, Y, Rx, Ry and Rz in such a way that the 2 spot grids are produced in the same Z plane, at the same Y height above the stage and that the grids are properly clocked (rows are parallel to the stage translation direction)

8.2.2 Tools

- ObjInf: An optical device that provides an extended object (like an F) at infinite distance
- Pointer: A device that produces a collimated laser beam of 1-2mm of diameter. This device is mounted on the Periscope Rotator and aligned in such a way that materializes the Periscope Rotator mechanical axis in both translation and angle. This device can shine the beam in both direction (inside and outside the NGS WFS board) and it is used for the internal alignment and the alignment of the NGS WFS with the external optics. This device can be mounted in the Periscope Rotator both when the Barrel is removed and when it is installed.
- F/13.4 source: A device that produces a laser F/13.4 beam with a pupil image at infinite mimicking the telescope NGS beam. This device is mounted outside of the NGS board to reproduce the on-axis telescope beam. It is aligned to the NGS WFS axis using the Pointer shining outside the NGS WFS board.
- Shearing Interferometer: A commercial shearing interferometer to check beam collimation
- CameraFlange: A device that is mechanically identical to the flange of the CCD camera and materializes the nominal plane on which the detector is located with the respect to the external mount of the CCD Camera. It is used to properly conjugate the lenslet array plane with the pupil image.
- AlignmentCamera: A laboratory small camera without optics used for alignment purpose.
- LCB: A large (same diameter as the periscope barrel) collimated beam like the one produced by a Wyko Interferometer
- Periscope Auxiliary Mirror: A flat mirror that can be mounted on the periscope rotator on the side facing the WFS board to retroreflect the beam entering the WFS. It can be adjusted to be perpendicular to the periscope rotator mechanical axis.

8.2.3 Alignment procedure

Alignment will be done accordingly to the following steps:

1. Periscope unit alignment
 - a. Periscope Auxiliary Mirror alignment
The Barrel is dismounted and the Periscope Auxiliary Mirror (PAM) is installed on the rotator. The PAM surface is made perpendicular to the rotator axis using an external collimated beam.
 - b. LCB alignment
The LCB is shined through the periscope rotator bearing illuminating the PAM. LCB tilt is adjusted in order to reach auto-collimation.
 - c. Periscope mirrors alignment
The Barrel is mounted in the Periscope rotator without the Entrance Lens
The mirrors inside the Barrel are adjusted in order to reach auto-collimation of LCB.
This condition should be verified for any rotator angle.
 - d. Entrance Lens alignment

| | | | |
|---|--|--|---|
| <p style="text-align: center;">ERIS Consortium</p> | <p style="text-align: center;">ERIS Documentation Standards</p> | <p>Doc.-Ref. Issue Date Page</p> | <p>: VLT-TRE-ERI-14403-3001 : 1.0 : 05.12.15 : 122 of 136</p> |
|---|--|--|---|

The PAM is removed and the Pointer is installed in the Periscope rotator shining inside the Barrel

We store the position of the Pointer beam on the AlignmentCamera

The Entrance Lens is installed in the periscope Barrel and its X, Y are aligned to restore the position of the Pointer beam on the AlignmentCamera

2. K mirror alignment

a. Z alignment.

The K mirror must be positioned along the Z axis to have the pupil plane imaged on its first optical surface. The pupil plane Z position on the board is determined using the ObjInf device. A mechanical reference is positioned on the board.

b. X, Y, Rx, Ry alignment

The K mirror devices is mounted on the board in the Z position found in the previous step. The Entrance Lens is removed and replaced by the Pointer shining inside the LGS board. The X, Y, Rx and Ry degrees of freedom are adjusted minimizing the wobble of the Pointer beam on the AlignmentCamera when the K mirror is spinning.

3. Dichroic alignment

a. The Dichroic is inserted in the optical path centered on the Pointer beam and Rx, Ry angles are adjusted to center the Pointer beam in the center of the Pupil Stabilization Mirror

b. The AlignmentCamera is installed on the beam reflected by the Dichroic. Rx is adjusted to keep the beam's height over the board constant. This is checked translating the AlignmentCamera on the board.

4. Pupil Stabilization Mirror

a. Z alignment

The F/13.4 source is used. The Entrance Lens and the Periscope Barrel are mounted. The PSM is adjusted to have its surface in the focal plane produced by the F/13.4 source.

b. Rx alignment

The Entrance Lens and the Periscope Barrel are removed and the Pointer is used toward the inside of the NGS board. The AlignmentCamera is installed on the PSM reflected beam. PSM Rx is adjusted to keep the beam's height over the board constant. This is checked translating the AlignmentCamera on the board.

c. Ry alignment

The Folding Mirror is mounted in the nominal position and the PSM Ry angle is roughly adjusted to center the reflected beam on the Folding Mirror center.

5. Folding Mirror

a. Rx alignment

The AlignmentCamera is installed on the Folding Mirror reflected beam. Folding Mirror Rx is adjusted to keep the beam's height over the board constant. This is checked translating the AlignmentCamera on the board.

b. Ry alignment

The CameraFlange is mounted in the nominal position of the CCD Camera and the Ry angle is roughly adjusted to center the reflected beam on the CameraFlange target.

| | | | |
|-------------------------------|--|--|---|
| <p>ERIS Consortium</p> | <p>ERIS Documentation Standards</p> | <p>Doc.-Ref. Issue Date Page</p> | <p>: VLT-TRE-ERI-14403-3001 : 1.0 : 05.12.15 : 123 of 136</p> |
|-------------------------------|--|--|---|

6. Filter wheel
 - a. Filter wheel

The filter wheel is installed in its nominal position and centered on the Pointer beam

7. Collimator Lens
 - a. Z alignment

The F/13.4 source is used. The Entrance Lens the Periscope Barrel are mounted. The Collimator Lens (CL) is installed in its nominal position and Z is adjusted using the Shearing Interferometer checking that the output beam is collimated. A mechanical reference for the CL Z-position is installed on the board.
 - b. X, Y alignment

The Pointer is used toward the inside of the NGS board. The Alignment Camera is mounted after the Collimator Lens. The Collimator Lens is removed and the Pointer beam position is stored. The Collimator Lens is mounted back and its X, Y are adjusted in order to restore the Pointer beam position.

8. ADC
 - a. Z alignment

The ADC is installed in its nominal position
 - b. Rx, Ry alignment

The Pointer is used toward the inside of the NGS board. The Alignment Camera is mounted after the ADC. The ADC is removed and the Pointer beam position is stored. The ADC is mounted back and its X, Y are adjusted in order to restore the Pointer beam position.

9. CCD Camera
 - a. Z alignment

The CCD Camera is temporarily set to nominal position in Z.
 - b. X, Y, Rx, Ry alignment

The Pointer is used to materialize the optical axis on the CCD Camera (the Pointer propagated through the NGS optics should provide a beam of about 2mm diameter). The Camera is panned to roughly center the spot on the CCD array central pixel. The Camera is Rx, Ry tilted using back-reflection from the CCD window.

10. Lenslet switch
 - a. Z alignment

The ObjInf device is used, the Pointer is removed and the Entrance Lens and Periscope Barrel are installed. The Lenslet Switch is adjusted in Z in order to have the pupil image conjugated to the lenslet plane. A mechanical reference is installed on the board.
 - b. Rx, Ry alignment

The F/13.4 source that produces a collimated beam on the lenslet is used. The lenslet switch unit Rx and Ry are aligned using back reflection from the first flat surface of the lenslet array. A mechanical reference is installed on the board.
 - c. X, Y alignment

| | | | |
|-------------------------------|--|--|---|
| <p>ERIS Consortium</p> | <p>ERIS Documentation Standards</p> | <p>Doc.-Ref. Issue Date Page</p> | <p>: VLT-TRE-ERI-14403-3001 : 1.0 : 05.12.15 : 124 of 136</p> |
|-------------------------------|--|--|---|

The F/13.4 source is used. The stage is stepped until the envelope of the grid spots is properly filling the CCD area. The Y direction is similarly adjusted shimming the lenslet switch unit.

11. CCD camera focus refinement

The F/13.4 source is used as source and the lenslet array switch is set to the Low Order position. A dedicated tool is used in order to keep the camera X,Y, Rx,Ry fixed while the camera can slide along the Z axis. The CCD camera is positioned in intra and extra focal positions in order to identify the best focus from the spot size measurements. The camera is set in the best focus Z position and the tool removed.

8.3 Warm Optics and WFS boards alignments on ERIS Optical Plate

At INAF premises (Arcetri), all the optics will be aligned with respect to the mechanical axis of the Cassegrain Interface Flange of the ERIS central structure. The alignment of the ERIS mechanical axis to the telescope optical axes will be performed during commissioning directly at the telescope. In the following sections, we describe the alignment procedure to align the warm optics, the LGS and the NGS WFS units to the mechanical axis of the Cassegrain Interface Flange.

8.3.1 Telescope’s mechanical axis materialisation

The Cassegrain Interface Flange (CIF), the support conical structure and the ERIS Optical Plate will be delivered to Arcetri Observatory to proceed to preliminary alignment test. We will use CIF as absolute reference to materialise the CIF mechanical axis. Thus, the mechanical reference for the horizontal plane is the CIF’s top surface and the mechanical reference for the centring will be provided by using tiny crossed wires secured on dedicated mechanical references of the CIF.

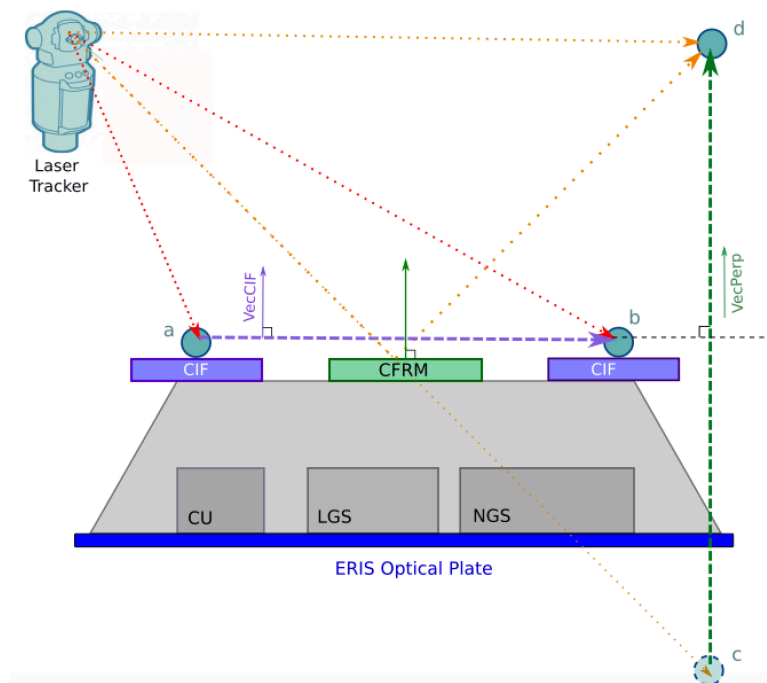


Figure 82 Alignment setup for the CFRM with respect to the CIF using a laser tracker.

To materialise the telescopes mechanical axis we will use a flat mirror with its two faces polished, aluminized and with a high grade of parallelism. We will refer to this optic as Cassegrain Flange

| | | | |
|---|--|--|---|
| <p style="text-align: center;">ERIS Consortium</p> | <p style="text-align: center;">ERIS Documentation Standards</p> | <p>Doc.-Ref. Issue Date Page</p> | <p>: VLT-TRE-ERI-14403-3001 : 1.0 : 05.12.15 : 125 of 136</p> |
|---|--|--|---|

Reference Mirror (CFRM). For alignment easiness, the CFRM will be installed in a tip-tilt mechanical mount. We will align the CFRM making its axis parallel to the CIF's one. For the axis angle alignment, we will use a laser tracker using a method we successfully experienced for the LBT FLAO system. This device provides 3-dimensional coordinate measurements with an accuracy of 1-10 microns, depending on the used setup. Figure 82 shows a schematic of the alignment setup of the CFRM. The laser tracker must be set aside the interface flange. The laser tracker retroreflector must be hold against the CIF mechanical reference surface in many locations around the CIF to identify its plane and, consequently, its normal vector Vec_{CIF} . The laser tracker retroreflector is then placed in position "d" and two additional measurements are taken: one through the reflection on the CFRM (at equivalent location "c"), and one directly between the tracker and retroreflector (at location "d"). This second set of measurements allows determining the normal vector to the CFRM, " Vec_{Perp} " in the schematic. Knowing Vec_{CIF} and Vec_{Perp} , the CFRM position can be adjusted in tip-tilt to position it parallel to the CIF. Laser tracker measurement is iterated until alignment is reached.

The centre of the CIF will be identified using mechanical reference and marked with a crosshair on the bottom surface of the CFRM. This will identify the position of the incoming optical axis. Once the CFRM is properly aligned to the CIF, its bottom reflective surface will be used as reference to materialise the telescope mechanical axis during the alignment of the warm optics and WFS boards.

8.3.2 Alignment of warm optics and WFS boards

The CFRM is now used to align WO and WFS units to the identified CIF axis.

Alignment procedure:

AP1. LGS WFS setup

Set the LGS WFS board on ERIS Optical Plate in its nominal position. Insert the alignment laser shining outward of the WFS board¹⁹.

AP2. Warm optics setup

Set on ERIS Optical Plate the LGS fold mirror, the WFS dichroic and the Instrument dichroic in their nominal positions.

AP3. LGS fold mirror an Instrument dichroic

Shine the alignment laser from the LGS WFS toward to the LGS folding mirror (see Figure 83). Then, adjust tip and tilt of LGS folding mirror and Instrument dichroic in order achieve auto-collimation (with the beam back reflected by the CFRM), together with centring with respect to the crosshair on the CFRM. At this point we have the telescope axis propagated through the warm optics coinciding with the LGS WFS one.

Note that the back surface of the Instrument dichroic has a curvature. However, its curvature ($R > 60m$) is very weak and the Instrument dichroic XY positioning does not require an optical feedback.

AP4. Telecentric lens

Install the telecentric lens in its nominal position. Then, check if the auto-collimation condition is still satisfied. If not, adjust the XY position of the Telecentric lens in order to restore

¹⁹ This is the same laser used in sect 8.1 for the internal alignment of the board. A Thorlabs Amber (590nm) Fiber-Coupled LED (coupled with a fiber optics collimator) will be used in order be properly transmitted through the WFS dichroic.

| | | | |
|-----------------|------------------------------|-----------|--------------------------|
| ERIS Consortium | ERIS Documentation Standards | Doc.-Ref. | : VLT-TRE-ERI-14403-3001 |
| | | Issue | : 1.0 |
| | | Date | : 05.12.15 |
| | | Page | : 126 of 136 |

it. Due to its long curvature radius, the positioning in Z of the telecentric lens does not require an optical feedback.

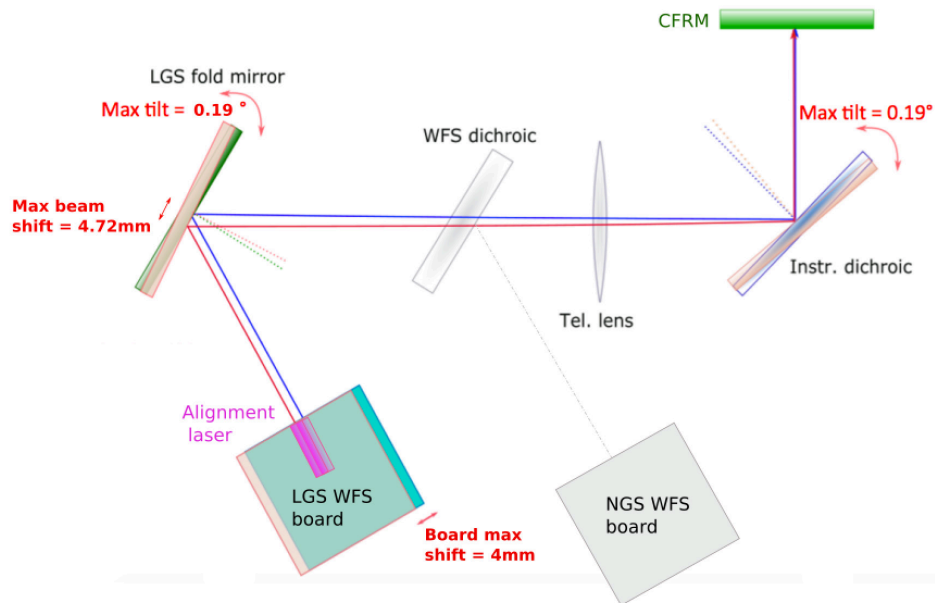


Figure 83 Sketch of the nominal optical path (blue) after the alignment (red) compensating for an error (4mm) in LGS WFS unit placement.

AP5. NGS WFS and WFS dichroic

Set the NGS WFS board on ERIS Optical Plate in its nominal position. Insert the alignment laser, shining outward of the WFS board, as done for the LGS WFS in AP1. Shine the laser toward the WFS dichroic and use WFS dichroic tip/tilt and NGS WFS field movements (X-stage and periscope) in order to achieve the auto-collimation (again with the beam back reflected by the CFRM) and centring on the crosshair. The X-stage and the periscope ranges will be oversized so that the displacement required by the alignment will not impact on the WFS patrol field.

AP6. LGS WFS alignment check

The WFS dichroic alignment done in AP5 can degrade the alignment of the LGS WFS board. Install the laser back on the LGS WFS and check if the auto-collimation and centring conditions is still valid. If not, start again from step AP3.

Because LGS and NGS WFS alignment are not independent, this results in an iterative process where a few iterations can be required.

| | | | |
|-----------------|------------------------------|------------------------------------|---|
| ERIS Consortium | ERIS Documentation Standards | Doc.-Ref. Issue Date Page | : VLT-TRE-ERI-14403-3001 : 1.0 : 05.12.15 : 127 of 136 |
|-----------------|------------------------------|------------------------------------|---|

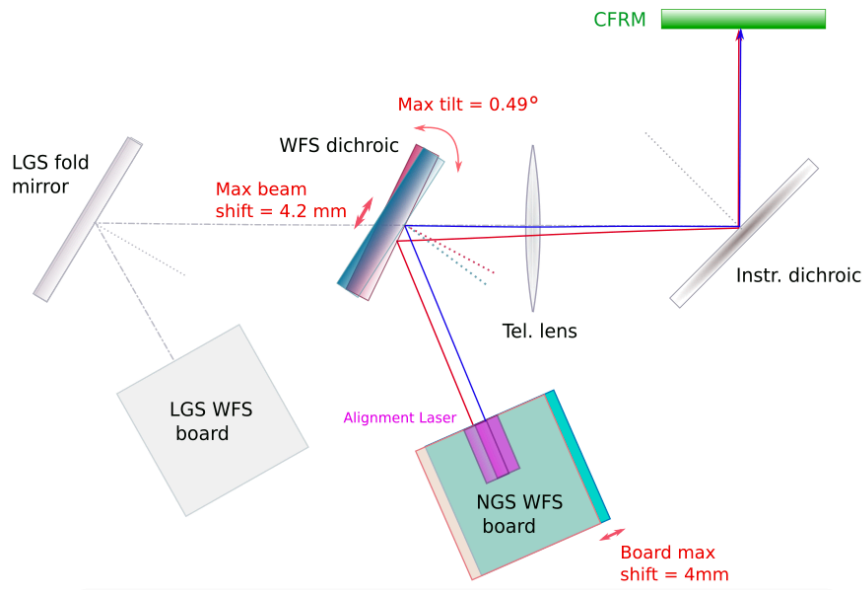


Figure 84 Sketch of the nominal optical path (blue) and after the alignment (red). A combination of tilt of WFS dichroic and stage travel is used.

9 Error Budget

The error budget collects all the contributions that are identified to evaluate the performance of a given specification. Three error budgets have been identified for the preliminary design:

- **TS-ERIS-PER-007 – NGS mode performance on-axis, requiring:**
 - $SR(K_s) \geq 68\%$ for a $mR=8$ NGS (class G2)
 - $SR(K_s) \geq 10\%$ for a $mR=15$ NGS (class G2)
 - 15 min observation at 30deg zenith with standard atmosphere (TS-ERIS-PER-005)
- **TS-ERIS-PER-008 – LGS mode performance on-axis:**
 - $SR(K_s) \geq 54\%$ for a $mR=12$ NGS (class G2)
 - $SR(K_s) \geq 10\%$ for a $mR=19$ NGS (class G2)
 - 15 min observation at 30deg zenith distance with standard atmosphere (TS-ERIS-PER-005)
 - on-axis NGS
- **TS-ERIS-PER-001 – Image motion, requiring**
 - max 30 mas PTV (10 mas PTV as a goal)
 - 1 hour observing block with zenith distance up to 30deg, bright AO guide star and standard atmosphere (TS-ERIS-PER-005)
 - NGS can be off-axis

For the first two budgets, it shall be assumed that the following parameters are perfectly known:

1. The science beam effective wavelength
2. The spectral type of the NGS
3. The science and NGS coordinates
4. The relevant atmospheric data (Temperature, Pressure, Humidity).

| | | | |
|----------------------------|---|-----------|--------------------------|
| ERIS Consortium | ERIS Documentation Standards | Doc.-Ref. | : VLT-TRE-ERI-14403-3001 |
| | | Issue | : 1.0 |
| | | Date | : 05.12.15 |
| | | Page | : 128 of 136 |

For the Image motion budget, this includes:

1. offsetting errors
2. field selector pointing errors
3. user-provided NGS colour errors
4. science beam effective wavelength
5. relevant atmospheric characteristics
6. inelastic flexures
7. thermal expansion

For the Image motion budget, only point 1, 2 and, in general, the effects producing image drift due to AO opto-mechanics are considered in the present report.

There are two types of contributions in the error budgets: random errors and drifts/offsets. Drifts and offsets, when repeatable, are calibrated and compensated in open loop using a LUT. For error budget purposes we assume that the LUT correction produces a residual error between 20% to 30%, depending on the hysteresis degree of the process generating the drift.

Random errors will be converted in WFE rms σ_{WFE} , summed in quadrature and Maréchal's approximation will be used to compute the corresponding SR attenuation factor:

$$SR = \exp \left[- \left(\frac{2\pi}{\lambda} \sigma_{WFE} \right)^2 \right]$$

On-sky angular drifts and corresponding LUT correction residuals are modelled as uniform drift at constant rate v (e.g. in mas/h) during the duration of the exposure T giving a Peak-to-Valley $PtV = vT$ and a rms $\sigma = vT/\sqrt{12}$ (see RD19). On-sky angular rms σ is converted in WFE rms $\sigma_{WFE} = \sigma D/4$ (D is the telescope entrance pupil diameter) and the Maréchal's formula is used again for computing SR attenuation.

We remind that the NGS WFS is the reference of tilt and focus for both NGS and LGS mode, then flexures of the LGS WFS are not relevant for the budget.

The following LUT will be considered here as major contributions:

- Differential focus between NIX and NGS WFS due to gravity change:
 - 4.5 nm RMS/h (see Sec. 7.1.3), no internal flexures in NIX are considered
- Differential TT between NIX and NGS WFS due to gravity change:
 - 32 mas/h (see Sec. 7.1.3), no internal flexures in NIX are considered
- On-axis NCPA LUT:
 - allocated budget of 20 nm rms WFE as bias error in NCPA identification/application
 - NIX contribution: 32 nm rms (fig. 5-13 in RD20, 90% confidence of on-axis Cam2 tolerance analysis)
 - IR/VIS dichroic: 8 nm rms, allocation buffer (contributions in Sec. 7.1.4 negligible)
 - HO NGS WFS (NGS-mode): 10 nm rms (Sec. 7.2.1)
 - LGS WFS (LGS-mode): 58 nm rms, VIS/VIS dichroic contribution (Sec. 4.8.2)
- LUT to compensate PSF drift due to pupil rotator:
 - rate per degree of instrument rotator: 1.1 mas/deg (see Sec. 7.2.2)
 - at 30 deg zenith distance the instrument rotator angle in 15min is 6.9 deg, in 1h is 27 deg

| | | |
|------------------------|-------------------------------------|---|
| ERIS Consortium | ERIS Documentation Standards | Doc.-Ref. : VLT-TRE-ERI-14403-3001 Issue : 1.0 Date : 05.12.15 Page : 129 of 136 |
|------------------------|-------------------------------------|---|

9.1 WFE budget

Table 45 shows the terms contributing to the WFE budget that are in common with NGS and LGS modes. The LUT efficiency column reports the fraction of drift/error effectively compensated by the LUT. The total contribution is 50 nm rms and it is dominated by the M1 optical figure.

The error budget for the NGS-mode is reported in Table 46, where the contribution of the common terms is also included. A buffer allocation of 40 nm rms WFE has been added to take in account the analysis that has not yet performed like thermal distortion and drifts, internal flexures, board stage stiffness, FEA refinement, etc.

Vibration WFE residuals are from average Case 2 described in the Sec. 4.7.12. The 1 kHz loop results are used for magR=8, the 500 Hz loop case are used for magR=15.

The specification **TS-ERIS-PER-007** is fulfilled with a WFE margin (contingency) of 143 nm rms for magR=8 and 377 nm rms for magR=15. The WFE difference between the total budget and the end-to-end (E2E) simulation provides the SR attenuation factor used for scaling down the simulated performances as reported in Sec. 4.7.8.

Apart from atmospheric correction residual, **vibrations are the dominant contribution in the budget, therefore it has to be considered a risk requiring mitigation action.** In the NGS-mode case this term is particularly important because the current implementation of the SPARTA RTC does not provide a Vibration Control function similar to the one already implemented in the LO NGS loop for the LGS-mode.

An assessment of Cassegrain Focal station vibration scenario is mandatory for likely performance estimation. The possibility to implement a Vibration Control algorithm in the HO NGS loop could be considered a valuable risk mitigation, especially in the case vibration frequencies above 48 Hz are present.

Table 45. WFE Budget: Common terms

| On-axis error terms, z=30deg, 15min exp.time WFE Budget: Common items | | | LUT | LUT | LUT | Reference |
|---|--------------|--------------|------------|-----------|--------|-------------------------------------|
| | WFE rms [nm] | SR@Ks | effic. % | max value | units | |
| Ks band [nm]: 2145 | | | | | | |
| Entrance Pupil Diameter [m]: 8.12 | | | | | | |
| WFS unit focal plane scale [mm/as] 0.528 | | | | | | |
| HO contributions | | | | | | |
| DSM best flattening | 18.0 | 0.997 | | | | RD14: VLT-TRE-OAA-11250-4054 Tab.5 |
| DSM fitting error of BFL500 conic constant | 10.0 | 0.999 | | | | AD3: VLT-TRE-ERI-14401-1010 Sec.4.4 |
| M1 High Spatial Frequency error | 40.0 | 0.986 | | | | RD1: VLT-TRE-ESO-14400-5563 |
| Differential focus LUT residual (between NIX and HO/LO NGS WFS) | 0.3 | 1.000 | 70% | 1.1 | nm RMS | Sec. 7.1.3 LUT change in 15 min |
| Strhel reduction due to scintillation | 10.0 | 0.999 | | | | RD1: VLT-TRE-ESO-14400-5563 |
| LO contributions | | | | | | |
| Differential TT LUT residual (between NIX and HO/LO NGS WFS) | 6.8 | 1.000 | 0.7 | 70% | 8.0 | mas |
| NGS WFS Stage positioning error | 18.6 | 0.997 | 1.9 | | | Sec. 4.9.2.1: repetability 1um |
| Total for common | 50.18 | 0.979 | 2.0 | | | |

Table 46 – WFE Budget: AO NGS-mode

| On-axis error terms, z=30deg, 15min exp.time NGS-mode | mR8 | | | mR15 | | | LUT eff. % | LUT max value | LUT units | reference |
|---|---|--------------|----------------|--------------|--------------|----------------|---------------|---------------|-----------|--|
| | WFE rms [nm] | SR@Ks | ang. rms [mas] | WFE rms [nm] | SR@Ks | ang. rms [mas] | | | | |
| | Ks band [nm]: 2145 Entrance Pupil Diameter [m]: 8.12 | | | | | | | | | |
| Performance from E2E simulation | 111 | 0.900 | | 329 | 0.396 | | | | | |
| Total from Common part | 50 | 0.979 | | 50 | 0.979 | | | | | |
| Other HO contributions | | | | | | | | | | |
| NCPA | | | | | | | | | | |
| Unmeasured NCPA | 20 | 0.997 | | 20 | 0.997 | | | | | Reserved budget |
| Residual error of NCPA compensation | 7 | 1.000 | | 7 | 1.000 | | 80% | 34 | nm rms | Sec.4.7.14 |
| Pupil X-Y misregistration on SH mask | 21 | 0.996 | | 21 | 0.996 | | | | | Sec.4.7.14 |
| Pupil rotation misregistration on SH mask | 5 | 1.000 | | 5 | 1.000 | | | | | Reserved budget (noise and aging) |
| Interaction Matrix calibration noise | 20 | 0.997 | | 20 | 0.997 | | | | | |
| Other LO Contributions | | | | | | | | | | |
| Vibrations | 82 | 0.946 | 8 | 113 | 0.902 | 11 | | | | Sec.4.7.12, Vibration case 2 |
| Pupil re-rotator: Correction residual of PSF drift LUT | 2 | 1.000 | 0 | 2 | 1.000 | 0 | 80% | 4.1 | mas | |
| Buffer allocation | 40 | 0.986 | | 40 | 0.986 | | | | | Thermal, internal flex.,etc(studies to do) |
| Total Error NGS-mode | 156 | 0.811 | | 355 | 0.339 | | | | | |
| Without E2E simulation performance contribution | 110 | | | 135 | | | | | | |
| Specification | 212 | 0.680 | | 518 | 0.100 | | | | | |
| Contingency | 143 | 0.838 | | 377 | 0.295 | | | | | |

The error budget for the LGS-mode is reported in Table 47, where the contribution of the common terms is also included. A buffer allocation of 40 nm rms WFE has been added to take in account the analysis that has not yet performed like thermal distortion and drifts, internal flexures, board stage stiffness, FEA refinement, etc.

Vibration WFE residuals are from average Case 2 described in the Sec. 4.7.12. The 500 Hz loop case are used both for magR=12 and 19 because the SPARTA baseline maximum speed of the LO NGS loop limited to 500 Hz.

Table 47 WFE Budget: AO LGS-mode

| On-axis error terms, z=30deg, 15min exp.time LGS-mode | mR12 | | | mR19 | | | LUT eff. % | LUT max value | LUT units | reference |
|---|---|--------------|----------------|--------------|--------------|----------------|---------------|---------------|-----------|--|
| | WFE rms [nm] | SR@Ks | ang. rms [mas] | WFE rms [nm] | SR@Ks | ang. rms [mas] | | | | |
| | Ks band [nm]: 2145 Entrance Pupil Diameter [m]: 8.12 | | | | | | | | | |
| Performance from E2E simulation | 198 | 0.714 | | 276 | 0.521 | | | | | |
| Total from Common part | 50 | 0.979 | | 50 | 0.979 | | | | | |
| Other HO contributions | | | | | | | | | | |
| NCPA | | | | | | | | | | |
| Unmeasured or miscalibrated NCPA | 20 | 0.997 | | 20 | 0.997 | | | | | Reserved budget |
| Residual WFE increase when using NCPA in the loop | 14 | 0.998 | | 14 | 0.998 | | 80% | 68 | nm rms | Sec.4.7.14 |
| Pupil X-Y misregistration on SH mask | 21 | 0.996 | | 21 | 0.996 | | | | | Sec.4.7.14 |
| Pupil rotation misregistration on SH mask | 5 | 1.000 | | 5 | 1.000 | | | | | Sec.4.7.14 |
| Interaction Matrix calibration noise | 20 | 0.997 | | 20 | 0.997 | | | | | Reserved budget (noise and aging) |
| Truth sensor sensitivity (active optics SH) | 41 | 0.986 | | 41 | 0.986 | | | | | Sec. 4.7.16: 30nm Astig, 20nm Coma, 20nm Trefoil |
| Focus truth sensing (LO NGS WFS) | 50 | 0.979 | | 50 | 0.979 | | | | | Sec. 4.7.16 |
| Other LO Contributions | | | | | | | | | | |
| Vibrations | 113 | 0.902 | 11 | 113 | 0.902 | 11 | | | | Sec. 4.7.12, Vibration case 2 |
| Pupil re-rotator: Correction residual of PSF drift LUT | 8 | 0.999 | 1 | 8 | 0.999 | 1 | 80% | 4.1 | mas | |
| Buffer Allocation | 40 | 0.986 | | 40 | 0.986 | | | | | Thermal, internal flex.,etc(studies to do) |
| Total Error NGS-mode | 249 | 0.589 | | 314 | 0.429 | | | | | |
| Without E2E simulation performance contribution | 150 | | | 150 | | | | | | |
| Specification | 268 | 0.540 | | 518 | 0.100 | | | | | |
| Contingency | 100 | 0.917 | | 412 | 0.233 | | | | | |

| | | | |
|---|--|--|---|
| <p style="text-align: center;">ERIS Consortium</p> | <p style="text-align: center;">ERIS Documentation Standards</p> | <p>Doc.-Ref. Issue Date Page</p> | <p>: VLT-TRE-ERI-14403-3001 : 1.0 : 05.12.15 : 131 of 136</p> |
|---|--|--|---|

The specification **TS-ERIS-PER-008** is fulfilled with a WFE margin (contingency) of 100nm rms for magR=12 and 412nm rms for magR=19. The WFE difference between the total budget and the end-to-end (E2E) simulation provides the SR attenuation factor used for scaling down the simulated performances as reported in Sec. 4.7.8.

Even in the LGS-mode case, apart from atmospheric correction residual, **vibrations are the dominant contribution in the budget**. However SPARTA supports Vibration Control algorithm that represents already a risk reduction item.

9.2 Image Motion Budget

A quite detailed image motion budget breakdown has been derived in RD19 for SINFONI. The related analysis in this section is using that work as guideline. image motion budget is evaluated considering the following contributions reported in RD19:

1. VLT guiding error: due to the telescope guide probe located far off-axis. From RD19 the error is <7.2 mas/h for $z > 2$ deg with 1 arcmin off-axis guide star.
2. Guiding wavelength error: due to the error in sending the offset commands to the NGS field selector to compensate for the differential drift between WFS wavelength (visible) and science wavelength (IR). This error is mainly due to the uncertainty in the estimation of the guiding wavelength. From Table 1 in RD19 we have 8.8 mas/h when guiding effective wavelength is 720nm and uncertainty of wavelength is 20nm.
3. Air-Mass variations: the star spectrum is dynamically dispersed depending on the air mass and produces an additional shift of the NGS centroid during observations. This error is mainly due to the uncertainty in the estimation of the guiding wavelength. From RD19: 6 mas/h when uncertainty of wavelength is 20nm.
4. Meridian rotation: the field selector shift speed depends also on the rotation speed of the meridian. This error is mainly due to the uncertainty in the estimation of the guiding wavelength. From plot in RD19 the contribution is 8.8 mas in 1 hour at $z=30$ deg.
5. Instrument flexures: these are the differential flexures between the AO path and the science path. We use the estimation from Sec. 7.1.3: 32 mas/h. No internal flexures in NIX/SPIFFI are considered here. This effect is mostly compensated using a pre-calibrated LUT to offset the NGS stages. We assume here that the efficiency of the LUT correction is 70%.

According to RD19, the Meridian rotation error and the combination between the Guiding wavelength and Air-mass variation errors are exclusive, therefore the combined image motion is the largest of the two effects.

The presence of the DSM as AO corrector requires a pupil rotator in the NGS (and LGS) WFS units to keep the DSM actuator map aligned with the SH lenslet array when the instrument rotator tracks the field. The opto-mechanical tolerances of the pupil rotator assembly produce a wobbling of the PSF that evolves with the same rate of the instrument rotator angular speed and then increasing when reducing the zenith distance of the NGS. This contribution was not present in the analysis for SINFONI, having the DM on the AO bench.

The drift introduced by the pupil rotator is estimated in Sec. 7.2.2 to be 1.1 mas per degree of instrument rotator. We assume this effect is mostly compensated using a pre-calibrated LUT to offset the NGS stages. We assume here that the efficiency of the LUT correction is 80%, considering that it is easily calibrated and regularly checked using the on-board technical camera.

The error budget for the Image Motion error taking into account all the above contribution is reported in Table 48 for 30deg zenith distance showing a total image motion of 18 mas in 1h. Moving

closer to the Zenith this value increases as shown in Figure 85. The threshold of the specification (30 mas) is crossed at z=9 deg, showing that the requirement is fulfilled in 91% of the specified sky area (z<30deg).

Table 48 – Image Motion Error Budget

| On-axis error terms, z=30deg, 15min exp.time Image Motion Budget | | | | LUT | LUT | LUT | LUT | LUT | reference |
|--|---------------|---------------|---------------|----------|-----------|-----------------|------|------------|---|
| | ang.PtV [mas] | ang.PtV [mas] | ang.PtV [mas] | effic. % | max value | max value units | rate | rate units | |
| Ks band [nm]: 2145 | | | | | | | | | |
| Integration time [h]: 1 | | | | | | | | | |
| Zenith distance [deg]: 30 | | | | | | | | | |
| Ins rotator angle in 1h [deg]: 27.1 | | | | | | | | | |
| NGS off-axis angle [as]: 60 | | | | | | | | | |
| Pupil rotator misalignment | 9 | | | 70% | 30.1 | mas | 1.11 | mas/deg | LUT rate in mas per deg of instrument rotator |
| Differential Flexures (NGS WFS wrt NIX) | 10 | | | 70% | 32 | mas | 32 | mas/h | Sec. 7.1.3 |
| Guiding error | 7 | | | | | | | | RD18: <50mas/h w off_axis=7arcmin and z>2deg |
| Wavelength error + airmass | | 11 | | | | | | | RD18: Wl error and airmass quadratic sum |
| Guiding wavelength estimated error | | | 9 | | | | | | RD18: 8.8 mas/h with NGS wl=720nm, z=30deg. 20nm wl uncertainty |
| Air Mass variation | | | 6 | | | | | | RD18: 6 mas/h, 20nm wl uncertainty |
| Meridian rotation | | 9 | | | | | | | RD18: from the plot image_motion vs z at meridian |
| Max between Meridian rot. and WL error+airmass | 11 | | | | | | | | |
| Total image motion error | 18 | | | | | | | | |
| Specification | 30 | | | | | | | | |
| Contingency | 12 | | | | | | | | |

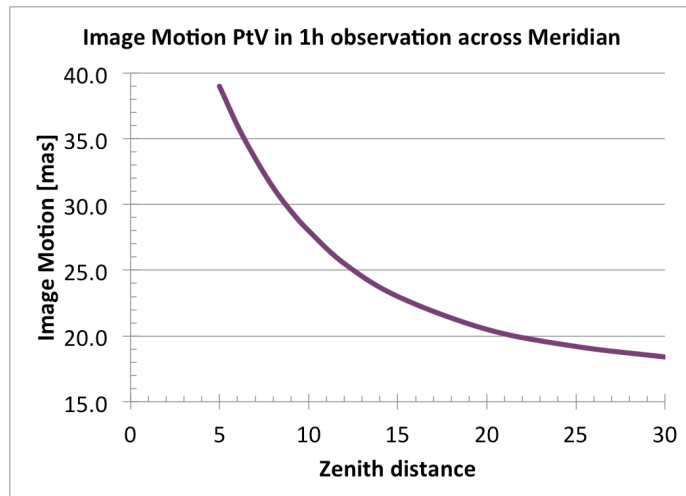


Figure 85 – Image motion budget in 1h observing time as a function of the Zenith distance. The specification (30 mas in 1h) is crossed at z=9 deg.

| | | |
|----------------------------|---|---|
| ERIS Consortium | ERIS Documentation Standards | Doc.-Ref. : VLT-TRE-ERI-14403-3001 Issue : 1.0 Date : 05.12.15 Page : 133 of 136 |
|----------------------------|---|---|

10 Compliance Status

We report here only the Verification Matrix items that are related to Adaptive Optics and Warm Optics. For a system-level Verification Matrix refer to AD13. For Software Level Verification Matrix refer to AD11. For Electronics Level Verification Matrix refer to AD12.

| ID | TS | TS title | Requirement | Compliance | Reference |
|----|-----------------|-------------------------------|--|------------|---|
| 2 | TS-ERIS-GEN-002 | Instrument Concept 2 | Pre-testing as single unit | 75%, D | The instrument will undergo verification testing following the MAIV plans. AO testing with the deformable secondary can only be performed at the telescope. During AO MAIV only functional test are possible (see AD7). |
| 7 | TS-ERIS-GEN-008 | Test equipment | Need for test equipment | 100%, D | AO MAIV Plan AD7 |
| 12 | TS-ERIS-GEN-013 | Accessibility | Accessibility requirements | 100%, D | No AO parts require regular maintenance or replacement |
| 15 | TS-ERIS-GEN-021 | Use of the AOF | Use of DSM and 4LGSF | 100%, D | This document |
| 16 | TS-AO-GEN-028 | AO correction | Modes of AO correction | 100%, D | This doc Sec. 4.5 |
| 17 | TS-AO-GEN-029 | AO module wavelength range | Wavelength range used by AO module | 100%, D | This document |
| 18 | TS-NIX-GEN-030 | NIX Wavelength range | Minimum wavelength range for NIX | 100%, D | This doc Sec. 4.8.2 for the instrument dichroic of Warm Optics |
| 21 | TS-NIX-GEN-055 | NIX FoVs | Minimum FoVs for NIX set-ups | 100%, D | This doc Sec. 4.8.2 for the instrument dichroic of Warm Optics |
| 29 | TS-ERIS-INT-015 | Telescope optical I/F | Optical prescription and interfaces to the VLT-UT4 | 75%, D | Change request for modification to BFL=500mm. See this doc Sec. 4.1 and AD3 |
| 31 | TS-ERIS-INT-021 | Interface to 4LGSF | I/F to the 4LGSF | 100%, D | This document |
| 32 | TS-ERIS-INT-024 | I/F to NGC | I/F to ESO's detector controllers | 100%, D | This doc Sec. 4.2 |
| 33 | TS-ERIS-INT-027 | I/F to the Real Time Computer | I/F to ESO's RTC | 100%, D | This doc Sec. 4.2 |
| 35 | TS-ERIS-INT-031 | Vibrations | Vibrations from ERIS | 100%, D | No fans or vibrating elements in WO and AO design inside the ERIS central structure. |
| 40 | TS-ERIS-STD-002 | Mechanical Standards | Comply with ESO's me- | | |

| | | |
|----------------------------|---|---|
| ERIS Consortium | ERIS Documentation Standards | Doc.-Ref. : VLT-TRE-ERI-14403-3001 Issue : 1.0 Date : 05.12.15 Page : 134 of 136 |
|----------------------------|---|---|

| ID | TS | TS title | Requirement | Compliance | Reference |
|----|-----------------|--|---|------------|--|
| | | | chanical standards | | |
| 41 | TS-ERIS-STD-003 | Moving mechanisms | Comply with ESO's standards for moving mechanisms | 95%, D | Only stepper motor of rotary stage of pupil rotator has no encoder. Substitution with different model if needed. |
| 43 | TS-ERIS-STD-010 | Control Electronics standards | Comply with ESO's electronics standards | 100%, D | This document |
| 44 | TS-ERIS-STD-011 | Detectors control electronics standard | Comply with ESO's NGC standards | 100%, D | This document |
| 45 | TS-ERIS-STD-013 | Real Time computer standards | Comply with ESO's RTC standards | 100%, D | This document |
| 46 | TS-ERIS-STD-014 | Wavefront Sensor Cameras standards | Comply with ESO's WFS cameras standards | 100%, D | This document |
| 49 | TS-ERIS-STD-025 | Environmental standards | Use of defined ESO's environmental conditions | 100%, D | |
| 53 | TS-ERIS-FUN-020 | Small offsets | Small offsets in close loop | 100%, D | |
| 54 | TS-ERIS-FUN-025 | Large offsets | Large offsets in open loop | 100%, D | |
| 57 | TS-AO-FUN-050 | RTC data recording | RTC data logging | 100%, D | See AD10 |
| 58 | TS-AO-FUN-055 | AO NGS acquisition | Automated NGS acquisition | 100%, D | This document and AD11 |
| 64 | TS-ERIS-OPS-010 | Staring mode | Definition of staring mode | 100%, D | |
| 65 | TS-ERIS-OPS-011 | Dithering mode | Definition of dithering mode | 100%, D | |
| 66 | TS-ERIS-OPS-012 | Chopping | Definition of chopping mode | 100%, D | See AD10 |
| 67 | TS-ERIS-OPS-013 | Moving targets | Definition of non-sidereal modes | 100%, D | Required coordination of periscope and stage motion (Sec. 4.10) |
| 68 | TS-ERIS-OPS-014 | Pupil tracking mode | Definition of pupil-tracking mode | 100%, D | Stopping Pupil rotator |
| 72 | TS-AO-OPS-030 | Seeing Limited Mode | Definition of seeing limited mode | 100%, D | This doc Sec. 4.5.1 |
| 73 | TS-AO-OPS-031 | Closed loop on LGS | Closed loop operations using LGS+ LO NGS | 100%, D | This doc Sec. 4.5 |
| 74 | TS-AO-OPS-032 | Closed loop on NGS | Closed loop operations using a HO NGS | 100%. D | This doc Sec. 4.5 |
| 75 | TS-AO-OPS-033 | Seeing enhancer mode | Definition of seeing enhancer mode | 100%, D | This doc Sec. 4.5.1 |
| 80 | TS-ERIS-PER-001 | Image motion | Maximum allowed image motion seen by the instruments in closed loop | 91%, D | This doc Sec. 9.2 |
| 81 | TS-ERIS-PER-005 | Atmosphere model | Model to be used for simulations | 100%, D | This doc Sec. 4.7.1.1 |
| 82 | TS-ERIS-PER-007 | NGS mode performance | Strehl ratio for NGS mode as a function of on-axis | 100%, D | This doc Sec. 4.7.8 |

| | | |
|------------------------|-------------------------------------|---|
| ERIS Consortium | ERIS Documentation Standards | Doc.-Ref. : VLT-TRE-ERI-14403-3001 Issue : 1.0 Date : 05.12.15 Page : 135 of 136 |
|------------------------|-------------------------------------|---|

| ID | TS | TS title | Requirement | Compliance | Reference |
|-----|-------------------|---------------------------------------|--|------------|---|
| | | on-axis | NGS reference magnitude | | |
| 83 | TS-ERIS-PER-008 | LGS mode performance on-axis | Strehl ratio for LGS mode as a function of on-axis NGS reference magnitude | 100%, D | This doc Sec. 4.7.8 |
| 85 | TS-ERIS-PER-010 | Offset accuracy | Accuracy of offsets | 100%, D | For the AO HW part: accuracy of stages: 1um=2mas |
| 86 | TS-AO-PER-014 | Max brightness limit of NGS reference | Max brightness for NGS reference | 100%, D | filters for bright objects (filter wheel in NGS WFS) |
| 87 | TS-AO-PER-015 | Sodium laser guide star flux | Collected photon flux from LGS | 100%, D | Sec. 4.7.1.5 |
| 88 | TS-AO-PER-016 | Extended objects as NGS reference | Using extended objects as NGS reference | 100%, D | Only baseline (1.5as Object). FoV of NGS is 2.5as |
| 89 | TS-AO-PER-017 | Loop stability NGS mode | Conditions under which loop remains closed in NGS mode | 100%, D | Stability of loop against seeing change in 4.7.13. Reduction of controlled modes before DSM force limit occurs. |
| 90 | TS-AO-PER-018 | Loop stability LGS mode | Conditions under which loop remains closed in LGS mode | 100%, D | Reduction of controlled modes before DSM force limit occurs. |
| 112 | TS-SPIFFI-PER-175 | Instrument swap | Overheads for NIX/SPIFFI swaps | 100%, D | For the WO side: Implementation of NIX selector mirror |
| 130 | TS-ERIS-ENV-010 | Gravity loads | VLT Altitude axis operational ranges NGS and LGS | 100%, D | Sec. 7.1.3 |
| 134 | TS-ERIS-RAM-020 | Line Replaceable Units (LRU) | Use of LRUs | 100%, D | For CCD220 and electronics components |
| 137 | TS-ERIS-RAM-023 | Treatment of surfaces | Treatment against corrosion | 100%, D | |
| 150 | TS-ERIS-SAF-025 | Disassembling | Assembly instructions, tools | 100%, D | AO MAIV plan |

| | | | |
|-------------------------------|--|--|---|
| <p>ERIS Consortium</p> | <p>ERIS Documentation Standards</p> | <p>Doc.-Ref. Issue Date Page</p> | <p>: VLT-TRE-ERI-14403-3001 : 1.0 : 05.12.15 : 136 of 136</p> |
|-------------------------------|--|--|---|

11 Conclusions

The preliminary design for the AO module of the ERIS instrument fulfils the specification in terms of system performance, optical, mechanical and electronics interfaces. The designed AO module fits in the volume allocated in the ERIS central structure.

The AO module preliminary design identified the following critical items:

1. Vibrations at 48 and 97 Hz are poorly rejected if not amplified by the system. An assessment of Cassegrain Focal station vibration scenario is mandatory for a performance estimation. In case 48 and 97 Hz vibration are confirmed at the level experienced in RD14, advance Vibration Control Algorithm have to be implemented in the HO NGS loop control of SPARTA. Currently only available in LO NGS loop of the LGS mode.
2. The image stability requirement of 30mas over 1 hour for Zenith distance up to 30 degrees is fulfilled for $z > 9\text{deg}$ covering 91% of the specified sky area around the Zenit.
3. the IR/VIS dichroic has been assessed to be critical in terms of manufacturing. Prototype of this unit is required as risk mitigation during Final Design phase
4. the Aerotech dual-axis stage moving the NGS WFS unit should be purchased and tested in the lab to verify critical specification, like stiffness, positioning accuracy and stability

End of document